SCUOLA DI DOTTORATO IN SCIENZE DELL'INGEGNERIA

CORSO DI DOTTORATO IN INGEGNERIA CIVILE, AMBIENTALE, EDILE E ARCHITETTURA

XXX CICLO

Optimization of building performance via model-based predictive control

Doctoral thesis by:

Mariangela Benedettelli

Supervised by:

Chiar.mo Prof. Ing. Berardo Naticchia

Prof. Ing. Alessandro Carbonari

Dott. Ing. Massimo Vaccarini

To Fabio

To my family

Acknowledgements

I would like to express my sincere gratitude to all people who in some way contributed to this thesis.
First of all, I would like to thank my tutor Prof. Ing. Naticchia, who trusted in me and offered me this great opportunity. Besides my tutor, I would like to thank Prof. Ing. Carbonari and Ing. Vaccarini for their continuous support of my PhD study and research, for their patience, motivation, and for all they taught to me.
My sincere thanks goes to people who work in my Department, Giuliana, Monica and Serena, they made me feel like home every time.
I thank my PhD colleagues and friends of these three years, especially Sara and Simona for the unforgettable moments shared together.
I would like to thank Giulia and Claudia, my dear friends, for their support in many situations during these years.
A special thanks to Chiara, the best friend I could wish for.
Last but not the least, I would like to thank my family: my parents and my sister for their unconditional love and for supporting me throughout writing this thesis and during my life in general.
All my love and my thanks to Fabio who was always there for me.

Summary

Model Predictive Control (MPC) is an advanced control technique which has played an important role in the management of many processes in the industry sector. Nowadays, thanks also to the increasing attention placed on the energy efficient management of buildings, the exploitation of this strategy is proving to be a promising solution for minimising overall energy consumptions and costs. However, while significant effort has been spent in simulated applications of MPC, investigations on the feasibility of the technique in real existing buildings are at an initial stage.

Hence, the main outcome of this dissertation is the design and development of a prototype hardware and software set up for on-field testing of a model-based predictive control system, integrating a virtual predictive model of the portion of the building under investigation, the controller and the interface to the monitoring and regulation devices used. Moreover, this research is addressed to investigate the technical feasibility of the development and deployment of a typical MPC system, which includes a monitoring sub-system, a data acquisition set up and a system identification method to obtain the model for the controller by means of a grey-box modelling approach. The modelling phase and the empirical approach developed are presented in the first part of this research thesis, while the core part concerns the development of the MPC prototype, within a virtual instrument (VI) of LabVIEW software. Subsequently, it is described the experimental test, which was carried out during heating season, ensuring normal building operation during the entire monitoring period. As a result, it is showed how an MPC system can be integrated in existing buildings and it is explained how the architecture of the controller can be designed and implemented in LabVIEW.

Finally, this dissertation presents the study developed in simulation environment to investigate the potential of the control logic for the evaluation of retrofitting scenarios. The focus is on the definition of the main MPC simulator components and on the results obtained by testing one of the intervention scenarios. The dissertation concludes by outlining the main contributions of the research carried out and recommending interesting research topics for future developments.

Italian version

Il controllo predittivo basato su modello (MPC) è una tecnica di controllo avanzata che ha svolto un ruolo importante nella gestione di molti processi nel settore industriale. Oggi, grazie anche alla crescente attenzione posta sulla gestione efficiente dell'energia degli edifici, l'utilizzo di questa strategia si sta dimostrando una soluzione promettente per ridurre al minimo i consumi e i costi energetici complessivi. Tuttavia, sebbene sia stato impiegato uno sforzo significativo nelle applicazioni simulate di MPC, gli studi sulla sua fattibilità tecnica in edifici esistenti sono ancora in una fase iniziale.

Pertanto, il risultato principale di questa tesi è la progettazione e lo sviluppo di un prototipo hardware e software per la verifica sul campo di un sistema di controllo predittivo, basato su modello, integrando un modello predittivo virtuale della porzione dell'edificio in esame, il controllore e l'interfaccia grafica per i dispositivi di monitoraggio e regolazione utilizzati. Inoltre, particolare attenzione è stata posta sulla fattibilità tecnica relativa all'implementazione di un tipico sistema MPC, che include un sottosistema di monitoraggio, un set di acquisizione dati e un metodo di identificazione del sistema per ottenere il modello per il controllore, mediante un approccio di modellazione grey-box. La fase di modellazione e l'approccio empirico sviluppato sono presentati nella prima parte di questa tesi di ricerca, mentre la parte centrale riguarda lo sviluppo del prototipo di controllo predittivo, basato su modello, all'interno di uno strumento virtuale (VI) del software LabVIEW. Successivamente, viene descritto il test sperimentale, che è effettuato durante la stagione di riscaldamento, garantendo la normale operatività dell'edificio durante l'intero periodo di monitoraggio. Di conseguenza, viene mostrato come un sistema MPC può essere integrato negli edifici esistenti e viene spiegato come progettare e implementare l'architettura del controllore in LabVIEW.

Infine, è presentato lo studio sviluppato in ambiente di simulazione per indagare il potenziale della logica di controllo per la valutazione di scenari di riqualificazione. Il focus è sulla definizione dei principali componenti del simulatore MPC e sui risultati ottenuti testando uno degli scenari di intervento. La tesi si conclude delineando i principali contributi della ricerca svolta e suggerendo argomenti di ricerca interessanti per sviluppi futuri.

Contents

ACKNOWLEDGEMENTS I
SUMMARY III
CONTENTS VI
LIST OF ACRONYMS X
LIST OF FIGURES XII
LIST OF TABLES XVIII
LIST OF EQUATIONS XX

CHAPTER 1: INTRODUCTION TO THE THESIS 1

1.1 Introduction 1
1.2 Problem statement 1
1.3 Aim and objectives 3
1.4 Overview of the research methodology 4
1.5 Outcomes and limitations 4
1.6 Thesis structure 6

CHAPTER 2: STATE OF THE ART ON REDUCED ORDER MODELS FOR BUILDINGS 9

2.1 Introduction 9
2.2 Reduced Order Modelling 10
2.3 Early works 11
2.4 A model for the thermal dynamics of buildings 13
2.5 Identification procedure of suitable ROMs 15
2.6 Grey-box models 16
2.7 Implication of the results 18

CHAPTER 3: STATE OF THE ART ON MODEL PREDICTIVE CONTROL FOR BUILDINGS 21

3.1 Introduction 21
3.2 Overview of Model Predictive Control strategy 21
3.3 Development of MPC for management of building systems 24
3.4 MPC design 28

3.5 Implication of the results ... 32

CHAPTER 4: DEVELOPMENT OF AN EMPIRICAL APPROACH TO DERIVE GREY-BOX MODELS ... 36

4.1 Introduction ... 36

4.2 Preliminary study ... 36

4.2.1 Sensors deployment ... 38

4.2.2 RC-networks ... 39

4.2.3 Estimation results and model validation ... 41

4.2.4 Implication of the results ... 44

4.3 Development of the identified procedure in a real case study ... 44

4.3.1 Case study description ... 44

4.3.2 Definition of objectives ... 47

4.3.3 Sensors identification and deployment ... 47

4.3.4 The experimental campaigns and data elaboration ... 52

4.3.4.1 Summer campaign ... 53

4.3.4.2 Winter campaign ... 59

4.3.5 The Grey-box modelling ... 64

4.3.5.1 The Grey-box model for the summer season ... 64

4.3.5.2 The Grey-box model for the winter season ... 68

4.3.6 Validation of the models ... 71

4.3.6.1 Methodology ... 72

4.3.6.2 Summer validation ... 78

4.3.6.3 Winter validation ... 79

4.4 Conclusions ... 81

CHAPTER 5: DEVELOPMENT OF A MPC PROTOTYPE ... 83

5.1 Introduction ... 83

5.2 Methodology ... 83

5.3 Monitoring system ... 84

5.4 Control management ... 87

5.5 The Grey-box model for the controller ... 89

5.6 The MPC prototype ... 92

5.6.1 Design phase ... 92

5.6.2 Development in LabVIEW ... 94

5.7 The experimental test ... 100

5.8 Results ... 101

5.9 Comfort and energy assessment ... 103

5.9.1 Indoor thermal comfort ... 105

5.9.2 Energy consumption ... 117

5.10 Conclusions *120*

CHAPTER 6: DEVELOPMENT OF A MPC SIMULATOR **123**

6.1 Introduction *123*

6.2 Methodology *123*

6.3 The Detailed Model *124*

6.4 MPC framework in simulation environment *129*

6.4.1 Input parameters 130

6.4.2 The Grey-box model 131

6.4.2.1 Model estimator 131

6.4.2.2 Kalman filter 132

6.4.3 The controller 133

6.5 Modelling results *136*

6.5.1 Model identification 136

6.5.2 Model validation 143

6.6 MPC results *152*

6.6.1 Horizons tuning 153

6.6.2 Adaptive modelling 160

6.7 Conclusions *165*

CHAPTER 7: FINAL CONCLUSIONS **167**

7.1 Main contributions and implications of this research *167*

7.2 Further research *168*

REFERENCES 171

PUBLICATIONS 178

APPENDICES 180

APPENDIX A. TECHNICAL SPECS OF HOBO WIRELESS SENSORS 181

APPENDIX B. OFFICE WALLS COMPOSITION 183

APPENDIX C. FCU TECHNICAL DATA 185

APPENDIX D. INDIRECT MEASUREMENTS 186

APPENDIX E. CTSM-R GUIDE 190

APPENDIX F. SENSORS NETWORK GENERAL DATA 198

APPENDIX G. MATLAB CODE FOR WUFORECAST SUBVI 200

APPENDIX H. MATLAB CODE FOR MPC SIMULATOR 205

APPENDIX I. TUNING OF MPC PARAMETERS 213

List of Acronyms

HVAC	Heating Ventilation and Air Conditioning
BEMS	Building Energy Management Systems
MPC	Model Predictive Control
ROM	Reduced Order Model
FDD	Fault Detection and Diagnostics
FBDD	Frequency Based Damage Detection
MBDD	Mode-shape Based Damage Detection
PRBS	Pseudo Random Binary Signal
TES	Thermal Energy Storage
GPC	Generalized Predictive Control
PMV	Predicted Mean Vote
PPD	Predicted Percentage of Dissatisfied
MBPC	Model Based Predictive Control
COP	Coefficient Of Performance
CTSM	Continuous Time Stochastic Modelling
AHU	Air Handling Unit
VAV	Variable Air Volume
FCU	Fan Coil Unit
RMSE	Root Mean Square Error
MISO	Multiple-Input Single-Output
RTD	Resistance Temperature Detector
FMI	Functional Mock-up Interface
FMU	Functional Mock-up Unit
SL	Shading Level
GP	General Problem

List of Figures

FIG. 1.1 OVERVIEW OF THE RESEARCH METHODOLOGY. 5

FIG. 2.1 EXAMPLES OF SIMPLE THERMAL NETWORKS (SOURCE: RABL, 1988) 12

FIG. 2.2 THERMAL NETWORK OF A BUILDING ZONE (SOURCE: MATHEWS AND RICHARDS, 1989) 12

FIG. 2.3 THE "TWO-TIME CONSTANT" MODEL (SOURCE: MADSEN ET AL., 1993) 14

FIG. 2.4 MODEL SELECTION PROCEDURE (SOURCE: BACHER AND MADSEN, 2011) 15

FIG. 2.5 THE FINAL SELECTED REDUCED-ORDER MODEL (SOURCE: BACHER AND MADSEN, 2011) 16

FIG. 2.6 RC-ANALOGY OF REDUCED ORDER BUILDING MODELS (SOURCE: REYNDERS ET AL., 2014) 17

FIG. 3.1 MPC STRATEGY 23

FIG. 3.2 KEY COMPONENTS OF A MPC FOR BUILDINGS 29

FIG. 4.1 OVERVIEW OF THE LABORATORY AND THE MAIN TESTING AREA. 37

FIG. 4.2 TEST-ROOM AND BOUNDARY PLACES. 37

FIG. 4.3 PLAN OF THE LABORATORY WITH THE HOBO NETWORK DEPLOYMENT. 38

FIG. 4.4 SENSORS POSITIONING IN THE ARCHIVE (A), IN THE CHANGING ROOM (B) AND IN THE LABORATORY (C). 39

FIG. 4.5 RC-NETWORKS OF THE GREY-BOX MODELS: 1ST, 2ND, 3RD ORDER MODELS, FROM LEFT TO RIGHT. 41

FIG. 4.6 VALIDATION RESULTS OF THE THREE REDUCED-ORDER MODELS TESTED 42

FIG. 4.7 A) SATELLITE LOCALIZATION, B) VIEW OF THE SOUTH FULLY-GLAZED FAÇADE, C) VIEW OF THE INTERIORS. 45

FIG. 4.8 THE TEST ROOM: VIEWS OF THE OFFICE 90 ON THE THIRD FLOOR. 46

FIG. 4.9 THE FALSE-CEILING BEFORE THE SENSORS INSTALLATION: A) EXTERNAL VIEW AND B) INTERNAL VIEW OF THE FCU 46

FIG. 4.10 THE CONFIGURATION OF THE SENSOR NETWORK BY MEANS OF HOBOWARE PRO SOFTWARE AND THE RECEIVER CONNECTED VIA USB CABLE TO THE PC 47

FIG. 4.11 A) ROUTER INSTALLED INSIDE THE TEST ROOM AND B) ONE OF THE ROUTERS PLACED ALONG THE WEST CORRIDOR 48

FIG. 4.12 DEVICES INSTALLED IN THE PLANT DUCTS TO MONITOR THE SUPPLY AIR FLOW: A) DURING THE SUMMER CAMPAIGN AND B) THE WINTER CAMPAIGN. 49

FIG. 4.13 THE MAP OF THE HOBO SENSORS NETWORK INSTALLED ON THE THIRD FLOOR 50

FIG. 4.14 THE WEATHER STATION INSTALLED ON THE ROOF OF THE BUILDING 50

FIG. 4.15 THE TWO PYRANOMETERS INSTALLED IN THE TEST ROOM 51

FIG. 4.16 TREND OF THE INTERNAL TEMPERATURE OF OFFICE 90, THE TEST ROOM. 55

FIG. 4.17 TREND OF THE OUTLET AIR TEMPERATURE FROM THE VENTILATING SECTION IN THE FALSE-CEILING OF THE TEST ROOM. 55

FIG. 4.18 TREND OF THE CORRIDOR TEMPERATURE, IN FRONT OF THE TESTING OFFICE. 56

FIG. 4.19 TREND OF THE OUTDOOR TEMPERATURE, MEASURED BY THE WEATHER STATION ON THE ROOF. 56
FIG. 4.20 TREND OF THE GLOBAL HORIZONTAL RADIATION ACQUIRED BY THE WEATHER STATION. 57
FIG. 4.21 TREND OF THE SOLAR RADIATION ACQUIRED BY THE INTERNAL VERTICAL PYRANOMETER. 57
FIG. 4.22 TREND OF THE VENTILATION POWER DURING THE SELECTED SUMMER CAMPAIGN. 58
FIG. 4.23 TREND OF THE COOLING POWER DURING THE SELECTED SUMMER CAMPAIGN. 58
FIG. 4.24 TREND OF THE INTERNAL TEMPERATURE OF OFFICE 90, THE TEST ROOM. 60
FIG. 4.25 TREND OF THE OUTLET AIR TEMPERATURE FROM THE VENTILATING SECTION IN THE FALSE-CEILING OF THE TEST ROOM. 60
FIG. 4.26 TREND OF THE OUTLET AIR TEMPERATURE FROM THE HEATING SECTION IN THE FALSE-CEILING OF THE TEST ROOM. 61
FIG. 4.27 TREND OF THE CORRIDOR TEMPERATURE, IN FRONT OF THE TESTING OFFICE. 61
FIG. 4.28 TREND OF THE OUTDOOR TEMPERATURE, ACCORDING TO DATA FROM WU WEB SITE. 62
FIG. 4.29 TREND OF THE GLOBAL SOLAR RADIATION, ACCORDING TO DATA FROM CAMS RADIATION SERVICE OF SODA WEB SITE. 62
FIG. 4.30 TREND OF THE VENTILATION POWER DURING THE SELECTED WINTER CAMPAIGN. 63
FIG. 4.31 TREND OF THE HEATING POWER DURING THE SELECTED WINTER CAMPAIGN. 63
FIG. 4.32 THE BEST GREY-BOX MODEL OF THE SUMMER SEASON: STRUCTURE OF THE 2C2R MODEL. 65
FIG. 4.33 THE BEST GREY-BOX MODEL OF THE SUMMER SEASON: STRUCTURE OF THE 2C2R MODEL. 66
FIG. 4.34 THE BEST GREY-BOX MODEL OF THE WINTER SEASON: STRUCTURE OF THE 2C2R MODEL. 69
FIG. 4.35 THE BEST GREY-BOX MODEL OF THE WINTER SEASON: STRUCTURE OF THE 2C2R MODEL. 70
FIG. 4.36 INSTANCES OF: A) THE MODELICA STANDARD LIBRARY, B) THE MODELICA BUILDINGS LIBRARY. 73
FIG. 4.37 IMPLEMENTATION OF THE DATA SET FOR THE MODEL VALIDATION IN DYMOLA. 74
FIG. 4.38 UNIT CONVERSION AND TEMPERATURE INITIAL VALUE FOR THE HEAT CAPACITOR COMPONENT 75
FIG. 4.39 UNIT CONVERSION AND TEMPERATURE INITIAL VALUE FOR THE THERMAL RESISTOR COMPONENT. 76
FIG. 4.40 MODELICA LIBRARY BLOCK REPRESENTING THE COEFFICIENT (AW) OF THE SOLAR RADIATION (PS) 76
FIG. 4.41 SIMULATION SETTINGS FOR RUNNING THE MODEL VALIDATION. 77
FIG. 4.42 EXTRACT OF THE MODELICA TEXT FOR THE CALCULATION OF ERRORS TO TEST THE MODEL IN VALIDATION 78
FIG. 4.43 BEST GREY-BOX MODEL FOR THE SUMMER SEASON BUILT UP IN DYMOLA ENVIRONMENT. 78
FIG. 4.44 RESULTS OF MODEL VALIDATION FOR THE BEST GREY-BOX MODEL OF THE SUMMER SEASON. 79
FIG. 4.45 BEST GREY-BOX MODEL FOR THE WINTER SEASON BUILT UP IN DYMOLA ENVIRONMENT. 80
FIG. 4.46 RESULTS OF MODEL VALIDATION FOR THE BEST GREY-BOX MODEL OF THE WINTER SEASON. 81
FIG. 5.1 PLAN LOCALIZATION AND VISUALIZATION OF THE INDOOR MONITORING SYSTEM. 85
FIG. 5.2 COMFORTSENSE SYSTEM INSTALLED INSIDE THE TEST ROOM 87
FIG. 5.3 A) ORIGINAL CONNECTION, B) SCHEME OF THE BUFFER BOARD AND C) CONNECTION IMPLEMENTED TO CONTROL THE FAN COIL MOTOR. 89
FIG. 5.4 SCREENSHOT OF THE FRONT PANEL OF THE VIRTUAL INSTRUMENT DEVELOPED IN LABVIEW TO MANAGE THE DATAFLOW. 90
FIG. 5.5 RESULTS OF THE PARAMETERS ESTIMATION RUNNING IN R-STUDIO, USING THE CTSM PACKAGE 91

FIG. 5.6 LABVIEW BLOCK DIAGRAM OF THE "MPC CONTROLLER SUBVI", INCLUDING THE "STATE-SPACE MODEL", THE CONSTRAINTS AND THE WEIGHT MATRICES, ALL INPUTS FOR THE MPC CONTROLLER. 92
FIG. 5.7 THE MP LOCAL CONTROL DEVELOPED WITHIN THE MAIN VI OF ACQUISITION IN LABVIEW: PORTIONS OF THE FRONT PANEL AND BLOCK DIAGRAM, SHOWING THE CONNECTION BETWEEN THE MPC SUBVIS. 96
FIG. 5.8 IMPLEMENTATION OF THE EFFECTIVE TIME (TPAR) CORRESPONDING TO THE PREDICTED CONTROL ACTION..... 96
FIG. 5.9 BLOCK DIAGRAM OF THE VIRTUAL INSTRUMENT CREATED IN LABVIEW FOR THE MPC PROTOTYPE. 97
FIG. 5.10 BLOCK DIAGRAM OF THE "WEATHER FORECAST SUBVI" IN LABVIEW. 99
FIG. 5.11 FRONT PANEL AND BLOCK DIAGRAM OF THE "SETPOINT SUBVI" IN LABVIEW. 99
FIG. 5.12 MPC PROTOTYPE INTEGRATED INSIDE THE VI OF DATA ACQUISITION IN LABVIEW: A) THE FRONT PANEL AND B) THE BLOCK DIAGRAM. 100
FIG. 5.13 USER INTERFACE OF THE MPC PROTOTYPE DURING THE EXPERIMENTAL TEST. 101
FIG. 5.14 FROM TOP TO BOTTOM: TRENDS OF THE INTERNAL TEMPERATURE, THE PREDICTED POWER SUPPLY TO THE FAN COIL AND THE SOLAR RADIATION DURING THE TEST PERIOD. 102
FIG. 5.15 THE CROSS CORRELATION OF THE TWO SERIES OF CONTROL ACTION AND SOLAR RADIATION. 103
FIG. 5.16 GLOBAL COMFORT ASSESSMENT: TIME TRENDS OF OPERATIVE TEMPERATURE AGAINST SETPOINT THRESHOLD, SOLAR RADIATION AND CONCOMITANT FAN SPEED. 110
FIG. 5.17 GLOBAL COMFORT ASSESSMENT: HISTOGRAMS OF OCCURRENCES - OPERATIVE TEMPERATURE OFFSET FROM THE SETPOINT. 111
FIG. 5.18 GLOBAL COMFORT ASSESSMENT: HISTOGRAMS OF OCCURRENCES - PMV VALUE..... 111
FIG. 5.19 LOCAL COMFORT ASSESSMENT: TIME TRENDS OF THE DRAUGHT RATE AT 0.1M AND OF THE VERTICAL GRADIENT AGAINST THE RESPECTIVE COMFORT LIMITS AND THE CONCOMITANT FAN SPEED. 113
FIG. 5.20 LOCAL COMFORT ASSESSMENT: HISTOGRAMS OF OCCURRENCES – VERTICAL THERMAL GRADIENTS. 114
FIG. 5.21 LOCAL COMFORT ASSESSMENT: THERMAL DISTRIBUTION OF THE MAXIMUM SURFACE TEMPERATURES ON THE GLAZED FAÇADE. 116
FIG. 5.22 ENERGY ASSESSMENT: HISTOGRAMS OF OCCURRENCES – FAN SPEEDS. 118
FIG. 5.23 ENERGY ASSESSMENT: TIME TRENDS OF THE ENERGY CONSUMPTIONS AGAINST SOLAR RADIATION AND THE SIMULTANEOUS OFFSET FROM THE SETPOINT. 119
FIG. 6.1 THE DETAILED MODEL OF "POLO EUSTACHIO" DEVELOPED IN DYMOLA: THE THIRD FLOOR AND THE PLANT COMPONENTS USED IN THE SIMULATOR. 125
FIG. 6.2 THERMAL ZONES SUBDIVISION FOR THE THIRD FLOOR..... 126
FIG. 6.3 THE THIRD FLOOR BUILT UP IN DYMOLA AND USED AS VIRTUAL REALITY FOR THE SIMULATOR. 127
FIG. 6.4 FANGER MEAN ICON IN DYMOLA: ON THE LEFT, INPUTS TO BE PROVIDED AND, ON THE RIGHT, OUTPUTS RETURNED. .. 127
FIG. 6.5 MODIFYING THE GLAZED COMPONENT TO INTRODUCE THE SOLAR SHADING IN THE DETAILED MODEL. 128
FIG. 6.6 THE MPC FRAMEWORK IN SIMULINK ENVIRONMENT. 129
FIG. 6.7 THE "MODEL ESTIMATOR" BLOCK FOR GENERATING THE STATE SPACE MODEL. 132
FIG. 6.8 THE MASK OF THE "KALMAN FILTER" BLOCK IMPLEMENTED IN THE SIMULATOR. 133

FIG. 6.9 THE MASK OF THE "MPC" BLOCK IMPLEMENTED IN THE SIMULATOR. 135
FIG. 6.10 THE "DATASETGENERATION" IN SIMULINK TO GENERATE DATA FOR THE MODEL IDENTIFICATION. 136
FIG. 6.11 TREND OF THE COOLING POWER DURING THE SELECTED PERIOD. 137
FIG. 6.12 TREND OF THE VENTILATION POWER DURING THE SELECTED PERIOD. 137
FIG. 6.13 TREND OF THE GLOBAL SOLAR RADIATION, ACCORDING TO WEATHER DATA OF YEAR 2016, DOWNLOADED BY "WEATHER UNDERGROUND" WEBSITE. 138
FIG. 6.14 TREND OF THE OUTDOOR TEMPERATURE, ACCORDING TO WEATHER DATA OF YEAR 2016, DOWNLOADED BY "WEATHER UNDERGROUND" WEBSITE. 138
FIG. 6.15 TREND OF THE AIR TEMPERATURE OF THE CORRIDOR, IN FRONT OF THE TEST-ROOM, DERIVED BY THE SIMULATION DURING THE SELECTED PERIOD. 139
FIG. 6.16 TREND OF THE INTERNAL TEMPERATURE OF THE TEST ROOM DURING THE SELECTED PERIOD. 139
FIG. 6.17 THE 3C5R NETWORK OF THE FOURTH GREY-BOX MODEL IDENTIFIED USING THE DATA SET 14-22 JULY. 142
FIG. 6.18 TREND OF THE COOLING POWER DURING THE SELECTED PERIOD. 143
FIG. 6.19 TREND OF THE VENTILATION POWER DURING THE SELECTED PERIOD. 144
FIG. 6.20 TREND OF THE GLOBAL SOLAR RADIATION, ACCORDING TO WEATHER DATA OF YEAR 2016, DOWNLOADED BY "WEATHER UNDERGROUND" WEBSITE. 144
FIG. 6.21 TREND OF THE OUTDOOR TEMPERATURE, ACCORDING TO WEATHER DATA OF YEAR 2016, DOWNLOADED BY "WEATHER UNDERGROUND" WEBSITE. 145
FIG. 6.22 TREND OF THE AIR TEMPERATURE OF THE CORRIDOR, IN FRONT OF THE TEST-ROOM, DERIVED BY THE SIMULATION DURING THE SELECTED PERIOD. 145
FIG. 6.23 TREND OF THE INTERNAL TEMPERATURE OF THE TEST ROOM DURING THE SELECTED PERIOD. 146
FIG. 6.24 THE 2C2R NETWORK OF THE FIRST GREY-BOX MODEL IDENTIFIED USING THE DATA SET 11-24 JULY. 147
FIG. 6.25 RESULTS OF MODEL VALIDATION FOR THE FIRST GREY-BOX MODEL TESTED. 148
FIG. 6.26 THE 2C2R NETWORK OF THE SECOND GREY-BOX MODEL IDENTIFIED USING THE DATA SET 14-22 JULY. 148
FIG. 6.27 RESULTS OF MODEL VALIDATION FOR THE SECOND GREY-BOX MODEL TESTED. 149
FIG. 6.28 THE 2C2R NETWORK OF THE THIRD GREY-BOX MODEL IDENTIFIED USING THE DATA SET 14-22 JULY. 150
FIG. 6.29 RESULTS OF MODEL VALIDATION FOR THE THIRD GREY-BOX MODEL TESTED. 151
FIG. 6.30 RESULTS OF MODEL VALIDATION FOR THE FOURTH GREY-BOX MODEL TESTED. 152
FIG. 6.31 SIMULATION RESULTS OF THE MPC SIMULATOR OPERATING DURING ONE MONTH OF THE COOLING SEASON, WITHOUT SOLAR SHADING MANAGEMENT. 155
FIG. 6.32 SIMULATION RESULTS OF THE MPC SIMULATOR OPERATING DURING ONE MONTH OF THE COOLING SEASON, WITH SOLAR SHADING MANAGEMENT. 156
FIG. 6.33 TOTAL ENERGY ABSORBED BY THE PLANT IN THE SIMULATION PERIOD FOR EACH PREDICTION TIME. 157
FIG. 6.34 COMFORT ASSESSMENT: HISTOGRAMS OF OCCURRENCES - PMV VALUE. 157
FIG. 6.35 COMFORT ASSESSMENT: FREQUENCY DISTRIBUTION - PMV VALUE. 158
FIG. 6.36 TOTAL ENERGY ABSORBED BY THE PLANT IN THE SIMULATION PERIOD FOR EACH HORIZON TESTED. 160

FIG. 6.37 COMFORT ASSESSMENT: FREQUENCY DISTRIBUTION - PMV VALUE..... 162
FIG. 6.38 COMFORT ASSESSMENT: FREQUENCY DISTRIBUTION - PMV VALUE..... 162
FIG. 6.39 SIMULATION RESULTS OF THE MPC SIMULATOR OPERATING DURING ONE MONTH OF THE COOLING SEASON, WITH ADAPTIVE MODELLING..... 163
FIG. 6.40 SIMULATION RESULTS OF THE MODEL PARAMETERS ESTIMATED BY THE "MODEL ESTIMATOR", WHILE THE MPC SIMULATOR WAS WORKING..... 164

List of Tables

TABLE 4.1: DESCRIPTION OF LUMPED PHYSICAL PARAMETERS AND RELATIVE UNITS. 41
TABLE 4.2: PARAMETER ESTIMATION IN CTSM-R FOR THE BEST 2ND REDUCED-ORDER MODEL. 43
TABLE 4.3: PARAMETER ESTIMATION IN CTSM-R FOR THE BEST 2ND REDUCED-ORDER MODEL WITH FIXED KA. 43
TABLE 4.4: TEMPERATURES FROM DATA ACQUISITION USED FOR THE MODELLING PROCEDURE 52
TABLE 4.5: VARIABLES CONSIDERED IN THE DATA SET OF THE SUMMER CAMPAIGN. 54
TABLE 4.6: VARIABLES CONSIDERED IN THE DATA SET OF THE WINTER CAMPAIGN. 59
TABLE 4.7: RESULTS OF THE PARAMETERS ESTIMATION FOR THE BEST MODEL OF THE SUMMER SEASON. 66
TABLE 4.8: CUMULATED PERIODOGRAM AND RMSE VALUES FOR THE BEST MODEL OF THE SUMMER SEASON. 67
TABLE 4.9: CUMULATED PERIODOGRAMS AND RMSE VALUES IN SIMULATION FOR THE OTHER TESTED MODEL OF THE SUMMER SEASON. 67
TABLE 4.10: RESULTS OF THE PARAMETERS ESTIMATION FOR THE BEST MODEL OF THE WINTER SEASON. 69
TABLE 4.11: CUMULATED PERIODOGRAM AND RMSE VALUES FOR THE BEST MODEL OF THE WINTER SEASON. 70
TABLE 4.12: CUMULATED PERIODOGRAMS AND RMSE VALUES IN SIMULATION FOR THE OTHER TESTED MODEL OF THE WINTER SEASON 71
TABLE 5.1: MEASUREMENTS USED TO BUILD UP THE MODEL FOR THE CONTROLLER AND RUN THE PREDICTIVE CONTROL. 87
TABLE 5.2: REPRESENTATIVE DAYS: AVERAGE WEATHER CONDITIONS 104
TABLE 5.3: STANDARD COMFORT CATEGORIES. 107
TABLE 6.1: RESULTS OF THE PARAMETERS ESTIMATION FOR THE FIRST GREY-BOX MODEL TESTED. 140
TABLE 6.2: RESULTS OF THE PARAMETERS ESTIMATION FOR THE SECOND GREY-BOX MODEL, IDENTIFIED USING THE "FMINCON" ALGORITHM OF MATLAB. 140
TABLE 6.3: RESULTS OF THE PARAMETERS ESTIMATION FOR THE THIRD GREY-MODEL, IDENTIFIED USING THE MLE OF CTSM-R. 141
TABLE 6.4: RESULTS OF THE PARAMETERS ESTIMATION FOR THE FOURTH GREY-BOX MODEL TESTED, THE 3C5R NETWORK 142
TABLE 6.5: RMSE VALUES IN SIMULATION OF THE GREY-BOX MODELS TESTED. 143
TABLE 6.6: RMSE VALUES IN SIMULATION OF THE GREY-BOX MODELS VALIDATED. 152
TABLE 6.7: RMSE VALUES OBTAINED SIMULATING THE MPC DURING THE TUNING OF NP 157
TABLE 6.8: RMSE VALUES OBTAINED SIMULATING THE MPC DURING THE TUNING OF NC 159

List of Equations

Eq. (2.1): First order network 11
Eq. (2.2)-(2.3): two-time constant model 14
Eq. (2.4): discret time measurement equation 16
Eq. (3.1)-(3.2)-(3.3)-(3.4)-(3.5): MPC optimisation problem 29
Eq. (3.6): energy cost function 30
Eq. (3.7)-(3.8)-(3.9): MPC constraints 31
Eq. (3.10)-(3.11): discrete state space form 31
Eq. (3.12): MPC-horizons 31
Eq. (3.13): MPC-cost function 32
Eq. (4.1)-(4.2): state space representation 39
Eq. (4.3): first-order model 40
Eq. (4.4)-(4.5): second-order model 40
Eq. (4.6)-(4.7)-(4.8): third-order model 40
Eq. (4.9): output measurement equation 41
Eq. (4.10): stochastic differential equation with “K” coefficient 42
Eq. (4.11)-(4.12): best grey-box model for summer season 66
Eq. (4.13)-(4.14): best grey-box model for winter season 69
Eq. (4.15): discrete time measurement equation 69
Eq. (4.16): root mean square error 77
Eq. (5.1): differential stochastic equations in matrix form 91
Eq. (5.2): state space representation in compact form 91
Eq. (5.3): MPC-cost function (J) 93
Eq. (5.4): MPC-linear constraint 94
Eq. (6.1): heat flow transmitted through window 130
Eq. (6.2): coefficient of attenuation for solar radiation 131
Eq. (6.3)-(6.4): discrete-time equations of Kalman filter 132
Eq. (6.5)-(6.6)-(6.7)-(6.8): process noise and white measurement noise 133
Eq. (6.9)-(6.10): general problem (GP) 134
Eq. (6.11)-(6.12): MPC simulator-constraints 134
Eq. (6.13): MPC simulator-cost function 134

Chapter 1

Introduction to the thesis

1.1 Introduction

This chapter provides an introduction to this thesis as a fulfilment for the title of Doctor by the Università Politecnica delle Marche. Relating to the field of building performance management, it states the problem, outlines the main aims and objectives of the research project and sets out the scope of the work, its limitations and delimitations. An overview of the methodology implemented, as well as a description of the structure of this dissertation, are also included.

1.2 Problem statement

Strategies to manage the energy and needs of buildings are becoming increasingly necessary. In fact, buildings are one of the major responsible for energy use, accounting for up to 40% of overall energy consumption, and consequently play a relevant role in global warming, accounting for about 36% of CO_2 emissions (Carrascal et al., 2016).

Energy efficiency has become one of the main policy goals in the European Union and its objective of 20% reduction on primary energy consumption was identified in the Commission's Communication on Energy 2020 as a key step towards achieving our long-term energy and climate goals, the EU energy targets for 2030, which are:

- 40% cut in greenhouse gas emissions compared to 1990 levels;
- at least a 27% share of renewable energy consumption;
- at least 27% energy savings compared with the business-as-usual scenario (Bertoldi et al., 2016).

Between 1990 and 2015, economic sectors showed different final energy consumption trends, mainly related to structural changes in the EU economy, i.e. the transition from an energy-intensive industry to a service-based economy. In 2015, the majority of final energy was used in transport with a 33.2 % share, followed by industry and the residential sector with shares of 25.3 % each. The services sector was responsible for 13.6 % and agriculture and forestry for 2.2 % of final energy consumption.

Although some enhancements have been done in terms of reduction of energy consumption, substantial potential for cost-efficient improvements in energy efficiency was not exploited. There is, for example, specific scope for savings in transport, building refurbishment, industrial processes and along the energy supply chain ("Europe 2020 indicators - climate change and energy - Statistics Explained," n.d.).

The strategy pursued by US and EU for energy saving in building includes both high-performance new construction and retrofitting old ones. Developed countries have been devoted in energy saving buildings for more years. These countries earned many valuable experiences in energy efficient buildings. However, it is evident that stricter regulations especially in existing buildings need to be further stressed by focusing on both new technology development and more educationally-related approaches to energy savings (Berardi, 2015).

It is also stated that strategies involving enhancement of building components or introduction of high-performance insulating materials can be considered passive improvements of new buildings or in the rehabilitation of the old ones. The development of a control to improve the energy efficiency in the use of the climate control systems within the required comfort parameters can be considered an active improvement (Carrascal et al., 2016).

Especially in existing buildings, during the operational phase, a substantial amount of energy is spent for conditioning of spaces (HVAC systems). In larger buildings, like office buildings, Building Energy Management Systems (BEMS) are usually designated to guarantee energy saving. Careful design of BEMS along with a good energy concept can yield effective and harmonious energy usage while achieving good thermal comfort conditions for the building occupants (Kontes et al., 2014).

In this regard, in last years, many research groups have focused their attention on building climate control and related savings, proposing the Model Predictive Control (MPC) techniques is a good solution for an effective BEMS design. In fact, several recent studies have shown that MPC, which has already been widely implemented in the industry sector, has proved to be a promising advanced control strategy also for buildings, because it is able to minimise energy consumption without compromising comfort and services. The MPC approach for thermal control outperformed PID controllers, showing a total system improvement through the reduction of thermal discomfort (Hazyuk et al., 2014). Besides, by exploiting MPC for system optimisation, it is possible to introduce occupancy schedules and weather forecasts into optimal temperature control. However, one major reason for a slow application of MPC in this field was the initial difficulty in obtaining a building model suitable for being included in the MPC controller and the related costs. In the last decades, experimental applications have increased significantly, due to the powerful improvement in computational technology, as well as to the wider use of simulation tools and the better quality of

weather predictions. Moreover, the rise in energy consumption/costs has highlighted the extreme urgency of efficiency improvement in building climate control to reduce peak electricity demand, while avoiding discomforts for users (Oldewurtel et al., 2012). The design of a model predictive control goes through the completion of specific steps for the MPC controller to solve the optimisation problem. First of all, with regard to the inputs of the MPC controller, it is required to specify time-varying parameters, such as energy price and comfort criteria as well as weather forecasts and occupancy schedules. It is then necessary to choose the cost function and define control constraints so as to achieve the desired building behaviour. All these components must be integrated into the controller, which, so far, has been developed mainly in virtual and simulation environments. On the contrary, to the best of the authors' knowledge, few experimental analyses aimed at assessing the technological feasibility of the technique have been provided (Široký et al., 2011). In this regard, the prototype implementations of MPC clearly demonstrated the high potential of a theoretically well-developed method, but only very few experts in the field know how to set up and commission such a control system successfully (Killian and Kozek, 2016). Another issue is the inference of an adequate dynamic building model for the controller. This last point is particularly tricky and requires considerable design effort, especially with regard to existing buildings, which are often affected by a significant lack of information. Finally, the integration of design, support and control optimisation tools into the building system needs to be promoted, as investigated in (Yuan et al., 2016). About this last point, the fact that MPC is not a proliferated technology implies the need for portable software components that can be easily adjusted to a given target building, and that allow for the flexible and safe experimentation with the underlying optimization task (Jirı Cigler et al., 2013).

1.3 Aim and objectives

According to what has been stated in the Problem statement section, the aim of this dissertation arises from the observation of the most common obstacles encountered in the application of the MPC strategy, which are mainly due to three issues inferred from the analysis of the relevant research works.

In order to provide an answer to the issues highlighted, the research conducted in this thesis, focuses on the development of a model-based, predictive control in a real case, an existing building of high complexity.

Hence, the main objectives of this research work are:

1. the identification of a suitable building model for the controller, which contributes to the quality of the control algorithm, reducing the computational effort of the controller, while ensuring a reasonable level of reliability;

2. the development of a real-time application in an existing building, as to demonstrate the high potential of the theoretically, well-developed MPC method and for supporting similar application in real cases;
3. the definition of the technological implementation pursued to support the proliferation of this advanced control strategy, by simplifying the design and implementing process.

1.4 Overview of the research methodology

The research methodology directs the course of activities to be undertaken during the research. To achieve the research aim and objectives, the activities are planned as illustrated in Figure 1.1.

1.5 Outcomes and limitations

The development of a prototype of model-based, predictive control, in a real existing building is the main outcome of this dissertation.
Obviously, this outcome is strictly connected to those equally relevant to the other two objectives, previously presented in par. 1.3. The first goal has been achieved by the adoption of reduced-order models, in particular grey-box models, to feed the controller. The last outcome concerns the technological implementation (hardware and software) of the MPC application, which is easily reproducible and expandable, and it can rely on a graphical, user-friendly interface.

However, some issues are still open and require further investigations. In this direction, further large-scale projects are necessary to extend the local procedure, providing for an integration with the central plant and automating the restitution of some variables input for the controller. Another issue, which is connected to the implementation of the MPC, concerns the model for the controller which requires a systematic identification during the operation of the control. Really, this aspect has been partly debated at the end of this dissertation by exploiting the MPC simulator. Anyway, a more in-depth analysis is necessary, also in technological field, to get a real “plug and play” application. Besides, in order to achieve a comprehensive automatic management of the building, the advanced control of the HVAC system should be integrated with the other services of the building. This could include also services, actually not present, to be provided for building retrofitting, following the line of investigation already undertaken, within the MPC simulator, with the introduction of the solar shading.

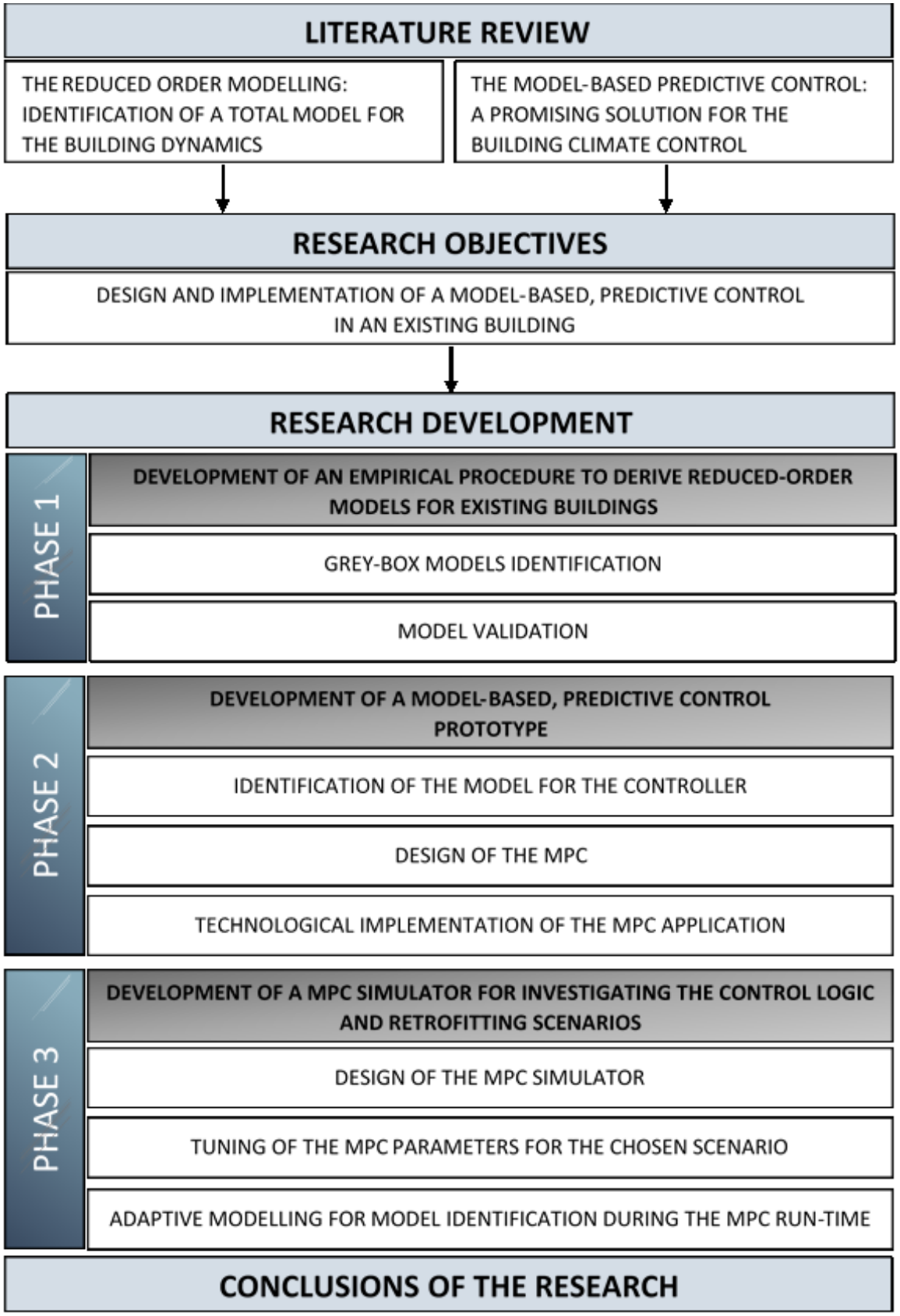

Fig. 1.1 Overview of the research methodology.

1.6 Thesis structure

This thesis describes the research undertaken as a fulfilment for the title of Doctor by the Università Politecnica delle Marche. It is structured as follows:

Chapter 1 provides an introduction to this thesis, presenting the problem statement, the main aim and objectives of the research and sets out the scope of the work and its limitations. The overview of the methodology implemented, as well as the description of the structure of this dissertation are also included.

Chapter 2 presents in the first part an overview on the state of the art about reduced order modelling related to buildings thermal dynamics. The second part is devoted to a particular type of Reduced-Order Models, the Grey-box models, highlighting the relevant contributions made to the development of this dissertation.

Chapter 3 presents a critical literature review of the existing knowledge on Model Predictive Control (MPC) with particular regard to building applications. This chapter focuses on those research projects that have demonstrated the MPC potential in providing substantial energy savings and improving indoor comfort, as compared to traditional control approaches. The results obtained in this chapter, together with the literature review in Chapter 2, serve as justification of the research undertaken within this thesis.

Chapter 4 and 5 detail the work undertaken to meet the research project's aim and objectives. Both chapters are aimed at the development of a model-based predictive control to support building energy management systems. Chapter 4 presents the leading case study and it is aimed at developing an experimental approach to establish an effective procedure for the identification of reduced-order models, in particular for existing buildings. Chapter 5 focuses on the development of a prototype of Model Predictive Control (MPC) that is presented together with a detailed description of its main components. The last part of the chapter is aimed to provide the results of the experimental test carried out inside the case study.

Chapter 6 is connected to Chapter 5 and it presents the development of the same model-based predictive control in simulation environment. This chapter is aimed at completely investigating the potentiality of the MPC application experimentally developed and offering suggestions for renovations scenarios and further applications.

Chapter 7 concludes with the summary of the key findings of the research and sets out how the project contributes to knowledge and practice, and presents areas suitable for further research.

Appendices A to I include additional supporting material as evidence of research undertaking.

Chapter 2

State of the art on Reduced Order Models for buildings

2.1 Introduction

Several research groups have been basing their work on modelling of the building heat dynamics for the development of management control strategies. Therefore, several different approaches have been described and many different methods for the dynamic analysis of energy use in buildings have been developed. In literature, the problem of deriving a suitable reduced model is solved referring to three different approaches. The first one is the so-called white box modelling, a detailed physical modelling in which the system is decomposed into elementary components problem of which are known the mathematical model and the value of parameters involved. Nevertheless, despite of theoretical precision of this modelling, the inaccuracy of control strategies relying on these detailed models represents a clear weakness, since the real building parameters are often unknown in existing buildings (Reynders et al., 2014). The second approach is the black-box modelling, a reducible model in which are unknown the equation of the system, so are the basic principles that govern the phenomenon. These relations are found using only measured inputs, measured output and statistical relations, but the parameters of the system have only mathematical significance and the model risks to be suitable only for a single case-study. The third way is represented by grey-box modelling, a compromise between the two previous methods; in this case physical principles are partially known and parameter were estimated with statistical relations. Furthermore, it is possible to obtain models with a limited set of data collected and estimated parameters have physical significance.

Thus, this chapter provides an overview of the relevant research that has been conducted within the area of reduced order modelling focusing on those approaches related to the identification of a total model for the building heat dynamics. First, reduced order modelling is analysed, describing the versatility of ROMs in building applications and underlying its increasing role in the perspective of real-time control of complex buildings. Then, different methods of using reduced modelling for the

thermal building simulation, are described. All the studies presented, from the oldest works to the newest researches, have a common matrix based on the simplification of the building heat dynamics with a thermal network, exploiting the analogy with the electric circuit. Finally, the Grey-box models are investigated in their contribution to the growth of the experimental approach of this dissertation.

2.2 Reduced Order Modelling

Reduced order modelling showed its reliability and usefulness for simulations, advanced controls, real-time predictions and, recently, it is widely used to improve energy management strategies. Nevertheless, this approach can be applied in many other fields in construction. In this regard, a real-time estimation of the occupancy in a large building is a challenging problem, due to the high uncertain nature of occupancy dynamics. In (Liao and Barooah, 2010) the authors propose an integrated approach to model and estimate the occupancy. Their strategy is based on two-level modelling: the development of an agent-based model to simulate the behaviour of all the occupants of a building (validated with sensor data), and the extraction of reduced-order graphical models from Monte-Carlo simulations of the agent-based model. A reduced-order graphical model identifies correlations among room-level occupancy, also predicting occupancy in locations without sensors based on measured data in other locations. Another two-tier approach to detect performance regards the actuator fault detection and diagnostics (FDD) in heating, ventilation and air conditioning (HVAC) systems (Weimer et al., 2012). This method includes a dynamic model-based detector and a fast deciding steady-state detector for testing whether an actuator is stuck in a single position. The quantitative model-based approach, referred to the model-based detector, does not require the full model knowledge; in fact, a simplified thermodynamic model represents it sufficiently. This approach is correlated to a qualitative one, referred to the steady-state detector, which makes a decision whether the actuator is working and utilises logical relations. In (Kim et al., 2003) a methodology is presented to non-destructively locate and estimate the size of damage in structures, for which two frequencies and/or mode shapes are available. Two methods are outlined: a frequency-based damage detection (FBDD) method and a mode-shape-based damage detection (MBDD) method. The first one is based on a damage-localization algorithm that locates damage from changes in natural frequencies and on a damage-sizing algorithm, which estimates crack-size from natural frequency perturbation. The MBDD method, instead, is based on a damage-index algorithm that locates and estimates severity of damage from changes in modal strain energy. By applying the two approaches to the test structure, damage has been located with a small localization error and the sizes of the cracks have been accurately estimated.

Finally, dealing with the predictive control, it is necessary a forecasting model of the building that requires to be controlled. For this use in the MPC, an important requirement of the dynamic model is the simplicity to overcome the too slow times of prediction that characterize the detailed models with large state spaces (Goyal and Barooah, 2012). Therefore, reduced models can predict long-term energy performance with short-term operation data monitoring (Wang and Xu, 2006). The MPC, recently developed also for buildings, employs a reduced-order model of the building dynamics and solves an optimization problem to determine the optimal control inputs. In terms of building climate control, this means that at the current point in time, a heating/cooling plant is formulated for next several hours to days, based on predictions of the upcoming weather conditions and of any other disturbances, e.g. internal gains, dynamic electricity prices, thermal comfort range, etc. (Oldewurtel et al., 2012). In conclusion, reduced order modelling represents a promising tool to manage buildings, accelerating energy audit processes and facility management. Thus, in the next paragraphs the development of the empirical procedure behind this approach will be investigated.

2.3 Early works

First thermal models date back to 1988 when, in its review, Rabl underlines the requirement of a simple building model, for a dynamic analysis of energy data, whose parameters can readily be adjusted by a statistical fit to the data. Thermal networks offer the simplest approach because the building is approximated by a simple network with a few resistances and capacitances (Rabl, 1988). A dynamic model must contain at least one resistance and one capacitance, which resides in the internal air, but it's almost an unrealistic condition. Therefore, one can adjust this narrow approximation by adding one or more resistances and capacitances. Some examples of simple thermal networks are showed in Fig. 2.1.

It is important to realize that for a successful dynamic simulation one may have to choose numerical values of the resistances and capacitances that are quite different from the static properties of the components; therefore, the parameters in these simple networks must be interpreted as equivalent thermal parameters. To use a thermal network for calculations, one writes down the differential equations that describe the energy balance at each node. For example, for the first order network (1R1C), the equation is (2.1):

$$Q = \frac{\left(T_{\text{int}} - T_{ext}\right)}{R} + C\frac{dT_{\text{int}}}{dt} \tag{2.1}$$

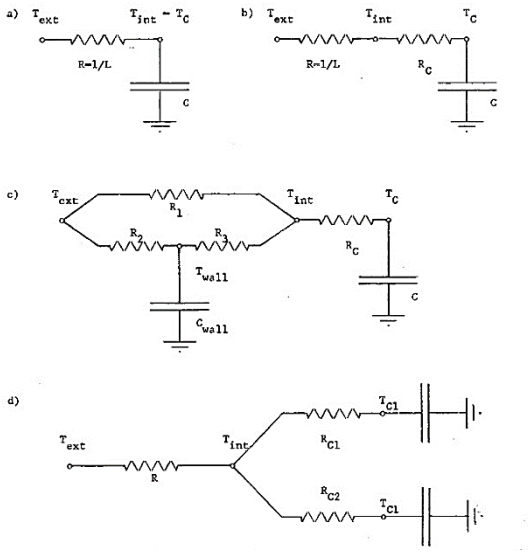

Fig. 2.1 Examples of simple thermal networks (Source: Rabl, 1988)

After choosing a model, the identification process requires to determine the coefficients of the model by fitting the data. For data fitting, one can use the finite difference approximation or an integrated version. Rabl (Rabl, 1988) underlines the power of the differential equations, which can be integrated analytically, but at the same time, he points out that the process of casting suitable differential equations for data fitting is quite laborious. One year later, Mathews and Richards (Mathews and Richards, 1989) described a thermal design tool to predict dynamic air temperatures in naturally ventilated buildings and dynamic sensible heating and cooling energy loads in conditioned buildings. Their simplified method was validated in some different types of real buildings, comparing the temperature measurements with the computer predictions. The proposed tool models the thermal interactions in a building by an extremely simplified thermal network of a building zone. The thermal network is shown in Fig. 2.2 and some thermal properties can be identified: the time-dependent inputs, which are the radiative heat source $Q_r(t)$, the sol-air temperature $T_{sa}(t)$, the convective heat source $Q_c(t)$, and the outdoor air temperature $T_o(t)$.

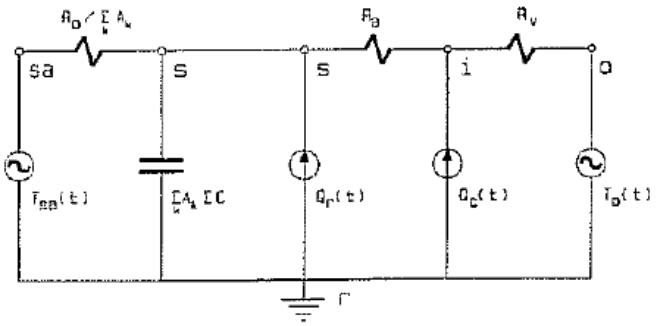

Fig. 2.2 Thermal network of a building zone (Source: Mathews and Richards, 1989)

There are three resistances in the network, namely R_o, R_v and R_a. The first is the resistance calculated from the sol-air node through the shell to the indoor surfaces in terms of the shell area $\sum_k A_k$. R_v is the ventilation resistance, given by $3,6/(Vol*\rho*ach*c_p)$, where Vol is the internal volume of the zone, ρ the air density, ach is the air change rate per hour, c_p is the specific heat and R_a is the resistance between the indoor air and the interior surfaces. A_k denotes the area of each exposed building element k. The capacitor $(\sum C)$ in the network represents the active thermal capacity of the building zone and it's expressed per unit shell area $\sum_k A_k$ (Mathews and Richards, 1989). It's defined active because it is the effective part of the building zone that stores heat; it consists of an internal mass, an exposed shell and a floor component. Only this active part is calculated for the indoor environment, taking into account the relative position and thermal properties of mass and insulation as the fact that different temperatures exist across a building element. The solution of the Mathews' network, that is the required unknown variable, the indoor air temperature $T_i(t)$, can be obtained by the convolution of the forcing temperatures and heat source inputs with relevant impulse responses of the network. Finally, the proposed simulation model was validated by comparing temperature predictions with measured values for 42 cases in 8 different types of buildings. An acceptable level of confidence was achieved. However, the modelling of infiltrations and ventilation flow rates was proved to be the most significant source of error in thermal simulation, suggesting a statistical approach instead of a deterministic one.

2.4 A model for the thermal dynamics of buildings

A significant contribution to this dissertation is provided by the activity of Henrik Madsen and his research group in Denmark that produced several works about the modelling of buildings' heat dynamics. The first work analysed, dating back to 1993, is the final report of a research project about "Short time investigation of heat consumption of houses". In this report (Madsen and Schultz, 2003), they describe a tool to identify the characteristic thermal parameters, such as heat loss coefficient and heat accumulation; the aim is to find a statistical method to develop models for an accurate determination of the heat consumption and heat capacity of buildings within a reasonable short time of data collection (16 days in this case). The proposed method is based on the estimation in continuous time of linear differential equations, which are generated from a lumped parameter model of the building. The experimental work was performed in the Passys test cell, which was chosen for the simple geometry and the high level of insulation. The heating system in the test room consisted of four 75 W electric bulbs and three 500 W electric heaters. For controlling the heat input of the system, it was used a PRSBS-signal, consisting in two different signals designed for each of the expected time constants of the test cell: a short time related to the heat capacity of the indoor air, and

a long-time constant related to the walls, floor and ceiling. At these signals, a sampling time of 5 minutes and 1 hour corresponded, respectively. The lumped model describing the test cell is a second order model with two capacitances and two resistances (Fig. 2.3).

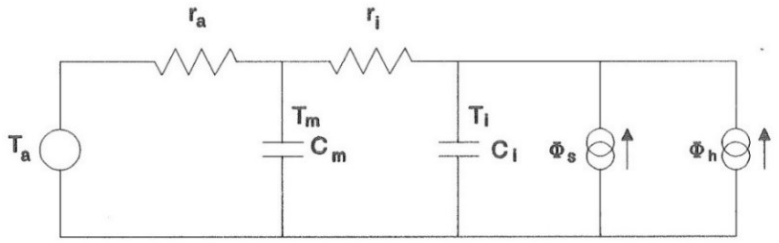

Fig. 2.3 The "two-time constant" model (Source: Madsen et al., 1993)

The identification of the four thermal parameters was carried out by comparison of the measured indoor air temperature and the indoor air temperature calculated by the model, supplying as input the measured climatic data and the heat input. The differential equations of the system are (2.2-2.3):

$$c_m \frac{dT_m}{dt} = \frac{1}{r_a}(T_a - T_m) + \frac{1}{r_i}(T_i - T_m) \tag{2.2}$$

$$c_i \frac{dT_i}{dt} = \frac{1}{r_i}(T_m - T_i) + \Phi_s + \Phi_h \tag{2.3}$$

The maximum likelihood estimation is the crucial part of this identification method to obtain the estimates of parameters from the system of linear stochastic differential equations. Based on the estimates of this iterative process, it is possible to estimate the performance of the model for forecasting the indoor air temperature. The standard error in the case of a horizon of 5 minutes was 0.024 °C, and it was 0.079 °C for the horizon of one hour. The largest differences between the observed and the predicted temperature, were evident just after the heating system was turned off or on. This reveals that the dynamic of the heating system need to be included in the model. Except for this aspect, an analysis of the residuals demonstrates that the model is able to describe all the dynamics variations (Madsen and Schultz, 2003). Madsen's studies, to derive a total model for the heat dynamics of a building, continued in the following years, supported by other experimental campaigns on test cells or test buildings. The papers published, after 1993 until 2011, retain the same continuous time modelling procedure, based on a statistical approach with a stochastic framework, against a traditional approach closed in a deterministic framework. The attention was focused on identifying a suitable model of a building by adopting selection strategies, namely likelihood-ratio testing.

2.5 Identification procedure of suitable ROMs

Most recent Madsen's experiments were carried out in the Flex House at RisØDTU in Denmark during winter in 2009. The building, which is a one only storey of 120 m^2, is a part of the experimental distributed energy system, Syslab. The objective of the experiments was to provide data for models of the thermal dynamics of the building. Five experiments were carried out, two with PRBS signals controlling the heaters, and three with thermostatic control. Tests followed a line from controlled conditions toward normal living conditions, providing the possibility to study model results under relevant variation of conditions (Bacher and Madsen, 2010). The following year (Bacher and Madsen, 2011), the authors described the identification procedure of suitable models for heat dynamics, using data from the "Flex House", their case of study. The procedure (Fig. 2.4) was based on likelihood-ratio testing combined with a forward selection strategy.

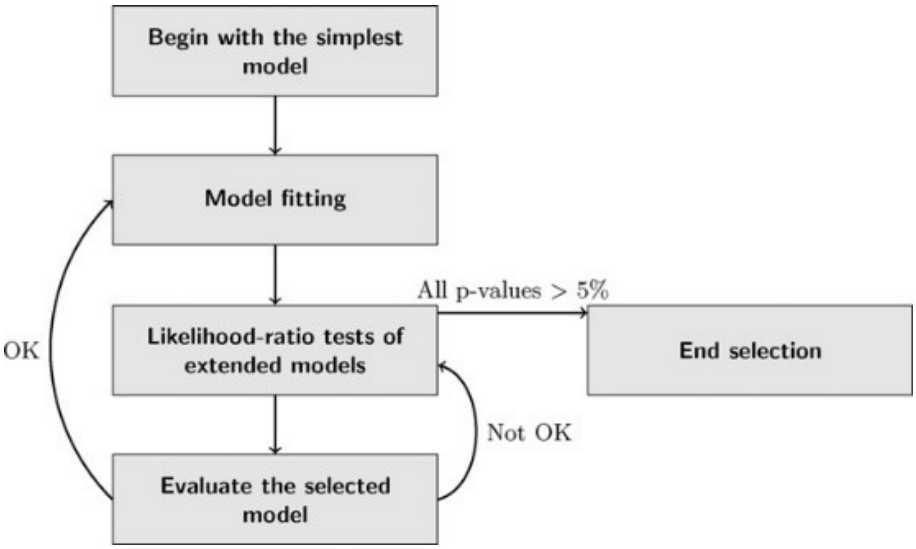

Fig. 2.4 Model selection procedure (Source: Bacher and Madsen, 2011)

The model validation required a combination of appropriate statistics and physical interpretation of the results, which came out from the iterative process of identification. The most suitable model was identified from a set of models of increasing complexity, beginning from the simplest model. The suitable model (Fig. 2.5) was the smallest model that describes all information embedded in the data (Bacher and Madsen, 2011).

The proposed models are defined grey-box models because they are a combination of prior physical knowledge and data-driven modelling. The physical knowledge is formulated by a set of first-order stochastic differential equations, which define a lumped parameter model of the heat dynamics of the building.

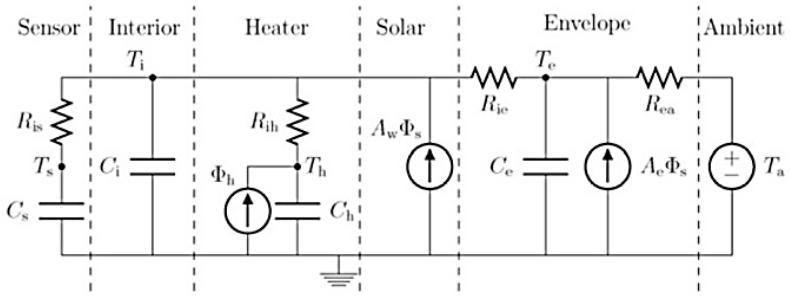

Fig. 2.5 The final selected reduced-order model (Source: Bacher and Madsen, 2011)

The physical interpretation of the parameters is dependent on how the building is divided into entities in the model. The data-driven part is represented by the discrete time measurement equation (2.4):

$$Y_k = T_{ik} + e_k \tag{2.4}$$

where k is the point in time t_k of a measurement, Y_k is the measured interior temperature and e_k is the measurement error, which is assumed to be a Gaussian white noise process with variance σ^2. The inputs used for modelling are the following data: climate data, measured at the location; measurements of the indoor temperature and a PRBS controlled heat input. The evaluation of results reveals that the selected model meets the assumptions of white noise residuals, therefore this identification procedure can be applied to give reliable estimates consistent with reality and the results are statistically validated.

2.6 Grey-box models

The last work analysed is dating back to 2014 and it represents both the summary of the system identification to identify suitable reduced order models, both the starting point of this dissertation. Firstly, in (Reynders et al., 2014), the usefulness of grey-box models, for day-ahead predictions and simulations of the thermal response of a dwelling, was described. In fact, active control of indoor temperature of buildings requires advanced control strategies, as model predictive control (MPC), in order to activate buildings thermal mass as a thermal storage capacity. However, an efficient application of MPC, demands for reduced-order models to predict the future heat demand of the building with minimal computational effort. Thus, reduced-order models represented by grey-box models are strongly suggested. Grey-box models are the best choice because they are relied on the physical knowledge about system dynamics to define the model structure, but they overcome white-box models using statistical methods, typical of the black-box models, to estimate the unknown parameters. In fact, especially dealing with existing buildings, data-driven system identification methods are required to estimate unknown thermal properties, meanwhile the relation with the

physical behaviour of the system avoids considering inconsistent results, coming from black-box models. In (Reynders et al., 2014), data used for the identification process were obtained from detailed simulations using the white-box models of two detached single-family dwellings. The use of a detailed physical model to generate a data-set facilitates virtual measurements of all temperatures and heat flows that occur in the model. These virtual measurements were used to select a minimal data-set necessary to obtain a robust grey-box model. The grey-box model structures derived from resistance-capacitance networks analogue to electric circuits, as just seen for previous works (Fig. 2.6). The ambient air temperature, the heat emitted by the radiators, the effective internal and solar gains were used as inputs for both models. Finally, the small differences in model structure observed in the two investigated dwelling models indicated that only few model types are enough to represent most of buildings.

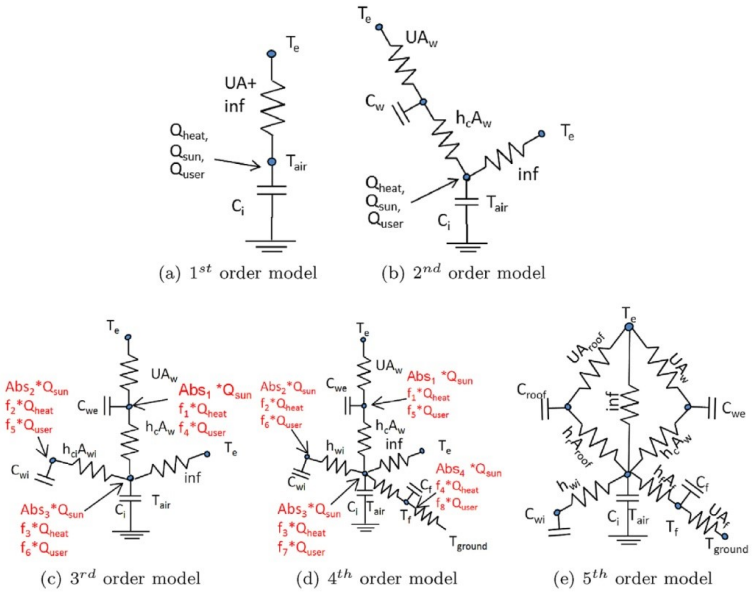

Fig. 2.6 RC-analogy of reduced order building models (Source: Reynders et al., 2014)

At the end, unbiased random distributed noise (white noise) was added on both the observation measurements and the inputs signals. Its influence represents measurement inaccuracies using calibrated sensors. In addition, the biased random distributed noise (coloured noise) was introduced on for the observation measurements to quantify the influence of inaccurate sensor placement on the estimated parameters. The resulting effect was an increase of the uncertainty level of the estimated values for both the noises with some difference. The introduction of white noise did not change significantly the estimated physical properties; this fact demonstrates that small measurement noise could be handled using grey-box modelling. However, to not affect the estimated parameters, sensor bias due to inaccurate placement or experiment design should be avoided.

2.7 Implication of the results

Literature about reduced-order models of buildings, of which most relevant works were reported in previous paragraphs, suggests the importance of an accurate building thermal modelling to implement any energy control strategy (Zhou et al., 2008). In this regard, system modelling and identification techniques have been extensively developed on a theoretical base, though their application in real buildings is trickier mainly due to the number of states, the nonlinearities and the lack of information in the models. Yet, advanced control applications require a dynamical model of the system that is preferably to be a low-linear model. In fact, a low-order thermal modelling can reduce the computational effort and expedite the completion of the computer-based optimisation (Ramallo-González et al., 2013), thus it is suitable for model-based HVAC control techniques, such as Model Predictive Control (Goyal and Barooah, 2012). For this purpose, ROMs represented by Grey-box models are the best compromise to obtain a robust model, unifying the physical system knowledge inside their structure of lumped-parameter model with black-box identification methods to establish the model parameters.

Yet, literature mainly reports case studies created ad hoc to obtain such reduced models (Andersen et al., 2000; Bacher and Madsen, 2011; Jiménez and Madsen, 2008), or the use of detailed models to derive simulated data on which identify Reduced-Order Models (Hazyuk et al., 2012; Reynders et al., 2014), threatening the need to simplify the modelling part in building control processes.

Although on the market there are dedicated software tools to simulate building thermal behaviour that produce detailed models clearly linked to system physics, these models are too complex and of high order to be suitable for the use in the development of control algorithms.

On the other hand, generating the reduced model from the simulated data provided by the detailed model of the same building allows to set special conditions to have data records variations, like pseudo-random binary sequence (PRBS) for the heat input (Madsen and Schultz, 2003). In fact, to obtain a good quality model the input signals must have a large spectrum to excite the system modes and the output signal must have enough variations to observe them (Hazyuk et al., 2012).

However, the experimental identification of the model parameters demands for input/output data acquired in the real building. In this regard, contrary to the previous statement for detailed models, in inhabited buildings the range of variation for the input data, as the heat flux, is very limited because it must compare with thermal comfort norms expected for the tested environments. Besides, other two problems with inhabited buildings are: the costs of testing, which often result prohibitive and the presence of unexpected heat sources of disturbance (e.g. free gains from occupants, electrical equipment), which affect the indoor temperature and, consequently, the quality of the simplified model. Therefore, the adoption of input data for the identification process generated by performing

specific simulations, could eliminate sources of disturbance and identify any non-linear behaviour in the building system to isolate it (Hazyuk et al., 2012).

Lastly, a crucial aspect is related to the estimation of thermal model parameters, of which values are bounded in order to keep their physical insight. The Grey-box models, seen previously, referred to Madsen's identification procedure, which is based on the of MLE algorithm. Applying this method, it is necessary to set initial and boundary conditions for all the parameters to be estimated. Sometimes this implies inadequate estimates of the parameters, so loss of accuracy for the identified model, which works properly only around the range in which it is identified (resulting too dependent on the data that generated it).

In order to support Building Energy Management Systems, mostly in advanced control processes, this dissertation is aimed at developing an empirical approach to derive grey-box models to be applied in the existing building stock. Models will be identified from experimental data acquired in short time and integrated in a MPC framework that will be tested and simulated.

For the purpose of this research, the empirical approach for the estimation of the Reduced-Order Models will be developed following the basic theoretical principles suggested by the literature. To doing so, a preliminary case study will be investigated to understand strength and weakness of the identification procedure analysed and define the experimental approach to be adapted and implemented in real cases. Then, the identified experimental procedure will be applied in a complex existing building, exploiting the adoption of the preliminary study. Components required for the modelling process will be definitely defined and the model validation will be examined, revising the one proposed by literature (see Chapter 4).

Later, the modelling approach experimented will be integrated in a MPC prototype for real-time controlling of the case study (see Chapter 5). Finally, exploiting simulations of the detailed model of the case study, will be evaluated the robustness of the grey-box model identified for its support and reliability in model predictive control strategies (see Chapter 6).

Chapter 3

State of the art on Model Predictive Control for buildings

3.1 Introduction

This chapter provides an overview of the relevant research that has been conducted within the area of model based predictive control strategy. Firstly, a brief introduction in the field of MPC technology, focusing on the explanation of this kind of advanced control and its already well-established applications. Secondly, an overview of MPC development for building climate control will be provided by means of the main research studies, underlining through their applications the advantages and limitations for the implementation in the construction field. Finally, the MPC structure and its components will be analysed in detail to support the following development of this dissertation.

3.2 Overview of Model Predictive Control strategy

Model Predictive Control (MPC) originated about 40 years ago, in order to support the processing industry, as reported in (Richalet et al., 1978) and in (Cutler and Ramaker, 1980), and since then, it has seen an increasing development. The acronym MPC does not imply a single control strategy, but includes a wide range of control methods based on an explicit model of the process to predict the future response of a plant (Qin and Badgwell, 2003). The MPC strategy refers to an iterative procedure to obtain real-time the optimal control signal for the actuators of a plant. The MPC central idea is based on the receding horizon principle, which was proposed for the first time by Propoi (Propoi, 1963). Different RHPC (Receding Horizon Predictive Control) algorithms can be applied in the control process, they only differ amongst themselves in the model used to represent the process, the noises and cost function to be minimized. Even though there are different MPC algorithms, they share the same basic principles, that are (Camacho and Bordons, 2007):

- use of an explicit process model to predict the system response at future time instants;

- calculation of a control sequence minimizing an objective function;
- application of a receding strategy, so that at each control interval the optimal control sequence is calculated, but only the first control signal is applied. Then, the entire calculation is repeated at subsequent control intervals.

The MPC was initially developed to fulfil specific control needs of power plants and petroleum refineries. Later, the industry processes became the main application field, particularly for chemical industries due to the use of a simple algorithm and an intuitive impulse or step response model. A complete review of MPC applications and implications in petrochemical sector during the eighties is provided by Garcia et al. (García et al., 1989). Now this advanced control technology is widely applied in different areas including, in addition to chemicals, food processing, automotive, and aerospace applications. The good performance of these applications shows the capacity of the MPC to achieve highly efficient control systems able to operate during long periods of time with hardly any intervention.

Comparing with other control methods, the MPC presents a series of advantages (Camacho and Bordons, 2007):

1. The control concepts are very intuitive, thus easily applicable and at the same time the tuning is relatively simple.
2. It can be used to control a great variety of processes, from those with relatively simple dynamics to more complex ones.
3. It can manage the multivariable case.
4. It has compensation for dead times.
5. It introduces feed forward control in a natural way to compensate for measurable disturbances.
6. The controller is the result of the easy implementation of the control law.
7. Its extension to the treatment of constraints is conceptually simple, and these can be systematically included during the design process.
8. It is very useful when future references (robotics or batch processes) are known.
9. Its characteristic of open methodology allows for future extensions.

On the other hand, the control logic has also its drawbacks. One of these refers to the controller derivation, which is more complex than that of the classical PID controllers. That derivation can be done beforehand if the system dynamic does not change, otherwise all the computation has to be carried out at every sampling time, as in the case of adaptive control. Regarding point 7, the introduction of constraints in the optimization problem requires a higher computational effort that

should be considered when the control is implemented in industrial process to avoid lacks for purposes other than the control algorithm itself (communication, dialogues with the operators, alarms, recording, etc.). Anyway, the greatest drawback is the need for an appropriate model of the process to be available. The design algorithm is based on prior knowledge of the model and is independent of it, but it is obvious that the benefits obtained will be affected by the discrepancies existing between the real process and the model used.

The methodology of all the controllers belonging to the MPC family is characterized by the following strategy, depicted in Fig. 3.1:

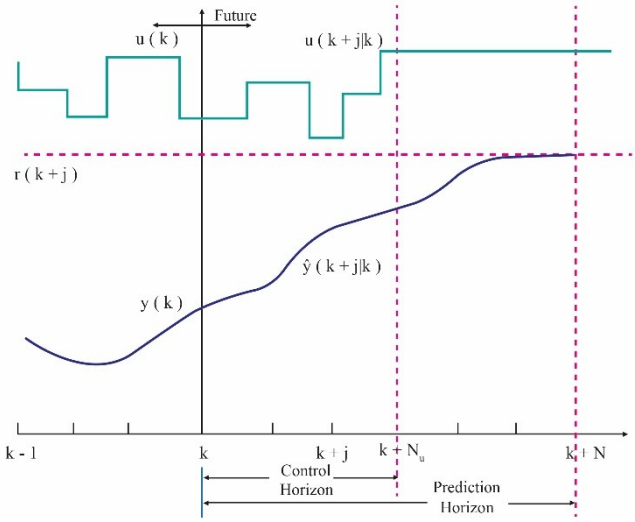

Fig. 3.1 MPC strategy

The outputs of the system are predicted, at each instant k, for a specified prediction horizon N. These future outputs, y(k+j| k) for j = 1. . .N, depend on the known values up to instant k (past inputs and outputs) and on the future control signals u(k+j | k), j = 0. . . N−1, which are those to be calculated and sent to the system (The notation (k+j | k) indicates the value of the variable at the instant k+j calculated at instant k).

The set of future control signals is calculated by means of the optimisation of a quadratic function of the errors between the predicted output signal and the predicted reference trajectory r(k+j), usually represented by the setpoint or its approximation. An explicit solution can be obtained if the criterion is quadratic, the model is linear, and there are no constraints; otherwise an iterative optimisation method should be used. Some assumptions about the structure of the future control law are also made in some cases, such as that it will be constant from a given instant.

The control signal u(k|k) is the only of the calculated control sequence to be sent to the process, because at time (t+1), the output y(k+ 1) is already known and step 1 is repeated with this new value and all the sequences are brought up to date. Therefore, the u(k + 1 | k + 1) is calculated and, applying

the receding horizon principle, it will be different from the u(k + 1 | k) due to the new information available.

At this point, it is possible to define the core of MPC, based on two components: a model and a controller. The first is used to predict the future plant outputs, based on past and current values and on the future control actions. The other fundamental component is the controller, which calculates the control actions within the optimisation process, as previously explained, considering eventual constraints. The process model is crucial for the efficient operation of the controller, because it must capture the process dynamics to precisely predict the future outputs.

Dealing with models, The Truncated Impulse Response Model is very appreciated in industry field because it is very intuitive and can also be used for multivariable processes, although it requires many parameters and only open-loop stable processes can be described in this way. The Step Response Model is quite like the previous one, but obtained when the input is a step.

The State Space Model, popular in the academic research community, is characterized by an easy derivation of the controller, even for the multivariable case. The state space description allows for an easier expression of stability and robustness criteria. The Transfer Function Model is also used in the academic research community and although the derivation of the controller is more difficult, it requires fewer parameters. This model is better than state space model for industry applications due to its basic concepts, usually employed also in industry.

The optimizer is the brain of the strategy as it provides the control actions. If the cost function is quadratic, its minimum can be obtained as an explicit function (linear) of past inputs and outputs and the future reference trajectory. In the presence of inequality constraints, the solution be obtained by providing a greater computational effort. The size of the optimization problems depends on the number of variables and the prediction horizons used and usually turns out to be a relatively modest optimization problem which does not require solving sophisticated computer codes. However, the amount of time needed for the constrained and robust cases can be largely different than the one needed for the unconstrained case and the bandwidth of the process to which constrained MPC can be applied is considerably reduced.

3.3 Development of MPC for management of building systems

Recently, model predictive control (MPC) techniques have been proposed towards effective BEMS design, with promising results for successful implementations (Kontes et al., 2014). The basic idea that contributed to the development of MPC for buildings was to efficiently use thermal storage by formulating an optimisation problem. First, as presented in (Grünenfelder and Tödtli, 1985), different control strategies, using weather forecasts and statistics, were applied to a solar domestic hot water

system. Simulation results demonstrated the potential in reduction of energy costs. Since then, the interest in the use of MPC for buildings and, in parallel, the need for higher computing power have considerably grown, as demonstrated by the number of related research works (Prívara et al., 2013). Earlier studies investigated the use of the building's thermal mass (Snyder and Newell, 1990). In particular, Henze et al. since 1997 (Henze et al., 1997) investigated the predictive control strategy, firstly developing and simulating an optimal controller for active thermal energy storage (TES) systems in order to reduce the cost of operating a central cooling plant. Results showed the performance advantages of the proposed controller over the conventional ones. Few years later, Henze et al. (Henze et al., 2004a) studied the benefits of combined optimal control of both passive building thermal capacitance and active thermal energy storage systems. The controller had to minimize an objective function constituted by the total utility bill of an office building, including the cost of heating and a time-of-use electricity rate. The office building was first modelled in EnergyPlus and subsequently a TRNSYS model was derived and validated. After the implementation of the optimization algorithms, findings revealed the importance of perfect weather forecasts and a building model which perfectly matches the actual building, as to have substantial utility cost savings and on-peak electrical demand reductions. Their further research (Henze et al., 2004b), always regarding the predictive optimal control of active and passive building thermal storage inventory, evaluated the impact of prediction uncertainty in the required short-term weather forecasts in the controller performance. It was demonstrated that weather predictions affect utility cost savings only marginally compared to a hypothetical perfect predictor that exactly anticipates the weather during the next planning horizon. This finding rests on the assumption of perfect match between the building model and the actual building behaviour. Instead, the impact of modelling accuracy on predictive optimal control was debated by Liu et al. (Liu and Henze, 2004) investigating five categories of building modelling mismatch. Performance analyses showed that building geometry and zoning does not affect significantly the optimal control response, in the case of an internal heat gain dominated commercial building. Therefore, reasonable model simplifications are acceptable, mostly to reduce computational effort. The same result was obtained for the mass of the internal structure, yet this acted in changing the building cooling load profile and consequently the operation of the active storage (TES) system. Construction material requires to be well modelled because of their impact on building passive thermal storage capacity. Besides, it turned out that internal gain mismatches should be avoided because setpoint profiles and TES performance are strongly affected by them. The same consideration is underlined for the efficiency of the building energy system, which affects both zone temperature setpoints (passive storage) and active storage operation. To completion the study of a predictive optimal controller for the combined usage of active and passive thermal storage, one year

later, another contribution (Henze et al., 2005) examined the role of the uncertainty in predictive variables and model mismatch. The work was developed in a test facility by means of a real-time control experiment of 5 days, which was later recreated in simulation environment. Simulated results showed that, even if the optimal controller is given imperfect weather forecasts and the building model did not match perfectly the actual building behaviour, utility cost savings achieved 17% relative to the base case and 27% to the reference case. Running in parallel, other simulation results demonstrated that the predictive control applied to radiant floor heating provided a superior control strategy, compared to that of conventional controllers. Chen (Chen, 2002) applied a generalised predictive control (GPC) to a floor radiant heating system in a test room. The system identification exploited the recursive least squares techniques deriving two different models for two different periods, night and day time. Experiment results confirmed the reliability of the strategy, because no significant difference was observed between temperature predicted and measured data. Moreover, simulation results demonstrated the efficiency of the GPC behaviour, compared to on-off and PI controllers. In addition, Braun (Braun, 2003) presented an overview of research about the building thermal mass for reducing the peak cooling loads in commercial buildings. Studies analysed, both in simulation and in laboratory, demonstrated significant potential savings for control building thermal mass and suggested the need of guidelines for application of expected savings from building thermal mass control strategies that can be used by controls engineers to facilitate implementation within control systems in large commercial systems. The assessment of the MPC performance through experimental campaigns on radiant heating systems was the subject of two recent papers. In the first study (Cho and Zaheer-uddin, 2003), a predictive control strategy is conducted to improve the energy efficiency of intermittently heated radiant floor heating systems. The predictive control method was simulated in a test facility by means of TRNSYS computer program, observing a more efficiently use the energy compared to the conventional control strategy. One reason for the higher energy efficiency was that the heat supply hours per day in the predictive control strategy was determined based on a forecast of hourly outdoor temperature, against the conventional method based on the daily minimum outdoor temperature. Besides, an experimental test of two days was conducted and performance results showed a reduction of energy consumption between 10% and 20% by using the predictive control technique instead of the conventional control scheme. In the second study (Prívara et al., 2011), the authors discussed MPC strategy applied to a real building of the Czech Technical University in Prague. Exploiting a real operation during the heating season, they proved the supremacy of the predictive controller tested over a well-tuned weather-compensated control, with energy savings of 17–24%. They highlighted the fundamental contribution of a proper model identification for the quality of the optimal control and, concurrently, the importance of a persistent

system excitation for quality in measurement data used by the identification process. The completeness of the MPC strategy, in terms of energy and comfort, is discussed in (Freire et al., 2008), where the methodology proposed connects energy savings to different thermal comfort criteria. The authors analysed the indoor thermal comfort problem in buildings equipped with HVAC systems exploiting two different MBPC (model based predictive control) algorithms, one based on the psychrometric chart and another based on the PMV index. In order to evaluate the MBPC performance, they simulated a BESTest single-zone building by means of PowerDomus, which is a whole-building hygrotermal and energy simulation software. Simulation results of two case studies testified the possibility of energy consumption reduction without compromising thermal comfort, which maintained 100% of the time in the comfort zone.

An interesting simulation study of an MPC was presented in (Ma et al., 2009), using a simplified model of a chilling system, for the campus at the University of California at Merced in USA, to predictive control building loads as to minimise energy costs, while exploiting time-varying electric energy prices. Preliminary simulation results showed a potential reduction of 24.5%, compared to the current heuristic manual control sequence.

Subsequently, based on the simplified load model of the previous work, the authors (Ma et al., 2010) developed a more detailed campus load model and validated using load measurements data. Model parameters were identified by using historical data collected in 2008, and minimizing the root mean square of the error between the model output and the measured load of the campus. An MPC algorithm was implemented in MATLAB to computes the setpoints for the chillers and cooling towers at the central plant, as to satisfy the required cooling load while minimizing the electricity costs. Three different types of scenario were studied, reaching an improvement of the central plant efficiency (COP) by 11.9% compared to baseline control.

Although these works are examples to demonstrate the potentiality of MPC, applications of this approach to the optimal control of real world buildings are very limited. Sticking to the general MPC framework, a crucial aspect is identified in the reduced-order modelling of the building to achieve a reliable level of predictive control. With this purpose, in (Prívara et al., 2013) an overview of building modelling for predictive control of the building climate is provided. Moreover, Privara et al. proposed a combined procedure of benefits from simulation tools and statistically-based algorithms to obtain a suitable building model.

Therefore, an adequate model for the MPC controller is a difficult goal to reach, because it should be reasonably simple and yet able to properly estimate thermal system dynamics, possibly in an explicit form. Normally, the modelling of building physics is carried out by means of simulation tools, e.g. Energy-Plus or TRNSYS, as shown in HVAC research (Orosa and Oliveira, 2011; Trčka

and Hensen, 2010). However, this kind of tools require considerable computational effort, which could be prohibitive for a real-time optimisation problem. Moreover, the implicit form of their models is not available. Besides, although they make it possible to carry out performance analyses on existing buildings, these tools do not ensure integration with high performance controllers, such as the model predictive ones (Afram and Janabi-Sharifi, 2014). A possible approach to overcome the problem, providing a more efficient model to the controller, was suggested by the literature on MPC with applied grey-box models, which describe building thermal dynamics in an explicit form, based on a thermal resistance capacitance (RC) network (Hazyuk et al., 2012; Ma et al., 2012; Široký et al., 2011). Carrascal et al. (Carrascal et al., 2016) presented a study on aged residential buildings without any rehabilitation exploiting the MPC strategy to improve building thermal quality. The MPC implementation in simulation environment was completed considering a grey box RC-model, identified as a 4^{th} order system by means of experimental measurements. Results of MPC performance, compared to those of hysteresis ON-OFF controls, achieved savings of 10-15 % in the energy consumption, which is similar to the ones of better quality buildings, as reported in literature. Thus, the grey-box models demonstrated their potential for modelling existing buildings with available data monitoring, because they combine physical insight and model structure from the white-box paradigm with parameter estimation and statistical framework from black-box models (De Coninck et al., 2014). One of the most recent works showing their quality is given by (Reynders et al., 2014), in which the overall model structure is derived from the analogy with electric circuits and the identification of the unknown parameters is carried out using the continuous-time stochastic modelling (CTSM) toolbox implemented in R (Juhl et al., 2013).

3.4 MPC design

The design of a model-based predictive control (Fig. 3.2) goes through the completion of specific steps for the MPC controller to solve the optimisation problem, that is minimise the use of energy while keeping the temperature within the comfort band (Carrascal et al., 2016). First, regarding the inputs of the MPC controller, it is required to specify time-varying parameters, such as energy price and comfort criteria as well as weather forecasts and occupancy schedules. It is then necessary to choose the cost function, generally subject to some control constraints, so as to achieve the desired building behaviour. All these components must be integrated into the controller, which, so far, has been developed mainly in virtual and simulation environments. Applying the receding strategy, at each iteration, the controller formulates the solution over a finite future time window, but only the first step of the control strategy is implemented. In fact, the MPC framework is integrated in the process, hence when the process moves a step forward, the prediction horizon is shifted forward and

the control signal is calculated again. This basic principle introduces feedback in the system, which means the new optimal control problem solved at the beginning of the next time step is a function of the new state at that point in time, therefore also of any disturbances that have acted on the building (Široký et al., 2011).

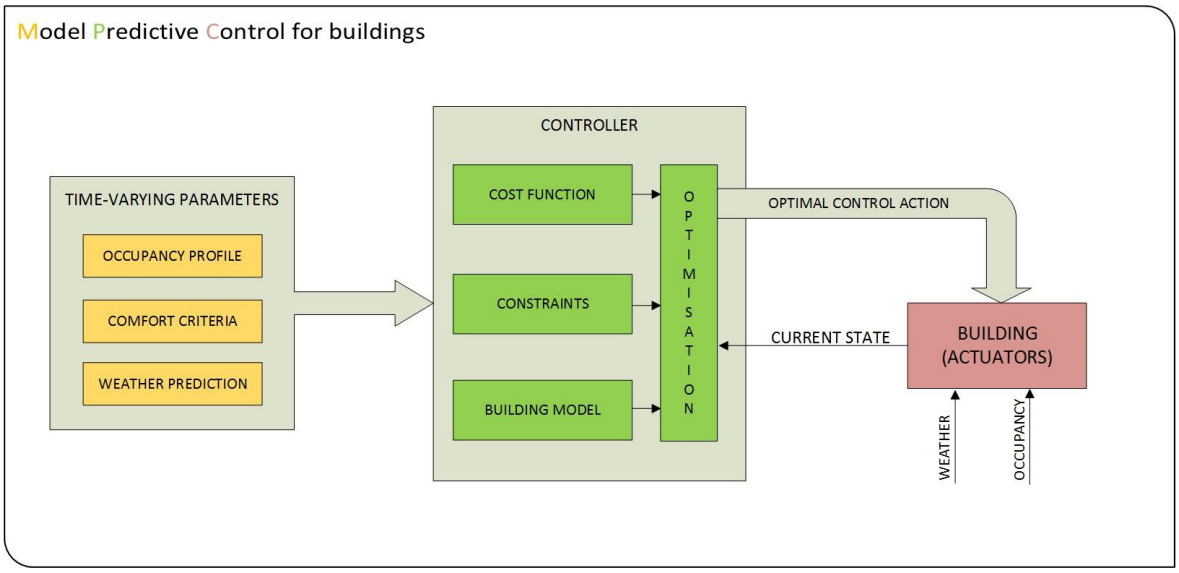

Fig. 3.2 Key components of a MPC for buildings

Time-varying parameters, namely weather prediction, occupancy and comfort criteria, are inputs for the controller (Fig. 3.2). At each sampling interval, measurements of the current state are provided to solve the optimisation problem, which requires the identification of the parameters to be controlled and the desired range in which the control must keep them. It is also possible to specify constraints related to the parameters.

The generic MPC framework is usually expressed in mathematical form as the components of the optimisation problem as follows:

Cost function

subject to

$$\min_{u_0,\dots,u_{N-1}} \sum_{k=0}^{N-1} l_{k(x_k,u_k)} \tag{3.1}$$

Constraints

$$(x_k, u_k) \in X_k \times U_k \tag{3.2}$$

Current state

$$x_0 = x \tag{3.3}$$

Dynamics – state update

$$x_{k+1} = f(x_k, u_k, w_k) \tag{3.4}$$

– system output

$$y_k = g(x_k, u_k, w_k) \tag{3.5}$$

where k is the discrete time step; N is the prediction horizon; $x_k \in R^n$ is the system state; $u_k \in R^m$ is the control input; $y_k \in R^p$ is the system output; $w_k \in R^l$ is the vector of the known/estimated disturbances acting on the system; X_k and U_k represent the constraint sets respectively of the states and inputs. The explanation of the components provided below is just introductory to the specific formulation that can be found in literature (Maciejowski, 2002).

Cost function

The cost function purpose is to provide the expected behaviour to the system (Oldewurtel et al., 2012). Generally, this can be achieved through:

- Stability. The choice of cost function structure should be such as to have the optimal cost forms a Lyapunov function for the closed loop system, in order to guarantee stability. This requirement is usually satisfied for stable systems with slow dynamics, such as buildings, enabling to select the cost strictly on a performance basis.
- Performance target. The cost usually represents a combination of performance targets, thus different cost weights can be used for different targets to specify a preference for one behaviour over another, e.g. minimizing energy or maximizing comfort in building climate control.

The main goal is to minimize energy cost, while respecting comfort constraints, generally formalized as presented in (Široký et al., 2011):

$$l_k = (y_k - y_{r,k})^T Q_k (y_k - y_{r,k}) + R_k u_k \tag{3.6}$$

where Qk and Rk are time-varying matrices of appropriate size and yr,k is the reference signal at time k. The proportion of the matrices Qk and Rk serves to balance the precision of reference tracking with the energy consumption. The reference tracking is usually expressed as a quadratic form because it significantly penalizes larger deviations from the reference. The function presented in Eq. 3.6 is not the only cost function applicable to building climate control, in fact it depends on the optimization problem to solve. Hence, several cost functions are in use, of which the most common are: Quadratic cost, Linear cost and Probabilistic cost. The Quadratic one (Eq. 3.6) was used for the MPC prototype of this dissertation, analysed in Chapter 5.

Constraints

The ability to specify constraints in the MPC formulation and to have the optimization routine handle them directly is the key strength of the MPC approach (Široký et al., 2011). Constraints can be fixed

on the states or the output, as well as on the input. Linear constraints are the most common type of constraint, which are used to place upper/lower bounds on system variables:

$$y_{min,k} < y_k < y_{max,k} \tag{3.7}$$

$$u_{min,k} < u_k < u_{max,k} \tag{3.8}$$

The limits can be constant, representing real-world limitations, or time-varying, to justify different comfort conditions. Linear constraints also result in the simplest optimization problems. Furthermore, one might want to constrain the rate of change, which is done by imposing a constraint of the form:

$$|u_k - u_{k-1}| < \Delta u_{max} \tag{3.9}$$

Current state

The system model is initialized to the measured/estimated current state of the building and all future (control) predictions begin from this initial state x. Depending on what the state of the building is describing, it might not be possible to measure everything directly. In this case, a Kalman filter can be used to estimate the current state of the building and the estimate is used as initial state.

Dynamics

The controller model, i.e. the mathematical description of the building dynamics is a critical piece of the MPC controller. For this dissertation, linear dynamics are used because they result in a convex and easily solvable optimization problem, in particular a discrete state space form is applied:

$$x_{k+1} = Ax_k + Bu_k \tag{3.10}$$

$$y_k = Cx_k + Du_k \tag{3.11}$$

To complete the overview of MPC design phase, it requires to define other two parameters: first, the prediction horizon (Np), which establishes the length of the future window for the evaluation of the system; then, the control horizon (Nc), that is the number of steps within computing the best control action. A long prediction horizon increases the predictive ability of the MPC controller. However, it decreases the performance of the MPC controller because of the extra calculations for the control algorithm. The two horizons are linked by this condition:

$$1 < Nc < Np \tag{3.12}$$

So, for the specified prediction and control horizons, the MPC controller returned the control action, u, by minimising the following cost function "J" (14), that is the one applied in this dissertation (see Chapter 5):

$$J(k) = \sum_{j=N_w}^{N_p} [\widehat{y}(k+j|k) - r(k+j|k)]^T \cdot Q \cdot [\widehat{y}(k+j|k) - r(k+j|k)] + \\ + \sum_{j=0}^{N_c-1} [\triangle u^T(k+j|k) \cdot R \cdot \triangle u(k+j|k)] \quad (3.13)$$

where j is the index along the prediction horizon; Nw is the beginning of the prediction horizon; Q is the output error weight matrix; R is the rate of change in control action weight matrix; by (k+j | k) is the predicted plant output at time k+j, given all measurements up to and including those at time k; r(k+j | k) is the output set-point profile at time k+j, given all measurements up to and including those at time k; Δu(k+j | k) is the predicted rate of change in control action at time k+j, given all measurements up to and including those at time k. As already underlined, it is necessary to specify weight matrices (Q, R) as well as constraints. The former adjust the priorities of the rate of change in control action and plant outputs, while the latter are limits applied to the states, the outputs or the inputs.

3.5 Implication of the results

Certainly, dealing with existing buildings, usually defined as very complex dynamic systems, represents a great challenge in terms of managing performances and real-time controlling. One of the main need arising in such buildings regards the balance between the maximization of user comfort and the minimization of energy consumption. In this optimisation direction, MPC technology, well developed for the industry sector, in the last few years, has achieved remarkable development and promising results also for the implementation in the construction field, for building climate control. Model Predictive Control (MPC) for buildings has gained a lot of attention recently. It has been shown that MPC can achieve significant energy savings in the range between 15-30% compared to a conventional control strategy, e.g., to a rule-based controller (Jiri Cigler et al., 2013). Acknowledged benefits of MPC in the field of building control are the optimal use of predictions (ambient temperature, radiation, occupancy) easy handling with large time-constants (large buildings in general have slow dynamics), and the possibility to simply include thermal and technical constraints into the underlying optimization (Killian and Kozek, 2016).

Although the great potential recognised, the development of this advanced control pointed out three main problems by the investigation of the best of authors' knowledge.

First of all, the analysed experiences of implementation revealed the difficulty of obtaining a reliable control in MPC algorithm due to the quality of the building model, which could be not well-identified and so reliable to represent building thermal dynamics. The use of a wrong strategy for the model identification often entails an extra effort that could compromise the predicted results or, even worse, represent a barrier for the controller development. Moreover, the building model should not make use of traditional modelling strategies because they are time consuming and not suitable to increase MPC performance for further commercial applications. Although at present there is no silver bullet to obtain a suitable model for MPC design (Killian and Kozek, 2016), investigations and preliminary tests have demonstrated that grey-box modelling can be applied to obtain the building model to be included in the controller, because it can be derived from short-term operation monitoring data and it represents a suitable choice to perform many prediction iterations in a short time.

Secondly, experimentations of MPC operation mainly referred to simulation studies, where the object of control is reproduced, or in some cases created, by means of simulation tools and the same happened for the controller. Experimental approaches constitute a limited part of knowledge acquired about MPC. Besides, the case studies are often pilot buildings and the prototypes developed not always concerned all disturbances affecting the internal temperature, like the experience presented in (Prívara et al., 2011), although the importance of completeness in disturbances predictions, such as solar and occupancy gains, was underlined.

Finally, a recent survey reported that most of publications on intelligent control schemes for optimized building control is based on MPC (Shaikh et al., 2014). Authors in (Kavgic et al., 2015) have recognised in office buildings and secondary schools, primary targets for a beneficial MPC. These building archetypes, indeed, both satisfy several criteria for effective MPC implementation. For that concerning offices, the significant thermal mass, joined to large passive solar gain through windows, occupancy scheduled periods and the opportunity to vary temperature setpoints represent points in favour. Moreover, offices are present in great quantity among the commercial building sector and in all climates. Finally, offices all provide for similar use characteristics (i.e. people, desks, computers, etc.) which lends itself toward a universal control solution for this building type. Linking to this concept, a typical observed disadvantage in MPC applications regards the lack of standardisation in the design procedure, usually fitting only to the specific building investigated.

Even though, according to literature provided, prototype implementations of MPC clearly demonstrated the high potential of a theoretically well-developed method, expertise in the field results insufficient in setting up and commissioning such this advanced control system successfully. To really contribute to the commercial growth of MPC for buildings, it is required to the automation suppliers to hire or train experts in the field of building modelling and MPC design, as stated in

(Killian and Kozek, 2016). This effort should be relied to a technological feasible implementation of MPC strategy that implies the need for portable software components that can be easily adjusted to a given target building and that allow for the flexible and safe experimentation with the underlying optimization task (Jırı Cigler et al., 2013).

The high potential of MPC usage in buildings control presented and its promising great benefits over the conventional controllers have justified the purpose of this research, which aims to facilitate the implementation of MPC for managing performances of existing buildings.

In the first instance, considering the significant impact of building modelling in the design phase of the model predictive controller, a modelling procedure will be defined combining suggestions from related literature with an experimental approach, paying attention to the reliability of the model for the controller (Chapter 4).

Then, exploiting the tested procedure, the main target of this dissertation will be the construction and implementation of a model predictive control in an existing building (Chapter 5), evaluating the real-time operation of the advanced control developed. The MPC application will be examined also in terms of technological feasibility, easy implementation and the capability to reproduce the same architecture by adequately expanding it for a different case.

At the end, further considerations on the opportunities of improvement scenarios for the building renovation will be provided by reproducing the same architecture in a simulation environment (Chapter 6). The simulated control represented also the possibility to deal with the tuning of the main controller parameters and to investigate the potential of the building model identification during the controller run-time.

Chapter 4

Development of an empirical approach to derive Grey-box models

4.1 Introduction

The main purpose of our experimental approach is the investigation of Reduced Order Models, using a grey-box modelling approach for simulating real and complex cases of the existing building stock, in order to implement it in advanced control strategies. Relevant literature provided many examples and case studies about modelling the energy dynamics of buildings. In fact, parameters of the reduced models are extracted in real time; this makes the estimation of the thermal response of a building in its current state feasible, and this information reusable to make predictions about its expected behaviour in further analyses. This work started with a fact-finding survey on the reduced-order models and the use of identification techniques from literature, see in Chapter 2. The robustness of such techniques was investigated, with the purpose of defining a mathematical model based on partial observations of the heat dynamics of the building. To fulfil this aim, a first controlled situation, based on theoretical principles suggested by the literature, was simulated in a machine laboratory of the DICEA Department at the Università Politecnica delle Marche and it will be described in the next paragraph. An empirical approach to derive reduced order models was identified by means of a limited data collection. Then, the identification procedure was extracted and implemented in a real case, increasing the complexity level, as to verify the reliability of the tested approach. The discussion of estimation procedure for the ROMs is split in two parts, corresponding to the two experimental campaigns carried out. Finally, the goodness of the derived models is analysed by means of the validation phase at the end of this chapter.

4.2 Preliminary study

The aim of our experimental approach is the investigation of grey-box modelling in simulating real and complex cases, in order to support advanced controls for managing existing buildings. To reach

this purpose, a single test-room, in which it was possible to easily manage all inputs, was used to define the model identification procedure, from the sensors deployment to the statistical estimation. The test-room is a changing room of a machine laboratory at the Università Politecnica delle Marche (Fig. 4.1). Being inside a building, the room is surrounded by different other rooms, in particular a bathroom, an archive and the same laboratory as shown in (Fig. 4.2). The ground effect was eliminated to further reduce inputs: 2-cm polystyrene sheets were placed on the floor of around 13 m^2 and over there a layer of bricks to make it walkable and increase thermal insulation. Moreover, an electric heater, of real measured power 377.6 W, was installed inside the test-room to simulate a real heating system. According to Madsen's work (Madsen and Schultz, 2003), even in this case switching on and off were managed by a timer, previously programmed with a signal PRBS.

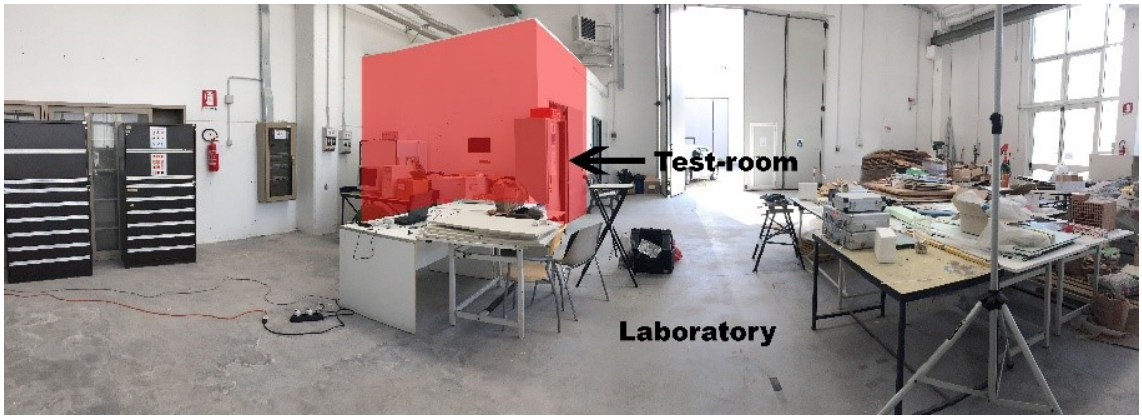

Fig. 4.1 Overview of the laboratory and the main testing area.

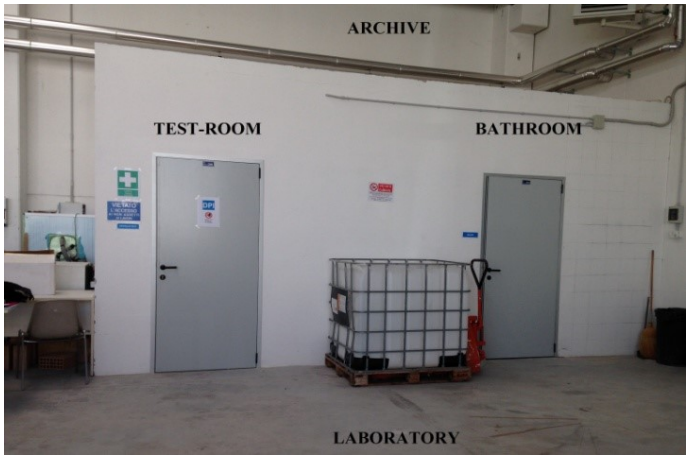

Fig. 4.2 Test-room and boundary places.

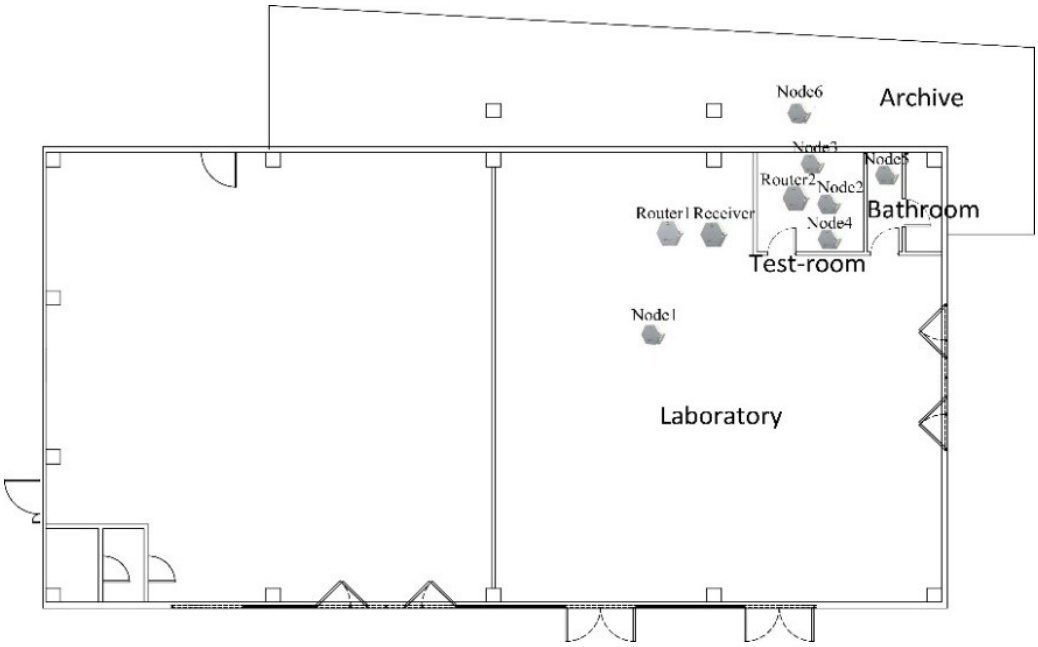

Fig. 4.3 Plan of the laboratory with the Hobo Network deployment.

4.2.1 Sensors deployment

A Hobo Zw Series Wireless Network, see specs in APPENDIX A, was installed in the test area to measure temperature and relative humidity of the different zones. This sensors network proved to be particularly fitting such applications because it is cheap, able to give back data in real time and equipped with internal memory and batteries, useful to overcome periods of electric blackout. Therefore, the six available sensors were installed in the area: three in the changing room, two of them applied on the two opposite internal walls and one hanging from the ceiling; one in the bathroom; another one in the laboratory and the last sensor was hung in the archive (Fig. 4.3). The sensor in the archive was hanged from a steel structure (Fig. 4.4a), while tripods were used for sensors placed in the centre of the other zones (Fig. 4.4b-4.4c). The applied data covered a period of about 18 days, from 2nd to 20th July 2015. The number of total observations was equal to 27131, corresponding to an acquisition per minute. Prior to estimating the model parameters, data of the first day of the test, July 2nd, were cancelled because corrupted and remaining data were resampled at a sampling time of 15 minutes. This sampling time was chosen to avoid problems of aliasing, according to Shannon's theorem, based on the smallest period of the electric heater that is 30 minutes. As better described in the following section relating to results, not all sensors were used for estimation. In fact, in the first estimations the two sensors fixed to the internal walls of the changing room were excluded because too much affected by the convective motion of the internal air. At the same time, also

temperature measurements of the bathroom were later excluded because they were too similar to the ones of the laboratory, so they did not bring any meaningful additional input into the model. Lastly, the small number of gaps present in the dataset was bridged with a linear interpolation.

Fig. 4.4 Sensors positioning in the archive (a), in the changing room (b) and in the laboratory (c).

4.2.2 RC-networks

The state-space representation of a grey-model is a mathematical description of a physical system using a vector of inputs and outputs tied together by a set of first-order differential equations. The state variables characterizing the system in each time step are gathered as a time varying state vector called system state. A typical representation with the state to which was added an error is shown below:

$$dX(t) = \mathrm{A}(\theta)\mathrm{X(t)dt} + \mathrm{B}(\theta)\mathrm{U(t)dt} + \sigma(\theta)\mathrm{d}\omega \quad (4.1)$$

$$Y(t) = C(\theta)X(t) + D(\theta)U(t) + \varepsilon \quad (4.2)$$

The states of the system are represented by the vector X(t) which correspond to the temperatures of the relevant building components, in the case of modelling the thermal response of buildings. U(t) is a vector containing the measured inputs of the system, which can be either inputs or controlled outputs (heating and ventilation system, solar gains, outdoor temperature, etc.). The measured output Y(t) is function of the states and the inputs by means of matrices C and D. A, B, C, D are nonlinear functions, depending on the parameters' vector θ. The matrix A characterizes the dynamic behaviour of the system and the matrix B concerns the influence of input signals entering the system. Matrices C and D are respectively how much the state and the error not affected by the state are reflected in the final output $Y(t)$. ω is a random function of time, assumed as a standard Wiener process with independent increments; the mutual independent ε is a white noise process representing the measurement error. To identify the unknown parameters of the vector θ, the ML estimation method is adopted (Bacher and Madsen, 2011; Madsen and Schultz, 2003). Maximum Likelihood estimation

is an analytic maximization procedure particularly useful in presences of a great number of data gathered, that maximizes the joint probability function between the observed samples and the individual parameters. Practically the search for parameters occurs through a process of numerical optimization of the objective function, by means of a statistical software R, using the package CTSM (Juhl et al., 2013). The structures for modelling the heat dynamics are derived from the analogy with electric circuits. According to the model order, the thermal mass of the building is lumped to a discrete number of capacitances. In the thermal network, the capacitors C_i represent the active thermal capacity of the building zone for storing heat, while the thermal resistances R_i are linked to material properties and affect the heat flow across building layers at different temperatures. Heat inputs and solar gains are representable like electric current while voltage generators are related to the external temperature. Temperatures of each modelled ambient or element are placed at the nodes. However, a given parameter is not identified with the same physical correspondence in each model. The models used in this preliminary study (Fig. 4.5) are referred to the 1st, 2nd and 3rd-order models. To simplify the problem, in this early stage, the testing area does not entail the internal and solar gains. The stochastic differential equations, related to the state space form, are deduced from principles of energy balance at nodes and of heat transfer. For the first order model (Fig. 4.5a), the only state is described by:

$$dT = \frac{1}{\mathrm{RC}}(\mathrm{T}_a - \mathrm{T})\mathrm{dt} + \frac{1}{\mathrm{C}}\Phi_h \mathrm{dt} + \sigma \mathrm{d}\omega \tag{4.3}$$

The two states grey-box model TiTe (Fig. 1b), is defined by the following equations:

$$dT_i = \frac{1}{\mathrm{R}_{ie}\mathrm{C}_i}(\mathrm{T}_e - \mathrm{T}_i)\mathrm{dt} + \frac{1}{C_i}\Phi_h \mathrm{dt} + \sigma_i \mathrm{d}\omega_i \tag{4.4}$$

$$dT_e = \frac{1}{\mathrm{R}_{ie}\mathrm{C}_e}(\mathrm{T}_i - \mathrm{T}_e)\mathrm{dt} + \frac{1}{\mathrm{R}_{ea}\mathrm{C}_e}(\mathrm{T}_a - \mathrm{T}_e)\mathrm{dt} + \sigma_e \mathrm{d}\omega_e \tag{4.5}$$

Consequently, the third order model (Fig. 1c) is represented by these ordinary differential equations:

$$dT_i = \frac{1}{\mathrm{R}_3\mathrm{C}_i}(\mathrm{T}_{23} - \mathrm{T}_i)\mathrm{dt} + \frac{1}{C_i}\Phi_h \mathrm{dt} + \sigma_1 \mathrm{d}\omega_1 \tag{4.6}$$

$$dT_{23} = \frac{1}{\mathrm{R}_3\mathrm{C}_{23}}(\mathrm{T}_i - \mathrm{T}_{23})\mathrm{dt} + \frac{1}{\mathrm{R}_2\mathrm{C}_{23}}(\mathrm{T}_{12} - \mathrm{T}_{23})\mathrm{dt} + \sigma_2 \mathrm{d}\omega_2 \tag{4.7}$$

$$dT_{12} = \frac{1}{\mathrm{R}_2\mathrm{C}_{12}}(\mathrm{T}_{23} - \mathrm{T}_{12})\mathrm{dt} + \frac{1}{\mathrm{R}_1\mathrm{C}_{12}}(\mathrm{T}_a - \mathrm{T}_{12})\mathrm{dt} + \sigma_3 \mathrm{d}\omega_3 \tag{4.8}$$

Symbols used in the previous equations with corresponding units are summarized in Table 4.1.

Table 4.1: Description of lumped physical parameters and relative units.

Symbol	Description	Unit
R_n	Resistances of the envelope	[°C/kWh]
C_n	Capacitances of the envelope	[kWh/°C]
C_i	Internal capacitance	[kWh/°C]
T_i	Internal temperature of the heated room	[°C]
T_a	Temperature of the archive	[°C]
T_l	Laboratory temperature	[°C]
F_h	Power of electric heater	[kW]

Whereas Φ_h and T_a constitute the input measured values of the power provided by the heater and the ambient temperature, the resistance/capacitance parameters (R and C), are estimated as well as the stochastic terms and the initial values of the other temperatures. The time is expressed in hours.

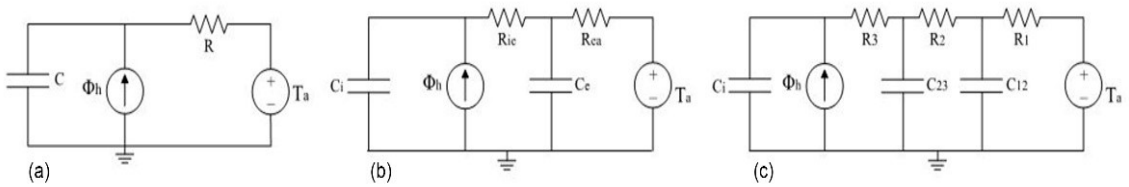

Fig. 4.5 RC-networks of the grey-box models: 1st, 2nd, 3rd order models, from left to right.

For every system of differential equations, the output equation is represented by the discrete time measurement equation, which takes into consideration the data-driven:

$$Y_k = T_{ik} + e_k \tag{4.9}$$

where k is the point in time t_k of a measurement, Y_k [°C] is the measured interior temperature, T_{ik} [°C] is the state at the time t_k and e_k [°C] represents the measurement error, which is assumed to be a Gaussian white noise process with variance σ^2 (Bacher and Madsen, 2011). In fact, a real context provides a number of disturbances to be taken into account in the modelling of the system, to not obtain largely distorted results.

4.2.3 Estimation results and model validation

The phase of system identification was conducted using the tool CTSM-R and testing three different orders of models (Fig. 4.5) in different days of the data collection period. In particular, four data periods were tested with different characteristics and lengths: 3-10 July, 8-15 July, 3-15 July and 3-20 July. The test started with the simplest model, the first order 1C1R (Fig. 4.5a), that turned out not to be conforming to reality. In fact, evaluating results of parameters estimation in CTSM-R, errors

were meaningful and model validation (Juhl et al., 2013) was not satisfied. Then, the second order model 2C2R (Fig. 4.5b) and the third order model 3C3R (Fig. 4.5c) were tested with different boundary conditions. In the first case, the ambient temperature was represented only by the laboratory temperature Tl. In the second case, the boundary condition of the system was represented by the average of the laboratory temperature (Tl) and the archive one (Ta), weighted on the respective surfaces. In the last case, a coefficient (Ka) was introduced to weight the archive temperature as compared to the one of laboratory. This coefficient was estimated by CTSM-R improving estimation results and the Equation 4.5 was rewritten in this way:

$$dT_e = \frac{1}{\mathrm{R}_{ie}\mathrm{C}_e}(\mathrm{T}_i - \mathrm{T}_e)\mathrm{dt} + \frac{1}{\mathrm{R}_{ea}\mathrm{C}_e}(K_a\mathrm{T}_a + (1-K_a)T_l - \mathrm{T}_e)\mathrm{dt} + \sigma_e \mathrm{d}\omega_e \qquad (4.10)$$

The root mean square errors in simulation of these two models were substantially better than the first order and similar each other. The evaluation of parameters in CTSM-R shows an overfitting of both models with some P-values over 0.05 for both models (Juhl et al., 2013). Nevertheless, the overfitting of the second order was not relevant because repeating estimation by fixing Ka, overfitting disappeared without changing any other estimated parameters value. The period, between those tested (3-10 July, 8-15 July, 3-15 July, 3-20 July), that showed a lower value of root mean square error was 3-15 July and with this period it was conducted the validation phase.

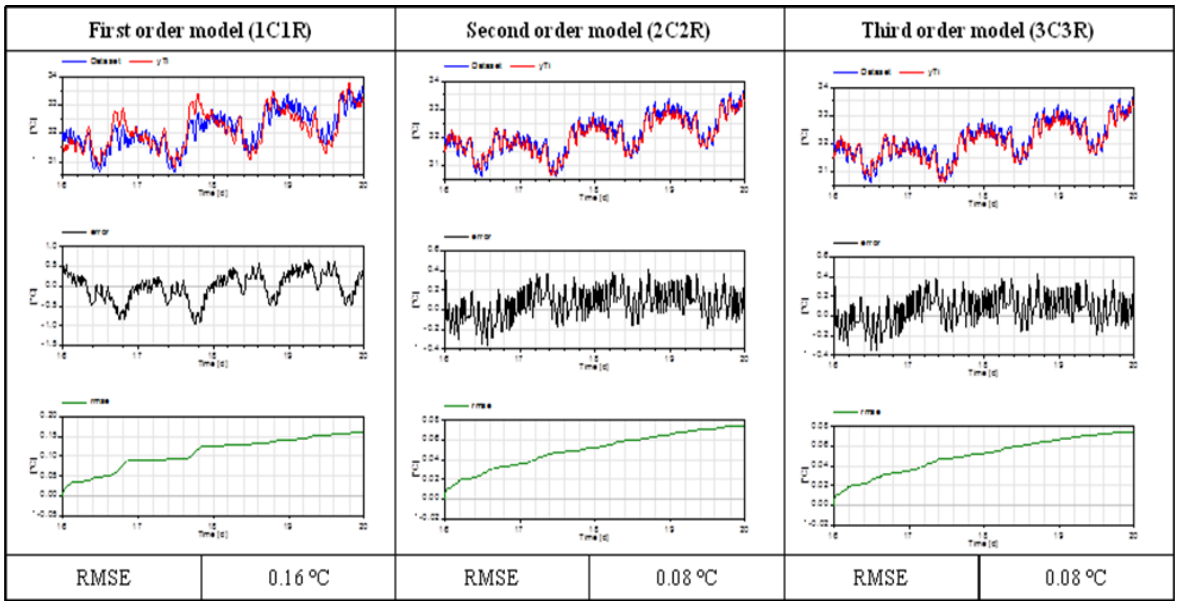

Fig. 4.6 Validation results of the three reduced-order models tested.

The last portion of data was used to validate the models. The validation was carried out by performing a simulation of the test-room indoor temperature from 16th until 20th July, reproducing the RC-

networks with their parameters values, previously estimated in CTSM-R. Results, (Fig. 4.6), continue to show the same results of the simulation phase: the first order model results as non-representative of the heat dynamics of the test room, while the models 2C2R and 3C3R have the same error also in validation. Anyway, the third order model, which fitted better, presented some parameters with a Pr-value over 0.05 that indicated an over-parametrization of the model. Thus, the second order model was considered the best choice in terms of structure simplicity and parameters validation in R (Table 4.2), while providing also an acceptable RMSE value in simulation.

Table 4.2: Parameter estimation in CTSM-R for the best 2nd reduced-order model.

VALORI DEI PARAMETRI STIMATI IN R				
Parametro	**Valore stimato**	**Pr(>|t|)**	**dF/dPar**	**dPen/dPar**
T_{i0}	2.9690e+01	0.0000e+00	-1.0788e-03	0e+00
T_e	2.9231e+01	0.0000e+00	7.5206e-06	0e+00
C_i	1.8778e-01	0.0000e+00	4.2141e-05	0e+00
C_e	7.2417e+00	7.9376e-02	3.9893e-06	0e+00
R_{ie}	3.3991e+00	0.0000e+00	-2.0544e-06	0e+00
R_{ea}	1.4982e+00	5.5475e-02	-1.8006e-06	0e+00
K_a	1.3307e-01	2.2220e-12	2.1635e-05	1e-04
p_{11}	1.3307e-01	0.0000e+00	-1.3475e-06	0e+00
p_{22}	-3.2885e+00	0.0000e+00	-2.2694e-05	0e+00
e_{11}	-2.1133e+01	9.5952e-02	3.2758e-06	0e+00

It was also possible to verify that replacing the Ka in the Eq. 4.10 with its estimated value, that was 0.13307, the results of the estimation were the best for model validation, without any Pr-value over 0.05, that is, the model is not over-parametrized (Table 4.3).

Table 4.3: Parameter estimation in CTSM-R for the best 2nd reduced-order model with fixed Ka.

VALORI DEI PARAMETRI STIMATI IN R				
Parametro	**Valore stimato**	**Pr(>|t|)**	**dF/dPar**	**dPen/dPar**
T_{i0}	2.9692e+01	0.0000e+00	-5.2349e-05	0.0000e+00
T_e	2.9224e+01	0.0000e+00	-4.8034e-06	0.0000e+00
C_i	1.7640e-01	0.0000e+00	5.2610e-05	0.0000e+00
C_e	7.4006e+00	9.7255e-14	-1.2173e-05	0.0000e+00
R_{ie}	3.4447e+00	0.0000e+00	-4.9613e-15	0.0000e+00
R_{ea}	1.4677e+00	-1.8006e-06	-1.3020e-05	0.0000e+00
p_{11}	-1.0883e-01	0.0000e+00	8.7844e-05	0.0000e+00
p_{22}	-2.9891e+00	0.0000e+00	2.1533e-05	0.0000e+00
e_{11}	-5.6405e+01	0.0000e+00	-4.9432e-06	0.0000e+00

In Table 4.3, the Pr-value represents the probability that the particular initial state or parameter is insignificant, i.e. equal to zero (Juhl et al., 2013). The variance of the system noise is represented in CTSM-R by the exponential function of the estimated parameters p11 and p22; while the variance

of the measurement error in the output equation (Eq. 4.9) is the exponential function of the estimated parameter e11.

4.2.4 Implication of the results

An empirical approach based on reduced-model strategy was derived to support modelling of existing buildings. A preliminary test of a controlled real situation was performed, starting from a very little set of data. In fact, this modelling approach requires a prior data acquisition campaign to run the model identification. For this purpose, sensors deployment is fundamental to create an adequate RC-network: environmental devices must be placed at least one for every thermal zone, in which the building is divided, as much as possible in the centre of each air volume, avoiding convective effects, to correctly acquire the internal temperature states. The same importance is conferred to boundary conditions: in this case, it is better to provide sensors for all boundary temperatures of the system, even though it is possible that parameters estimation is not affected by some of them. The influence of the data period is another crucial aspect to be considered and results, obtained with the preliminary study, show the importance of measurements containing adequate dynamics for the robustness of the identified reduced models. Besides, the best predictions were reached by estimating a 2nd-order model with only one week of data. This simple and easily manageable grey-box model extracted, was a good starting point to ponder the applicability of lumped parameters modelling in a real case, by extending the procedure in terms of complexity and inputs for the system. Further evaluation could be done on the modular implementation of the modelling procedure at a larger scale, classifying based on the modelling results different building types.

4.3 Development of the identified procedure in a real case study

4.3.1 Case study description

The monitoring campaign took place in one of the buildings (Polo Eustachio) composing the ensemble of the university polyclinic in Ancona (Italy). Polo Eustachio was built in the ‘90s to accommodate the medical school’s offices, classrooms and library. It is a multi-storey complex (6 floors, of which one is the basement) developed on two longitudinal blocks with a rectangular ground plan (Fig. 4.7a). The building represents a common case study for thermal discomfort, testified by its users. In fact, on the heliothermic axis are the fully-glazed façades (Fig. 4.7b and Fig. 4.7c), responsible of the overheating phenomena. The experimental activity took place on the third floor of the south block of the building. In particular, the development of the modelling procedure regarded a 3.70m x 5.64m x 3.00m south-exposed office room, currently in use by the staff, which is

representative of the local discomfort affecting the users, see Fig. 4.8. The double-glazed window of the office is split in three modules by aluminium uprights for a total area of 3.50m x 1.67m. A 1-metre high, shielded and insulated panel runs from floor level, juxtaposed to the internal side of the glass, to mitigate the energy loss through the façade: it consists of a 6-mm thick prepainted steel sheet and 55mm of hot-injected polyurethane foam at the interface with the window. In this way, the local thermal transmittance drops from 2.8 W/m^{2}K to less than 0.5 W/m^{2}K (thus reducing the magnitude of the overall heat transfer through the façade) and the penetration of solar beams is dampened. Yet, no remarkable relief to the overheating is provided since just a small portion of the indoor surface stays cooler throughout the day: the twilight zone reaches significative dimensions right approaching the sunset, thus not affecting the hours of maximum radiation. More details of the glazed façade and the walls' composition are given in APPENDIX B.

Fig. 4.7 a) satellite localization, b) view of the south fully-glazed façade, c) view of the interiors.

Fig. 4.8 The test room: views of the office 90 on the third floor.

Every block is served by a different conditioning and regulation system, even though the central plant is the same for the whole building. Three air handling units (AHU) are installed on the roof for mechanical air supply in the top three floors; seven AHUs are installed on the ground floor for mechanical air supply in the classrooms; lastly, variable air volume (VAV) systems are located inside the ceiling of the laboratory rooms and other open spaces of the 3rd, 4th and 5th floors. Hot and chilled water is provided by a central heating and a cooling plant, located, respectively, in the basement and on the roof. The testing office, like the other ones, is served by a horizontally recessed fan coil unit (FCU), which is installed inside a false-ceiling provided at the top by a vertical grid for the air supply and at the bottom by a horizontal grid for air return (Fig. 4.9). The FCU is connected to one of the three rooftop Air Handling Units (AHUs) supplying mechanical air to the top three floors: the primary stream (external air treated by the AHU) mixes with the secondary stream (return air, recirculated and conditioned by the room coil) in a dedicated plenum box attached directly to the supply outlet of the FCU, where the velocity pressure drops and equalize, the combined airflow gets uniformly dispersed and the momentum stabilizes. Thanks to such plant configuration the fresh and return air mixing is facilitated and both sensible and latent loads are controlled.

a) b)

Fig. 4.9 The false-ceiling before the sensors installation: a) external view and b) internal view of the FCU.

The technical specs of the FCU are summarized in APPENDIX C. The original operation of the 3-speed centrifugal fan was manual, exerted via a local thermostat.

4.3.2 Definition of objectives

This paragraph is aimed at the complete explanation of the approach adopted to derive grey-box models, in particular for existing buildings, by applying the procedure in a real case study.
Hence, the main objective is the identification of a suitable grey-box model to be implemented in the model-based predictive control that it will be described in detail, in Chapter 5.
Moreover, a second objective is to provide useful data from the monitoring campaigns carried out, in order to calibrated the detailed model built up, in another thesis, that will be exploited in Chapter 6 to realize the MPC for the case study in simulation environment.

4.3.3 Sensors identification and deployment

The Hobo sensor wireless network (APPENDIX A) was deployed along the third floor of the south block, where there is the office 90, that is the test room; meanwhile, other two sensors are positioned respectively on the second and fourth floor, vertically corresponding to the testing office, as to monitor the boundary conditions, according to previously considerations (par. 4.2.4). In addition to the RC-network logic analysed before, the layout of the network nodes was also conditioned by the availability of electrical outlets, necessary for the operation of the routers (with batteries only for the backup function). Furthermore, since one of the monitoring objectives was the identification of a reduced model for the office, object of study, it has been necessary to concentrate the equipment close to and inside the test room. The central component of the network architecture was a receiver connected to a PC via USB cable, both located in room 90. The Hoboware Pro Software was installed in the pc for configuring, monitoring and downloading the acquired data (Fig. 4.10).

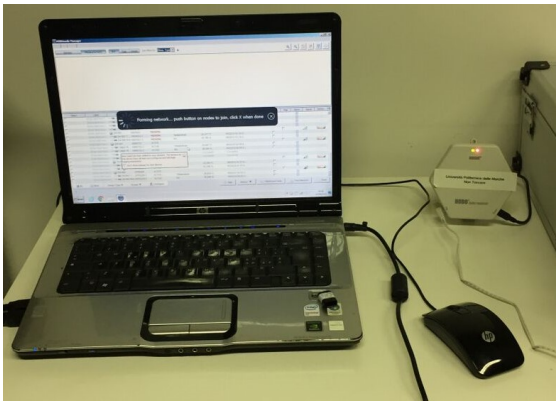

Fig. 4.10 The configuration of the sensor network by means of Hoboware Pro Software and the receiver connected via USB cable to the PC

Subsequently, the router backbone was settled, consisting of five devices: two Hobo Data Routers, three Hobo Data Nodes that were used in router function to increase data transmission stability in relation to the environments to be monitored. A Data Node Router was placed inside the office (Fig. 4.11a) and three other routers along the corridor to the west of the test room (Fig. 4.11b). One last router was placed about halfway of the east corridor, always referring to the test room.

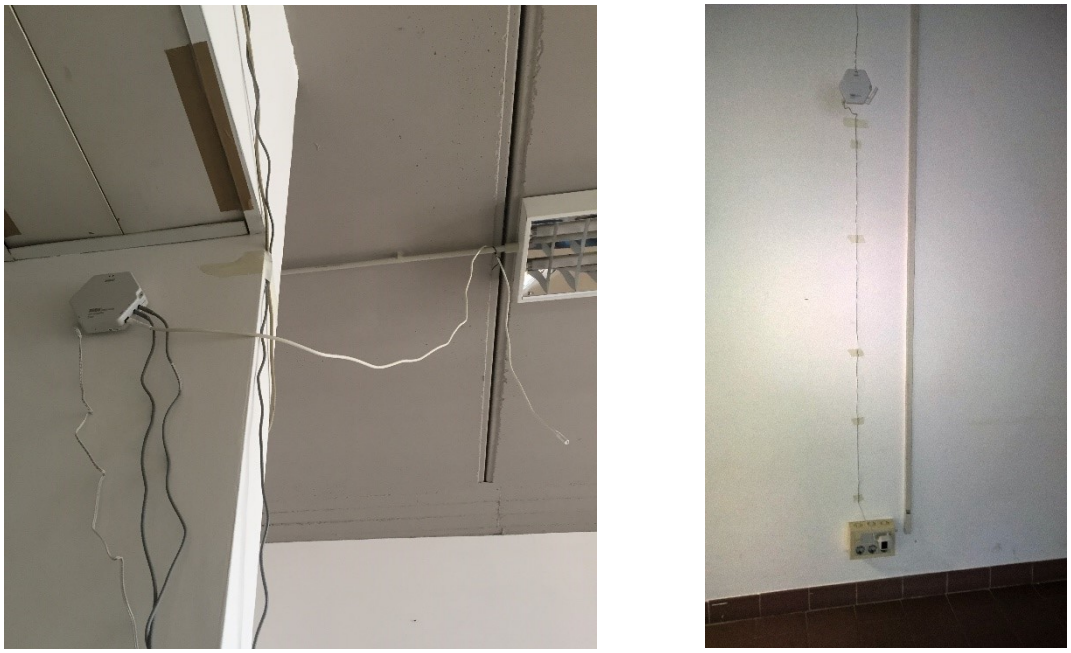

a) b)

Fig. 4.11 a) router installed inside the test room and b) one of the routers placed along the west corridor.

Connected to routers, battery-powered ZW-003 Data Nodes were the end network terminals, which captured temperature and relative humidity data by every minute and transmitted them to the nearest router with a 10-minute logging interval. Then routers transmitted data in turn directly to the receiver in the testing office. Four of these nodes were of the ZW-007 type, namely equipped with an external temperature probe and two additional analogue ports to connect analogue inputs. This latter aspect was exploited for the Data Node-Router placed at the entrance of the test room, using two additional analogue inputs: one to monitor the flow temperature of the duct of the AHU section and the other connected to an anemometer to measure the air velocity entering the room from the same duct (Fig. 4.12).

a) b)

Fig. 4.12 Devices installed in the plant ducts to monitor the supply air flow: a) during the summer campaign and b) the winter campaign.

This configuration was kept for the summer campaign and changed during the winter season by replacing the anemometer with a temperature probe for monitoring the supply air flow of the FCU. Three Data Nodes of the same type were installed: two in other offices of the third floor and one on the second floor in vertical correspondence with the testing area. Other ZW-003 Data Nodes, always with integrated T-RH sensor, were placed in other third-floor offices and one on the fourth floor vertically aligned with the room to be monitored. A complete map of the installation, extracted from the Hoboware Pro Software, is provided in Fig. 4.13.

Finally, a weather station was installed on the roof of the fifth floor (Fig. 4.14), positioned in correspondence to one of the transverse blocks, which link the two-longitudinal north/south blocks of the building. This zone was chosen because no obstructions were there and only authorized persons could access. Main components of this microclimatic control unit were:

- Temperature and Relative humidity sensor, a thermo-hygrometer. The thermosensitive element was a Pt100 thermal resistor, while the hygrosensitive one was an hygrocapacitous platter. Sensitive elements were protected by incident solar radiation by means of a double anti-radiation shield. The interior screen contained sensitive elements, while the outer one is a further protection consisting of a series of high reflective white fins.
- Wind speed and direction sensor, a tacho-gonianemometer.
- Global solar radiation sensor, a pyranometer. A white shield protected the probe from the overheating, while a capsule, containing hygroscopic salt, avoided damaging condensation ensuring the sensor operation in dry air.

Acquisition and processing of data were carried out via an E-Log that allowed timely programming of the acquisitions, setting of the measurements start, of the surveys frequency and their duration. Data transfer power cables, connected to the control unit, entered the building via the door on the back of the weather station, then they arrived in a technical room, provided by a data acquisition PC directly connected to the Data Logger.

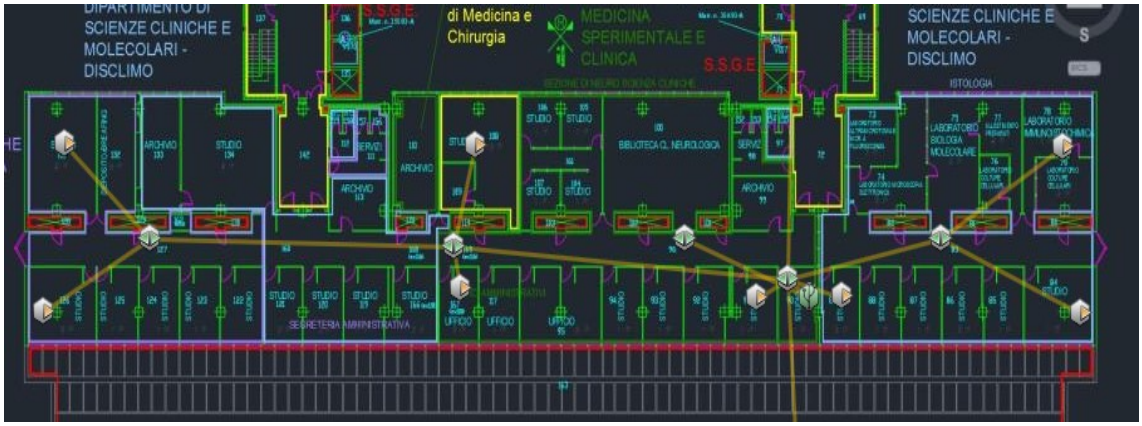

Fig. 4.13 The map of the Hobo sensors network installed on the third floor

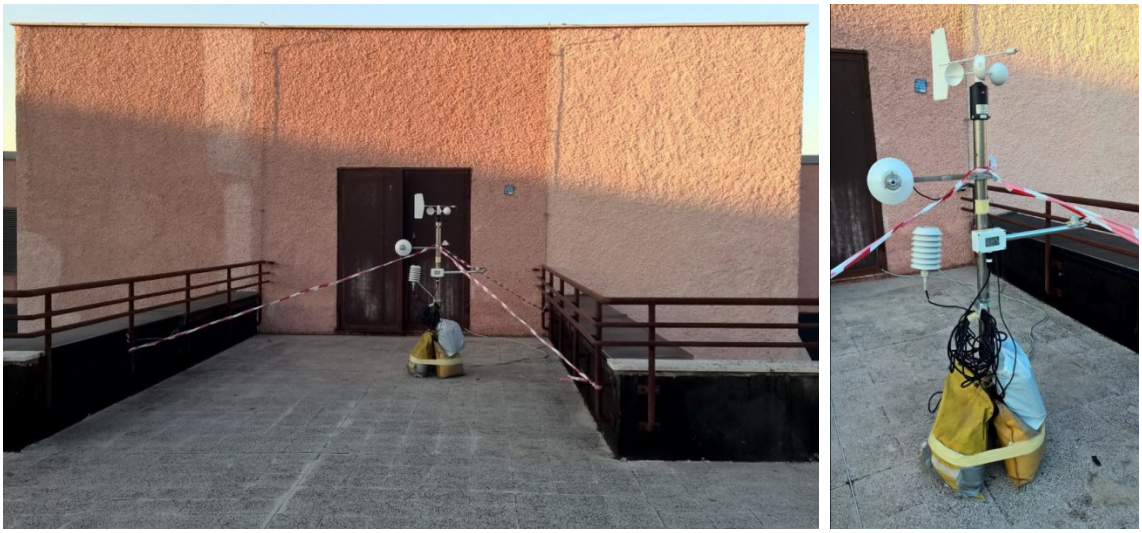

Fig. 4.14 The weather station installed on the roof of the building

Finally, two solar radiation (silicon pyranometers) sensors were placed, fixed to a tripod, near the window of the room (Fig. 4.15) as to monitor the solar radiation actually entering the test room. The devices, one orthogonal and one parallel to the glazed surface, were connected to a Data Logger. The Data Logger, placed in the test room, was electrical powered. The data acquisition range was the same as the wireless network as well as the software used to download the data.

Fig. 4.15 The two pyranometers installed in the test room

In addition, to support the modelling process in terms of data set for parameters estimation, the simulations of the detailed model and the implementation of the advanced control, two weather services were used:

A web site that detects weather conditions in real time, with advanced features such as user geolocation, interactive radar, satellite maps and alerts in case of an emergency. The reliability of the information and weather forecasts are guaranteed by the processing of data from a large number of detection stations, positioned worldwide. To download hystorical weather data, you had to refer to the "Hystorical weather" section and enter the location of interest and the time period in which you want to acquire the data. The weather is detected by the weather station closest to the site selected. Once the data is downloaded, the capture file is saved as a text file so that it can be easily imported into excel. For this work, only the dry bulb temperature values were considered.

The SoDa Service is a broker to a list of services and webservices related to Solar Radiation proposed by several providers in Europe and abroad. In particular, the CAMS radiation service provides time series of Global, Direct, and Diffuse Irradiations on horizontal surface, and Direct Irradiation on normal plane (DNI) for the actual weather conditions as well as for clear-sky conditions. The geographical coverage is the field-of-view of the Meteosat satellite, roughly speaking Europe, Africa, Atlantic Ocean, Middle East (-66° to 66° in both latitudes

and longitudes). The time coverage of data is from 2004-02-01 up to 2 days ago. Data are available with a time step ranging from 1 min to 1 month.

4.3.4 The experimental campaigns and data elaboration

The data acquisition campaign started on 22/04/2016, however during the first weeks of acquisition, data were not so stable to be used for model estimation. Thus, first useful data referred to acquisitions of May. They were extracted from Hoboware Pro Software in a text format file (.txt) that was imported in Excel to be modify and cleaned of unnecessary data. In fact, Hobo ZW-series sensors return also dew point and relative humidity for each measurement that they were not considered in this dissertation. Only dry bulb temperatures were considered for the modelling procedure. Besides, temperatures codified by sensors number were renamed, identifying those ones useful for the reduced model estimation, following considerations done on the preliminary study (par. 4.2.4), thus discarding temperatures not affecting the room internal dynamics. Instead, the total data set of temperatures was employed for the calibration of the detailed model, that will be partly discussed in Chapter 6. Temperatures initially selected for the model identification are listed in Table 4.4.

Table 4.4: Temperatures from data acquisition used for the modelling procedure

Name	Sensor	Definition
yTi	RTR ZW-007(723)	Internal Temperature (office 90)
Tr*	RTR ZW-007(723-3)	Temp. Probe for AHU section
Tc	RTR ZW-003(743)	Corridor temperature (3rd floor)
Ta89	ZW-003(744)	Internal Temperature (office 89)
Ta91	ZW-003(634)	Internal Temperature (office 91)
Tp4	ZW-003(221)	Internal Temperature (office 76)
Tp2	ZW-007(722)	Corridor temperature (2nd floor)
Ta	Weather station	Outdoor Temperature

*another Temp. Probe for FCU section was added during winter campaign.

The temperatures choice is justified by the position of the test room (office 90), which is between office 89 and 91 and adjoining a corridor on north. Moreover, being on the third floor, the office 76 on the 4th floor and the corridor on the 2nd floor represent other two boundary conditions for the test room, together with the ambient temperature. In the end, supply air temperatures of the plant, both in summer and winter season, were used to calculate the power of the plant, input for the system in the modelling phase. In this regard, the calculation of the plant power is provided in APPENDIX D. Refer to this appendix for a complete in-depth explanation about calculation of indirect measures.
The temperature data measured by the Hobo sensors were acquired with a 1-minute time interval, so it was necessary to re-sample them with a wider interval to prevent a slowdown of the procedure due

to an overload of information being estimated. It was considered adequate a sampling interval of 5 minutes. This choice was also related to the weather station data of outdoor temperature (Ta) and global solar radiation (Ps) that were acquired every 5 minutes. At the same time, measurements values from internal pyranometers were re-sampled with the same time step.

At this point, it was possible to search and identify the suitable data set for every campaign, divided in the two main seasons because of different plant operation. The definition of the optimal data set will be the subject of the next two sub-paragraphs. Before dealing with the specific campaigns and for better understanding related choices, just some considerations on the formulation of the data set are provided. This aspect is not obvious for the modelling approach followed in this dissertation. In fact, deriving a reduced model from experimental data requires a relevant level of variability in system input dynamics, as already stated. It is sufficient underlining that best results in reduced-model identification, according to investigated literature, exploited PRBS signals in input to the system. Even if it is an impossible condition to be recreated in reality, also results of a parametric study, carried out simulating the reduced model of the preliminary study (par. 4.2), confirmed the goodness of this assumption. Another important aspect regards the length of the data set to achieve reliability in model estimations. In this regard, the same parametric study mentioned before revealed that the optimal length was a month to obtain a limited RMSE in simulation. However, in real operating, usually it is required to reduce data acquisition periods and concurrently a large data set does not represent a plus for computational algorithm in parameters estimation phase. Moreover, keep the extended length of data set and increase the sample interval it is not a good choice in order to get a reliable estimate, without modifying the real dynamics of the system. At the end, to choose the suitable data set for applying the modelling procedure it was decisive to consider the setting and real operation of the plant as well as avoiding drawbacks periods in acquisition, while maintaining a quite limited data set with adequate dynamics.

4.3.4.1 Summer campaign

During the summer campaign, a first collection of data used for a preliminary estimation of the test room thermal characteristics was carried out by means of May measurements. Anyway, during May 2016, the plant was set to off until the 17th. Then, from the 18th till the end of May, only the ventilation (referring to AHU section) was provided in the test room to guarantee air recirculation. For this reason, to have a complete outline of the internal dynamics of the testing area with the plant in summer mode, it was considered a second campaign, relative to data acquired during July 2016.

The choice of the dataset for July was based solely on data days that were reliable without failures in acquisition. Since the second half of July the system was affected by discontinuous problems of

capturing weather data, a week of data (3-10 July 2016) was found out as adequate data set within the rest of July acquisition, also considering results of previous campaigns. During this July campaign, it was planned the starting of the plant, according to the real schedule of the building, usually manually regulated with the following time interval:

- From Monday to Friday, from 7am to 7pm;
- On Saturday, from 7am to 2pm.

For the rest of time the plant was turned off, hence it was set a zero value in the columns of data set relative to Pr and Pc, which were the input powers of AHU and FCU sections, respectively. All the variables involved were re-sampled with a 5-minute sampling time and they are summarized in Table 4.5. Analysing Table 4.5 compared to Table 4.4, it is evident that some temperatures are not considered in the formulation of the data set, this because the missing temperatures turned out to be not significant boundary conditions for the thermal parameters estimation of the test office, as resulted in the first campaign of May. On the other side, variables added represented internal gains for the system, as will be more clearly explained in par. 4.3.5. Trends of the variables involved are provided in Figg. 4.16-4.23, for the period of interest. The trends of Pr and Pc are generated based on the calculation in APPENDIX D, as already anticipated in previous paragraph.

Table 4.5: Variables considered in the data set of the summer campaign.

Symbol	Measure unit	Definition
yTi	°C	Internal Temperature (office 90)
Tr	°C	Air supply temperature (AHU section)
Tc	°C	Corridor temperature
Ta	°C	Outdoor Temperature
Ps	kW/m^2	Solar radiation (weather station)
Psv*	kW/m^2	Solar radiation (internal pyranometer)
Pr	kW	Ventilation Power (AHU section)
Pc	kW	Cooling Power (FCU section)

*Psv is referred to the pyranometer inside the test room and positioned parallel respect to the window.

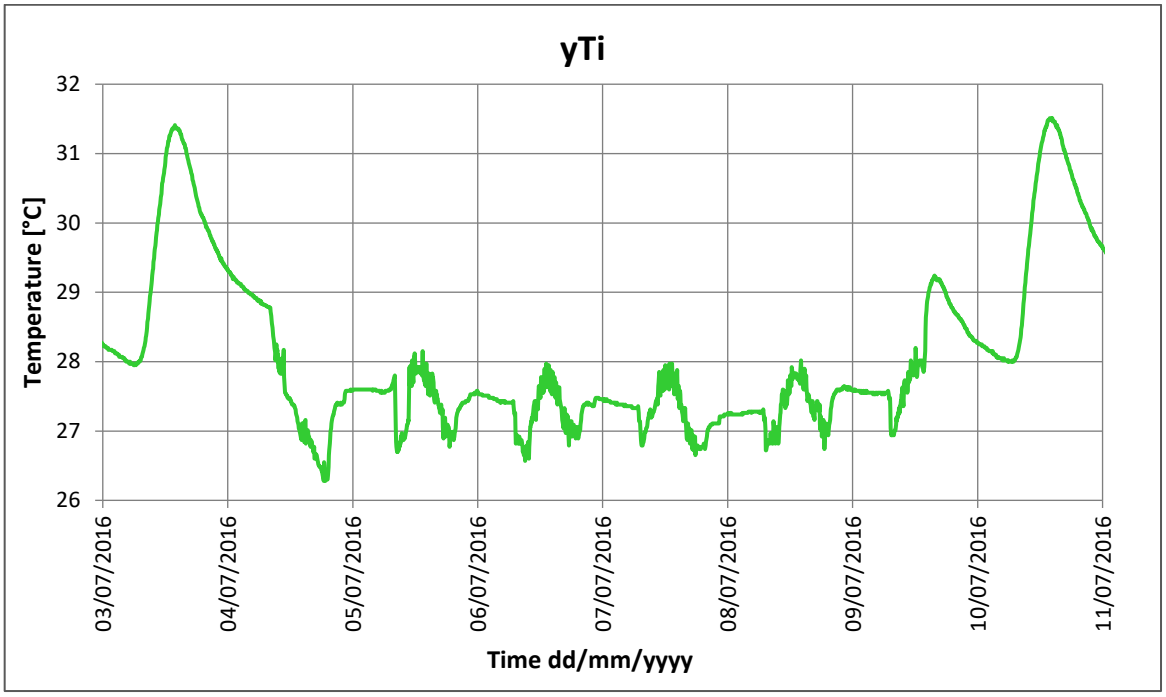

Fig. 4.16 Trend of the internal temperature of office 90, the test room.

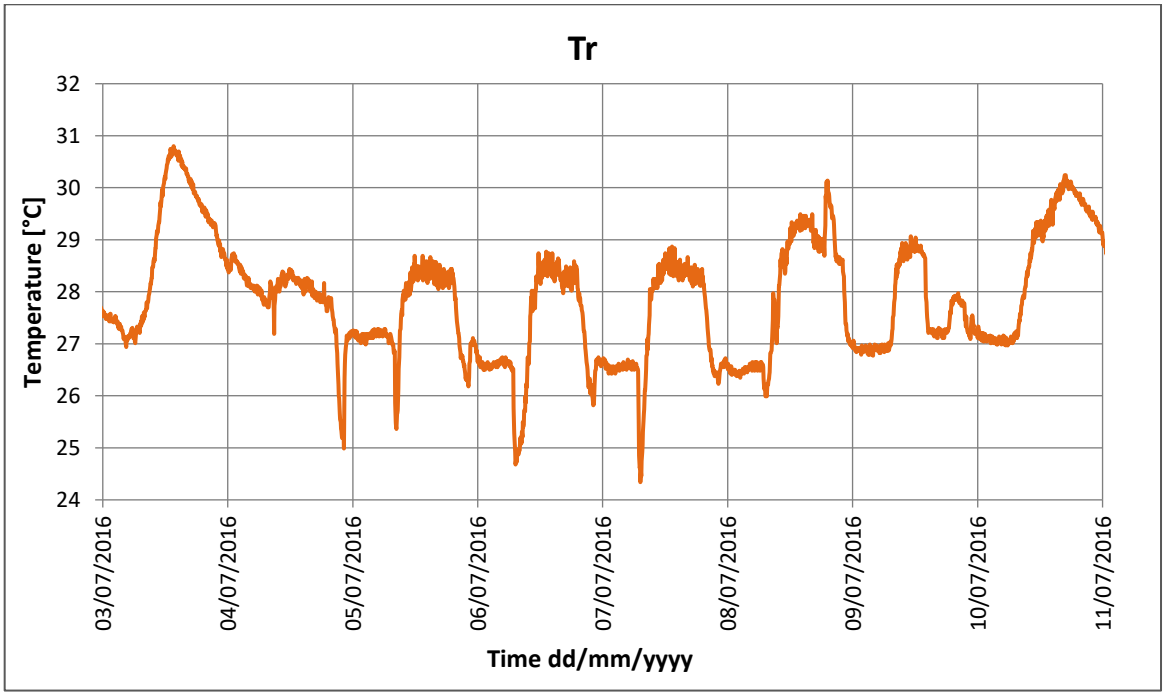

Fig. 4.17 Trend of the outlet air temperature from the ventilating section in the false-ceiling of the test room.

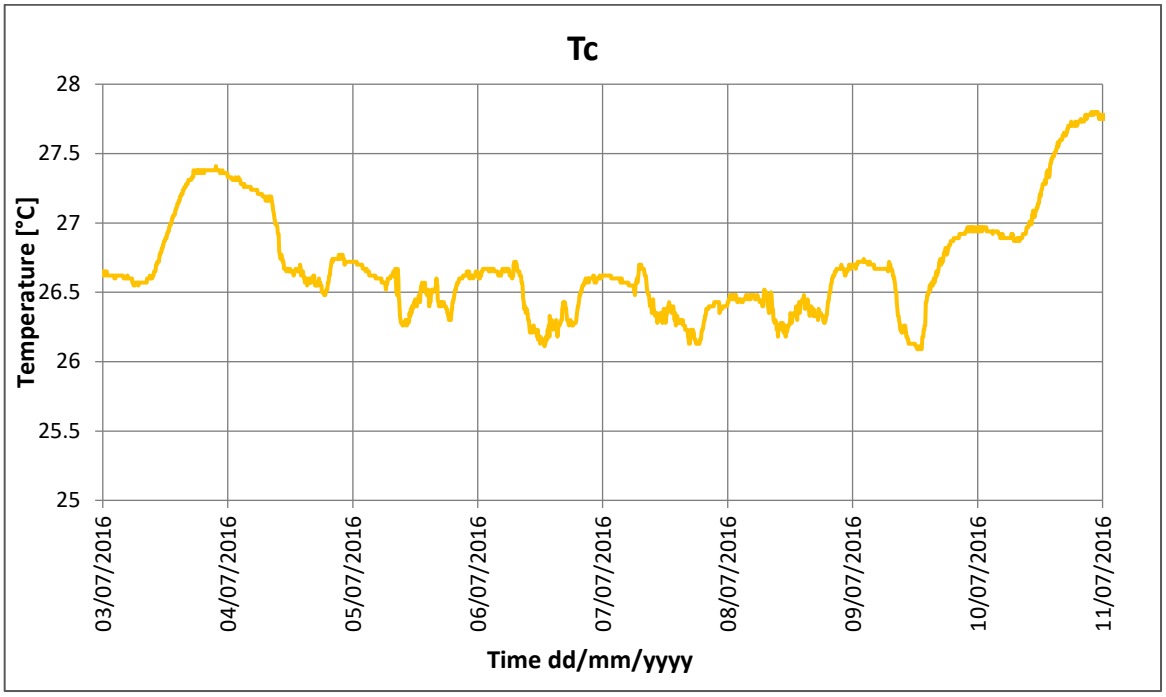

Fig. 4.18 Trend of the corridor temperature, in front of the testing office.

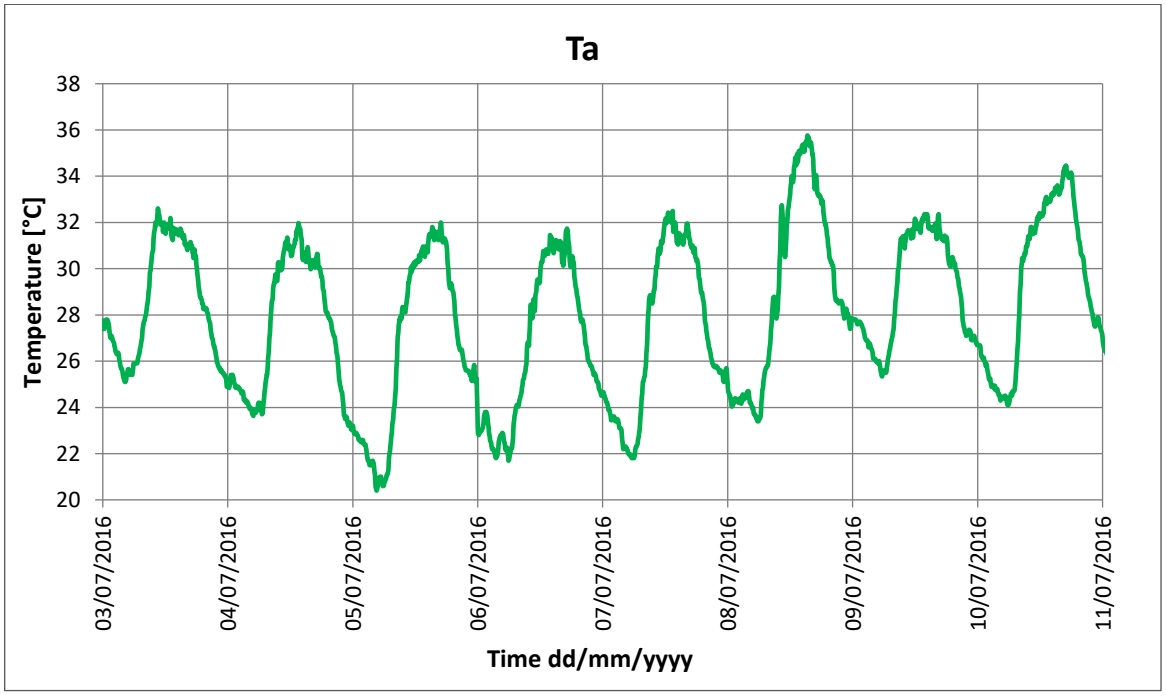

Fig. 4.19 Trend of the outdoor temperature, measured by the weather station on the roof.

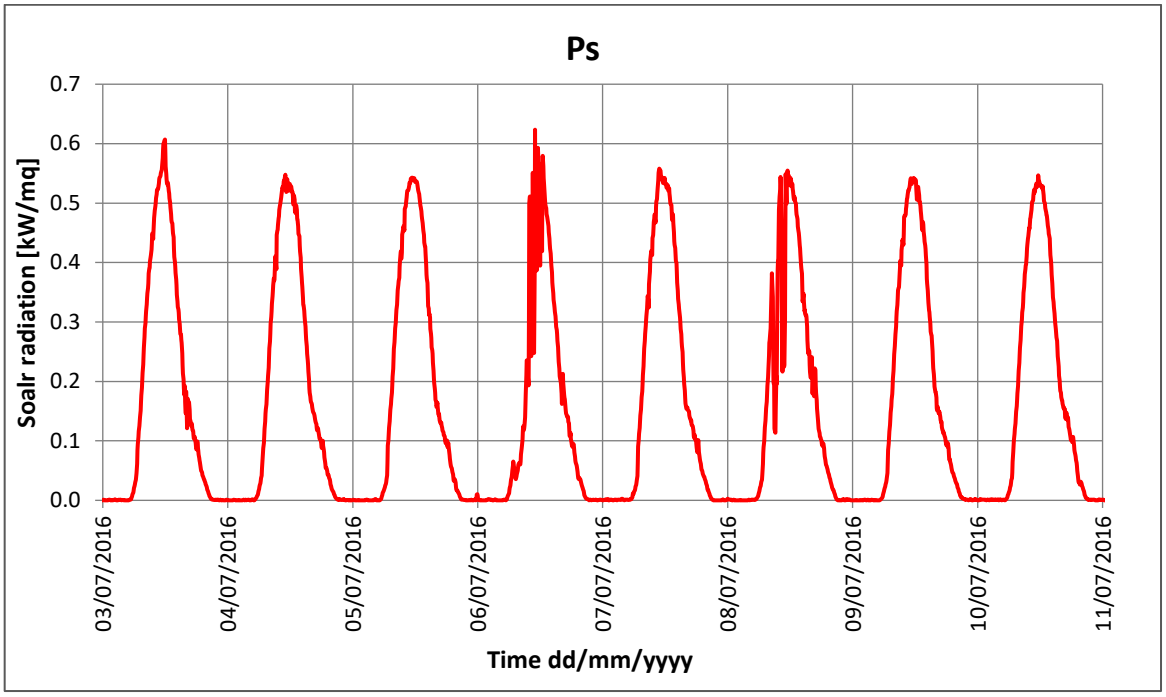

Fig. 4.20 Trend of the global horizontal radiation acquired by the weather station.

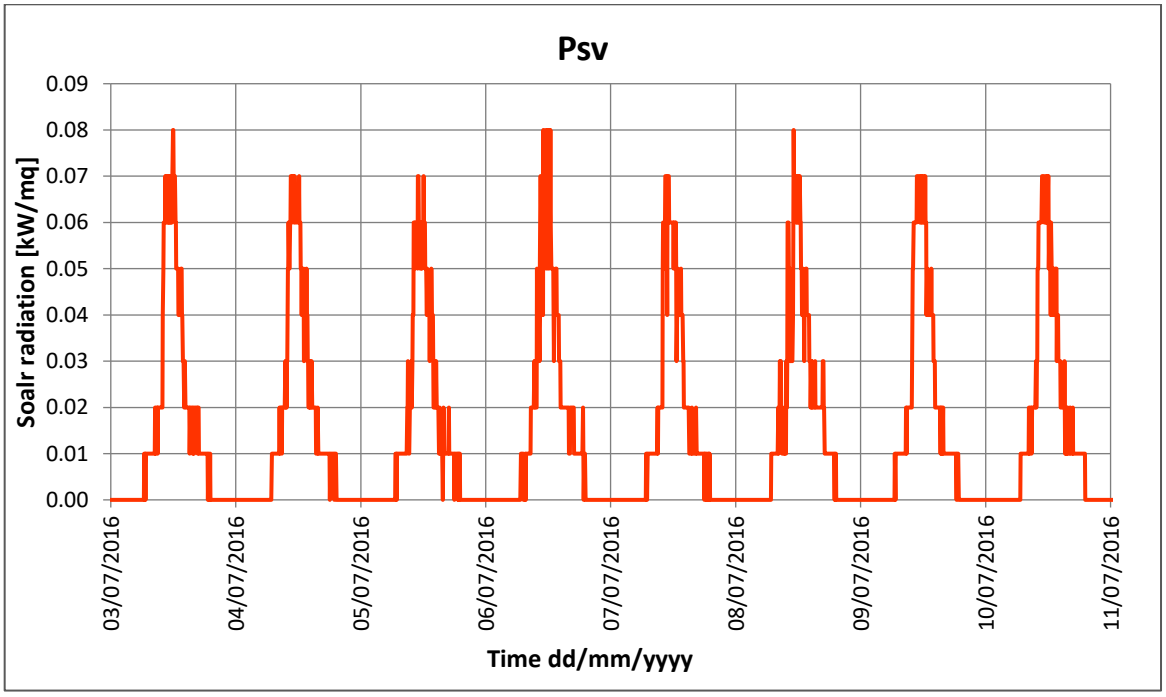

Fig. 4.21 Trend of the solar radiation acquired by the internal vertical pyranometer.

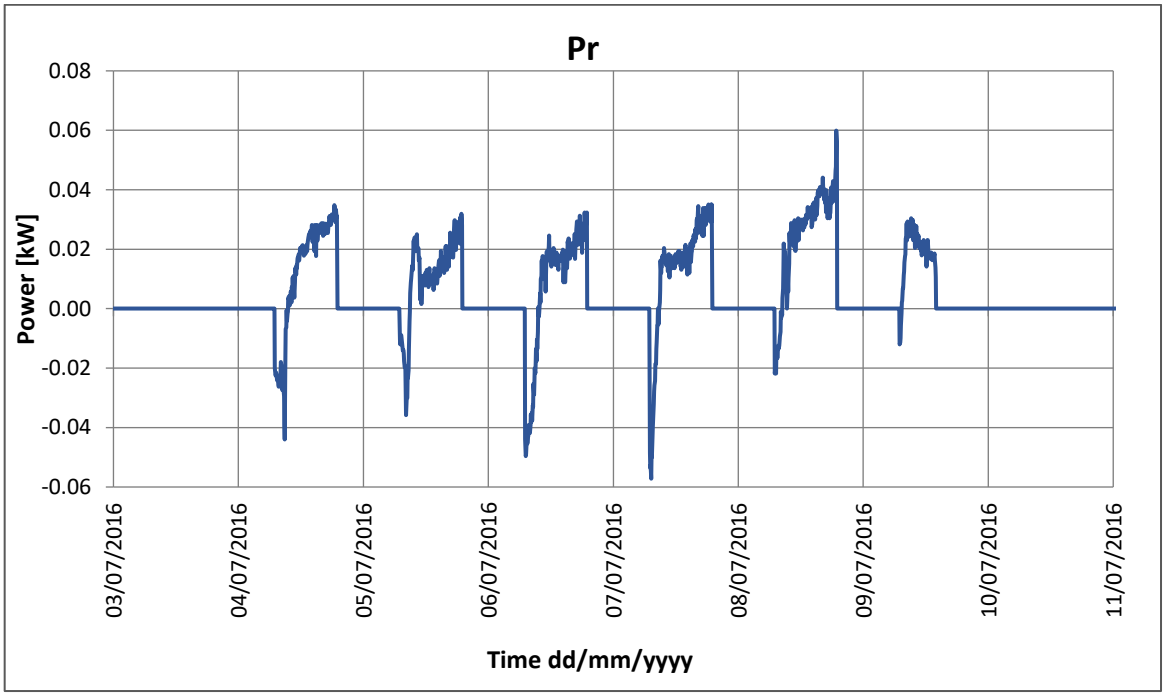

Fig. 4.22 Trend of the ventilation power during the selected summer campaign.

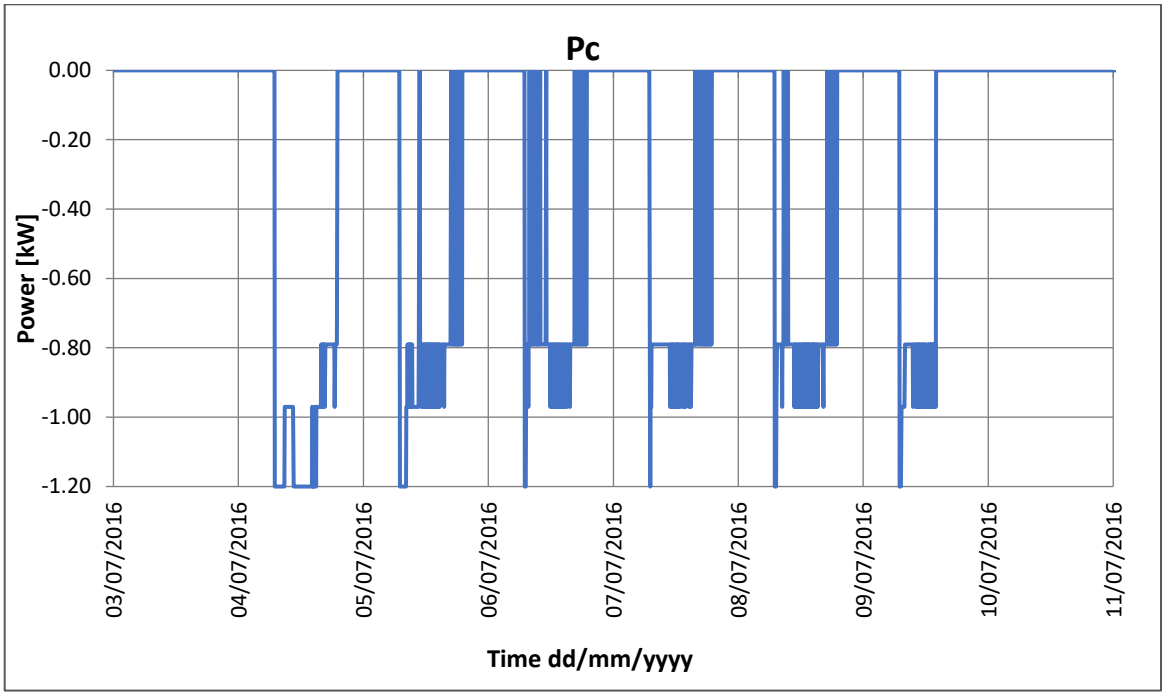

Fig. 4.23 Trend of the cooling power during the selected summer campaign.

4.3.4.2 Winter campaign

The winter campaign began in the second half of November and, exploiting knowledge acquired during the summer campaigns, suitable data for the winter estimation were chosen taking into account stability of data, lack of interruptions and the full operation of the plant in winter mode. Thus, the adequate collection of data was identified in measurements from 21st to 26th of November 2016. It is appropriate to report that during the winter campaign, the Hobo sensor monitoring the internal temperature of the test room was moved in the centre of the office, next to the user workstation. During this November campaign, it was planned the starting of the plant, according to the real schedule of the building, usually manually regulated with the following time interval:

- From Monday to Friday, from 7am to 7pm;
- On Saturday, from 7am to 2pm.

Unlike the previous campaign, data set columns relative to Pr and Ph, which were the input powers of the system plant, were calculated starting from the measurements of air supply temperatures for each plant section, that is the ventilation and heating units. The calculation procedure is the same mentioned for the summer campaign and provided in APPENDIX D. Then, all the variables involved were re-sampled with a 5-minute sampling time and they are summarized in the Table 4.6. Trends of all variables acquired by the sensors network are presented in Figg. 4.24-4.27, concerning the data set period identified. The weather station data were not available in this period, thus the weather data downloaded from the Weather Underground web site (Figg. 4.28-4.29), were used for the parameters estimation of the winter reduced model. About the absence of the internal pyranometer values, this was due to considerations made during modelling, see par. 4.3.5.1. Lastly, the power trend of the plant, represented by the Pr and Ph calculated, is provided in Figg. 4.30-4.31 for the interest period.

Table 4.6: Variables considered in the data set of the winter campaign.

Symbol	Measure unit	Definition
yTi	°C	Internal Temperature (office 90)
Tr	°C	Air supply temperature (AHU section)
Tf	°C	Air supply temperature (FCU section)
Tc	°C	Corridor temperature
Ta	°C	Outdoor Temperature (Weather Underground)
Ps	kW/m^2	Solar radiation (SoDa service)
Pr	kW	Ventilation Power (AHU section)
Ph	kW	Heating Power (FCU section)

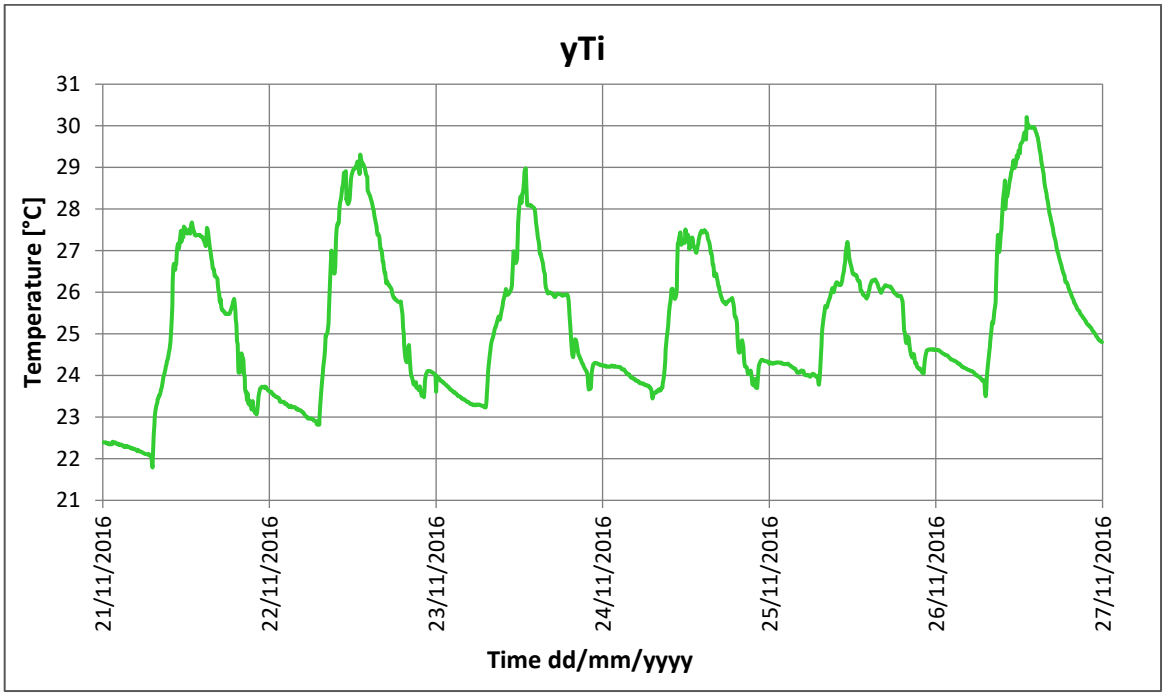

Fig. 4.24 Trend of the internal temperature of office 90, the test room.

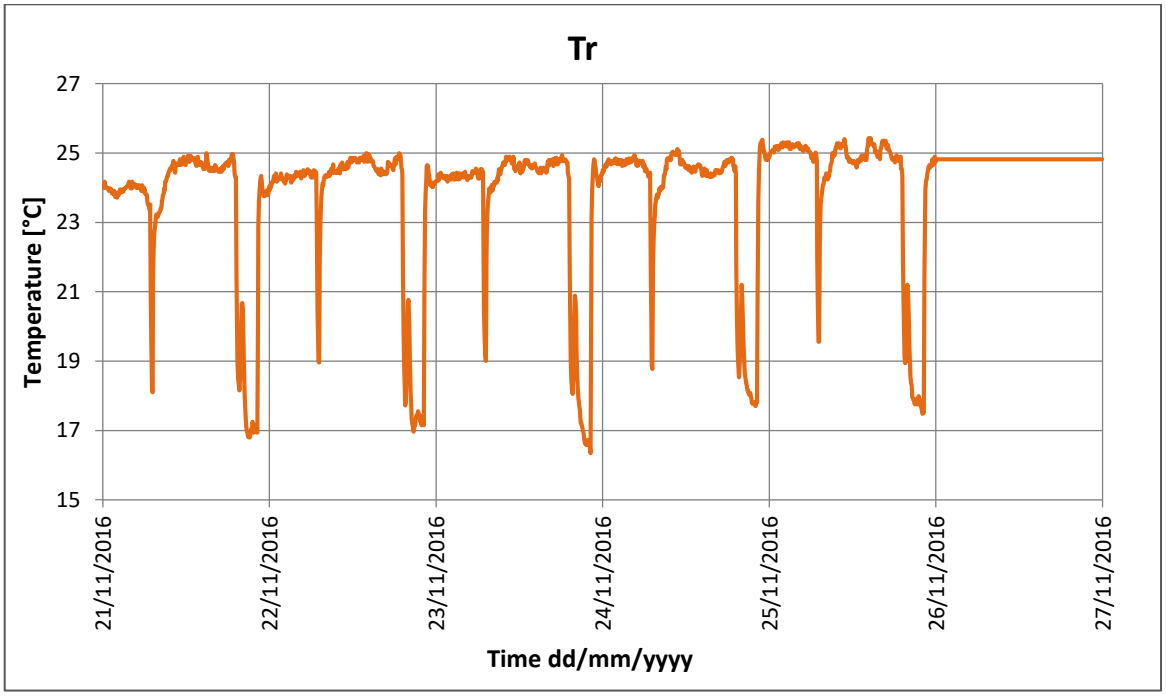

Fig. 4.25 Trend of the outlet air temperature from the ventilating section in the false-ceiling of the test room.

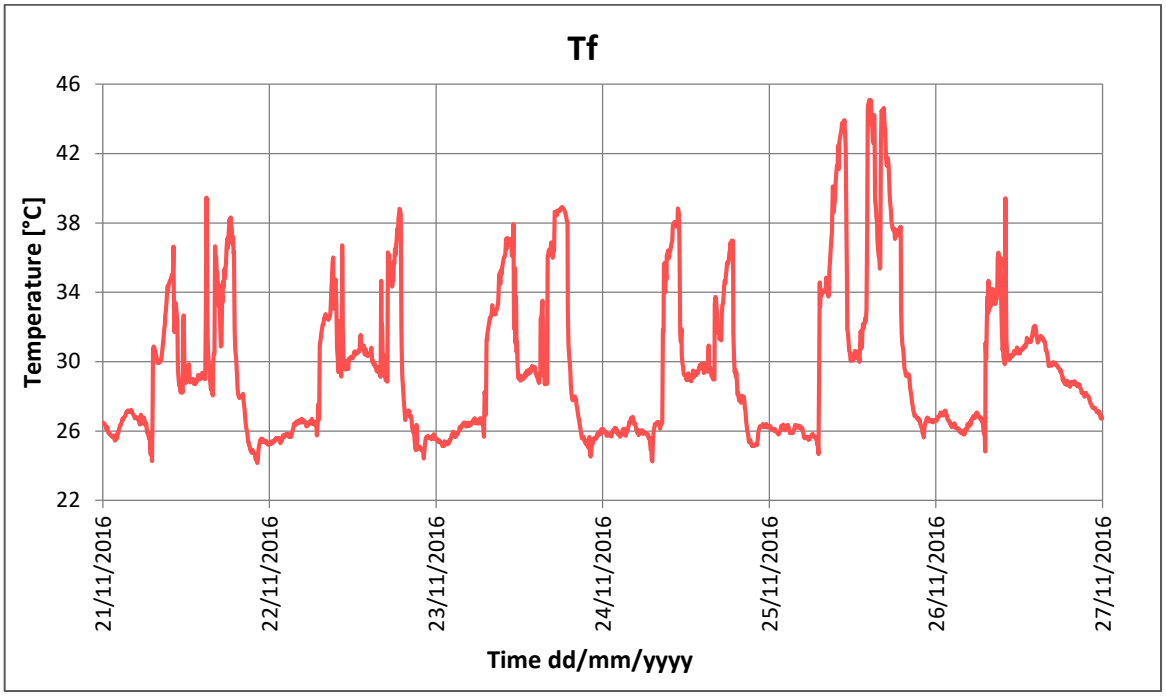

Fig. 4.26 Trend of the outlet air temperature from the heating section in the false-ceiling of the test room.

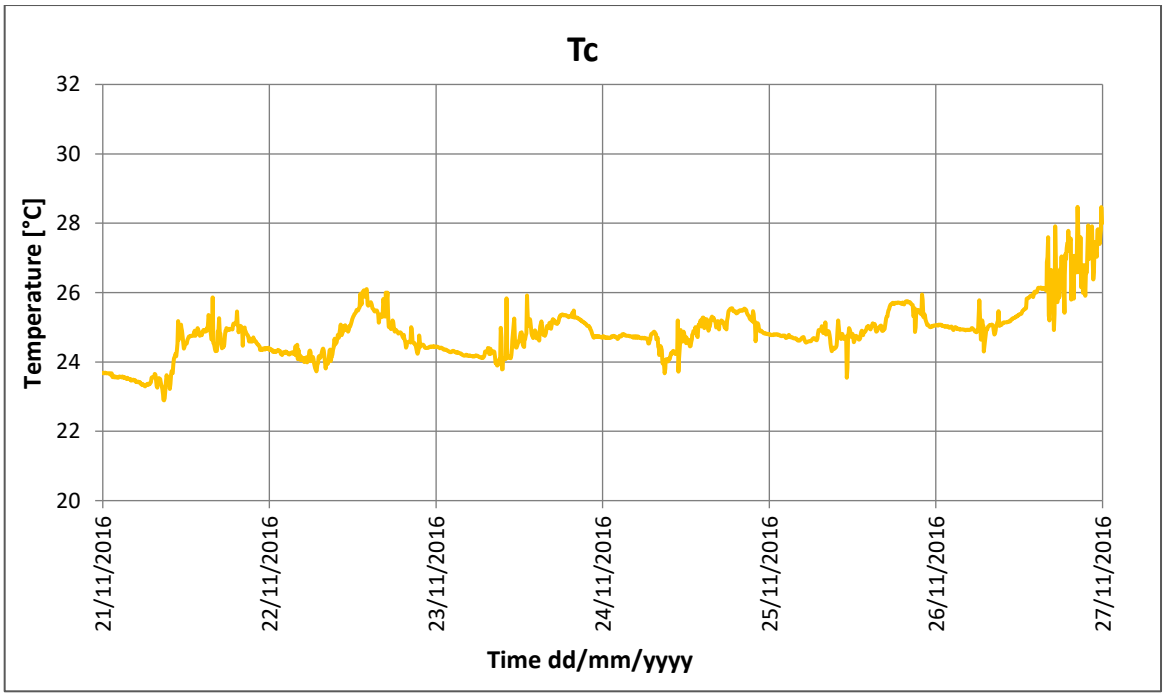

Fig. 4.27 Trend of the corridor temperature, in front of the testing office.

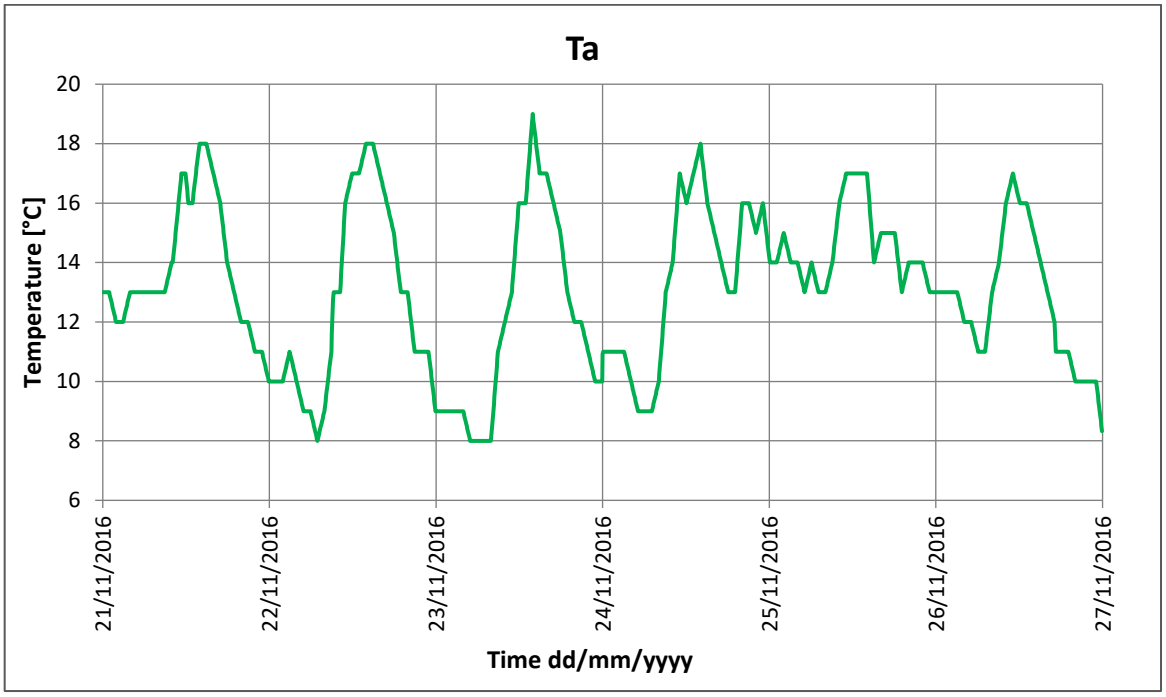

Fig. 4.28 Trend of the outdoor temperature, according to data from WU web site.

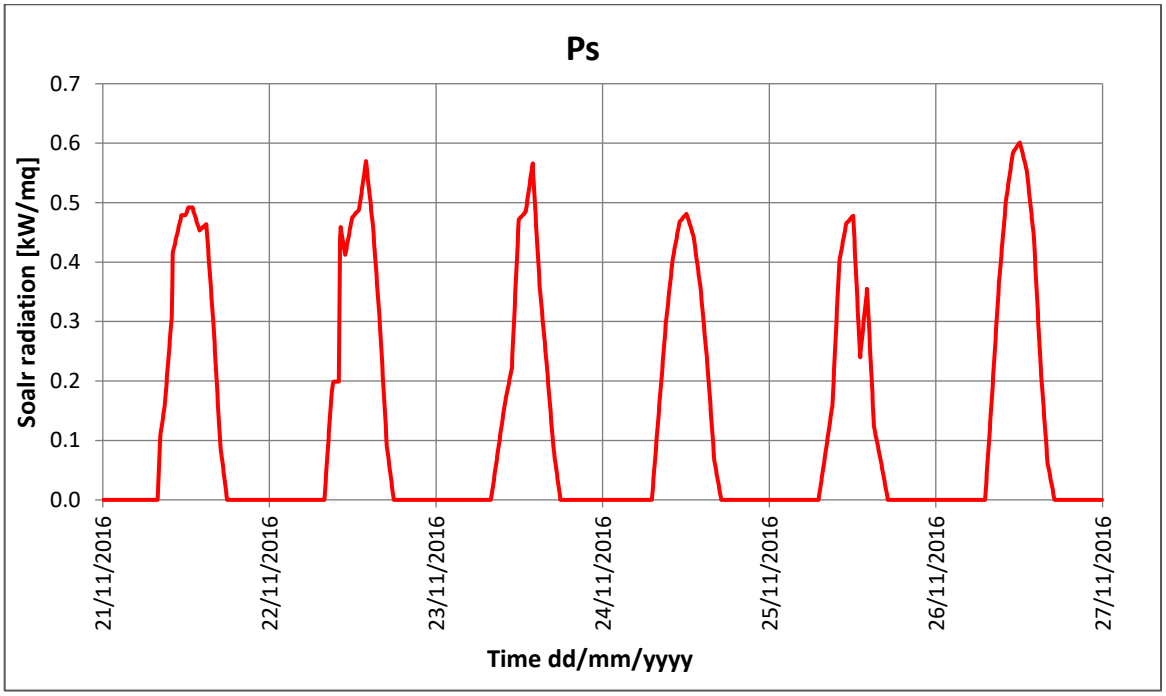

Fig. 4.29 Trend of the global solar radiation, according to data from CAMS radiation service of SoDa web site.

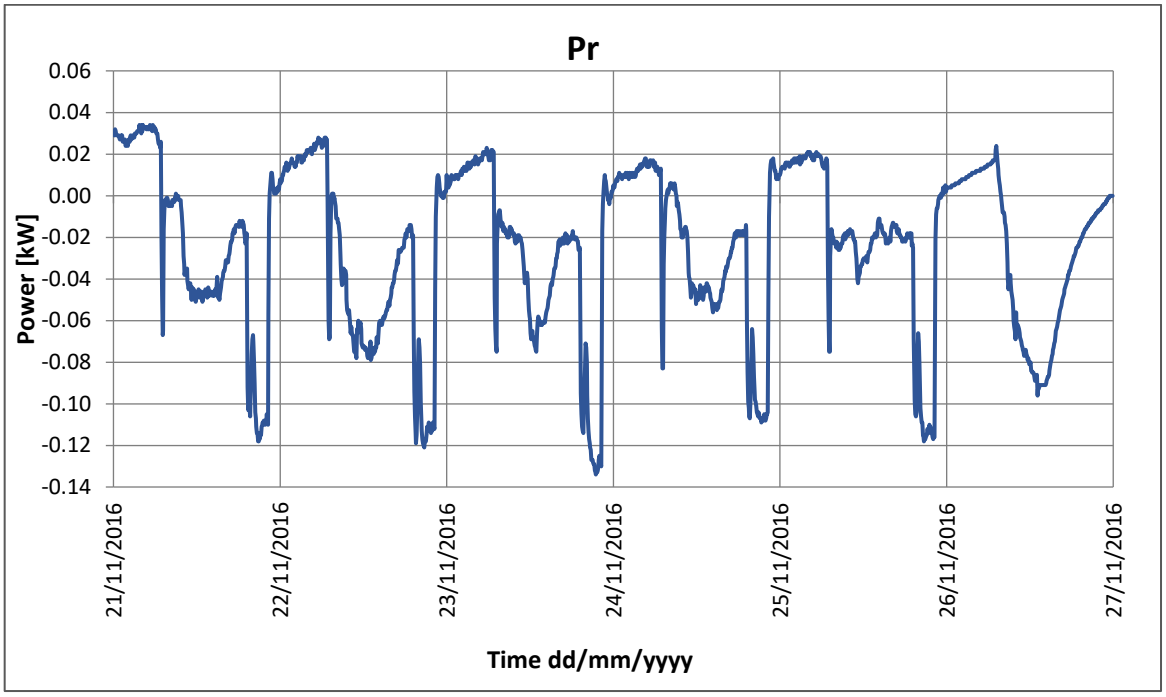

Fig. 4.30 Trend of the ventilation power during the selected winter campaign.

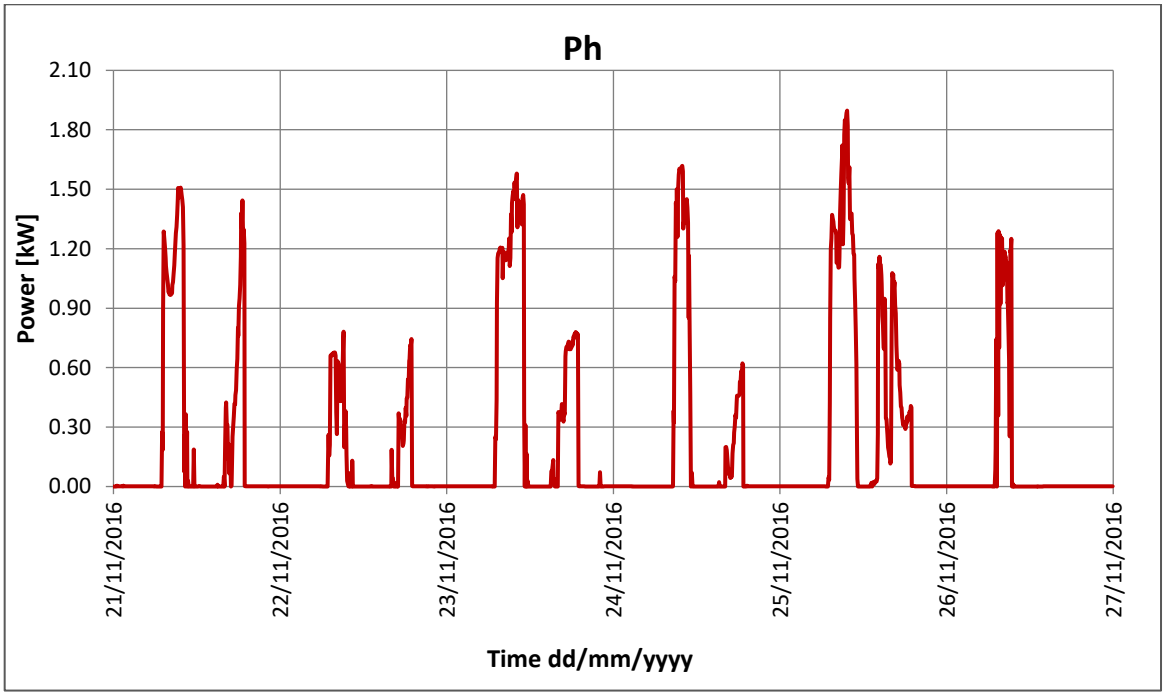

Fig. 4.31 Trend of the heating power during the selected winter campaign.

4.3.5 The Grey-box modelling

In order to derive suitable reduced-order models to be implemented in advanced controls, a grey-box modelling approach was followed, starting from the analysis of relevant applications in literature. Madsen's work was the main reference for the develop of the procedure, as underlined in Chapter 2. Thus, first of all, it is fundamental to create a script that must be processed by the statistical software R, using the CTSM package for the parameters estimation. The data sets provided in each estimation were the ones defined in the previous section. The structure of a grey-box model requires a prior system physics knowledge to include the dynamics involved. Generally, to define the most appropriate RC-network, the simplest model structure is considered, as partly explained in the preliminary study (par. 4.2). Then, the corresponding system equations are inserted in the script. After running of each estimation, results are evaluated in terms of parameters values estimated, residuals, root mean square error (RMSE) and verifying the validation parameters in R. Until enhancements in estimates are recorded, the procedure is repeated, changing conveniently the structure or parameters settings. Thereafter, when the model is substantially stable in terms of parameters estimates and the RMSE values are acceptable, the modelling phase stops and the identified reduced-model can be validated, with the procedure presented in par. 4.3.6. In the next two sub-paragraphs, the best model for each season will be mainly discussed, whilst the grey-box modelling, summarized above, is explained in depth in the APPENDIX E, examining step-by-step the script used by the identification procedure.

4.3.5.1 The Grey-box model for the summer season

The model for the summer season is derived by data of July campaign (par. 4.3.4.1). Anyway, the first campaign of May, when the plant was not fully operating, served to gain familiarity with the statistical software and define the adequate script. Moreover, by the first estimates, it was possible to identify main variables affecting thermal dynamics of the testing area and, consequently, discarding useless data and sensors providing redundant system information. Therefore, based on the results of the previous campaign, a second order model was initially considered. The outdoor temperature and the corridor temperature were identified as boundary conditions for the system, discarding temperatures of the other neighbouring areas, because they did not affect significantly the internal temperature trend of the office 90. To manage both boundary temperatures at the same time, a coefficient "K" was included in the equation of the state "Te" for linearly combining the two temperatures. This coefficient represented an added parameter to be estimated. Differently from the May campaign, in addition to the internal gain of Pr, was added the Pc, cooling power, as direct gain for the system under investigation. Since there was no user in the room, the internal gain for

occupancy was zero, but the heat gain from equipment installed in the test room must to be considered. Thus, it was put into the model equations as Pf and added to the parameters to be estimated by the CTSM-R software. After that, some attempts were made to return the best grey-box model verifying results according to the considerations explained in APPENDIX E, especially evaluating the best correspondence in simulation with measured data, that was translated as the lowest RMSE value. Six different models were considered, four second-order models and two third-order models, refer to (Bolognini, 2016) for the complete study of each model. Testing a greater complexity was justified by the introduction of the input gain Pc, however models resulted over-parameterized. The added heat capacity in the third-order models represented a further subdivision of the envelope to separate Tc and Ta (MOD 4-5). The differences between second-order models concerned: the choice of radiation for the data set between the data of weather station and those of internal pyranometer (MOD 1), the use of the Tr plus an associated resistance Rir (MOD 2) versus a direct power input Pr, the introduction of a solar gain (MOD 3) affecting the envelope surface (Ae*Ps) in addition to that acting directly indoor (Aw*Ps). At the end, the grey-box model that demonstrated to be more stable and reliable for the summer season was the 2C2R model presented below in its structure (Fig. 4.32) and relative system equations (Eq. 4.11-4.12). Only a solar gain, affecting internal temperature, was considered (Aw*Ps), whilst Ta and Tc were linearly combined by means of the K coefficient. Finally, powers for the plant and data from the weather station were used. For the best model, parameters estimates are provided in Table 4.7, final temperature and residuals plots in Fig. 4.33, whilst cumulated periodogram and RMSE values in Table 4.8. Different root mean square errors (RMSE) were calculated connected to a different time interval by considering that 1-step interval was equal to 5 min, according to the data set created. These values could be useful for the definition of the prediction horizon within the design phase of the model predictive controller. The last value in Table 4.8 is the RMSE in simulation. Results of other models tested for the summer season are presented in Table 4.9, in terms of cumulated periodogram and RMSE value in simulation.

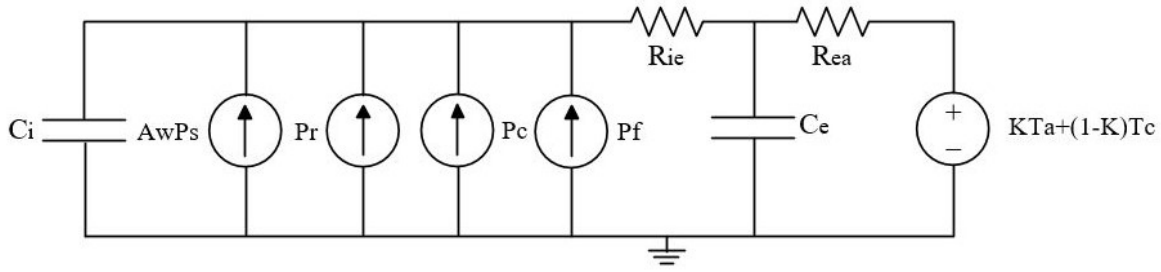

Fig. 4.32 The best grey-box model of the summer season: structure of the 2C2R model.

First-order stochastic differential equations implemented in the script for the parameters estimation:

$$dT_i = \frac{1}{\mathrm{R}_{ie}\mathrm{C}_i}(\mathrm{T}_e - \mathrm{T}_i)\mathrm{dt} + \frac{1}{C_i}P_r\mathrm{dt} + \frac{1}{C_i}P_c\mathrm{dt} + \frac{1}{C_i}P_f\mathrm{dt} + \frac{1}{C_i}A_wP_s\mathrm{dt} + \sigma_i\mathrm{d}\omega_i \quad (4.11)$$

$$dT_e = \frac{1}{\mathrm{R}_{ie}\mathrm{C}_e}(\mathrm{T}_i - \mathrm{T}_e)\mathrm{dt} + \frac{1}{\mathrm{R}_{ea}\mathrm{C}_e}(\mathrm{KT}_a + (1-\mathrm{K})T_c - \mathrm{T}_e)\mathrm{dt} + \sigma_e\mathrm{d}\omega_e \quad (4.12)$$

The output equation for the system is represented by the discrete time measurement equation, already seen in the preliminary study (Eq. 4.9).

Table 4.7: Results of the parameters estimation for the best model of the summer season.

Parameter	Estimated value	Pr(>|t|)	dPen/dPar
Ti0	2.8250e+01	0.0000e+00	0.0000
Te0	2.7324e+01	0.0000e+00	0.0000
Aw	1.9978e+00	0.0000e+00	0.0000
Ce	4.0914e+00	5.7573e-03	0.0000
Ci	8.6999e-01	0.0000e+00	0.0000
e11	-7.1820e+00	0.0000e+00	0.0000
p11	-1.7811e+00	0.0000e+00	0.0000
p22	-1.0365e+01	4.5262e-04	0.0000
Pf	2.1363e-01	2.6478e-10	0.0000
Rea	2.1345e+00	2.0331e-03	0.0000
Rie	3.3185e+00	0.0000e+00	0.0000
K	3.8102e-02	2.1947e-01	0.0000

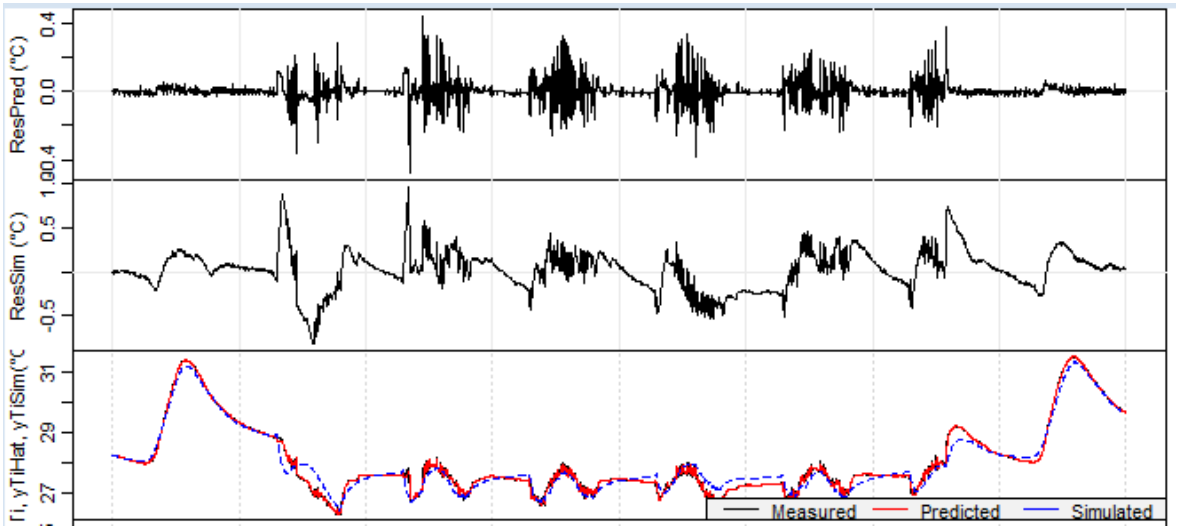

Fig. 4.33 The best grey-box model of the summer season: structure of the 2C2R model.

Table 4.8: Cumulated periodogram and RMSE values for the best model of the summer season.

2C2R Model
Best summer model
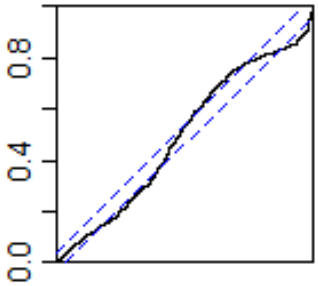
RMSE-1 STEP: 0.07 RMSE-2 STEPS: 0.08 RMSE-4 STEPS: 0.10 RMSE-6 STEPS: 0.12 RMSE-8 STEPS: 0.13 RMSE-10 STEPS: 0.14 RMSE-12 STEPS: 0.16 RMSE-24 STEPS: 0.20 RMSE in simulation: **0,23 °C**

Table 4.9: Cumulated periodograms and RMSE values in simulation for the other tested model of the summer season.

2C2R Model	2C3R Model	2C3R Model
MOD 1	*MOD 2*	*MOD 3*
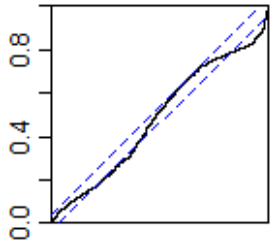	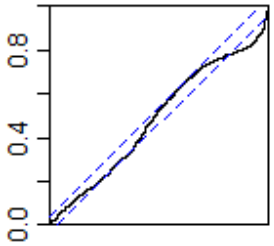	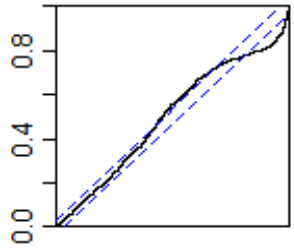
RMSE in simulation: **0,39 °C**	RMSE in simulation: **0,24 °C**	RMSE in simulation: **0,32 °C**

3C3R Model	3C4R Model
MOD 4	*MOD 5*
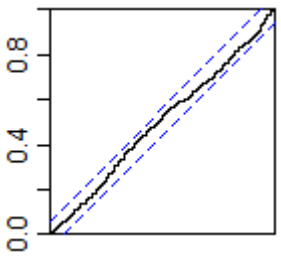	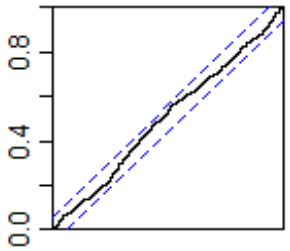
RMSE in simulation: **0,40 °C**	RMSE in simulation: **0,58 °C**

4.3.5.2 The Grey-box model for the winter season

The model for the winter season is derived by data of November campaign. This model identification exploited the results in previous campaigns, most of all the July campaign, in which the plant was fully operating. In this regard, the difference was represented by the heating power Ph, calculated by means of the thermal gradient between the internal temperature and the supply air temperature of the fan coil and the air velocity measured for each fan coil speed during the summer campaign, seen also APPENDIX D. For this model identification, the available data set was very limited, as observed in par. 4.3.4.2. Since for this period there were no data available from the local weather station, weather data (outdoor temperature, Ta, and global horizontal irradiation, Ps) were provided by the web services previously mentioned. The boundary conditions for the system were the outdoor temperature and the corridor temperature, according to the evaluations and results for the summer season. In first instance, these temperatures were maintained divided. Then, the coefficient "K", already introduced for the reduced-order model of July campaign, was included in the equation of the state "Te" for linearly combining the two temperatures. This coefficient represented an added parameter to be estimated. Attempts, like those of summer season, were made to return the best grey-box model verifying results according to the considerations explained in APPENDIX E, especially evaluating the best correspondence in simulation with measured data, that was translated as the lowest RMSE value. Six different models were considered, almost all second-order ones. Only a third-order model was tested to verify the ability of an adding state for the plant in returning heat dynamics of the test-room (MOD. 8). On the other side, differences between the tested second-order models concerned: the presence (MOD. 6) or not (MOD. 7) both of a solar gain affecting the envelope surface (Ae*Ps), in addition to that acting directly indoor (Aw*Ps), and a power contribution connected to equipment in the office. Lastly, evaluations of the data set length were made to provide more efficient dynamics for the parameter estimation for CTSM-R software. Therefore, for the last two models tested (MOD 9-10) and for the best winter model, the data set was respectively: 21-26 Nov, 21-24 Nov, 23-26 Nov. At the end, the grey-box model that demonstrated to be more stable and reliable for the summer season was again a 2C2R model presented below in its structure (Fig.4.34) and relative system equations (Eq. 4.13-4.14). The output equation for the system is always the same, provided for remember in Eq. 4.15. The initial data set was reduced to four days, 23-26 November 2016, anyway guaranteeing an acceptable level of approximation, even if worse than the model identified for the summer season. Carrying on with the description of the best model for wintry season, only a solar gain, affecting internal temperature, was considered (Aw*Ps), whilst Ta and Tc were linearly combined by means of the K coefficient. Finally, powers for the plant and data from the weather station were used. For the best model, parameters estimates are provided in Table 4.10, final

temperature and residuals plots in Fig. 4.35, whilst cumulated periodogram and RMSE values in Table 4.11. Different root mean square errors (RMSE) were calculated connected to a different time interval by considering that 1-step interval was equal to 5 min, according to the data set created. Such values, particularly for this model, will be useful for the definition of the prediction horizon within the design phase of the model predictive controller. The last value in Table 4.11 is the RMSE in simulation. Results of other models tested for the summer season are presented in Table 4.12, in terms of cumulated periodogram and RMSE value in simulation.

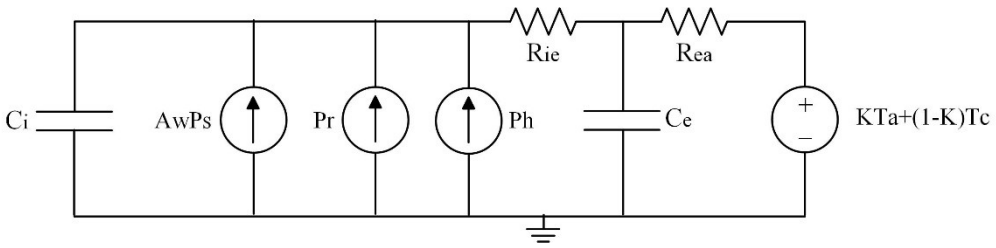

Fig. 4.34 The best grey-box model of the winter season: structure of the 2C2R model.

First-order stochastic differential equations implemented in the script for the parameters estimation:

$$dT_i = \frac{1}{\mathrm{R}_{ie}\mathrm{C}_i}(\mathrm{T}_e - \mathrm{T}_i)\mathrm{d}t + \frac{1}{C_i}P_r\mathrm{d}t + \frac{1}{C_i}P_h\mathrm{d}t + \frac{1}{C_i}A_wP_s\mathrm{d}t + \sigma_i\mathrm{d}\omega_i \quad (4.13)$$

$$dT_e = \frac{1}{\mathrm{R}_{ie}\mathrm{C}_e}(\mathrm{T}_i - \mathrm{T}_e)\mathrm{d}t + \frac{1}{\mathrm{R}_{ea}\mathrm{C}_e}(\mathrm{KT}_a + (1-\mathrm{K})T_c - \mathrm{T}_e)\mathrm{d}t + \sigma_e\mathrm{d}\omega_e \quad (4.14)$$

The output equation for the system is represented by the discrete time measurement equation, already seen in the preliminary study (Eq. 4.9):

$$Y_k = T_{ik} + e_k \quad (4.15)$$

Table 4.10: Results of the parameters estimation for the best model of the winter season.

Parameter	Estimated value	Pr(>|t|)	dPen/dPar
Ti0	2.3610e+01	0.0000e+00	0.0000
Te0	2.5329e+01	0.0000e+00	0.0000
Aw	4.1722e+00	8.2058e-06	0.0000
Ce	8.6243e-01	1.1815e-02	0.0000
Ci	6.6227e-01	2.5508e-11	0.0000
e11	-2.3489e+01	6.8058e-01	0.0000
p11	-2.2574e+00	0.0000e+00	0.0000
p22	-1.4148e-01	5.5814e-01	0.0000
Rea	1.5614e+00	5.7416e-05	0.0000
Rie	4.2946e-01	7.0325e-08	0.0000
K	8.1601e-02	2.2452e-09	0.0000

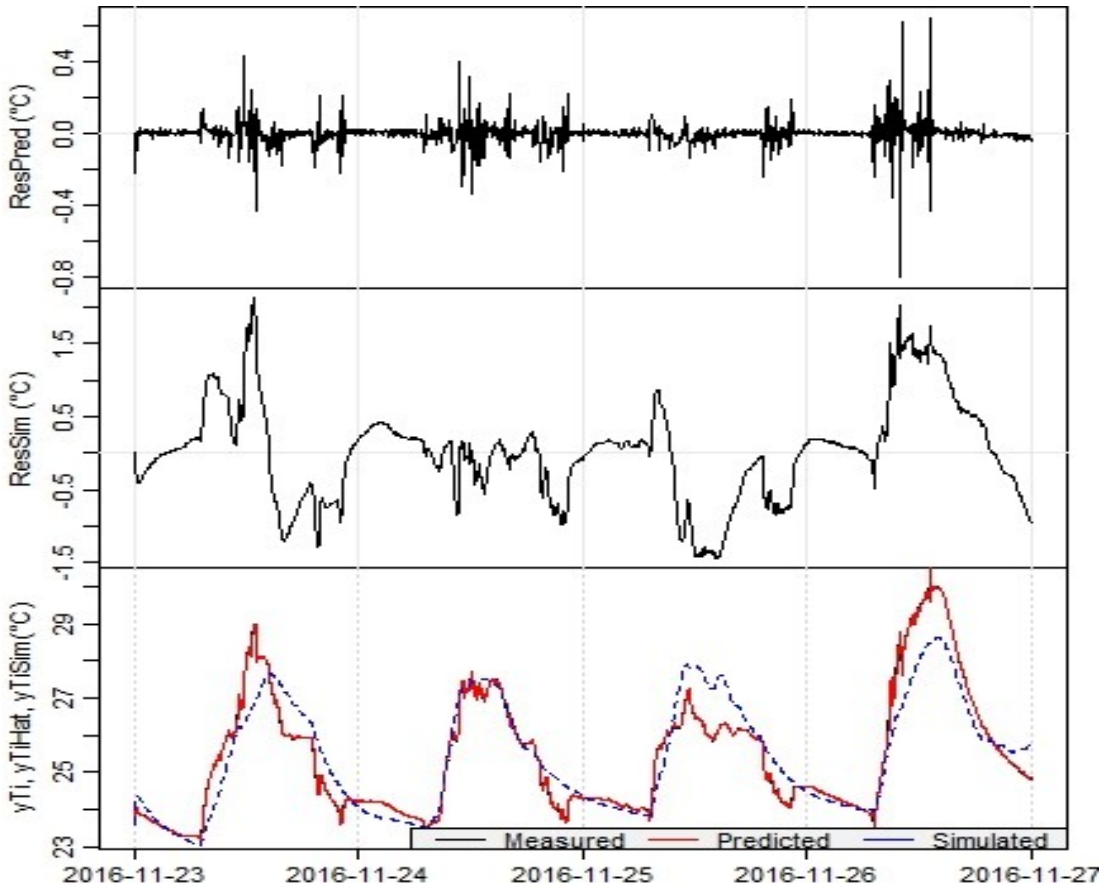

Fig. 4.35 The best grey-box model of the winter season: structure of the 2C2R model.

Table 4.11: Cumulated periodogram and RMSE values for the best model of the winter season.

2C2R Model
Best winter model
Cumulated periodogram
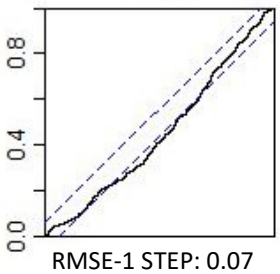
RMSE-1 STEP: 0.07
RMSE-2 STEPS: 0.12
RMSE-4 STEPS: 0.20
RMSE-6 STEPS: 0.26
RMSE-8 STEPS: 0.31
RMSE-10 STEPS: 0.34
RMSE-12 STEPS: 0.38
RMSE-24 STEPS: 0.54
RMSE in simulation: **0,67 °C**

Table 4.12: Cumulated periodograms and RMSE values in simulation for the other tested model of the winter season.

2C3R Model	2C3R Model	3C4R Model
MOD 6	*MOD 7*	*MOD 8*
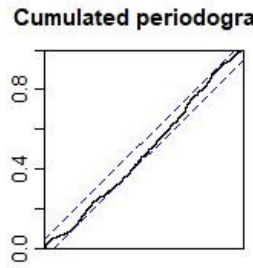	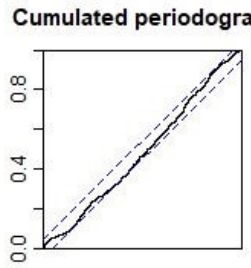	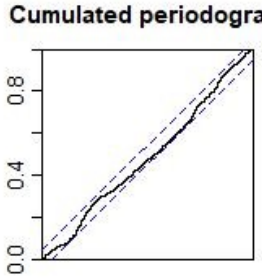
RMSE in simulation: **0,99 °C**	RMSE in simulation: **0,99 °C**	RMSE in simulation: **0,84 °C**

2C2R Model	2C2R Model
MOD 9	*MOD 10*
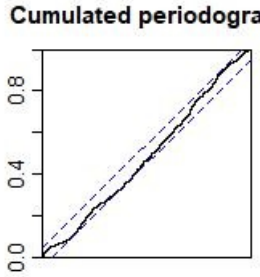	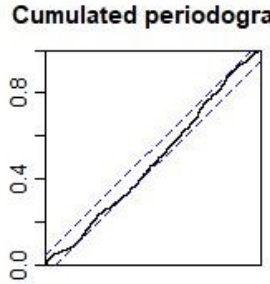
RMSE in simulation: **0,99 °C**	RMSE in simulation: **0,78 °C**

4.3.6 Validation of the models

The empirical approach, presented in par. 4.3.5, returns the values of the parameters that are needed to identify the model. However, such reduced-order model must be validated as to verify its reliability in representing the physics of the system. In fact, the usefulness of a model in explaining phenomena should overlook the sequence of data considered for its identification. Thus, a model is effective and objectively valid if it fits not only the available data, but mostly measured data acquired in different conditions from those of data set used in the identification procedure. For the model validation, it is necessary to use input data acquired from a campaign different from the one used for the parameters estimation. Anyway, it is recommended that the validation period falls within the same modelling season, not to risk the physical parameters are no representative of climate conditions and plant setting. The validation procedure can be done by means experimental or simulation testing. In this work, the second method was adopted to validate grey-box models and Dymola software was used

to carrying out the simulations. Below, in the methodology section, a description of the approach and software used for the model validation will be provided. Then, the last two sections will address the validation of the best models for the summer and winter season, previously identified.

4.3.6.1 Methodology

The validation procedure of this dissertation is based on a simulation approach. Before analysing the validation procedure for the grey-box model, a brief introduction about the tool used to run the required simulations.

Dymola is a complete tool for modelling and simulation of integrated and complex systems for use within automotive, aerospace, robotics, process and other applications. The main advantages it offers are:

- multi-engineering capabilities, which means that models can consist of components from many engineering domains. This allows for models of complete systems that better depict reality. In this regard, for many different engineering domains, libraries are available containing components for mechanical, electrical, control, thermal, pneumatic, hydraulic, power train, thermodynamics, vehicle dynamics, air -conditioning, etc.
- intuitive modelling, thanks to Dymola's graphical editor and the multi-engineering libraries provided. The libraries include elements corresponding to physical devices which are simply dragged-and-dropped to build the model. Interactions between the components are conveniently described by graphical connections that model the physical coupling of the components. This means that models are intuitively organized the same way as the physical system is composed.
- open and flexible structure, which allow users to introduce components that match their needs. This can be done either from scratch or by using existing components as templates. The Dymola environment is completely open in contrast to many modelling tools that have a fixed set of component models and proprietary methods for introducing new components. Dymola is based on Modelica®, which is an object-oriented language for physical modelling developed by the Modelica Association.
- interoperability options, among which one is mentioned the support of FMI Standard that allows any modelling tool to generate C code or binaries representing a dynamic system model, which may be integrated in another modelling and simulation environment. This latter aspect will be exploited in Chapter 6, by exporting our Dymola model as FMU (Functional Mock-up Unit) and importing it with Simulink. The great advantages is that,

after importing the FMU, you can access all the available parameters, to set their values or link them to Matlab workspace variables, and configure the outputs.

- unique and outstanding performance for solving differential algebraic equations (DAE). The key to high performance and robustness is symbolic manipulation which also handles algebraic loop and reduced degrees-of-freedom caused by constraints.

Referring to libraries, which are constantly developed and up-to-date, the relevant ones for this work are two:

- Model Standard Library
- Modelica Buildings Library

The Modelica Standard Library is also called Modelica Package and it provides model components in many domains that are based on standardized interface definitions. Main libraries provided by this Package (Fig. 4.36a) are:

- Electrical: contains electrical components to build up analog and digital circuits, as well as machines to model electrical motors and generators, especially three phase induction machines such as an asynchronous motor;
- Mechanics: includes components to model the movement of 1-dim. rotational, 1-dim. translational, and 3-dim. mechanical systems;
- Thermal: contains libraries to model heat transfer and fluid heat flow;
- Math: contains basic mathematical functions (such as sin(..)), as well as functions operating on vectors, matrices, nonlinear functions, and Boolean vectors;
- Constants: provides often needed constants from mathematics, machine dependent constants and constants from nature.

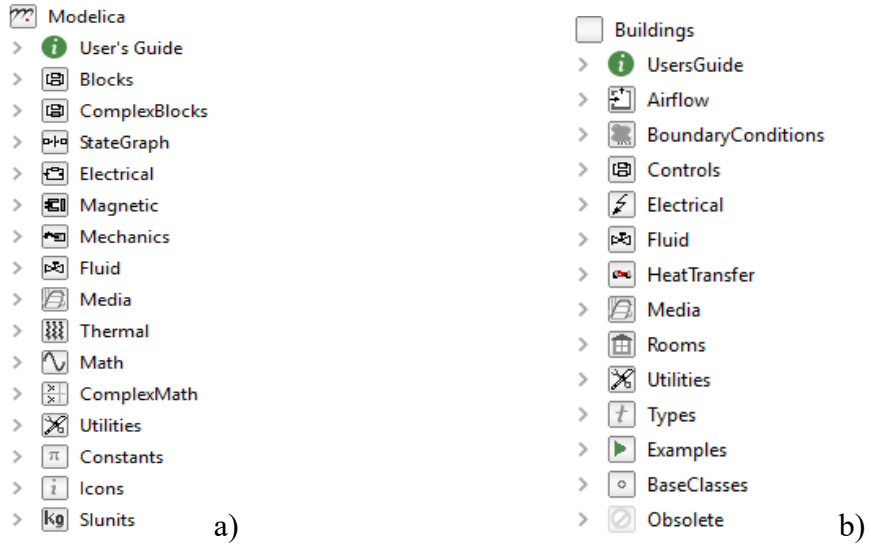

Fig. 4.36 Instances of: a) the Modelica Standard Library, b) the Modelica Buildings Library.

The Modelica Buildings library (Fig. 4.36b) is a free open-source library with dynamic simulation models for building energy and control systems. The library contains models for:

- HVAC systems;
- controls;
- heat transfer among rooms and the outside;
- multizone airflow, including natural ventilation and contaminant transport;
- single-zone computational fluid dynamics coupled to heat transfer and HVAC systems;
- data-driven load prediction for demand response applications;
- electrical DC and AC systems with two- or three-phases that can be balanced and unbalanced.

After this overview on the simulation tool, to validate the models, it is required the data set of the validation period, including all the time series of variables involved in the reduced-order model identified. The data set must be save in a standard text document (.txt). Then, the RC-network, each for the grey-box models previously determined, is built up in Dymola environment and the data set is uploaded by means of a *CombiTimeTable*, the library path of this object is: *Modelica.Blocks.Sources.CombiTimeTable* (Fig. 4.37).

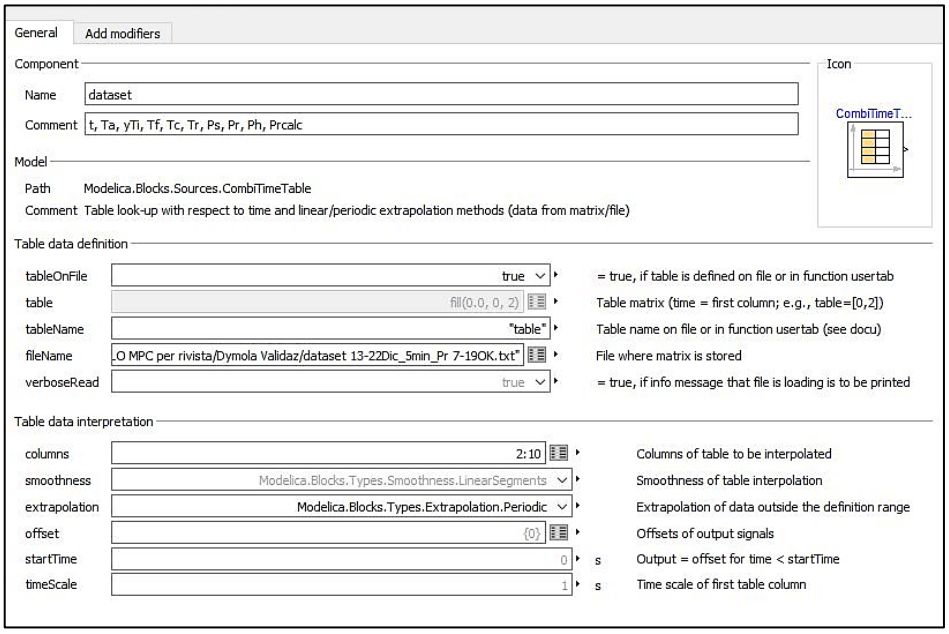

Fig. 4.37 Implementation of the data set for the model validation in Dymola.

Subsequently, model parameters estimated by R software are inserted in corresponding blocks of Dymola's RC-network, making necessary unit conversions: the capacity value was multiplied by 3600000 to obtain J/K while the value of resistances was divided by 1000, to obtain K/W (Figg. 4.38-4.39).

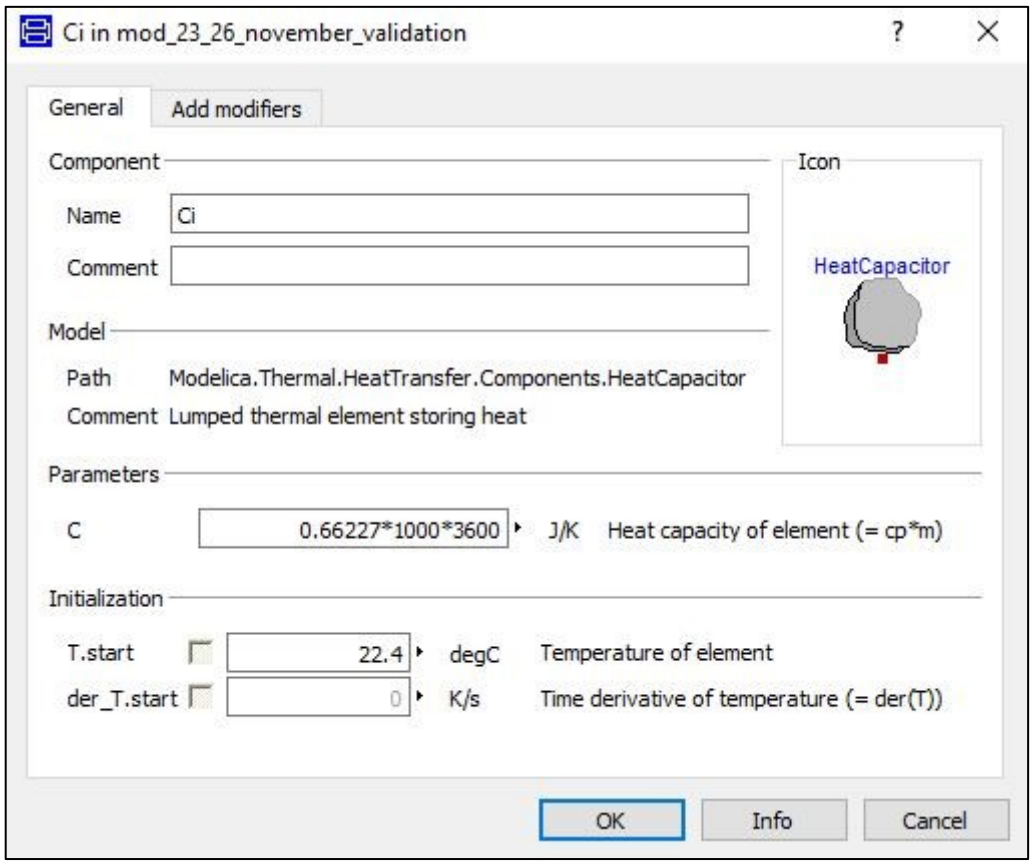

Fig. 4.38 Unit conversion and temperature initial value for the heat capacitor component.

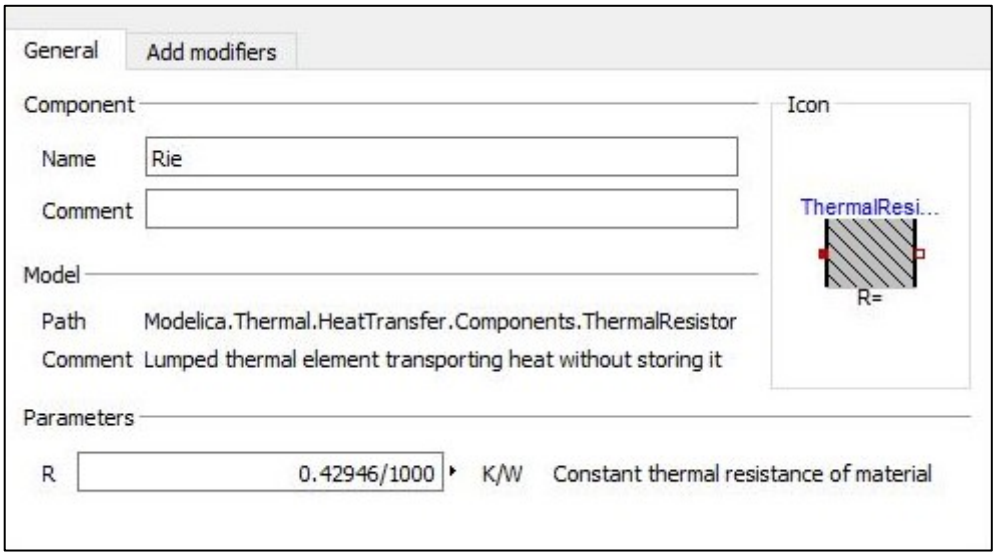

Fig. 4.39 Unit conversion and temperature initial value for the thermal resistor component.

The capacities were also provided by the initial temperature values, as inputs for simulation beginning. It was necessary to insert another instance, *Modelica.Blocks.Math.Gain*, that was used both to represent coefficients of the heat inputs of the system (Ps, Ph, Pc, Pf) and to linearly combine boundary temperatures. In Fig. 4.40, as an example, it is shown the coefficient (Aw) of the solar radiation (Ps).

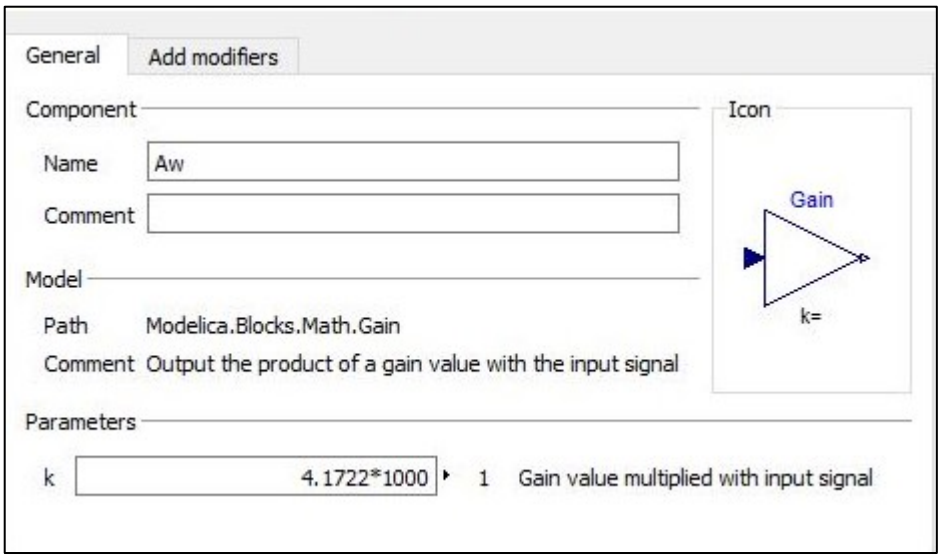

Fig. 4.40 Modelica Library Block representing the coefficient (Aw) of the solar radiation (Ps).

Finally, after running a check to avoid modelling errors, simulation settings were defined in terms of start/stop time, interval length, calculation algorithm and relative tolerance (Fig. 4.41). Then the simulation can be run.

Results of the validation phase both for summer and winter modelling are provided in next sections and they are expressed in terms of:

- *Error*, the difference between measured and simulated values of the internal temperature;
- *RMSE, the Root Mean Square Error* (Eq. 4.16), based on residuals to measure the spread of the observed values about predicted values of the internal temperature.

$$RMSE = \sqrt{\frac{\sum_{i=1}^{n}(y_i - \hat{Y}_i)^2}{n}} \tag{4.16}$$

Residuals are represented by the difference between observed value (y_i) and predicted values ($\hat{Y}_i$). Squaring the residuals, averaging the squares and taking the square root, you get the RMS error. The RMSE provides a quantitative indication of the model correspondence to real behaviour. The calculation instruction of the RMS error has been inserted inside Modelica text, as shown in Fig. 4.42.

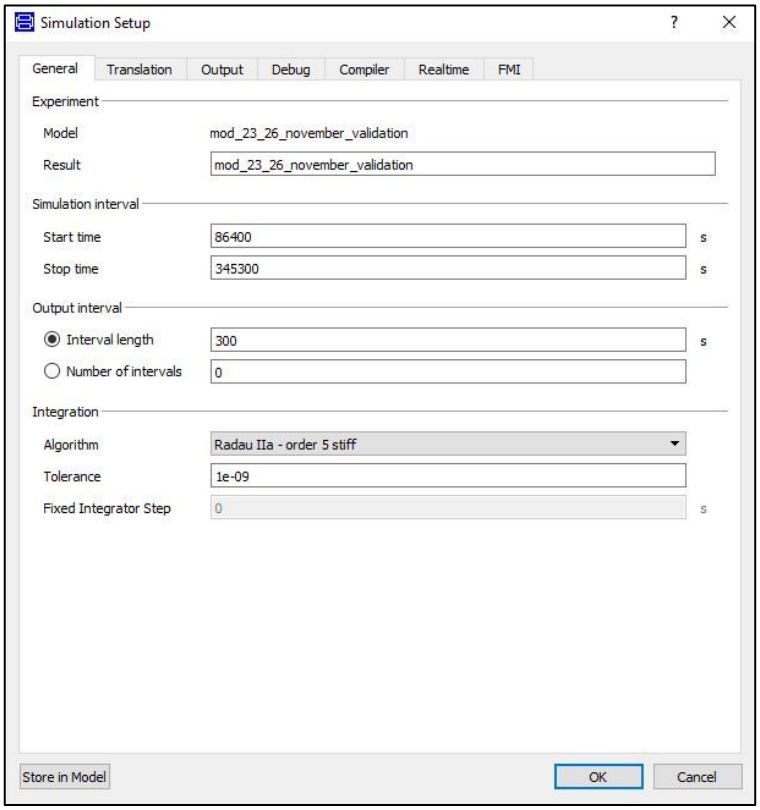

Fig. 4.41 Simulation settings for running the model validation.

```
model mod_23_26_november_validation

  Real error "Simulation error";
  Real mse "Mean Square Error";
  Real se "Square Error";
  Real rmse "Root Mean Square Error";

equation
  error = dataset.y[2] - (Ci.T-273.15);
  der(se) = error^2;
  time * mse = se;
  rmse = sqrt(mse);

end mod_23_26_november_validation;
```

Fig. 4.42 Extract of the Modelica text for the calculation of errors to test the model in validation.

4.3.6.2 Summer validation

Validation for the summer season was carried out over a period of data acquisition that was not used during the parameter estimation process, that was from 30 July to 5 August. Following the validation procedure described in par. 4.3.6.1, the grey-box models of the second-order identified in par. 4.3.5.1, were tested in validation by means of Dymola software. The best model in terms of parameters estimation was the best also in validation and plot of results are provided below in Figg. 4.43-4.44. The other models tested returned an RMS error greater than 0.65°C in validation.

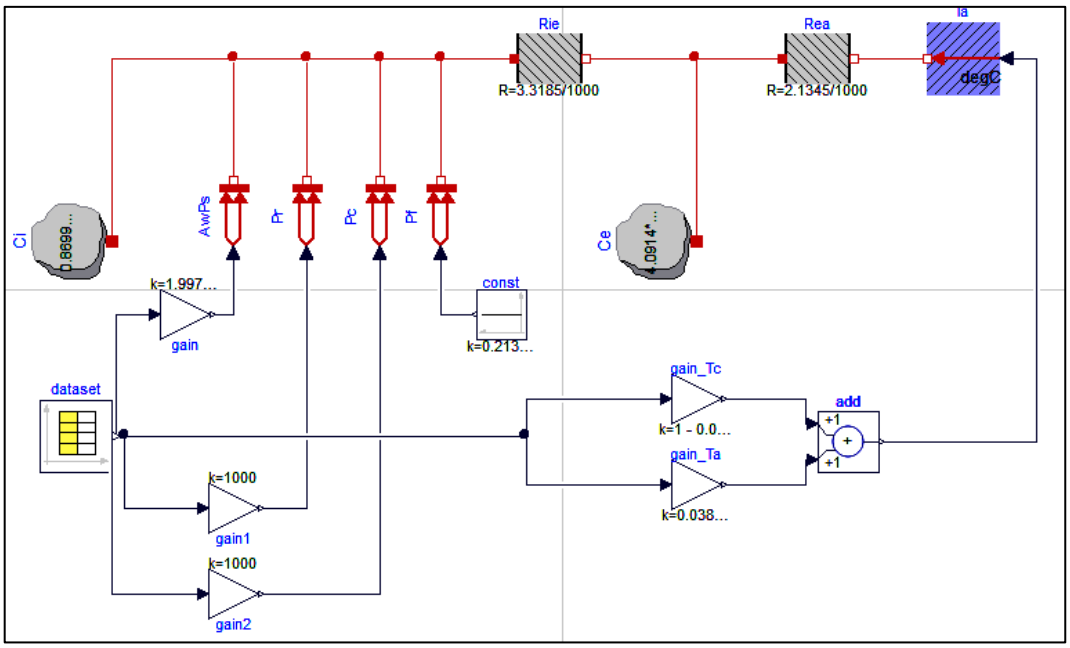

Fig. 4.43 Best grey-box model for the summer season built up in Dymola environment.

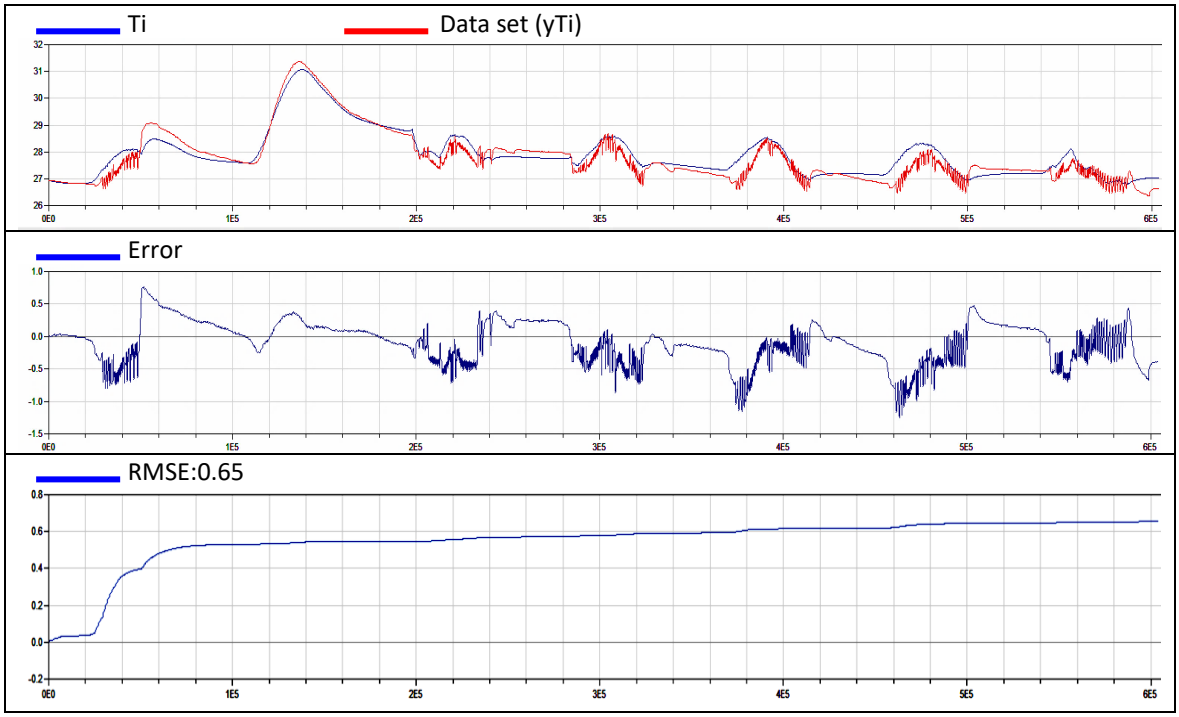

Fig. 4.44 Results of model validation for the best grey-box model of the summer season.

4.3.6.3 Winter validation

Since the reduced-order model of the winter season was applied in an advanced control, the model validation was carried out differently compared to summer validation. Model validation for the wintry season was performed by comparing the indoor temperature simulated by the grey-box model integrated in the MPC and the corresponding one measured by the sensor network during the time window when the controller was in operation (14-16 December 2016). Simulation was run by means of an RC-network model developed in the Dymola environment (Fig. 4.45), that was equivalent to the best two-state model of the test-room, described in par. 4.3.5.2. As shown in the plot of Fig. 4.46, the RMSE observed during the whole simulation period is always lower than 0.3°C, thus comparable with the sensors accuracy, as found in APPENDIX A.

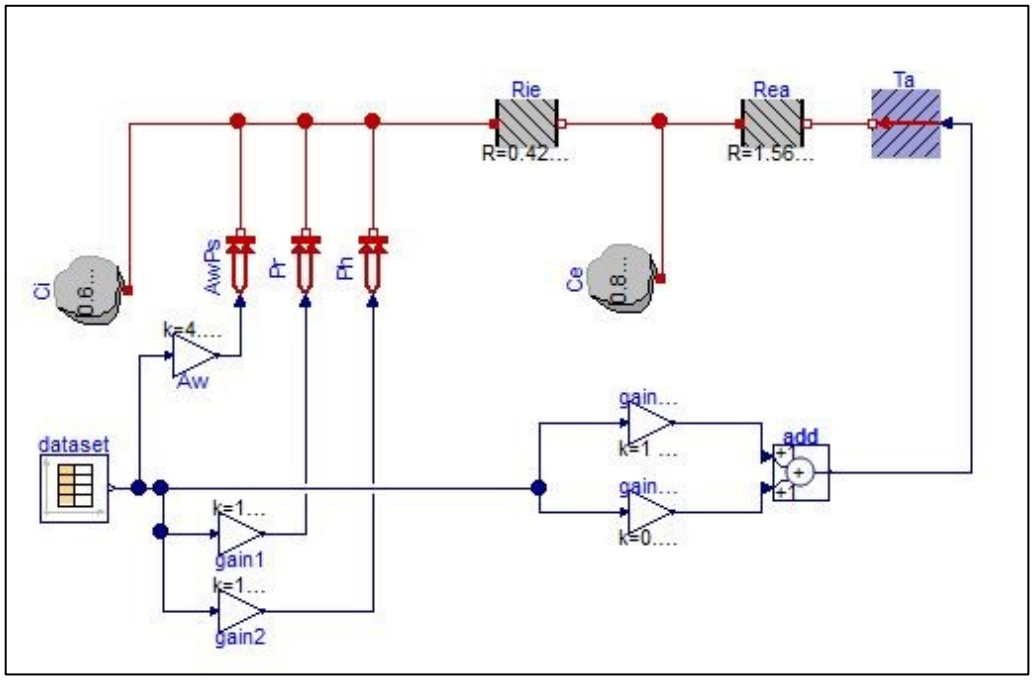

Fig. 4.45 Best grey-box model for the winter season built up in Dymola environment.

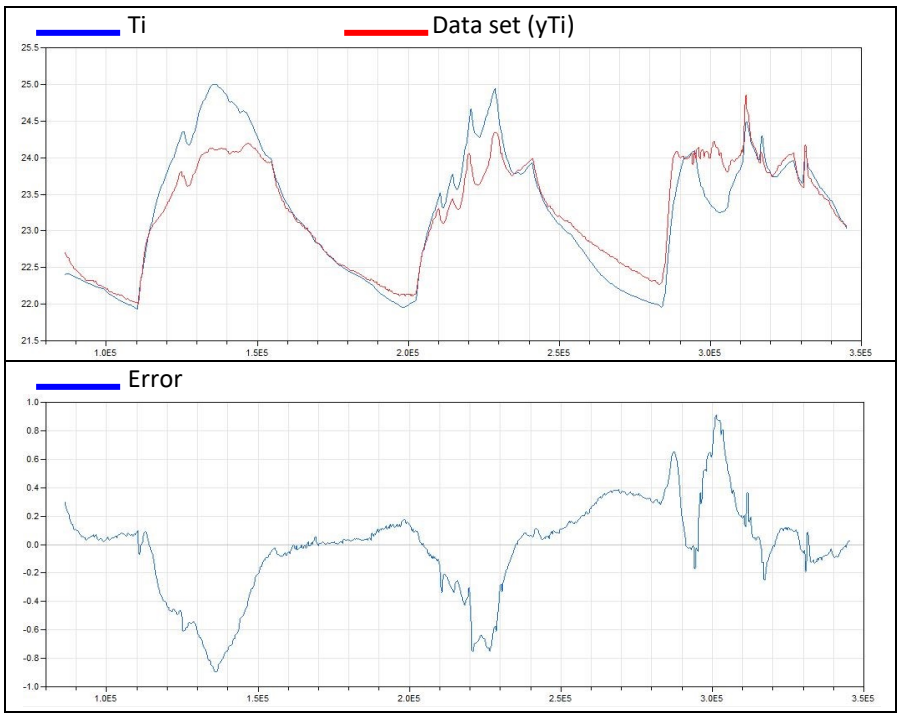

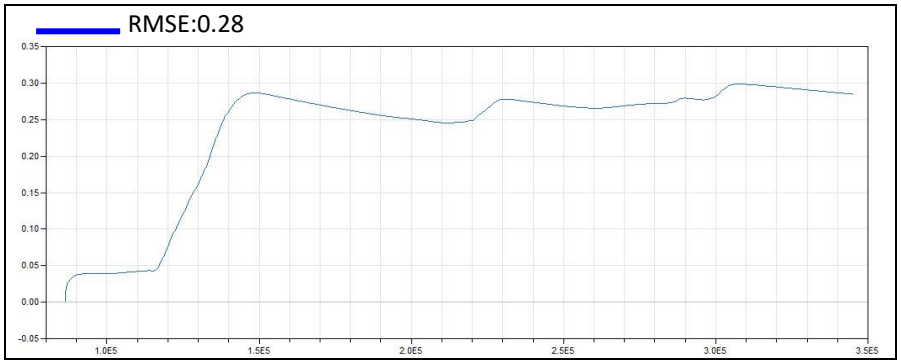

Fig. 4.46 Results of model validation for the best grey-box model of the winter season.

4.4 Conclusions

This chapter detailed an empirical approach to derive reduced-order models for existing buildings with the main objective of identifying an adequate building model for advanced control strategies, like model-based, predictive control.

Starting from the investigation of relevant identification techniques provided by literature, the grey-box modelling was pointed out to be the best to accomplish the set goal, as motivated in Chapter 2. Hence, a preliminary study was carried out to define the experimental procedure. The design phase of the approach pursued in this dissertation was confirmed and partly enriched by results obtained in the preliminary test.

Then, the confirmed procedure was applied in a more complex case, an existing building, within a testing area, selected to carry out monitoring campaigns for providing data to the model identification phase.

Two grey-box models were identified: the first was derived by means of data acquired during the summer campaign, whilst the second from data of the winter campaign.

Both of models were validated after the estimation of thermal parameters in order to provide an index of reliability for further applications. The best models were obtained just from a maximum of one week data set, with a maximum value of RMSE in simulation of 0.65°C, referred to the winter model. In order to prove the effectiveness of the empirical approach developed, despite the discrete value of RMSE achieved, this model has been chosen to be used within the architecture built up for the MPC prototype in Chapter 5.

Chapter 5

Development of a MPC prototype

5.1 Introduction

This chapter is aimed at the development of a MPC prototype, operating in a real building. The novel contribution introduced is a procedure, based on the collection of short-term environmental data, for working out a dynamic thermal model of the building to feed the controller. Moreover, result is achieved exploiting an interface designed to the regulation system of the real building and the real-time monitoring system that feeds the controller, and developing a sub-unit to gather forecasts about weather and occupancy of the building. Following, in the Methodology section, the main parts of this discussion will be identified.

5.2 Methodology

In order to test a real-time predictive control for buildings, a number of operational steps are required, thus the roadmap of this chapter was conceived, following the real prototype development, as:

1. definition of the case study so as to analyse relevant aspects for the application of the control strategy;
2. definition of the MPC logic to be tested: MPC framework, constraints, building modelling;
3. programming of a software for input acquisition and output actuation, to enable the automatic management of the MPC response;
4. deployment of a sensor network on-site, in order to assess indoor and outdoor climate conditions during operation as well as overall system performance;
5. definition of an experimental campaign to collect local and real-time data;
6. analysis of MPC performance during operation, by means of analytical assessments of controller output consistency with the cost function and reliability of the predictive model unit;
7. numerical and graphical assessment of the controller performance in terms of global comfort, local discomfort and energy consumption.

In the following, these main parts are treated in detail. Specific attention is paid to the design and development of a LabVIEW prototype integrated in a real building and in the arrangement of a procedure for building model identification.

5.3 Monitoring system

An articulated sensor network was designed, in collaboration with DIISM Department of this University, to get a global understanding of the thermal dynamics involved, with particular emphasis to collect the real-time measurements to fulfil the model predictive controller. The monitoring system (Fig. 5.1) consists of two main interconnected subsystems and two additional subsystems that will be described in detail below.

A Hobo ZW Series Wireless Network was installed on the 3rd floor to measure the temperatures of the various environments, as already seen in Chapter 4. In particular, four thermo-hygrometers were installed in the experimental area. Three sensors were hanging from the ceiling of the offices adjacent the test room and of the corridor to get the air temperature of the surrounding environments, while another one was placed in the testing office next to the comfort station. The network receiver located inside the test-room, was connected to a computer, which was used to set up the network and offload the data from the receiver on site. Two additional probes were added to characterize the airflow processed through the FCU and through the AHU, plus a KIMO anemometer (Ø 100 mm vane probe) was used for a spot measurement of the air velocity from the technical system, for each speed of the fan. Such measuring system was setup to feed the grey-box model of the controller with the necessary information about the power supply. The receiver and the router of the Hobo network were line powered (batteries were provided only for backup), while data nodes were battery powered. This deployment of sensors was required by the numerical identification techniques chosen and for the assessment of the general working conditions. Then, it was utilised to build up the mathematical model of the building embedded in the MPC. Data were acquired every minute with a logging interval of 10 minutes. The accuracy of data nodes was ±0.21°C over a 0 to 50°C range with a wireless transmission range of approximately 100 m, depending on interference or obstructions.

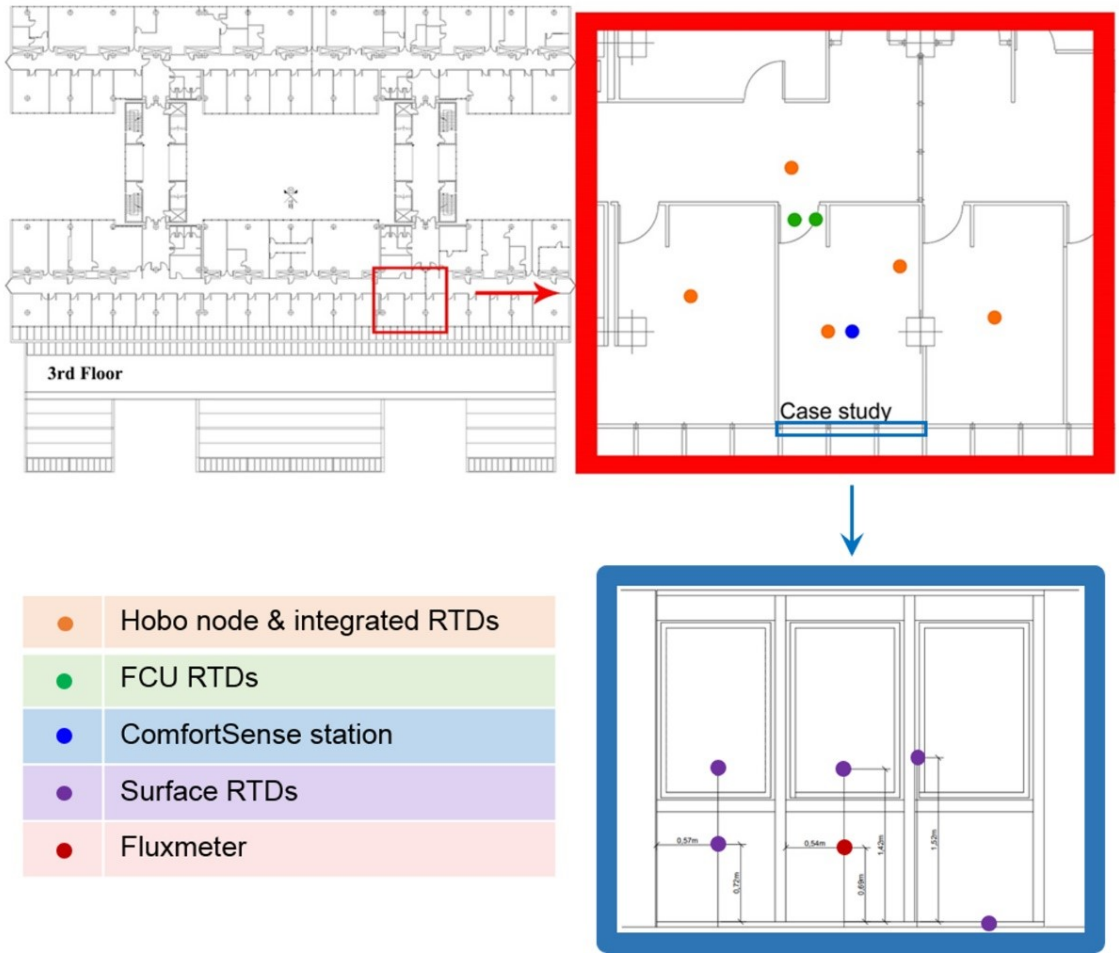

Fig. 5.1 Plan localization and visualization of the indoor monitoring system.

An indoor microclimatic station (Fig. 5.2), composed by the comfort-conceived ensemble by Dantec Dynamics, named ComfortSense Dantec, was installed to monitor the thermal comfort inside the test-room. This system consists of a main frame with input channels for up to 16 probes. It includes three draught probes to perform local discomfort analysis, a capacitive hygrometer to measure the moisture content in the air and an ellipsoidal-thermometer, which was inclined of 30° from vertical to get the mean radiant temperature in consideration of both the radiosity of the walls and the effective radiation area of a seated person. All the probes were connected to the main frame which logged and packed the dataflow through a National Instrument acquisition platform. A dedicated palette is embedded in LabVIEW to easily communicate with the station and perform the calculation of indoor comfort parameters, such as operative temperature, turbulence intensity, draught rate, PMV and PPD. The calculation of operative temperature and PMV might be misleading when performed in the middle of a room whose thermal conditions are expected to be non-uniform because of the presence of local heat sources and sinks, like a large window (Kalmár, 2016). Indeed, in order to test the comfort perceived by the occupants, the station was installed very close to the workbench, slightly

decentralized on the South-North axis towards the glazed façade and right in front of the central glazed module on the East-West axis. The draught probes were placed at 0.1m, 0.6m and 1.1m according to the standardized procedure (*ASHRAE Standard 55 - 2010*) when the user is expected to stay seated for the vast majority of time. To integrate the ComfortSense system in a complex measuring environment and synchronise it with other user developed programs, a LabVIEWToolbox (written in NI LabVIEW) is provided to assemble ComfortSense measurements by means of pre-programmed blocks and high-level virtual instruments (VIs). This programming aspect was fundamental for the development of the MPC in NI LabVIEW environment.

In addition, a glazed façade thermo-station was installed: the internal side of the south-exposed wall was littered with flat Resistance Temperature Detectors (Pt100) to map the surface temperature distribution and detect when and where the main alterations occurred, in function of:

- position (readings from the different glass modules and pieces of frame);
- materials and composition of the layers (readings from the frame, from the glass and from the horizontal shielded band).

Lastly, to check real outdoor conditions, a weather station was installed on the roof of the 5th floor (see par. 4.3.3, Chapter 4) and, among other data, measured data of external temperature and global horizontal radiation were acquired by means of a thermo-hygrometer (provided with an anti-radiation shield) and a pyranometer, respectively. As previously done, also measurements were integrated in one inclusive LabVIEW Virtual Instrument so as to be able to monitor all the parameters during the experimental campaign. Actual weather data were not used for the MPC algorithm since the predictive control requires weather forecasts to be provided as inputs. However, they were useful for comparisons and for data processing.

In conclusion, the following sensors were used in the system identification phase:

- one temperature probe inside the office room;
- two temperature probe external to the office room;
- one anemometer;
- one pyranometer;
- a national instrument board tracking the power level of the fan coil.

The following sensors and actuators were used also during the operation of the MPC prototype:

- one temperature probe inside the office room;
- one temperature probes external to the office room;
- a national instrument board tracking the level of the fan coil during the day.

Table 5.1: Measurements used to build up the model for the controller and run the predictive control.

Description	Measurements from sensors
Internal temperature (of the office)	Hobo ZW-007-Router; ComfortSense probe
Corridor temperature (next to the office)	Hobo ZW-003-Data Node
Air flow temperature (Fan coil, AHU)	Ext. temp. probes of Hobo ZW-007
Air velocity (Fan coil, AHU)	Anemometer Kimo VT 200
Outdoor air temperature and Solar radiation	Weather forecasts from internet website

Table 5.1 summarizes the several sensors and related measured parameters necessary to derive the reduced model for the controller and implement the predictive control. The output signals were logged every 5 minutes by a suite of acquisition cards by National Instruments (for what concerns the indoor stations), while the wireless sensors data were acquired every minute by means of a receiver connected to the PC inside the room and, later, re-sampled with a 5-min step. An additional module (NI 9401) transformed the output of the control algorithm into the digital command to the 220V electric motor of the FCU to set the defined speed. For the sake of safety, three static relays were interposed so that low voltage and high voltage circuits could be separated and potential competing requests to the fan averted. A detailed description of the specs and spatial distribution of the devices composing the monitoring system is given in APPENDIX F.

Fig. 5.2 ComfortSense system installed inside the test room

5.4 Control management

The output of the control algorithm was the power supply of the fan coil, which is the unit in charge of room conditioning. Given that the fan coil was driven by the room thermostat, a logical and

physical connection with it was built. In this way, the control was able to act directly on the room internal temperature. In this feasibility study the software used to manage the MPC system was LabVIEW 2015, provided by National Instrument S.r.l. The software managed the data-flow using a G-language (Graphic Language) to build up a Virtual Instrument (VI) which simulated the interaction between the physical devices. The feedback loop of the MISO (multiple-input, single-output) MPC controller repeated the following steps all over the time window of expected occupancy inside the office (7am to 7pm during weekdays, 7am to 2pm on Saturdays, full-day off on Sundays):

- input acquisition: the data from the monitoring stations were invoked and used to feed the controller, to perform comfort assessments, to check on the response of the glazed façade in terms of surface temperatures and display the weather data so as to visually strike correlations with the thermal evolution inside and outside the building;
- elaboration of the control action: the optimization problem was computed over a defined prediction horizon on the basis of the building model and of the objective function. The output was the speed of the fan necessary to track the setpoint;
- power supply to the electric motor of the fan via the digital output module and the buffer board hosting the static relays;
- data storing in a database application.

To better explain the third item of the previous action list, some additional information need to be provided about the original configuration. As depicted in Fig. 5.3a, a Honeywell thermostat drove the three-speed fan coil. The thermostat was also equipped with a sub-base that made it possible to adjust fan speed manually and switch the fan coil on and off. In order to drive the fan via LabVIEW, a bidirectional digital I/O module NI9401 was used. It provides 8-digital 5 V/TTL channels, only three of which were used as digital outputs for driving the three coils of the 220V electric motor. In order to electrically separate the low voltage and high voltage circuits, the thermostat with sub-base was temporarily replaced with a buffer board as shown in Fig. 5.3b. The three digital outputs (DIO 0, 1, 2) that provides TTL voltage and current levels are buffered by switching the transistors that drive 12V relays connected to the three coils of the motor. The relays guarantee ensures electrical separation and avoid the possibility of turning on multiple coils at the same time. In fact, relays are cascaded so that, for instance, when DIO 2 is set to ON, the corresponding coil is powered and the common terminals of the other relays are disconnected from power, thus avoiding both the other two coils to be powered even if DIO 1 or DIO 0 are wrongly set to ON. The new connection provided to the fan coil motor is shown in Fig. 5.3c.

Even if manual regulation was bypassed, LabVIEW allowed the user to change the MPC settings during the whole acquisition and it visualized the time trends of the following parameters: ambient

temperature [°C], outdoor temperature [°C] and solar radiation [W/mq], fan coil velocity and its actual power value [kW], air inlet and outlet temperatures [°C], percentage comfort values (PMV-PPD). Data from the weather station installed on the roof were collected in a shared folder, from which were invoked to be used inside the main VI. The front panel of the main VI (Fig. 5.4) was remotely managed via TeamViewer 10, for ongoing debugging, maintenance and data analysis.

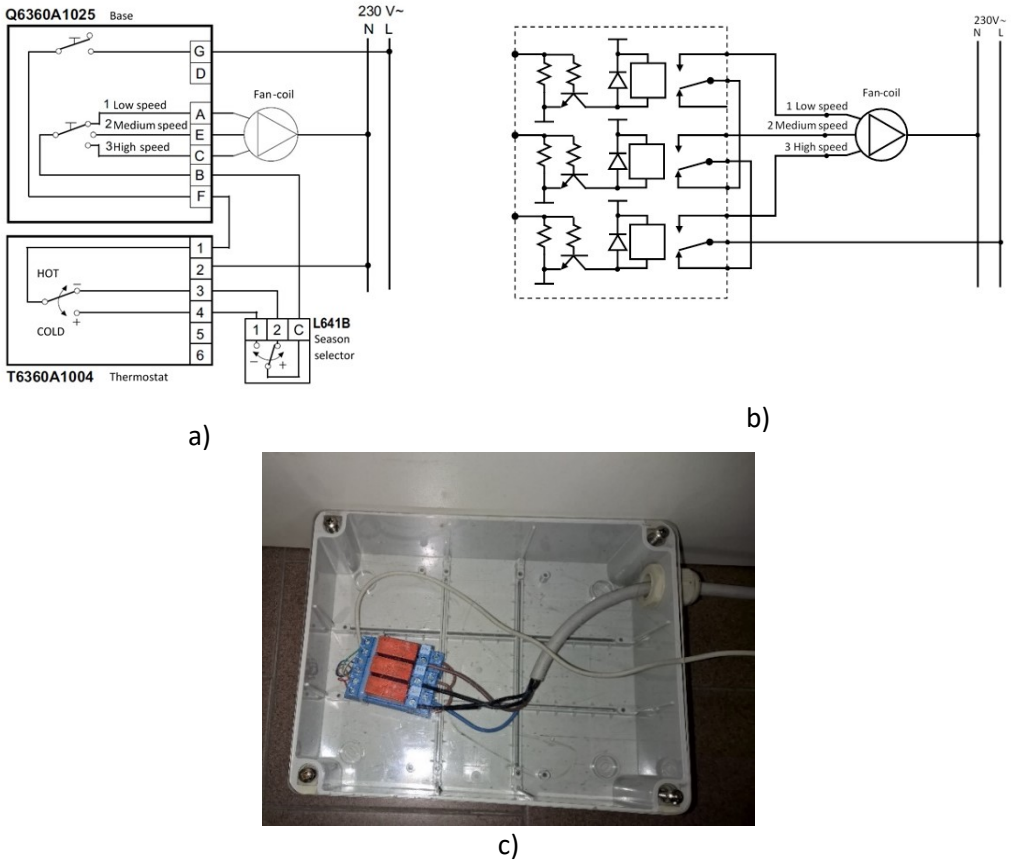

Fig. 5.3 a) Original connection, b) scheme of the buffer board and c) connection implemented to control the fan coil motor.

5.5 The Grey-box model for the controller

The reduced-order model for the controller is a crucial part of the prototype. As anticipated in Chapter 4, the data set used to derive the model referred to the winter season, in particular the period 23-26 November 2016. In this case, a 2C2R network was identified with 9 parameters to run the parameters estimation. Maximum likelihood estimation was carried out by means of the R package CTSM-R, which provides the necessary input data from monitoring and assigns the initial conditions and bounds for the parameters and the states. The best model for the controller was then chosen according to the identification procedure described in APPENDIX E and the RMSE value in simulation was 0.67°C. Thermal parameters relative to the best model, were obtained applying the empirical approach developed in Chapter 4 and they were extracted from the CTSM-R software (Fig. 5.5) to

build up the mathematical model for the controller. Refer to par. 4.3.5.2 for a complete explanation, in particular to Table 4.10.

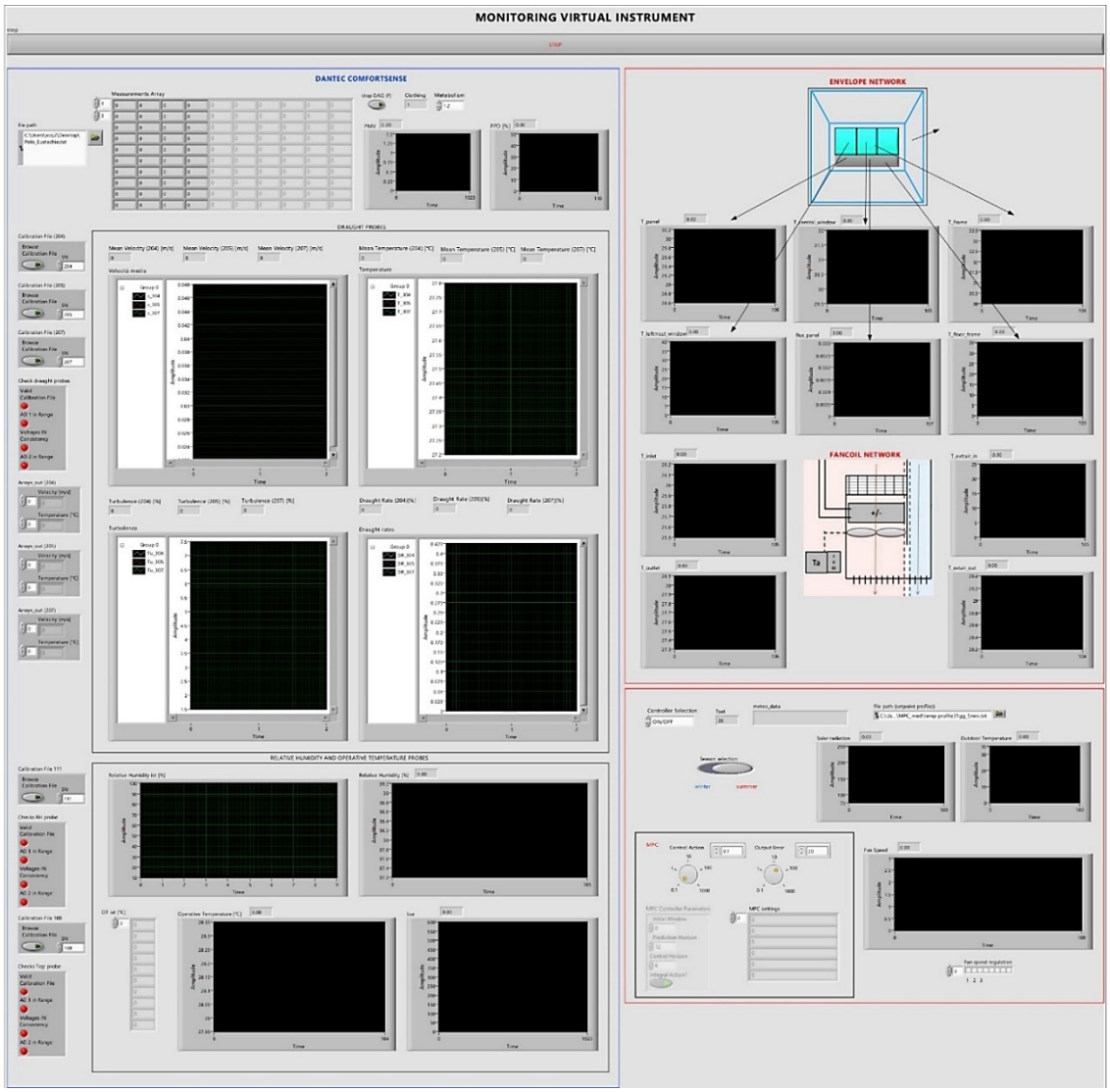

Fig. 5.4 Screenshot of the front panel of the Virtual Instrument developed in LabVIEW to manage the dataflow.

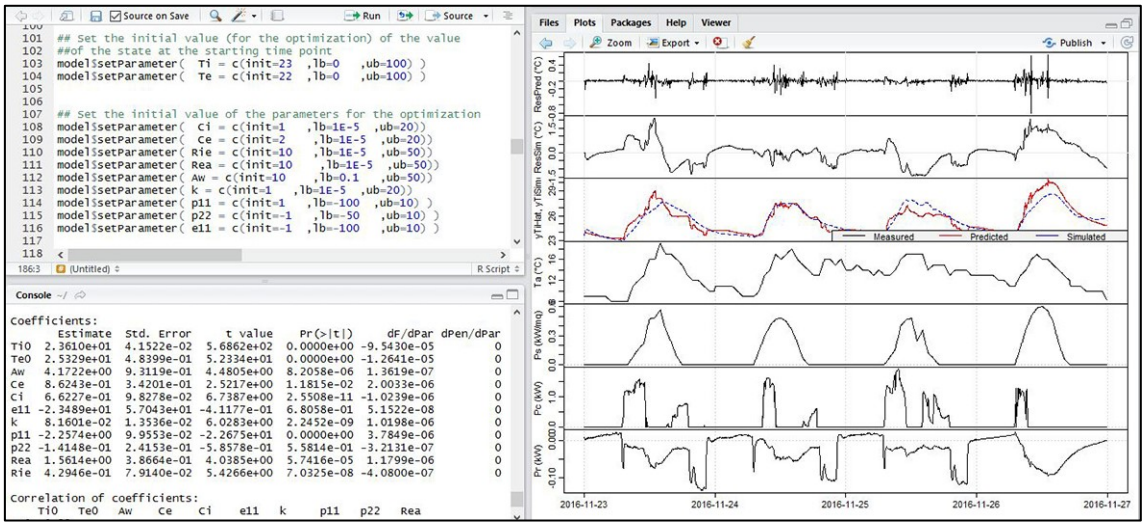

Fig. 5.5 Results of the parameters estimation running in R-Studio, using the CTSM package.

The grey-box controller model was implemented in the Virtual Instrument in LabVIEW, into the "MPC Controller subVI", using a specific tool for state space modelling (Fig. 5.6). For this purpose, the differential stochastic equations (Eq. 4.13 and 4.14, Chapter 4) were rewritten in matrix form, as in Eq. 5.1. By converting them into a more compact form, as in Eq. 5.2, it is possible to verify the correspondence with the structure of the grey-box models, that is the state space representation seen in Eq. 4.1 par. 4.2.2.

$$\begin{bmatrix} \mathbf{dT_i} \\ \mathbf{dT_e} \end{bmatrix} = \begin{bmatrix} -\frac{\mathbf{1}}{\mathbf{R_{ie}C_i}} & \frac{\mathbf{1}}{\mathbf{R_{ie}C_i}} \\ \frac{\mathbf{1}}{\mathbf{R_{ie}C_e}} & -\left(\frac{\mathbf{1}}{\mathbf{R_{ie}C_e}} + \frac{\mathbf{1}}{\mathbf{R_{ea}C_e}}\right) \end{bmatrix} \begin{bmatrix} \mathbf{T_i} \\ \mathbf{T_e} \end{bmatrix} \mathbf{dt} + \begin{bmatrix} \frac{\mathbf{1}}{\mathbf{C_i}} & \frac{\mathbf{A_w}}{\mathbf{C_i}} & \frac{\mathbf{1}}{\mathbf{C_i}} & \mathbf{0} & \mathbf{0} \\ \mathbf{0} & \mathbf{0} & \mathbf{0} & \frac{\mathbf{K}}{\mathbf{R_{ea}C_e}} & \frac{\mathbf{(1-K)}}{\mathbf{R_{ea}C_e}} \end{bmatrix} \begin{bmatrix} \mathbf{P_h} \\ \mathbf{P_s} \\ \mathbf{P_r} \\ \mathbf{T_a} \\ \mathbf{T_c} \end{bmatrix} \mathbf{dt} + \begin{bmatrix} \boldsymbol{\sigma_i d\omega_i} \\ \boldsymbol{\sigma_e d\omega_e} \end{bmatrix} \tag{5.1}$$

$$\boldsymbol{dT = ATdt + BUdt + \sigma d\omega} \tag{5.2}$$

In order to be passed to the MPC controller, the initial state-space model, defined by its matrices, must pass from a continuous stochastic form to a discrete stochastic form. As shown in Fig. 5.6, the state-space matrices A, B, C and D were added and also the stochastic part representing by the G and H matrices, related to states and the outputs respectively. Then, the “Statistical Noise Model” VI was specified. In LabVIEW, “w” is the noise process vector and “v” is the measurement noise vector. Hence, the noise model was constructed specifying the expected mean and auto-covariance of each noise vector, and the cross-covariance between the two vectors, using stochastic estimated values in CTSM-R. Thus, the form of the noise model was that presented in Fig. 5.6 by means of Q, R and N matrices. Q is the auto-covariance matrix of “w”, R is the auto-covariance matrix of “v” and N is the cross-covariance matrix between “w” and “v”.

After that, using the “CD Convert Continuous Stochastic to Discrete” VI, the continuous stochastic model and the associated noise model were discretized. This VI converts the deterministic matrices (A, B, C, D) using the Zero-Order-Hold method, whilst the other matrices (G, H, Q, R, N) are converted according the method you specify. In this case, we used the Numerical Integration, which is set up as default.

Lastly, the “CD Convert Stochastic to deterministic Model” VI was used to convert the model in a deterministic state-space model, as to be accepted by the controller. This VI removes the G and H matrices from the stochastic model equations. Refer to “LabView Control Design User Manual” for a more in-depth explanation.

The "State-Space Model" in LabVIEW is part of the “Model Construction” palette inside the “Control Design and Simulation” module, which includes also the “Predictive Control” palette for creating the MP controller, as shown in Fig. 5.6.

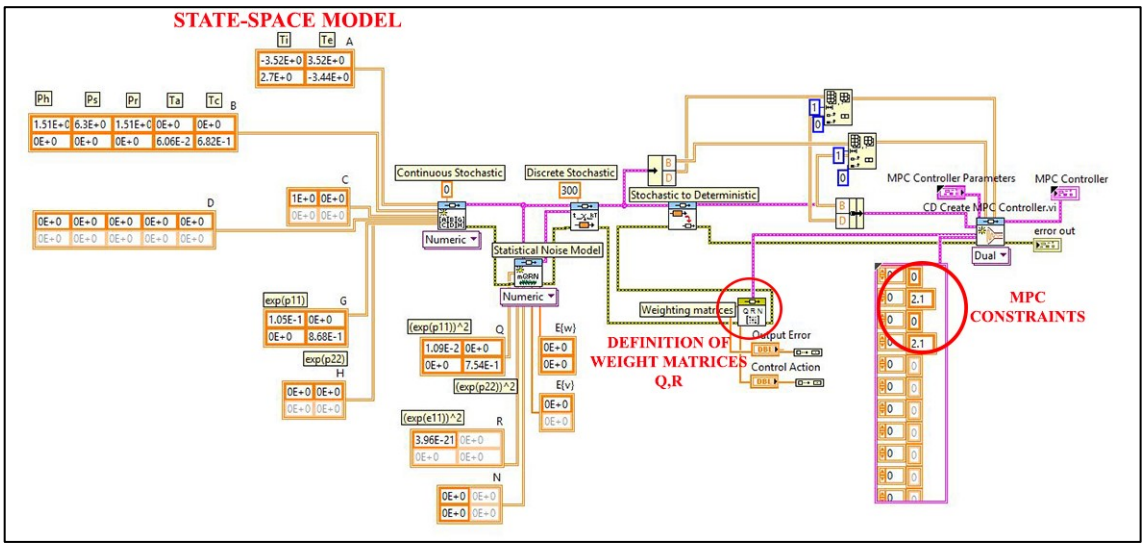

Fig. 5.6 LabVIEW block diagram of the "MPC Controller subVI", including the "State-Space Model", the constraints and the weight matrices, all inputs for the MPC Controller.

5.6 The MPC prototype

5.6.1 Design phase

MPC is a mathematical-model-based, constrained, feedback control. Its design requires the setting of multiple inputs and calculation procedures (Maciejowski, 2002). The basic functioning of such controllers relies on the optimization of an objective cost function which encapsulates the wished process evolution, on the basis of a reliable dynamic model of the phenomenology to be steered and

a suite of limitations to obey to physical laws, namely ranges and thresholds. The optimal control problem loops in feedback and in such receding horizon it propagates states, disturbances (i.e. internal gains), time-dependencies of input variables (weather forecasts, occupancy schedules, …) and constraints (comfort parameters, energy price, …) to properly conceive the corrective action fort the new state (Široky et al., 2011).

Basically, the configuration of the basic control scheme of a model predictive controller consists in designing its three main components:

1. Cost function J(k), formulized in equation (5.3):

$$J(k) = \sum_{j=N_w}^{N_p} [\hat{y}(k+j|k) - r(k+j|k)]^T \cdot Q \cdot [\hat{y}(k+j|k) - r(k+j|k)] + \sum_{j=0}^{N_c-1} [\triangle u^T(k+j|k) \cdot R \cdot \triangle u(k+j|k)] \quad (5.3)$$

"Np" and "Nc" are the prediction horizon and the control horizon respectively and they are connected by the inequality expressed in Eq. 3.12 (Chapter 3). "Nw" is the lower bound of the prediction horizon, equal or greater than one so as to exclude the current state (Nw=0) from the predictive term. "k" is the discrete time step for the completion of a single loop, "$\hat{y}(k+j|k)$", "$r(k+j|k)$" and "$\triangle u(k+j|k)$" are, in order, the predicted output, the output set-point profile and the predicted rate of change of the control action at time $k+l$ given all previous measurements (up to including those at time k), "Q" and "R" are weight matrices, the former referred to the output error (difference between $\hat{y}$ and r), the latter to the rate of change in control action ($\triangle u$) used to set priorities. At first instance, Q and R were set to 1 and 10 respectively so as to give to energy consumption and comfort level the same priority. Such values derived from the tuning procedure, run on the first day of monitoring: the differences between absolute maximum and minimum values of both ambient temperature and FCU power were used to set the respective operative ranges and so the terms of normalization (2.1 kW for the control action and 6.6 °C for the output error). Then, since $\hat{y} - r$ and $\triangle u$ are squared quantities in the cost function, Q and R were initially set on a one-to-ten ratio so as to harmonize the weights.

In first instance, the prediction horizon was fixed at 1 hour in consideration of the time lag between weather changes and indoor reactions, caused by the thermal mass of the glazed façade. According to the calculation methodology described in the standard UNI EN ISO 13786:2008 (*UNI EN ISO 13786:2008*), such delay amounts to 0.43 hours, based on the dynamic thermal characteristics of the layers composing the glass. A certain margin of safety was introduced to take into account potential slowdowns of the control system.

The control horizon "Nc" (a value between 0 and "Np") was tuned to 30 minutes, as trade-off between two competing objectives: on the one hand, the need to preserve the predictive nature of the MPC controller in place of a traditional feedback controller and, on the other hand, the wish to avoid abrupt changes in the control action, and so, the wear and tear of the system ("LabVIEW Control Design User Manual," 2008).

2. Constraints: given the technical specifications of the FCU, a linear constraint (Eq. 5.4) was applied to the control action to fix its lower and upper limits:

$$0 \leq u_k \leq 2.1 \text{ [kW]} \tag{5.4}$$

3. Dynamics/building model: as previously mentioned, the grey-box approach was here adopted to fill the lack of information based on a limited set of experimental data and thus estimate the necessary parameters without excessive computational load (which might had penalized the controller responsiveness). The model relied on building thermal physics laws (principles of energy balance and heat transfer), used to translate the building components into the corresponding elements of the analogous electric circuit. Its formalization is given by the following first-order stochastic differential equations, as already exhaustively explained in Chapter 4 and summarized in par. 5.5 for the aspects required by the controller design.

5.6.2 Development in LabVIEW

In order to test the feasibility of the model predictive control, Laboratory Virtual Instrumentation Engineering Workbench (LabVIEW) software was used to develop a prototype of the real-time control of the office room. LabVIEW is a graphical programming language that uses icons instead of lines of text to create applications, thus its graphical user interface makes it easier to handle such control systems. In contrast to text-based programming languages, where instructions determine program execution, LabVIEW uses dataflow programming, where the flow of data determines execution order.

Users interact with the Front Panel when the program is running. Users can control the program, change inputs, and see data updated in real time. Controls are used for inputs such as, adjusting a slide control to set an alarm value, turning a switch on or off, or to stop a program. Indicators are used as outputs. Every front panel control or indicator has a corresponding terminal on the block diagram. When a VI is run, values from controls flow through the Block Diagram, where they are used in the functions on the diagram, and the results are passed into other functions or indicators through wires.

At the beginning, a Virtual Instrument for data acquisition was created and provided by a Front Panel window, connected to a Block Diagram. Every time a new or existing VI is opened, the Front Panel window of the VI appears and functions as the graphical user interface or GUI of a VI. The source code that runs the Front Panel is provided on the Block Diagram. The front panel window contains a toolbar across the top and a Controls palette that you can access by right-clicking anywhere on the Front Panel.

The development of the MPC prototype in LabVIEW makes use of the "Control Design and Simulation" module and its user manual. Thus, the MP controller was integrated into the main VI of acquisition, defining constraints and specifying weights of the cost function, as detailed below.

Fig. 5.6 shows the definition of the MPC constraints connected to the control action u(k), that is the power of the fan coil (Eq. 5.4) and the subVI to obtain the weight matrices (Q, R) for the cost function (Eq. 5.3) as output.

The "MPC Controller subVI" (Fig. 5.6), containing the building model, must be connected to the "Implement MPC Controller VI" inside the main VI of data acquisition (Fig. 5.7), in order to solve the optimisation problem and predict the output to be sent to the actuator of the plant.

The key components of the MP controller introduced in Chapter 3 (Fig. 3.2), are developed as component of the MPC prototype in LabVIEW (Fig. 5.8):

- the controller (green circles);
- the time-varying parameters, inputs for the controller (yellow circles);
- the predicted output acting on the building by means of the actuator, i.e. the fan coil (red circles);
- the optimal control action calculated and the measurements of the current state at each sampling interval (grey circles).

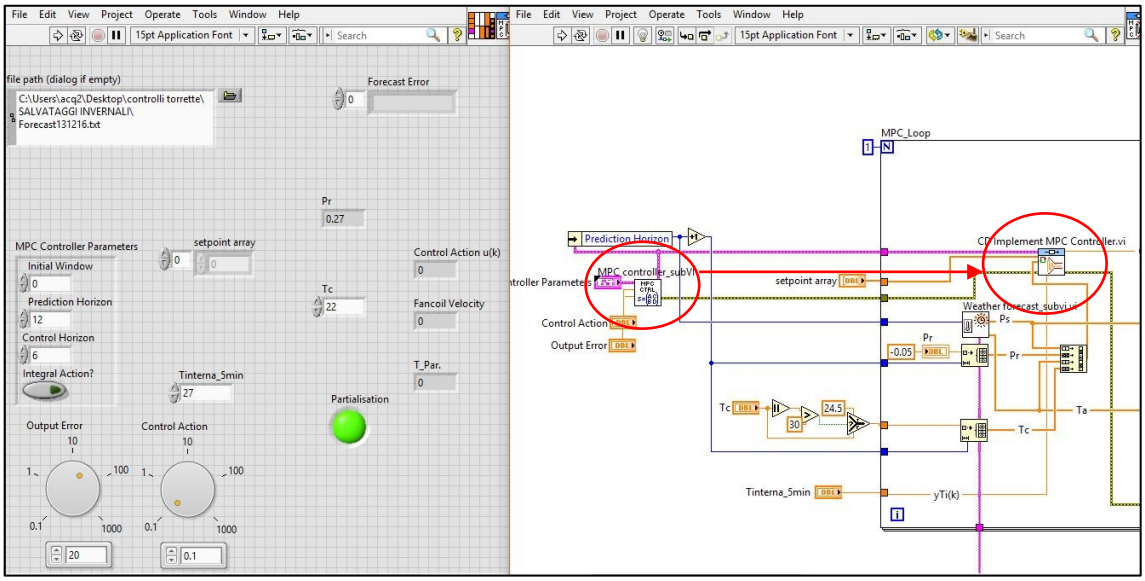

Fig. 5.7 The MP local control developed within the main VI of acquisition in LabVIEW: portions of the Front Panel and Block Diagram, showing the connection between the MPC subVIs.

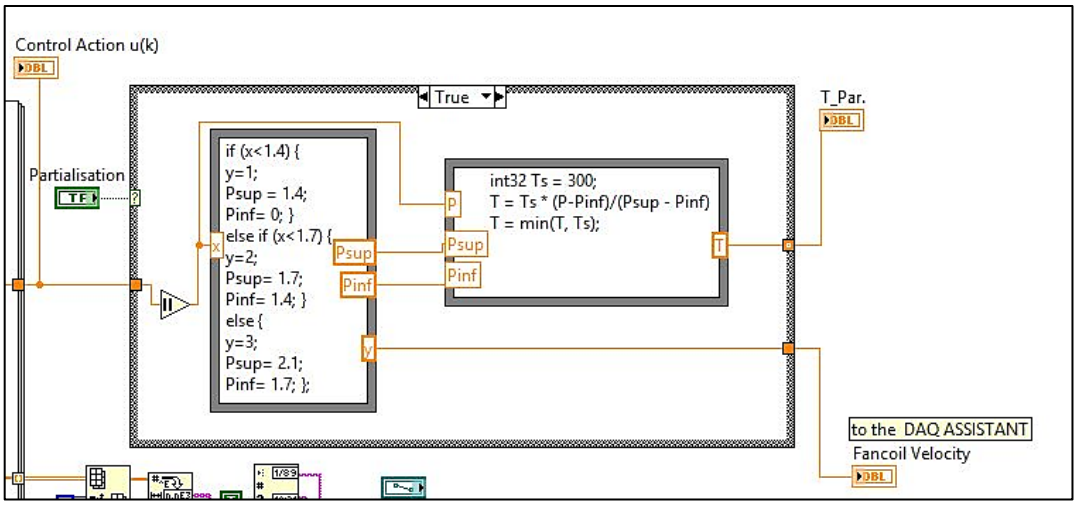

Fig. 5.8 Implementation of the effective time (Tpar) corresponding to the predicted control action.

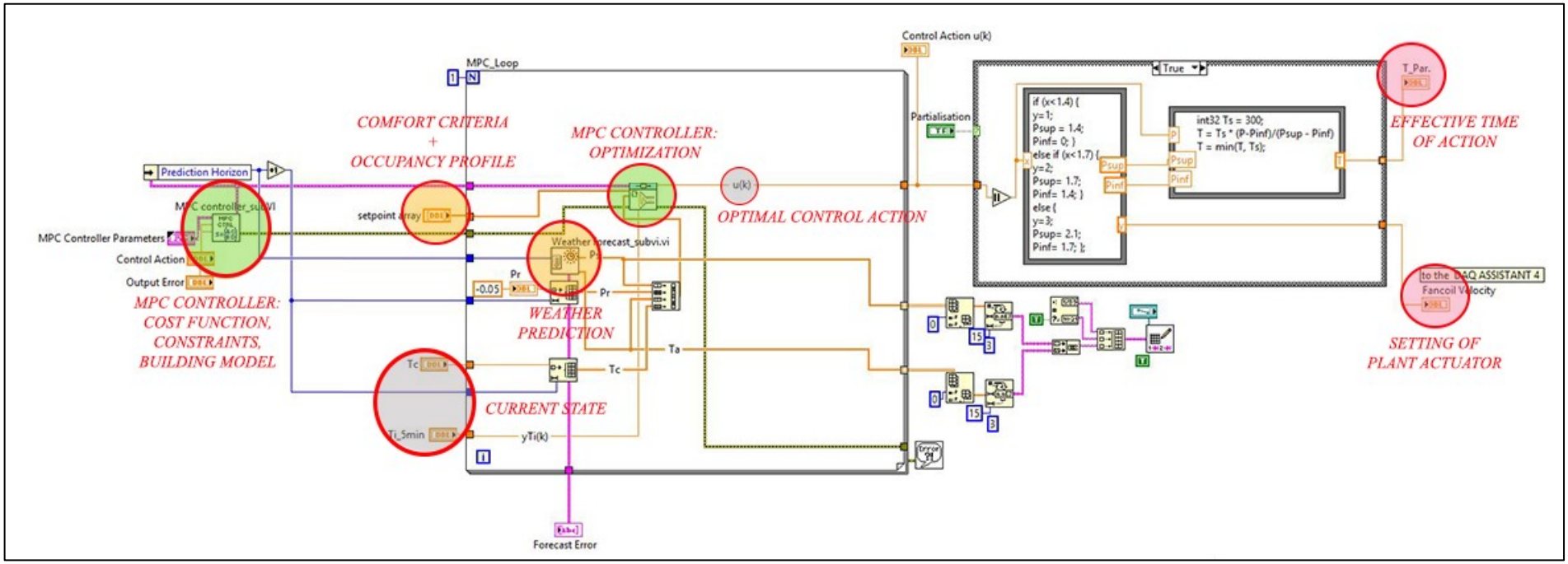

Fig. 5.9 Block Diagram of the Virtual Instrument created in LabVIEW for the MPC prototype.

An extract of the block diagram for the MPC prototype (Fig. 5.8) shows the code implementation of the effective time (Tpar) of duration, that is the time interval when the predicted control action is considered valid within the 5-minutes interval of data acquisition. In fact, the fan coil speed can be set to discrete speed levels (0-1-2-3), corresponding to nominal powers, whereas the control action u(k) [kW], see the grey circle in Fig. 5.9, is the real power that should be provided to the system. Thus, the adoption of the "Tpar" makes it possible to cope with this limitation, ensuring to keep an average of the power calculated by the controller within each interval.

With regard to the time-varying parameters provided as input to the controller, two SubVIs have been created: one for the weather predictions and the other for the occupancy/comfort profile. The "Weather Forecast SubVI" (Fig. 5.10) exploits a MATLAB script (APPENDIX G) implemented in LabVIEW in order to join a forecast website and download weather predictions for the MP controller. Weather data were referred to outdoor temperature [°C] and global horizontal radiation [kW/mq]. They were collected in two arrays, whose size corresponded to the prediction horizon (Np). Besides, also the current values of both the parameters were extracted. As output, the "Setpoint Profile SubVI" (Fig. 5.11) gives an array (size = Np+1) of temperatures required to guarantee comfort conditions within the office, according to the timetable of a typical user of this building: Mon-Fri 7:00-19:00, Sat 7:00-14:00. In our case, the setpoint temperature was set to 24°C. The control was integrated inside the LabVIEW VI of the monitoring and data acquisition system. Fig. 5.12a shows the front panel of the MPC, which represents the interface available for the interaction with the user and also the real-time graph of the fan coil velocity. The corresponding block diagram is provided in Fig. 5.12b and constitutes the highest level of the MPC prototype integrated in the main VI of data acquisition, the same of the ComfortSense system, seen in par. 5.3.

Besides, Fig. 5.12b depicts the connection between the control implemented in the MPC case (left) and the physical system (right) mentioned in par. 5.4 and here represented by the "DAQ subVI" inside the sequence structure. The "DAQ subVI" included the DAQ Assistant Express VI, a digital output module directly linked to the physical system to set the velocity of the fan coil motor.

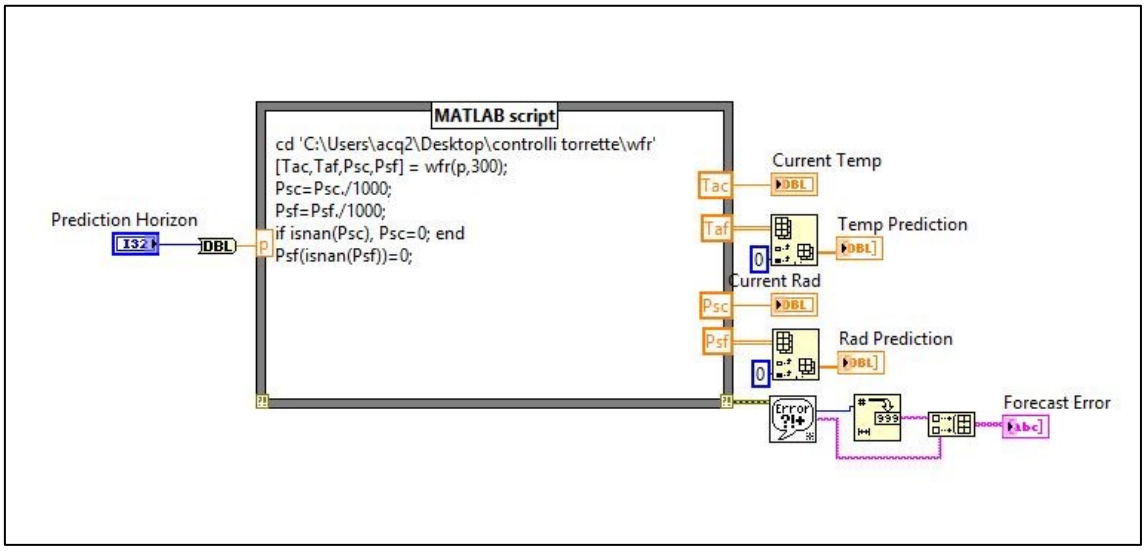

Fig. 5.10 Block Diagram of the "Weather Forecast SubVI" in LabVIEW.

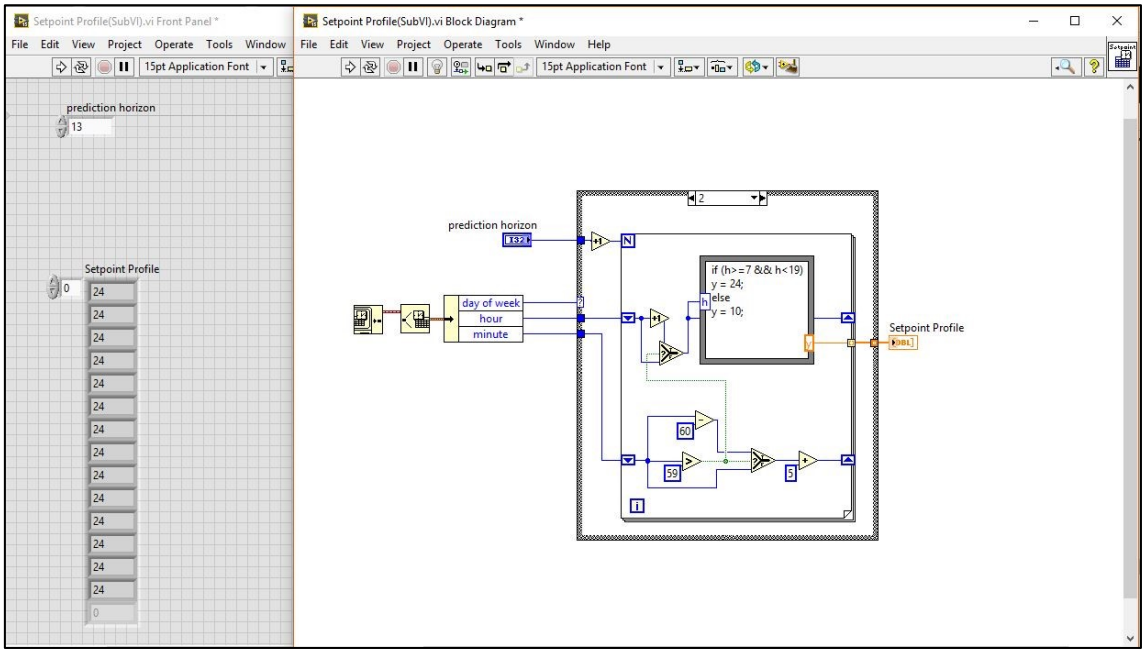

Fig. 5.11 Front Panel and Block Diagram of the "Setpoint SubVI" in LabVIEW.

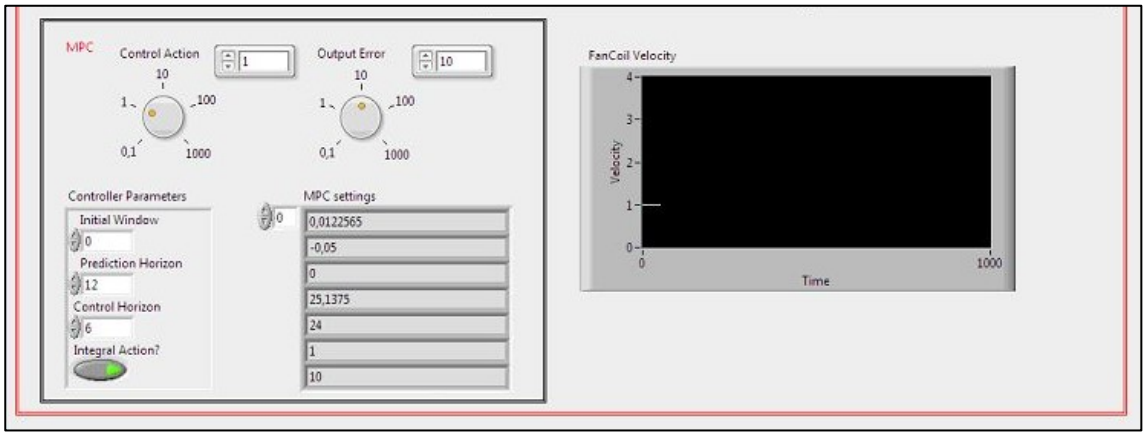

a)

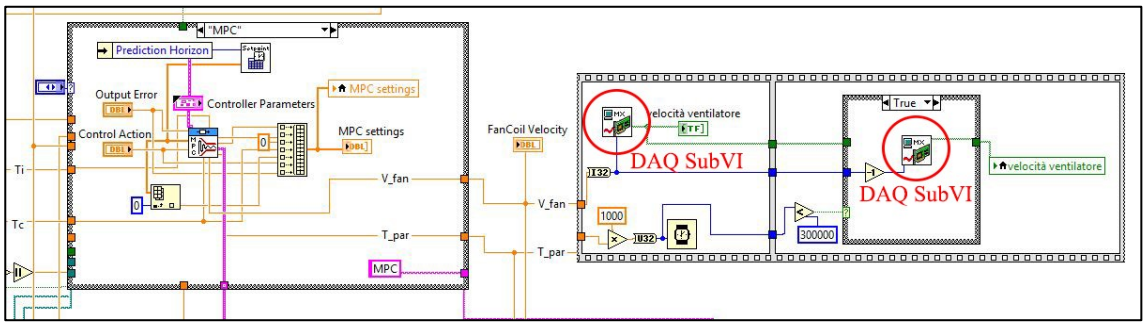

b)

Fig. 5.12 MPC prototype integrated inside the VI of data acquisition in LabVIEW: a) the Front Panel and b) the Block Diagram.

5.7 The experimental test

The test on the MPC prototype was carried out during heating season. The MPC prototype operated in the test room from the 13th to the 22nd of December 2016. In the case study presented, the fan coil, which represents the heating unit of the room, was the only actuator available for implementing the model predictive control. Thus, every 5 minutes the controller returned the adequate power to be supplied to the fan coil. This response was converted into the corresponding speed of the fan coil. Since the thermostatic control of the fan coil has a discrete regulation, at each time step, the right time of holding speed was calculated to simulate the effect of the real control action calculated. An example of the MPC prototype running is given in Fig. 5.13. On the left, the user can read the MPC parameters and the MPC settings from top to bottom:

- control action u(k) [kW];
- AHU power (Pr [kW]), which was fixed;
- internal gain, which was null in this case;
- boundary temperature (Tc [°C]);

- set-point temperature [°C];
- control action weight;
- output error weight.

The "Integral Action?" boolean control specifies whether the MPC controller includes integral action. It can be used to provide for possible inconsistencies between the plant and the reduced-order model. The real-time values calculated by the MPC controller are displayed on the top on the right side of the front panel in Fig. 5.13. The "Probe Watch Window" below gives the user the opportunity to read the output values of the SubVIs in real-time during operation. In this case, the values are computed by the "Implement MPC Controller VI", already presented in the block diagram of Fig. 5.7.

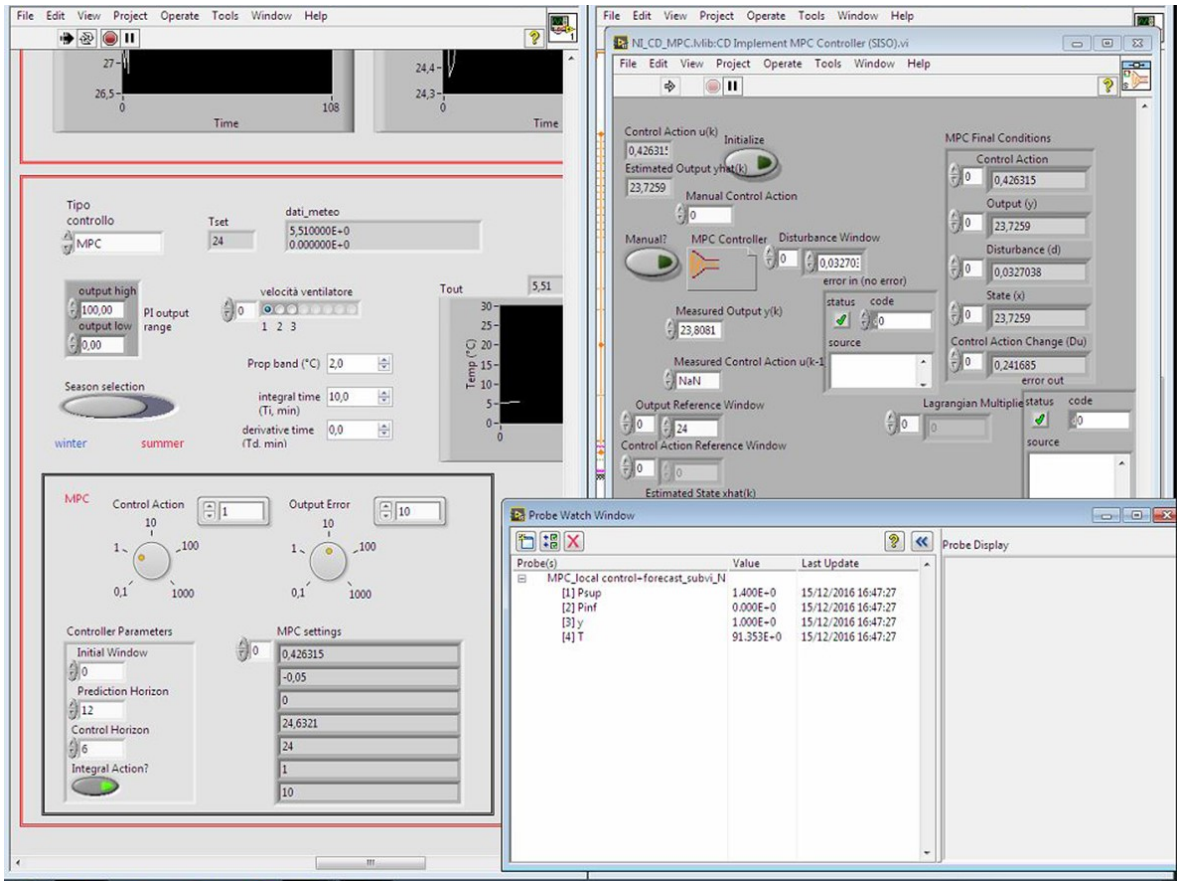

Fig. 5.13 User interface of the MPC prototype during the experimental test.

5.8 Results

The MPC prototype was tested inside the office on the 3rd floor for the entire period available, also at the weekend. No one entered the office during the test and no window was opened. The MPC parameters were set at the beginning of the test. The top and the middle diagrams in Fig. 5.14

illustrate, respectively, the trends of the indoor temperature of the room during all the test period and the operation of the MPC prototype in terms of predicted control action. Tuning was accomplished on the first day and the set point of the indoor temperature in the MPC was set at 24°C. Between the beginning of the second day and the first morning of the weekend, the MPC prototype operated as expected. The conditioning system was kept off during the rest of the weekend, as already said in par. 5.6.2. During the second week, the heating system was not triggered for most of the time due to warm weather conditions, e.g. high solar radiation, as depicted at the bottom of Fig. 5.14. Consequently, the following discussions about the results from the experimental campaign are related to the time period when the MPC worked regularly.

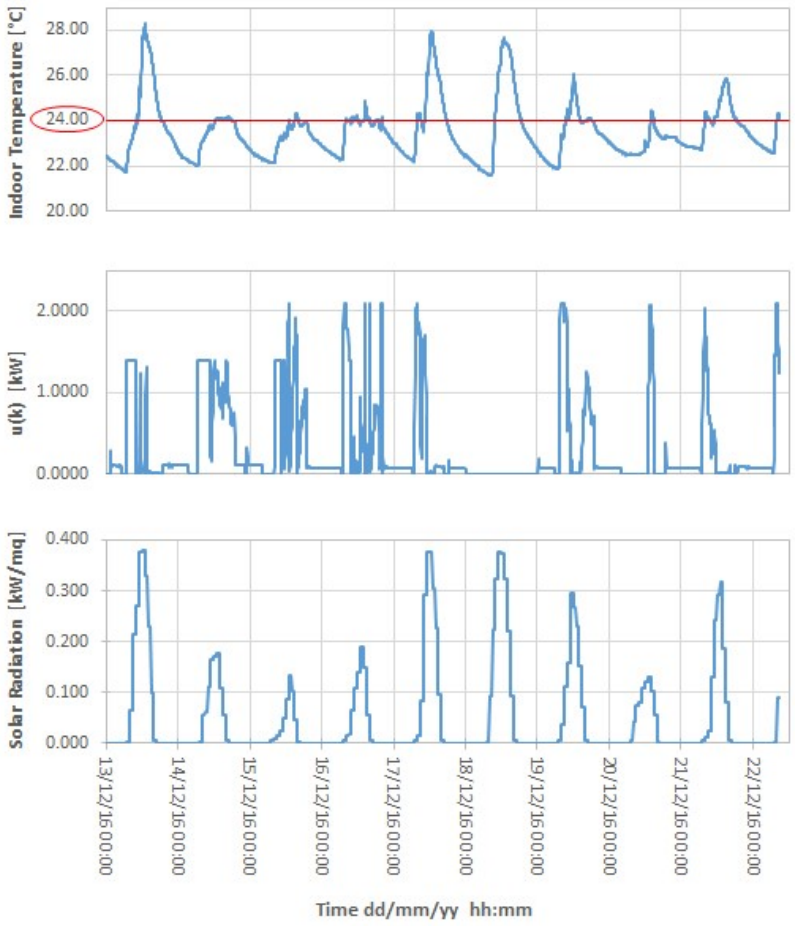

Fig. 5.14 From top to bottom: trends of the internal temperature, the predicted power supply to the fan coil and the solar radiation during the test period.

In order to demonstrate the predictive capability of the MPC prototype developed, a cross correlation function was implemented in MATLAB to measure the time shift between the two-series u(k) and Ps, which is the most relevant variable affecting indoor temperature. To avoid the effect of daily trends, the first order derivatives of the two variables were considered for the correlation. It was

verified that the control action anticipated the effect of solar radiation, as reported in Fig. 5.15, where it is noticeable that the control action u(k) and the solar radiation are shifted and the cross-correlation maximum falls at a lag of 50 minutes. The negative value of the correlation indicates that when one of the two variables increases the other one decreases, as expected.

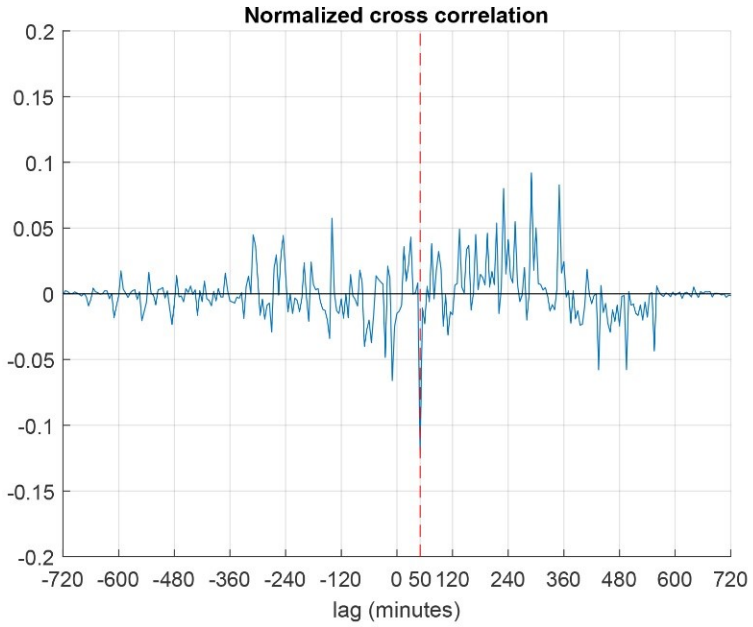

Fig. 5.15 The cross correlation of the two series of control action and solar radiation.

5.9 Comfort and energy assessment

This post-processing phase was primarily focus on comfort parameters, then on energy efficiency during the MPC operation. For this purpose, two representative days were selected: the most overcast (15th of December 2016) and the sunniest (16th of December 2016) over the entire observation period around the winter solstice (13rd-22nd of December). Such choice served the double purpose of investigating lower and upper limits for the overheating occurring inside the office and evaluating the performance of the controller under different borderline circumstances. Detailed information on the boundary conditions is provided in Table 5.2.

An indication of the energy benefit was included too, based on the frequency of activation of the three speeds of the FCU. Each assessment was performed over the hours of expected occupancy. It should be stressed here that, on the 15th of December some issues occurred with the technical system of the office, indeed no control action could be exerted before 8:00 in the morning (one-hour delay in respect of scheduled operation). Therefore, such anomaly has been contemplated in the assessment phase and served the purpose of checking on how the office would have thermally performed in free

running (without any intervention of the controller): in fact, before the implementation of the smart system, the FCU was manually controlled and thus activated just at the arrival of the workers (8:00am).

Table 5.2: Representative days: average weather conditions.

MONITORING CAMPAIGN: 13rd-22nd December 2016		
Controller	**Representative day**	
MPC	15/12/2016	
Average weather conditions during business hours		
Air Temperature [°C]	**Relative umidity [%]**	**Global Solar radiation [W/m²]**
5.40	33	40.75
Controller	**Representative day**	
MPC	16/12/2016	
Average weather conditions during business hours		
Air Temperature [°C]	**Relative umidity [%]**	**Global Solar radiation [W/m²]**
6,25	32	66,22

Comfort Assessment

When it comes to comfort-oriented controllers in mechanically ventilated buildings, the aspects to be taken into account are multiple since multiple are the ways the air jet affects the local and the global air volume in terms of temperature, stratification and turbulence. Indeed, each speed of the fan guaranteed a certain penetration of the air inlet both along the longitudinal axis (distance spanned) and along the transversal axis (effective area) resulting in different throws, spreads and drops. Consequently, each action and each switch of the controller caused a perturbation of the thermal field inside the room by mixing the air layers with different intensities and by triggering more or less pleasant draughts. Therefore, the comfort aftermaths were quantified by calculating the draught rate (DR) and the vertical gradient per each loop. Then the time trends were derived and chartered, together with the corresponding fan speed, so as to define whether the global thermal benefit - which might have been achieved at full-power activations - was counterbalanced by local discomfort phenomena. Finally, in order to address the magnitude of radiant asymmetry and check on the main reasons behind the increase of mean radiant temperature, the output of the RTD network installed on the glazed façade was analysed to:

- identify the maximum values per each of the materials and the positions involved in the measurements;
- investigate the time lag between maximum solar radiation and maximum surface temperatures.

Global comfort evaluations focused on both the environmental and the users' point of view: accordingly, the operative temperature trends and the PMV values were computed and analysed.

Besides, in order to strike potential causal correlations, the simultaneous levels of solar radiation and outdoor temperature were retrieved and comparatively assessed.
For each performance parameter, along with or in place of the graphical representation of the time trends, a suite of charts (histograms of occurrences) was produced to get the dimension of the dispersion around setpoint values and/or comfort limits, generally by splitting the datasets into progressively wider gaps from the ideal target. The occurrences refer to the 5-minute spaced recordings.

Energy Assessment

The energy consequences of the entrance of over-abundant solar gains through the glazed façade were addressed by investigating the need for higher or lower speeds of the fan as they stand for both electric and thermal consumptions. Furthermore, the thermal power supplied by the FCU was calculated based on the on-site, instantaneous measurements of the thermal difference between supply and indoor air and the velocity of the air jet. Such information was analysed in absolute and relative terms:

- by plotting the time trends of the energy consumption, together with the parallel solar radiation and difference between setpoint and operative temperature so as to strike correlations between the energy use and the main triggers for its demand;
- by comparing the frequency of activation of the 3 speeds so as to identify the proportion of corrective action in response to more or less solar gains.

5.9.1 Indoor thermal comfort

In order to comprehensively describe the way the fully glazed façade affected the indoor environmental conditions, both the global and local contribution of convective and irradiative heat flows were addressed to characterize the competing/mutual-empowering interactions between the entrance of solar radiation and the emission of cool air jets from the aeraulic system.
Local phenomena, in particular, were assessed in view of the extensive asymmetries triggered by both the envelope and the HVAC design: indeed, the presence of the large glazed area on one side and of the FCU on the other side (given that the outlet grids were not shaped to take maximum advantage of the Coanda effect) represented a major source for non-uniform distribution of the isotherms.

Global comfort assessment: operative temperature and PMV

The operative temperature (Top) was adopted in the context of this experimental activity since it is a particularly meaningful parameter when irradiative heat transfer plays a major role in the thermal

balance between occupants and surrounding environment: it is calculated as the average of the mean radiant and ambient air temperatures, weighted by the respective heat transfer coefficients.
The suitability of such approach is underpinned both by on-topic Standards (*ASHRAE Standard 55 - 2010*, *EN 15251:2007*, *UNI EN ISO 7730:2006*) and akin scientific papers addressing the same issue (Kalmár, 2016). In order to potentially intervene on the settings of the MPC at any given time on the basis of the achieved comfort performance, the calculation of the operative temperature was programmed in LabVIEW, within the same Virtual Instrument governing the control process. The time trend was chartered in the front panel together with the parallel speed of the fan (Fig. 5.4) so that a gross, prompt indication of the interrelation could be retrieved.
Thanks to such precaution, a strong overheating was notified since the first day of the monitoring activity which forced to correct the settings of the controller.
In fact, the MPC was originally tuned to track a setpoint of 20°C, in compliance with the standardized values afferent to the Italian legislation (*DPR 74/2013*).
De facto, on the 13th of December, the operative temperature never dropped below 20°C, thus forcing to raise the setpoint value to 24°C (still within the acceptable range of wintry operative temperatures and air speeds for the comfort zone according to the ASHRAE Standard 55 – 2010 (*ASHRAE Standard 55 - 2010*) in order to check on the performance of the controller.
Nonetheless, that was the major proof of the ongoing occurrence of uncomfortable conditions.
Therefore, it was unequivocally demonstrated that the vulnerability to overheating for such building typology is a major issue which might undermine the productivity of the occupants and trigger other-SBS related inconveniences/illnesses throughout the year.
Since no means of effective counteraction was identified neither in summer (the cooling load supplied by the FCU, even smartly controlled, was insufficient) nor in winter (the AHU did not operate in cooling mode during the heating season) a substantial retrofitting is apparently necessary (replacement of the current glazed solution with high-performance glasses or electronically switchable glasses, installation of external shadings, …).
The graphs in Fig. 5.16 plot the time trend of operative and outdoor temperatures along with global solar radiation (on the secondary y-axis) for both the days under investigation. The horizontal, thickest red line stands for the setpoint value, while the light-blue graduated scale on the left side defines the legend for the piled column chart representing the fan speeds.
Other two sets of charts are provided to comprehensively depict the global comfort condition:

- the histograms in Fig. 5.17, which display how many times the 5-minute readings of the operative temperature fell within progressively wider ranges around the setpoint value. Such

representation is illustrative of the stability of the control action according to different perturbing inputs from the outdoors;

- the histograms in Fig. 5.18, which show how many times the environmental conditions established inside the office fell within the different categories of comfort defined in the on-topic standards (*EN 15251:2007*, *UNI EN ISO 7730:2006*, *UNI EN 13779:2008*) and recapped in Table 5.3. The results are based on the 5-minute spaced calculation of the PMV index. It was assumed a metabolic rate of 1.2 met (equal to 70 watts per unit of body area), recommended for sedentary activities and a thermal resistance of the clothes equal to 1.0 clo (0.0775 m^2K/W), typical of wintry garments (*UNI EN ISO 7730:2006*).

Table 5.3: Standard comfort categories.

Category	Thermal Comfort Indices		Operative Temperature Ranges	
	PMV	PPD	Winter 1.0clo/1.2met	Summer 0.5clo/1.2met
	[/]	[%]	[°C]	[°C]
I	-0.2÷0.2	<6	21.0÷23.0	23.5÷25.5
II	-0.5÷0.5	<10	20.0÷24.0	23.0÷26.0
III	-0.7÷0.7	<15	19.0÷25.0	22.0÷27.0
IV	>0.7	>15	<19.0 v >25.0	<22.0 v >27.0

Note: In EN ISO 7730, EN15251 and EN 13779 categories are named differently, yet the comfort ranges they refer to are the same.

It should be stressed here that The Predicted Mean Vote is representative of the expected feedback on thermal sensation of a homogeneous sample of people living the thermodynamics of indoor environments (Fanger, 1970), thus it stands for the overall pleasantness of the microclimate. This means that it includes the negative effect of the unavoidable baseline of overheating that led to the adjustment of the setpoint value during the configuration of the controller. Consequently, closest sensations to thermal neutrality are concomitant with morning hours when lower temperatures persisted inside the office. Therefore, such analysis should not be considered representative of the quality of the MPC management (which tended to emphasize the occurrence of slightly warm conditions by tracking the 24°C setpoint), yet it truly depicts the drawbacks of over-abundant solar gains on the proper comfort-driven running of the FCU.

By analysing the trends in Fig. 5.16 it is possible to investigate the way the controller handled the information about current indoor and forecast outdoor parameters to keep the operative temperature in the closest possible neighbor of the setpoint.

Both on the 15th and the 16th of December, the controller started to manipulate the emission of heat when Top was approximately 22.5°C (in the first case around 8am, in the second at 7am) and initiated a progressive escalation of the fan speeds. Then, two different operative patterns were established on the representative days, due to the different start time and amount of solar gains affecting the room:

- on the 15th, speed 1 was initially activated and maintained (in view of the increase of solar radiation predicted for the following hours) until Top exhibited a trend reversal and stabilized

at a certain offset under the setpoint. Consequently, the controller corrected its action by boosting the fan from speed 1 to speed 2. Speed 3 was eventually reached because of the combination of Top below the target value and the forecast of decreasing solar radiation. The full power mode persisted (regardless of the increase of the outdoor temperature, expected for the next hour) until the setpoint was twice overtaken in a time slot of less than 10 minutes. The MPC logic intervened by drastically switching off the fan for a while. As soon as Top showed a mild, but steady decrease, the fan was activated again at minimum power. The maximum overshoot occurred because of the subsequent escalation to speed 2 and 3 around 3pm, in response to a quite stable Top and the prediction of sunset. This suggests that the controller slightly outweighed the effect of solar radiation when its predicted value approached zero and overreacted by releasing more heat than necessary. Indeed, once the overshoot was detected, the algorithm corrected the emission by stepping back directly to speed 1. From 4pm on, neither solar radiation nor outdoor temperature changes perturbed the thermal balance of the office; therefore speed 1 was enough to compensate the heat losses and keep a very stable operative temperature.

- On the 16th of December, the MPC rapidly proceeded through the three power levels to emphasize the natural rise of Top and quickly drive it to the target value. Until no significant increase of the solar radiation was forecast, speed 3 persisted without causing any relevant overshoot, even with Top very close to or slightly exceeding the setpoint. Such behaviour demonstrates the suitability of the developed grey-box model in depicting the sensitivity of the test room to solar gains so that the control action could be pondered on the right driving forces. At 9am the MPC detected a significant increase of solar radiation expected for the next hour and corrected the action by directly switching to speed 1. Such setting persisted until 2.15pm since a minimum heat influx was necessary to compensate the heat losses (thanks to more favorable weather conditions than those recorded the previous day). Given the dramatical drop of solar radiation predicted to occur at 3pm, a 20-minute-lasting action at maximum power was preventively adopted until a certain overshoot of the setpoint was detected. Another activation, even briefer, of speed 3 occurred in view of the sunset, thus remarking the potential room for improvement in the settings of the controller to better manage the forecast zeroing of the solar contribute.

Despite such occasional boosts of the fan, the controller succeeded in preserving a steady operative temperature close to the target value by resorting to the minimum power throughout the operative time frame. As regards the overheating affecting the building, from 7am to 8am on the 15th of December, when the system breakdown prevented any control action, the operative temperature rose

from around 20°C to 22.5°C as a result of the sole effect of solar gains entering through the glazed façade. Moreover, on the 13th of the month, when the test started and the MPC settings were defined, the operative temperature ranged between a minimum of 21.6°C and a maximum of 27.7°C in the time slot of expected occupancy, given an average solar radiation of 170 W/m^2 (higher than that experienced during the other days of monitoring of the MPC): this means that, around winter solstice solar gains are still so abundant to drive the operative temperature not just over the heating setpoint, but even over the cooling setpoint (26°C) without any active intervention. Moving on to the statistical figures, the histograms in Fig. 5.17 display how the operative temperature recordings distributed around the setpoint during the operation of the MPC, thus comparing the stability of the control action in response to the two different boundary conditions.

An additional set of histograms is provided to check on the differences with the performance of the fuzzy controller which piloted the FCU during the previous test, run in summertime. Even though the weather conditions that accompanied the two experimental rounds were completely different, such frequency distributions are representative of the level of indoor comfort achieved inside the office as a result of the smart management of cooling/heating loads. Therefore, some comparative conclusions can be drawn between the predictive, model-based logic and the heuristic approach.

The MPC proved to better master the building thermal dynamics on sunnier days. Indeed, on the 16th of December, its action was never belated and promptly compensated the predicted necessary corrections right before the steepest rises and falls of the solar radiation curve (at 10am and 3pm approximately). That caused minimum overshooting (even less than during more overcast days) and minimum offsets from the setpoint. In detail:

- on the 16th of December, the 5-minute-spaced Top measurements fell within the ±0.2°C range around the setpoint for more than the 77% of the time. The almost total remainder fitted the range ±0.2 to ±0.5°C.
- on the 15th of December, most of the readings were distributed between the two above ranges (35.4% of the time in the former and 25.4% in the latter) thus validating the quality of the control action in the event of diverse boundary conditions. The residual 40% was quite equally distributed among the other subsets in Fig. 5.17.

The limit of ±2°C was never exceeded. Then, analyzing the frequency distribution of the Predicted Mean Vote index (Fig. 5.18), is evident that Category IV conditions were always averted by the model-based predictive logic. Category II was ensured for the 85% and the 80% of the time on the 16th and the 15th of December respectively. The coldest temperatures on the overcast day allowed to establish even Category I conditions over a considerable time window (from 8am to 10am, standing for the 18% of the occurrences approximately), while the higher solar gains on the 16th

were responsible for non-negligible persistence (13.1% of the time) of Category III comfort levels (acceptable for existing buildings).

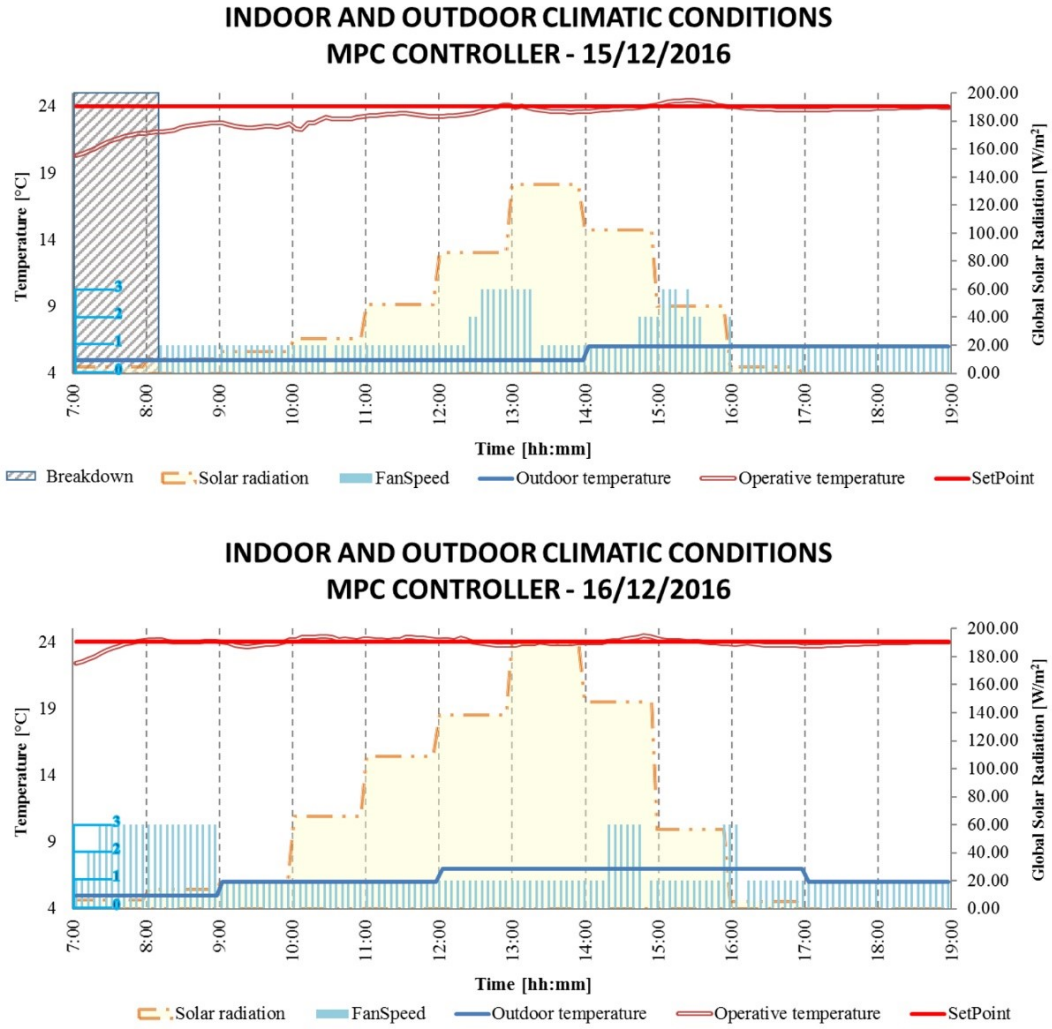

Fig. 5.16 Global comfort assessment: time trends of operative temperature against setpoint threshold, solar radiation and concomitant fan speed.

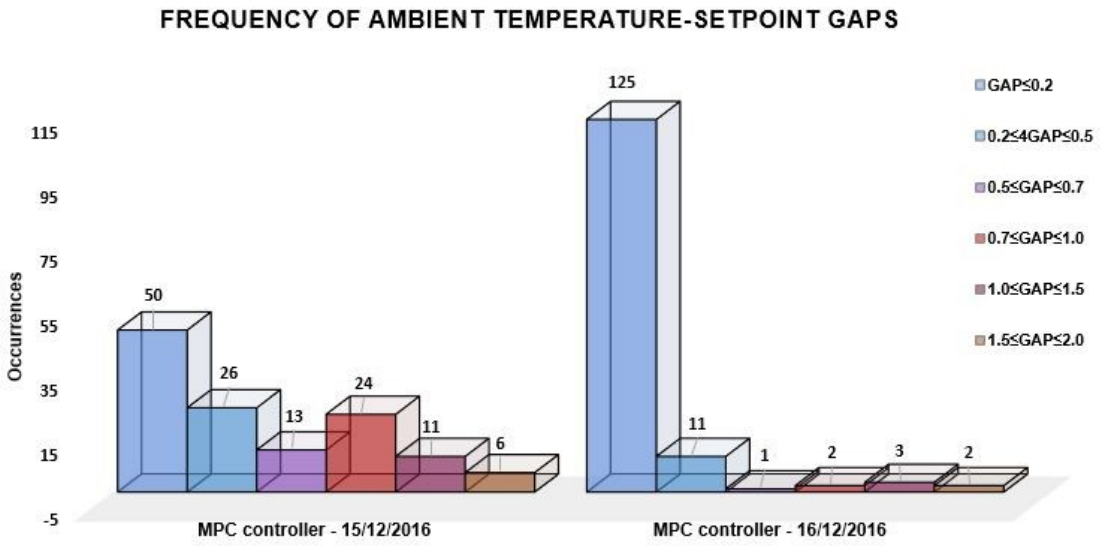

Fig. 5.17 Global comfort assessment: histograms of occurrences - operative temperature offset from the setpoint.

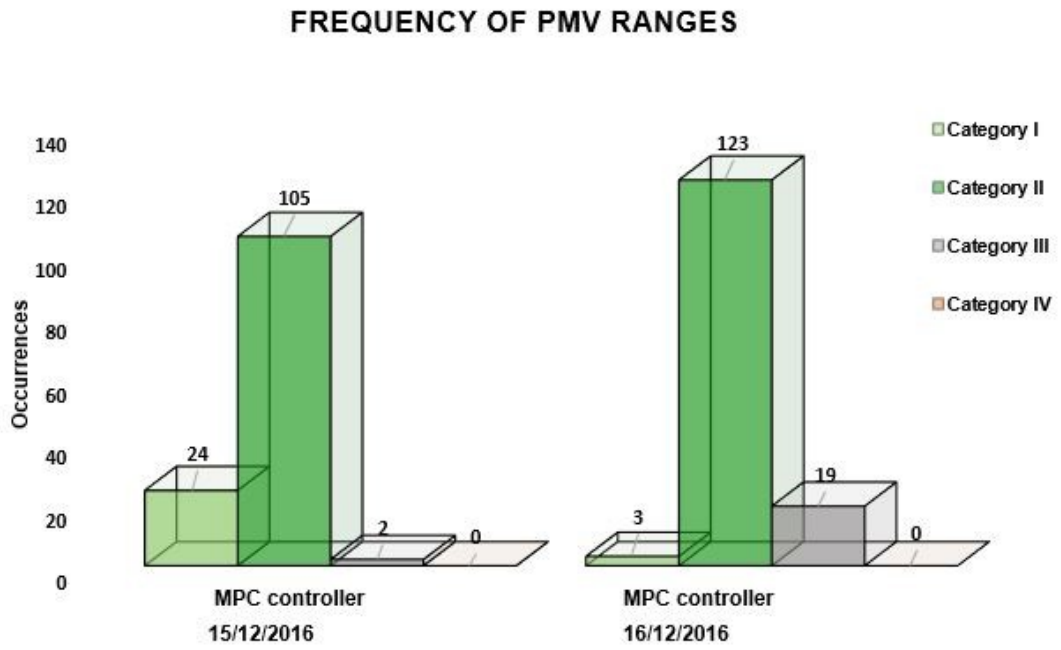

Fig. 5.18 Global comfort assessment: histograms of occurrences - PMV value.

Local comfort assessment

Although comfort criteria might be successfully fulfilled on a spatially-averaged scale, situations might differ on a local-scale. In presence of a single FCU serving a small indoor volume, the

likelihood of discomfort phenomena, namely drafts and vertical gradients, tends to be non-negligible. Besides, the presence of a single, very large glazed façade is a major trigger for asymmetries. Accordingly, a series of evaluations based on measured data was carried out to check on confined areas of high potential for thermal dissatisfaction.

In order to define the extent of the discomfort inside the office in object, the *occurrence of draughts* was investigated. The likelihood of excessive or excessively variable air velocity in the casuistry in object was mainly linked to:

- the protracted exposition to solar radiation, that heated up the internal surfaces, which, in turn, gradually released the stored energy to the neighboring air volumes thus creating a vertical thermal gradient and impelling convective updrafts;
- the air jet from the FCU, which was responsible for considerable air movement, beneficial in terms of mixing and homogenizing, yet detrimental in terms of local air acceleration and turbulence (sparsely tolerated in wintertime (*UNI EN ISO 7730:2006*)).

The second trigger for local environmental non-uniformities is the vertical thermal gradient. The vertical gradient of the air temperature depends on the distribution of the heat sources, especially along the height (AC systems. lighting, occupants…). Given the denial to access the room all over the monitoring campaign, the potential uneven stratification of the air could be directly related to the air jet from the fan coil and to the penetration of solar beams (no other internal gains).
Against this backdrop, the outputs of the draught probes were post-processed to calculate the draught rate (DR) and the vertical gradient at 1.1 m and 0.1m, according to the formulation in ISO 7730 and other Standards (*ASHRAE Standard 55 - 2010*, *UNI EN ISO 7730:2006*).
The analyses were performed for both the representative days, by producing:

- Plots of the time trends (Fig. 5.19), compared to the recommended upper limits in compliance with Category II requirements set out in EN ISO 7730 (20% for DR and 3°C for vertical gradients). On the secondary axis is reported the action of the FCU in terms of activated speed so as to strike causal links between the intensity of the local discomfort and the momentum of the air jet. It should be stressed that only the 0.1-metre value for the DR is displayed since the measurements at higher heights were negligible.
- Histograms (Fig. 5.20), which display how many times the 5-minute calculations of the vertical gradient fell within progressively wider ranges approaching the comfort limit. When mixing devices are deployed, instead of displacement ventilations, the thermal uniformity tends to be jeopardised when high airflow rates are activated (Lin et al., 2005). Therefore, the least the need for full-power air conditioning, the least the impact on local discomfort.

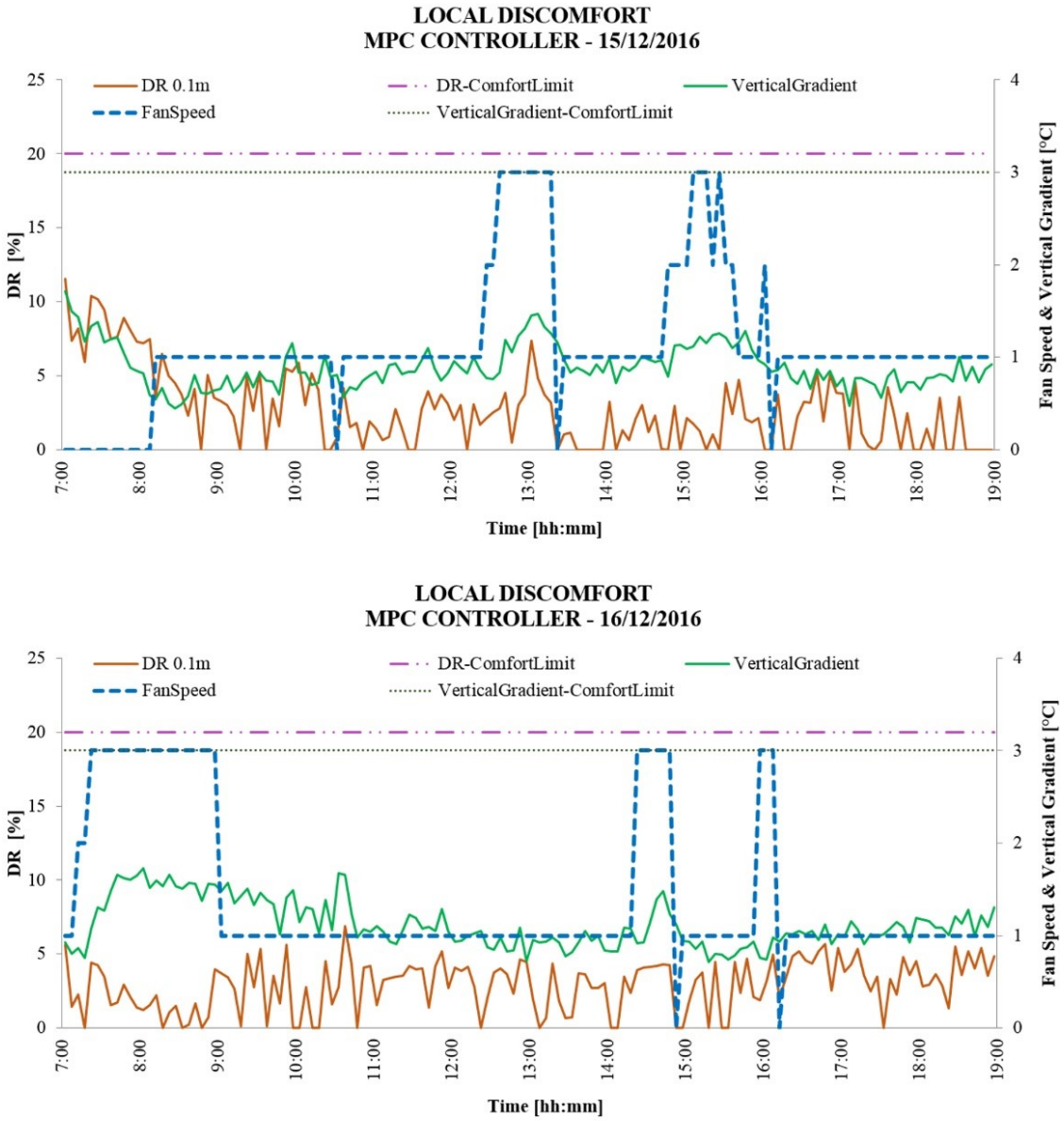

Fig. 5.19 Local comfort assessment: time trends of the draught rate at 0.1m and of the vertical gradient against the respective comfort limits and the concomitant fan speed.

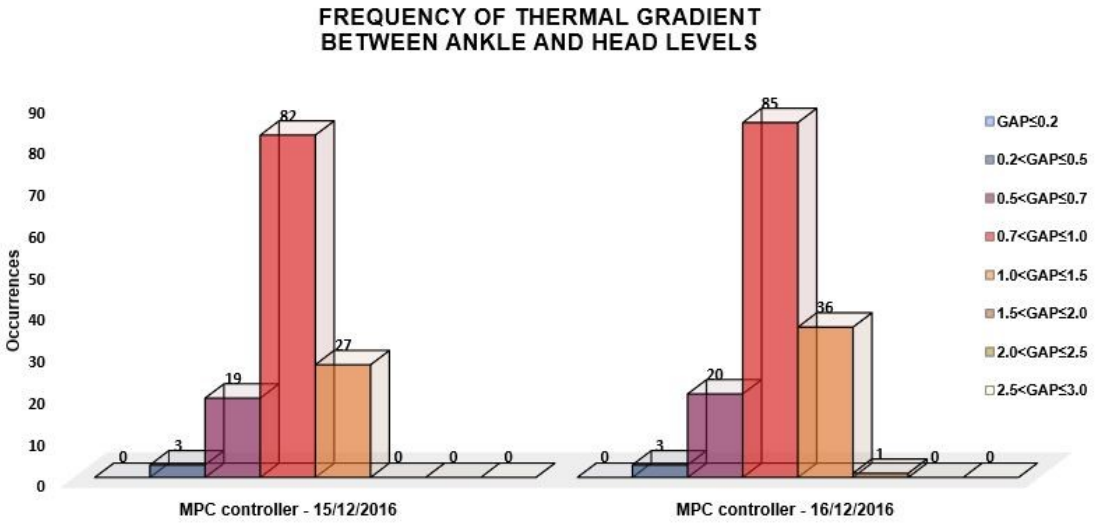

Fig. 5.20 Local comfort assessment: histograms of occurrences – vertical thermal gradients.

The main reason behind imparting predictive features to an AC controller was to prevent strong, delayed corrective actions and to distribute the energy loads on smoother, longer-lasting low-power calls. Consequently, the risk for strong vertical gradients was expected to get mitigated. The main observations can be recapped as follows:

- the comfort limits were never exceeded. Consequently, no local discomfort was generated by the control action pursued by the MPC;
- on the 15th of December, the maximum and average DR values at 0.1m (excluding the spikes due to the initial breakdown) were 7.4% and 2.0%, when speed 1 was activated, whereas the respective percentages under full-power air jets were 10.4% and 4.6% (speed 2 ran too briefly to be reasonably evaluated). The correspondent figures recorded on the 16th were 6.9% and 3.1% for speed 1, whilst 2.26% and 1.13% were detected for speed 3. This might be explained by contemplating the effect of solar radiation at ground level: on the 16th of December, the floor surface was more intensively heated up by the Sun, thus reaching a higher temperature and transferring more thermal energy to the air volumes blowing past it. Consequently, higher thermal uniformity was achieved throughout the room and lower turbulence was impelled since the warm fluid jet from the FCU better mixed with the local convective updrafts;
- on the 15th of December, the maximum, minimum and average vertical gradients were 1.46°C, 0.47°C and 0.88°C, when speed 1 was activated, whilst the respective values at speed 3 were 1.68°C, 0.71°C and 1.06°C. The correspondent figures recorded on the 16th were 1.38°, 0.45°C and 0.85°C for speed 1, whereas 1.73°C, 0.74°C and 1.38°C were detected for

speed 3. Therefore, on sunnier days, higher-power injects triggered more substantial thermal gradients, as expected. Instead, very cloudy conditions (predominance of diffuse radiation) led to a complete reversal of the usual thermal behaviour pattern: this suggests that more vigorous air mixing is beneficial when floor temperature is lower since it helps to amalgamate the stratified air layers.

Overall, the thermal gradients were more pronounced on the 16th, because of the protracted use of speed 3 in the early morning, when the indoor surfaces where still cold: in such conditions, the thermal gap between ankle and head level was remarkably higher since the momentum of the air jet could span a major area and cover a greater distance.

Finally, by plotting the different frequencies of progressively wider vertical gradients (Fig. 5.20), it was possible to underline whether the predictive nature of the MPC was beneficial in terms of air stratification. As expected, the vertical gradient never exceeded 2.0°C under the regulation of the predictive logic. The greater time percentages corresponded to the 0.7°C÷1.0°C and the 1.0°C÷1.5°C ranges all over the MPC control: 62.6% and 20.6% on the 15th of December versus 58.6% and 24.8% on the 16th.

Among the sources for local discomfort, non-uniform radiant distributions are prominent.

They can be measured as difference between the plane radiant temperature of the two opposite sides of a small plane sensitive element, placed in a representative point of the room under test and then compared to the comfort limits identified by (Fanger et al., 1985).

Asymmetric thermal radiation caused by warm vertical surfaces is expected to cause less than 5% of dissatisfied occupants when radiant asymmetry is below 10°C (*UNI EN ISO 7730:2006*). Yet, in the case of windows, further discomfort might come from direct sun beams and glare, especially if the glazed façade is large enough to let the sun penetrate throughout its diurnal path.

Among the environmental parameters, radiant asymmetry strongly depends on the surface temperature of the indoor elements.

Therefore, even though plane radiant temperature measurements were not performed during the monitoring campaign, some relevant information was derived by commenting on the temperature distribution on the internal side of the south-exposed façade, instrumented with the net of flat RTDs. On both the representative days of December, solar radiation peaked between 1pm and 2pm, while the maximum surface temperatures were recorded two hours later on the 15th and one hour later on the 16th. Fig. 5.21 maps the distribution of the maximum values. Multiple comparisons can be drawn.

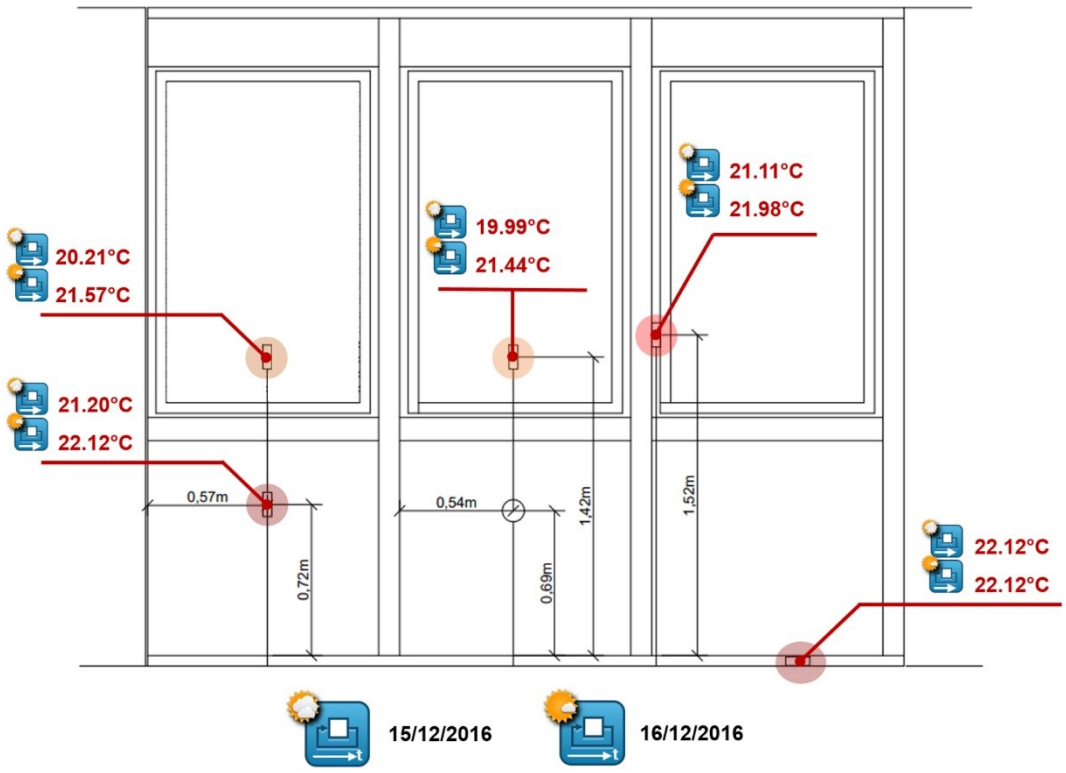

Fig. 5.21 Local comfort assessment: thermal distribution of the maximum surface temperatures on the glazed façade.

Firstly, by comparing the pairs of values displayed per each probe, it is possible to point out the differences between days dominated by direct or diffuse solar radiation.

Regardless of materials and position, on the 16th all surfaces reached higher temperatures and kept them longer. The only negligible increase is the one on the frame at floor level: this might be explained considering the shadowing effect of the shielded horizontal band in the first 1 meter of the façade which, de facto, annulled the local contribution of direct solar radiation.

As expected the maximum differences were recorded by the Pt100s installed on the glazed panes, in particular, +1.46°C on the central module and +1.37°C on the leftmost module. The different location, in fact, impinged on the amount of solar radiation received in the early morning, when the sunbeams on the lateral window were temporarily obstructed by the bordering construction elements. The shielded panel and the inter-window frame exhibited milder increments, yet close to 1°C (0.92°C and 0.86°C respectively), in view of their lower thermal transmittances.

Another consequence of the different resistances to the heat flow exerted by the variously composed portions of the south façade, is that the glazed components (and the opaque elements in close proximity) stayed cooler over the entire monitoring period, as the thermal gradient between outdoors and indoors impelled stronger heat transfers.

In fact, a second comparison between different materials (same height of the probes) revealed that the leftmost glazed module stayed 1°C and 0.55°C cooler than the shielded horizontal band directly below on the 15th and the 16th, while the recordings from the RTDs on the central windowpane and window frame differed by -1.12°C and -0.53°C respectively.
The gaps were halved on the sunnier day because the glazed components could absorb much more radiation.
A third comparison aimed at investigating the role of position by juxtaposing the pairs of values recorded on the same day and on equal materials, yet different heights of the probes.
Since the maximum levels of solar radiation were recorded in the afternoon, the leftmost elements were more intensely irradiated and heated up: accordingly, the probe on the lateral module detected a surface temperature greater than that recorded by the aligned probe on the central module by 0.22°C and 0.13°C on the 15th and 16th of December respectively. The difference was less noticeable on the sunnier day since the maximum surface values were reached one hour earlier (between 2:15pm and 3pm) than on the 15th when the sun was still high upon the horizon.
A substantial discrepancy (+1°C) arises by comparing the recordings of the probes on the frame, between floor level and window level in overcast conditions: that might depend on the higher thermal losses by conduction experienced by the aluminum uprights towards the adjacent cooler glazed surfaces when the direct sunlight was not sufficient to properly counterbalance. Conversely, the floor frame and the shielded horizontal band surface temperatures were always very close thus not impelling any significant conductive transfer (thereby keeping the frame warmer). On the 16th of December, such gap was dramatically reduced: the inter-window frame stayed just 0.15°C cooler than the floor frame. The reason is that the thermal gradient between frame and window was halved with respect to the correspondent recordings on the 15th, as previously discussed.

5.9.2 Energy consumption

Comfort and energy savings are commonly antagonist targets in building design. Nevertheless, in case the source of discomfort leads to the exacerbation of the cooling/heating loads the two purposes might align. Therefore, some of the conclusions drawn for the comfort assessment are de facto illustrative of the energy aspects too. The main indicator for energy consumptions is the fan speed, since each operative mode of the motor corresponds to different thermal/electric power levels (APPENDIX C). Accordingly, the histograms in Fig. 5.22 were produced to:

- investigate the differences occurring between a winter day of high solar radiation, when the sun deeply penetrated inside the office and a winter day when the sky was much more cloaked by clouds;

- verify if the controller pondered its control action in a reasonably balanced way or exhibited a remarkable, anomalous "preference" for any of the speeds which might have been re-allocated, avoided or mitigated in consideration of the environmental conditions simultaneously recorded in the room.

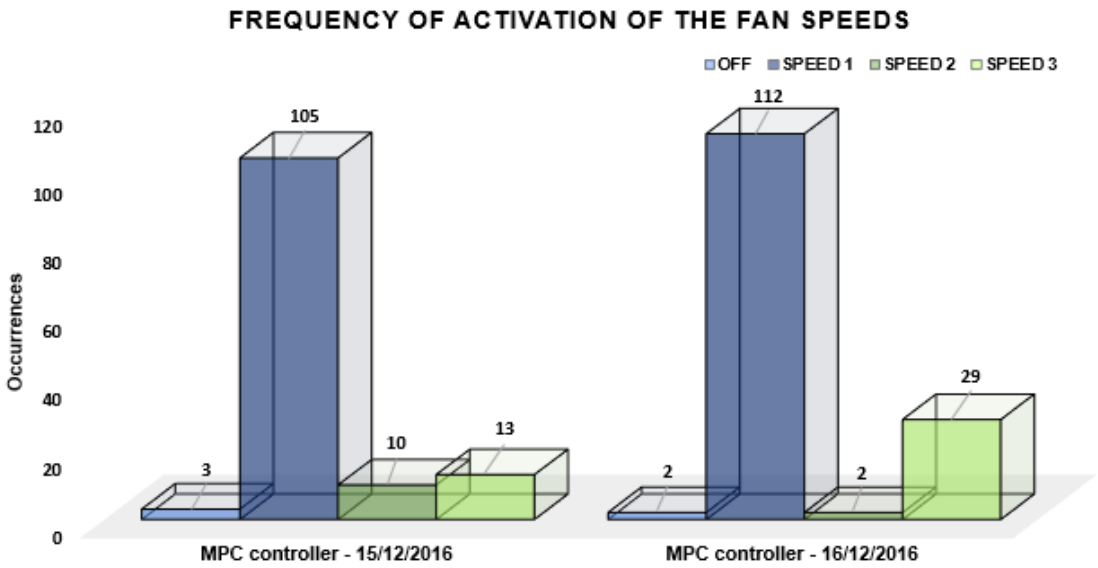

Fig. 5.22 Energy assessment: histograms of occurrences – fan speeds.

Finally, in order to strike causal relationships between the performance of the controller and the concomitant weather conditions, a further assessment was carried out. Thanks to the installation of the anemometer and the thermo-hygrometers upstream and downstream the heating terminal, it was possible to measure the power supply to the indoor environment and calculate the energy consumption. Fig. 5.23 displays its time trend, overlapped to the curves of solar radiation and of the distance between operative temperature and setpoint: these parameters were selected as major driving forces for the heating calls (since the perturbing action of outdoor temperature was found to be less extensive).

In terms of balanced operation, the MPC showed a systematic low utilization of the medium power, regardless of the specific boundary conditions: it seldom activated speed 2 for protracted time slots (7.6% and 1.4% on the sunnier and cloudier days), privileging quite abrupt switches from speed 1 to speed 3 and vice versa. Indeed, minimum power levels were deployed for the 80.2% on the 15th and the 77.2% on the 16th, while full-power runs occurred for the 10% and the 20% of the time respectively. Such result outlines that a certain scope for improvement, in terms of energy savings, might come from a different setting of the speed activation conditions so as to enlarge the

intermediate power zone and compress the time slots of maximum consumption. The FCU switched off over a very limited time window (2.3% on the 15th and 1.4% on the 16th in percentage terms) as it seldom occurred that the operative temperature was above the setpoint line in concomitance with high or predicted high solar radiation.

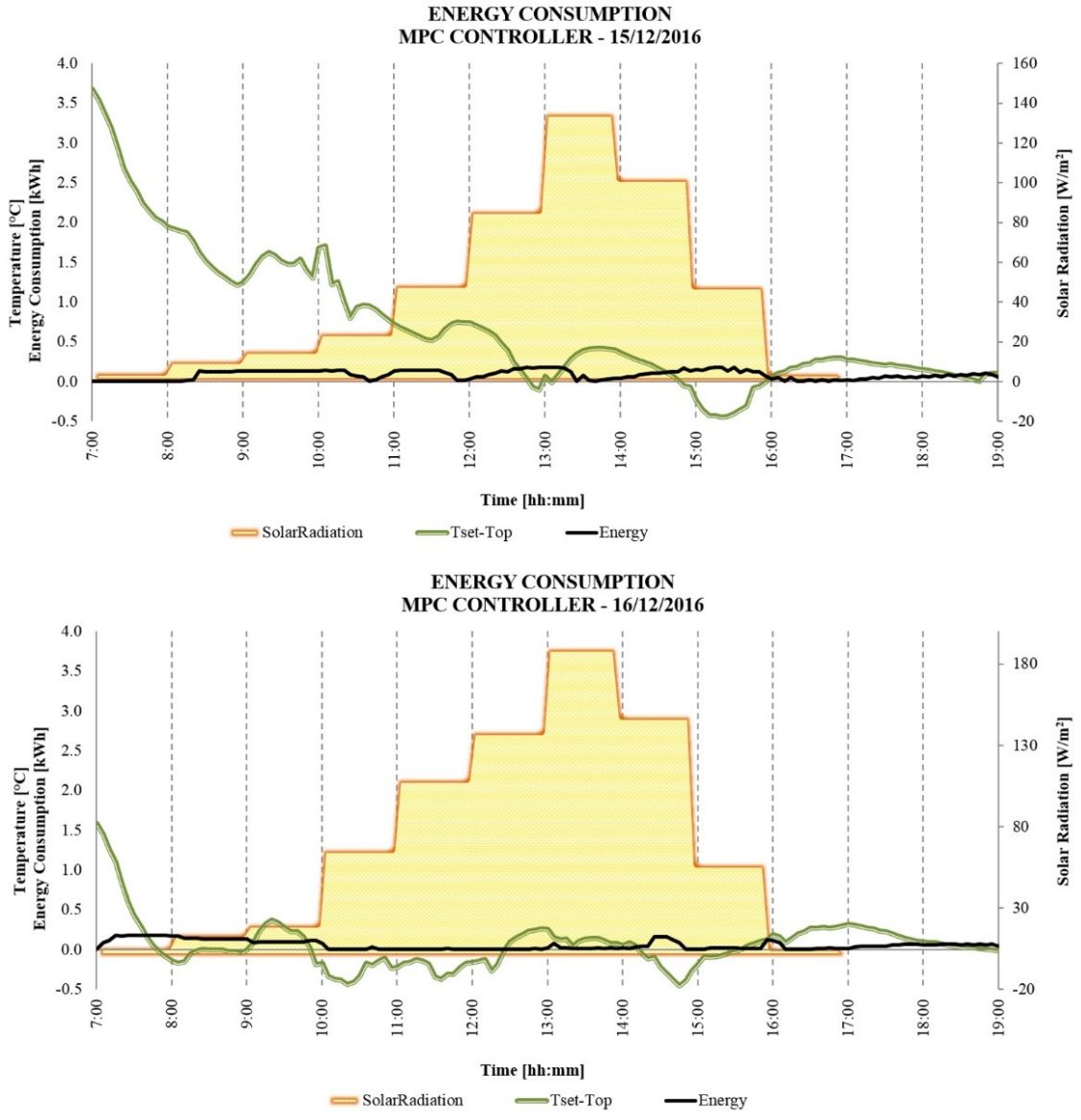

Fig. 5.23 Energy assessment: time trends of the energy consumptions against solar radiation and the simultaneous offset from the setpoint.

The time trends in Fig. 5.23 reveal that minimum energy consumptions occurred in three instances:

- peak hours of solar radiation, since little energy release was necessary to counterbalance the heat losses and contain the potential overheating, given that the predictive controller had already boosted its action in the hour before;

- operative temperature slightly below the setpoint and concomitant/forecast high radiation, since solar gains were predicted to suffice in maintaining comfort conditions;
- after sunset, since no significant perturbing action existed and the heat losses were mostly compensated by the heat re-emitted by the surfaces into the enclosed space.

On the other hand, maximum energy consumptions possibly occurred in three main occasions too:

- operative temperature considerably below the target value and concomitant/predicted low solar radiation;
- consistent predicted increments/decrements in the level of solar gains (especially right before sunset);
- operative temperature above the setpoint accompanied by concomitant/predicted high solar radiation.

The strongest control actions always occurred when the indoor temperature drifted: it is evident that the MPC better handled direct than diffuse radiation (given its mathematical-model-based nature) as both the major crests and the major troughs of the temperature offset took place on the 15th of December. The total energy consumption was 11.96 kWh/day and 7.82 kWh/day over the period of expected occupancy on the two consecutive representative days. It should be stressed here that the prominent call for heating concentrated in the first hour of operation (7am to 8am) when the operative temperature was far below the setpoint, thus the consumptions on the 15th of December were slightly underestimated because of the initial breakdown.

5.10 Conclusions

This chapter surveyed the feasibility of the MPC control, trying to bridge the lack of real-time applications by developing a MPC prototype of a test room in LabVIEW environment.

The grey-box model for the winter season developed in Chapter 4, was adopted for the test room in order to run a considerable number of iterations for the optimisation of the controller process in a short period of time.

It proved to be an effective solution to feed the controller, even if, in the validation phase, it reported a discrete RMSE value in simulation, as provided in par. 4.3.6.3 (Chapter 4).

During the experimental test, the MPC prototype revealed its predictive power, which has been detected by applying a cross correlation function between main variables involved, the control action on the FCU and the solar radiation. This demonstrated that the optimal control response provided by the controller, anticipated the effect of solar radiation inside the test room with a maximum shift of 50 minutes.

Moreover, the two days of maximum and minimum solar radiation were selected for assessment. The severity of global discomfort was evident from the very beginning of the field-test:
the MPC couldn't be tuned to track a setpoint value of 20°C , according to the Italian legislation (*DPR 74/2013*, n.d.) since the operative temperature naturally rose above such threshold all over the time window of expected occupancy (7am-7pm), thus forcing to raise the target value to 24°C.
Besides, during the first day of measurements (to tune the MPC), when the room was in free-running, the operative temperature ranged between a minimum of 21.6°C and a maximum of 27.7°C given an average solar radiation of 170 W/m^2.
The control action of the MPC strongly mitigated the risk of discomfort: it succeeded in preserving a steady operative temperature close to the target value by properly anticipating the perturbing action of weather changes and by pondering the power released by the FCU accordingly. Indeed:

- the operative temperature mostly fell within the ±0.5°C range around the setpoint (95.8% of the time on the sunnier day and 60.8% on the cloudier day). The limit of ±2°C was never exceeded. Given the almost optimal performance in conditions of high solar gains (and so higher surface temperatures of the glazed façade components), it was proved that the MPC mastered the thermal dynamics of the building by successfully preventing both the overshoot of the setpoint and considerable temperature drops;
- the PMV never exceeded Category III limits, while Category II conditions were satisfied for the 85% and the 80% of the time respectively;
- vertical temperature gradients and draught rates stayed always below the respective discomfort thresholds (maximum 1.7°C on the sunnier day and maximum 10.4% on the cloudier day);
- the fan operated at minimum speed for the greater time percentage on both the sunny and the cloudy day (77.2% and 80.2% respectively). Full-power activations occurred just for the 20% and the 10%of the time.

Overall, even though the overheating proved to be a major risk for the liveability of the indoors, even in winter time, the smart control of the technical system via MPC logic resulted in non-negligible improvements from all considered perspectives.

Chapter 6

Development of a MPC simulator

6.1 Introduction

The chapter presents the development of model-based predictive control, described in Chapter 5, in simulation environment. This chapter investigates the potentiality of the control logic and the procedure tuned, by testing different scenarios, which are prohibitive in the real building, as to provide a complete overview of the problem. Following, the methodology section better explains the goals of this last part of the research, underlining the differences compared to the experimental phase. Then, the focus is on the definition of the main simulator components and consequent results obtained through this approach.

6.2 Methodology

The application of model-based predictive control presented in this chapter, is based on promising results obtained during the experimental phase, using the MPC prototype. The need to suspend the experimental activity at the end of the year, has provided the inspiration for a simulation research, exploiting the already acquired knowledge and consolidated tools, to assess situations that could not be considered within the actual building.

By having available the detailed model of the building (the case study), it was created a predictive control simulator in Simulink, a modelling software closely integrated with MATLAB, proceeding similarly to what was done to realize the prototype. This choice allowed to investigate internal conditions by changing operation period, control settings (e.g. the tuning MPC parameters) but, most of all, it was possible to test effective solutions for the building renovation.

Since the most evident problem of this building was the discomfort, mainly caused by the overheating phenomena, it was assessed the introduction of solar shadings in the building model, which was relative to third floor of the building, more detailed for the test room previously described. The structure of the MPC, as it has been developed, provides the chance to consider more than a control action as output of the optimization problem. Thus, the adequate shading level for the test room, the

office 90, has been added as control variable, to be calculated at each time interval, together with the already defined control action for setting the fan coil velocity.

Comfort and energy assessments cannot leave the choice of MPC parameters out of consideration. If the weights of the cost function generally depend on priorities fixed by the policy of building management, the tuning of prediction and control horizon could be reasonably investigated to define ranges of empowering in building performance.

Therefore, as a first step, the detailed building model, representing the physical system, was connected to the simulator and the summer season was settled as control period as to have a complete overview on system operation.

Secondly, it has been necessary identify the components to feed the simulated control, on the track of the approach followed earlier and enriching the architecture by introducing new modules for testing more scenarios.

As previously underlined, the grey-box model for the controller takes on a core function in the MPC framework. Therefore, it was necessary to provide the controller with an appropriate model for the summer season identified on data, this time simulated by the detailed model, using a random input for the fan coil. The modelling procedure ended by the identification of the best model and its validation. After that, this model was integrated in the simulator architecture, linked to a new module to test the estimation of the model during the controller operating.

Then, all the input parameters needed for the prediction time window were added and connected to the controller.

The last design phase of the simulator concerned the configuration of the controller. The optimization function was implemented for calculating the output response both the FCU power and for the shading level. In fact, at the same time, these were also inputs for the detailed model, which represented the virtual reality.

6.3 The Detailed Model

In order to simulate the real physical system and communicate with the simulator, the detailed model of “Polo Eustachio” was used. The detailed building modelling is not the subject of this research, a more detailed explanation of its building up is found in (Piccinini, 2016). Here, only the information necessary to completely understand operation of the MPC simulator will be provided. Therefore, the detailed model was realized in simulation environment only for the south block of the total building volume, using Dymola software, version 2018, and Modelica Buildings library 3.0.0. This building zone can be considered both structurally and thermally as a block, this was evidenced also by the investigation of the original project.

The model should be complete and sufficiently representative of reality, also to planning future scenarios of renovation, thus the detailed model should rely on a solid basis of real information, many times available on project. Dealing with existing buildings, this is not taken for granted and often information is incomplete and does not reflect the current state, thus, to increase the accuracy of the building model, a survey campaign was conducted by installing wireless Hobo sensors on the third floor, as described in par. 4.3.3. Monitoring data were also used after the modelling process for the calibration of the various components of the plant, as anticipated in par 4.3.2.

Within the model, temperature and humidity sensors were placed inside the test room, the office 90, to have a direct feedback of indoor comfort level. In this dissertation, to feed the simulated controller, the focus will be limited only on the third floor and the test room of the detailed model. For this reason, the original model built up was simplified to keep the components useful to the simulator, as shown in Fig. 6.1.

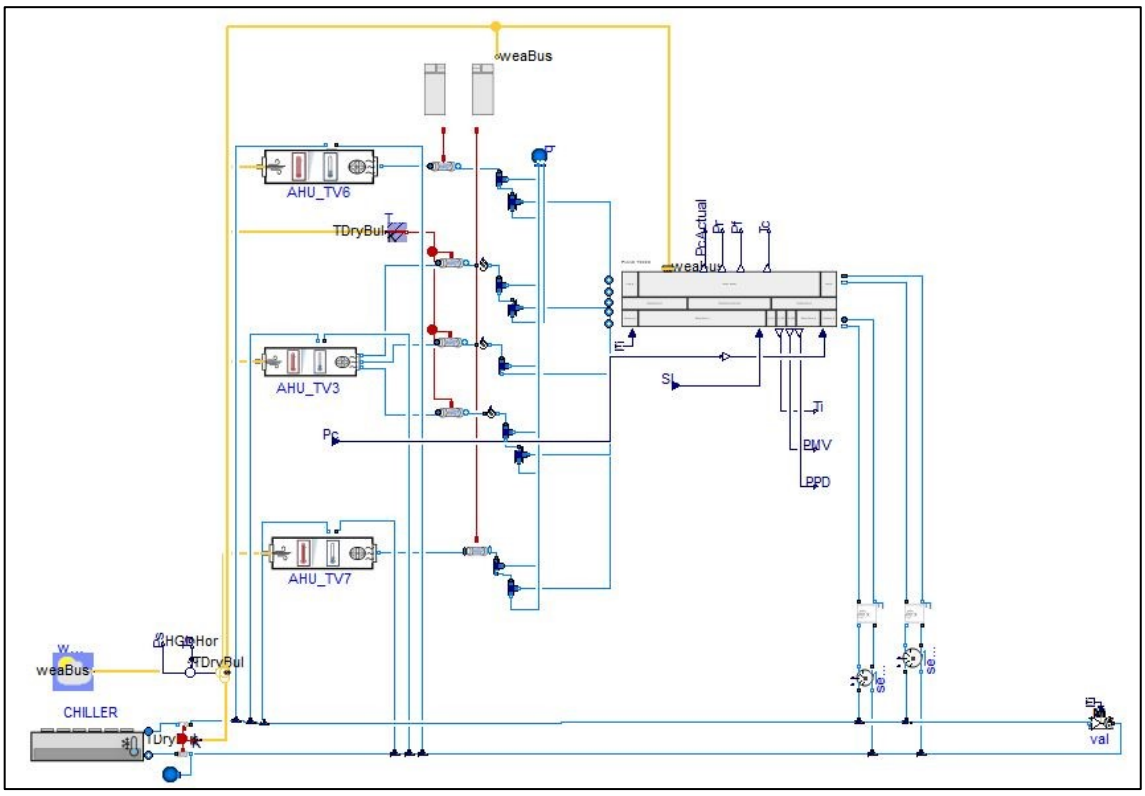

Fig. 6.1 The detailed model of "Polo Eustachio" developed in Dymola: the third floor and the plant components used in the simulator.

The investigated third floor was subdivided in thermal zones (Fig. 6.2), including the test room, and they were modelled by the "MixedAir Room", model of a room in which the air is completely mixed (Fig. 6.3). These instances are volumes with their own physical and technical characteristics and they must have linked each other coherently, correlating them with adequate information about:

orientation, weather data, opaque and transparent surfaces, boundary conditions, adjoining heat-exchange surfaces, direct connection between environments, fixed or variable heat inputs for the occupancy, lighting and equipment in the rooms, envelope layers.

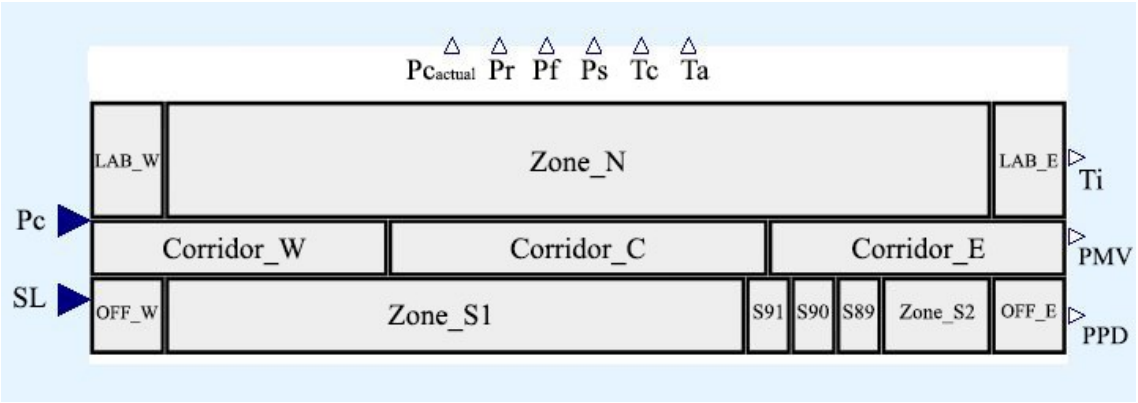

Fig. 6.2 Thermal zones subdivision for the third floor.

In this research phase, the summer season was simulated, consequently the plant components (Fig. 6.3) of the simplified model were: the AHUs (Air Handling Unit) supplying the third floor, the chiller for the production of the refrigerated fluid and the FCUs (Fan Coil Unit) for the air conditioning of each thermal zone. Besides, the entire air distribution system has been modelled and it is graphical represented by the light blue wires in Figg. 6.1-6.3.

The comfort assessment was performed with PMV and PPD comfort indices, introducing a specific component of Modelica Buildings library, "FangerMean", in the detailed model (Fig. 6.4). This thermal comfort model, created according to Fanger, as described in ("Buildings.Utilities.Comfort," n.d.) on Berkeley LAB website, was then compared with ranges imposed by reference comfort standards. The "FangerMean" instance was connected to the test room, office 90, that is the reference room of this study to the comfort assessment.

The Predicted Mean Vote (PMV) model combines four physical variables (air temperature, air velocity, mean radiant temperature, and relative humidity), and two personal variables (clothing insulation and activity level) into an index that can be used to predict the average thermal sensation of a large group of people. Clothing is defined in terms of clo units. Clo is a unit used to express the thermal insulation provided by garments and clothing ensembles, where *1* clo = *0.155* (m^2*K/W) ("Buildings.Utilities.Comfort"). In this study, the metabolic rate was fixed at 60 W/m^2, representing a sedentary activity, whilst an adaptive clothing was designed, so the value for clothing insulation varied depending on mean outdoor temperature.

The operative temperature is defined as the uniform temperature of an imaginary black enclosure in which an occupant would exchange the same amount of heat by radiation plus convection as in the

actual nonuniform environment. The operative temperature is computed as the average of the air temperature and the mean radiant temperature, weighted by their respective heat transfer coefficients.

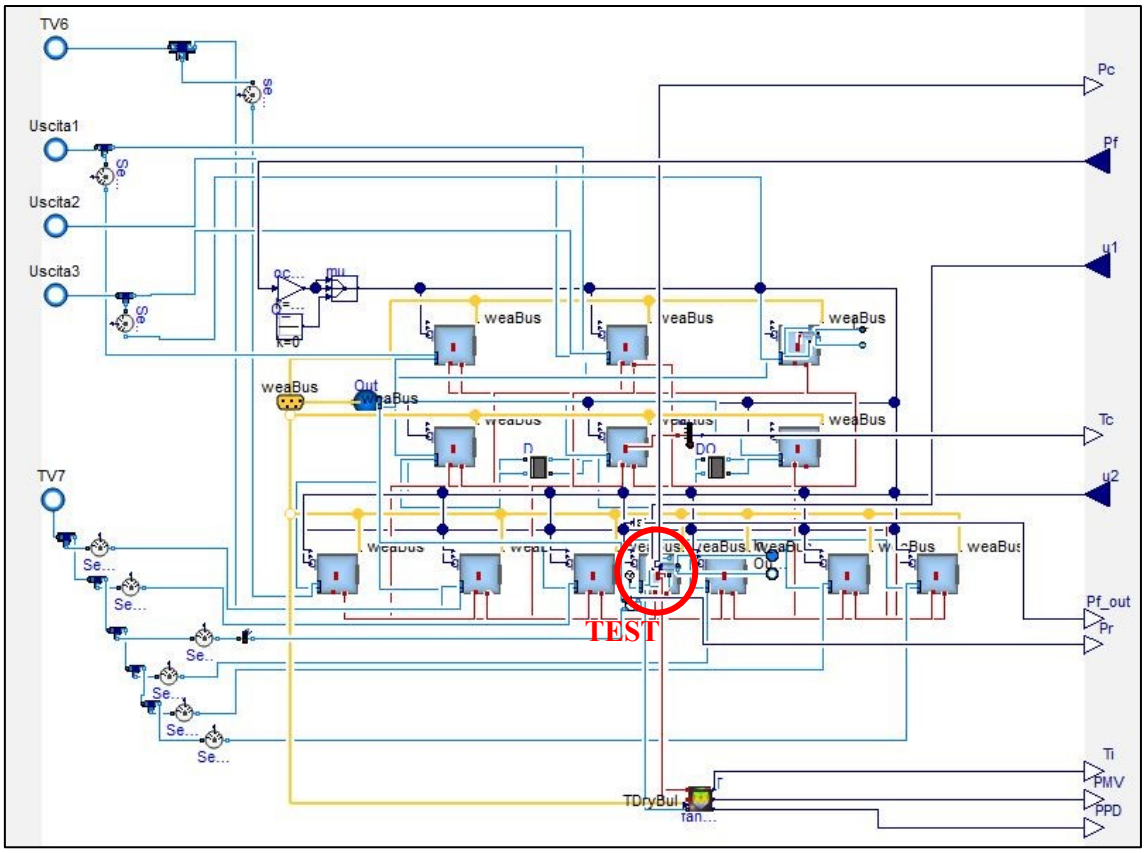

Fig. 6.3 The third floor built up in Dymola and used as virtual reality for the simulator.

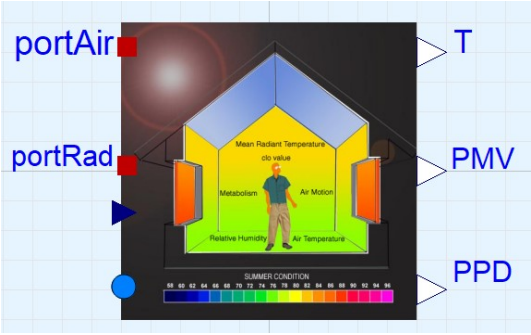

Fig. 6.4 Fanger mean icon in Dymola: on the left, inputs to be provided and, on the right, outputs returned.

According to this standard, for a given space, the optimum operative temperature for summer season (clothing= 0.5 clo) is 24.4°C, corresponding to PMV=0 (neutral). The PPD index, obtained from the PMV index, provides information on thermal discomfort (thermal dissatisfaction) by predicting the percentage of people likely to feel too hot or too cold in the given thermal environment.

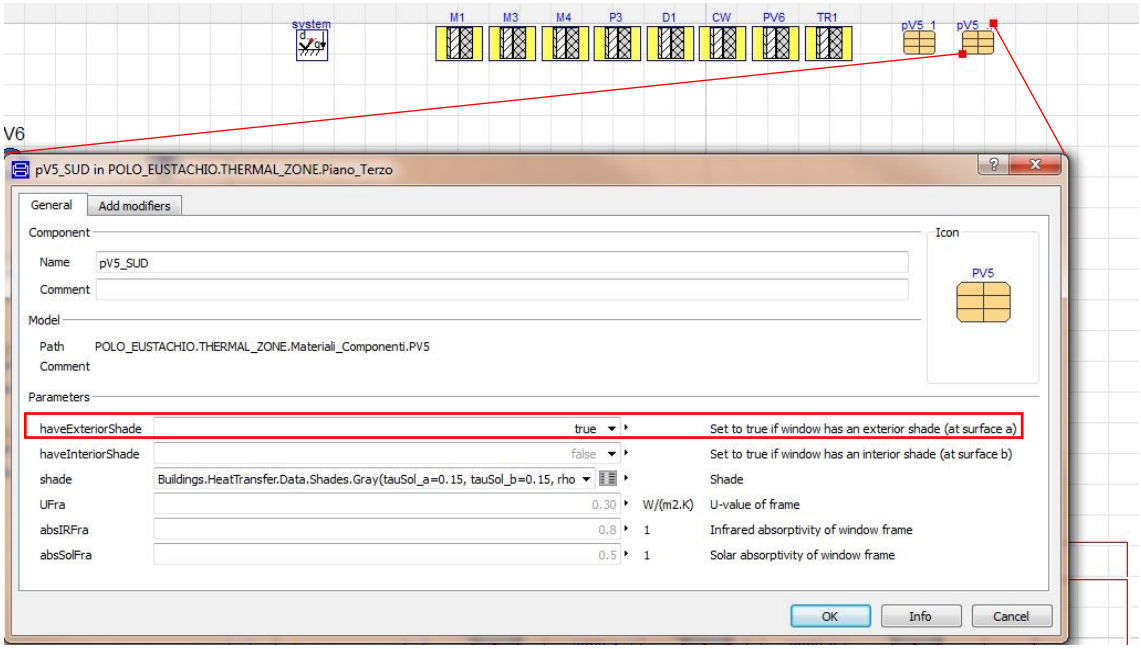

Fig. 6.5 Modifying the glazed component to introduce the solar shading in the detailed model.

A powerful aspect of the detailed model has been the chance to reproduce scenarios otherwise impossible to test in the real building. This was the case of the introduction of solar shading within the model, by modifying properties of glazed wall (Fig. 6.5) and consequently providing a connector (the "SL" blue triangle in Fig. 6.2) to manage the shading level (SL) directly by the controller simulator, as will be explained in next section.

Finally, the detailed model has been exported to be used in the simulator, built up in Simulink environment. In this regard, the FMI ("Functional Mock-up Interface") standard allows any modelling tool to generate C code or binaries representing a dynamic system model which may then be seamlessly integrated in another modelling and simulation environment. A model package implementing the FMI standard is called a Functional Mockup Unit (FMU). To generate FMU, you must go to the "Simulation" tab in Dymola and click on the menu arrow to the right of "Translate" icon and choose "FMU". A pop up window shows the settings options for exporting the FMU. In this specific case, to optimize simulation run-time, the exporting option of "Model exchange, and Co-simulation using Cvode" was chosen, then the FMU of the detailed model was generated, in Dymola working directory.

"FMI Kit" for Simulink contains a Simulink FMU block, which enables embedding of FMUs into Simulink models. The package for FMU import into Simulink together with the Dymola support for FMU export facilitates simulation of Dymola models in Simulink. In particular, this enables use of Dymola solvers in Simulink through the FMI Co-simulation interface. "FMI Kit" for Simulink has

full FMI support for both export and import, which means that both versions 1.0 and 2.0 of the FMI standard are supported for both Model Exchange and Co-Simulation. Supported MATLAB releases are R2010a to R2016b (32- and 64-bit). FMU export supports both Windows and Linux. FMU import is currently only supported on Windows. “FMI Kit” for Simulink can be used for free without any license key. In this study, the “FMI Kit” 2.4.0 and MATLAB 2015a versions were used.

The procedure to import an FMU into Simulink and the associated settings/configurations requires to open the Simulink library browser (View > Library Browser) and drag the FMU block from the FMI Kit library into the model. Double-clicking the FMU block, it is possible to load the chosen FMU. By default, the block has the output ports defined by the FMU, but it is allowed adding or removing output ports, selecting one or more variable in the specific “Variables” tab. The “Variables” tab shows all variables of the FMU. Input variables are marked with an arrow on the left, whilst output variables with an arrow on the right of the icon. The start value, unit and description of the variable are displayed in the “Start”, “Unit” and “Description” columns.

6.4 MPC framework in simulation environment

Following the steps previously defined in the Methodology section, after the FMU of the detailed model was imported into Simulink environment, the simulator was built all around, as shown in Fig. 6.6. Three main components of its architecture are highlighted with coloured rectangles and their function, within the simulator, will be explained in the next subparagraphs.

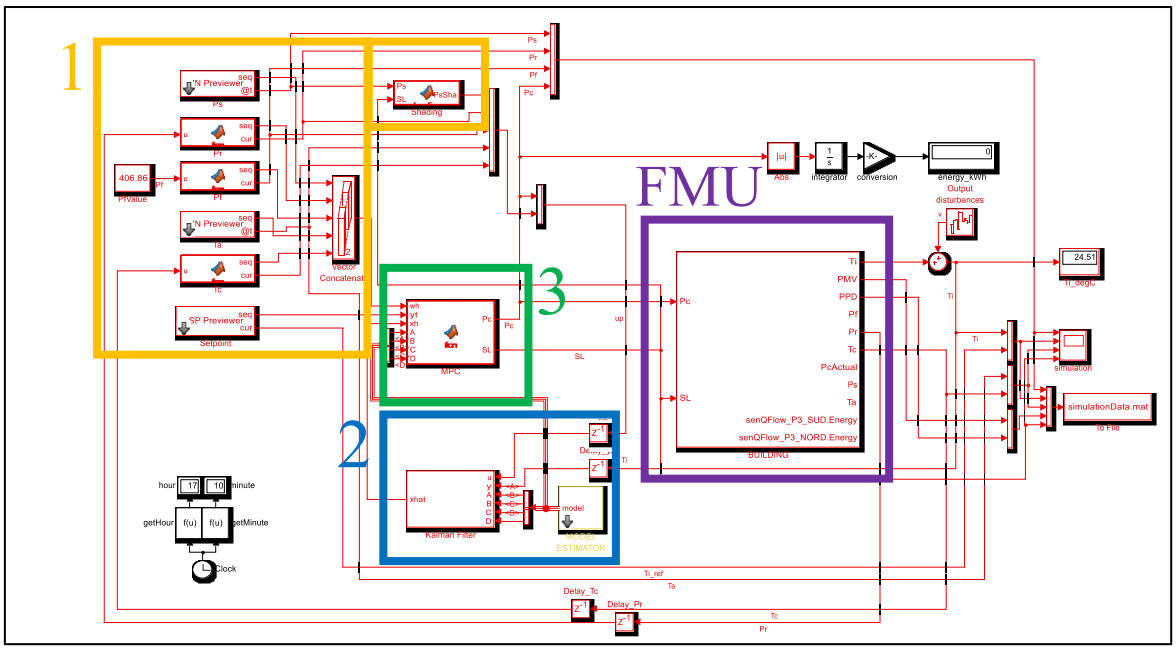

Fig. 6.6 The MPC framework in Simulink environment.

6.4.1 Input parameters

The bigger yellow rectangle in Fig. 6.6 concerns the time-varying parameters, in analogy to those presented in the scheme (Fig. 3.2 Chapter 3). Just like it did in the design phase of the experimental test, setpoint and disturbances generated an information profile to give in input to the controller. The information profile had dimension equal to the prediction horizon set up. For each variable, values provided to the controller were the current and the predicted ones at each time interval. Thus, the variables supplied in input were:

- the temperature setpoint of the test room (office 90), according to the occupancy schedule already mentioned in Chapter 5;
- the power of AHU (Pr), obtained in feedback by FMU output, corresponding to the measured value in the detailed model, and repeated for all the prediction horizon;
- the temperature of the corridor (Tc) in front of the office 90, obtained in feedback by FMU output, corresponding to the measured value in the detailed model, and repeated for all the prediction horizon;
- the heat gain of equipment (Pf), derived by the grey-box model identification and returned as a sequence of fixed value at each time interval;
- weather data of the global horizontal irradiance (Ps) and the outdoor temperature (Ta), extracted from the weather data of the year 2016, generated with a 5-minute time sample and loaded in the "Dataset2016.mat" file.

The "Display" menu in Simulink, under "Sample Time Legend" give the possibility to control the sample time of each variable.

The smaller yellow rectangle in Fig. 6.6 contains a block to consider the adding of solar shading within the model. Indeed, the solar gain was affected by the shading level (SL), thus the input provided dynamically to the grey-box model for the controller response must be computed accordingly, at each time interval. To reach this goal, the attenuation (α) of solar radiation (Ps) was introduced in that block of code, after doing a test to demonstrate the linearity between the attenuation coefficient (α) and the shading level (SL). The test was carried out in Dymola, using the building model and simulated it for two hours around the midday of the 1st of June 2016. The input function for the shading level was generated by the "Ramp" block of Modelica library, with a height of ramp settled to 1. Variables involved in the test were: the global horizontal irradiance (Ps), the window area (Aw) of the office 90 and the heat flow transmitted through the window (Qtra_flow), defined by the following equation (6.1):

$$\mathrm{Qtra_{flow}} = \mathrm{P_s} * \mathrm{A_w} * \rho * \alpha \tag{6.1}$$

ρ is a transmission coefficient that was found equal to 0.132, supposing SL = 0 (inactive shading), and kept fixed. For SL=1, shading 100% active, the lower bound of the attenuation (α_{min}) was calculated and it was 0.152. Results of simulation verified the linear dependence between the two variables, so the equation (6.2) was implemented into the simulator block, mentioned above.

$$\alpha = (\alpha_{\min} - 1) * \mathrm{SL} + 1 \tag{6.2}$$

The output of this block was the solar radiation attenuated (PsSha), result of the product: Ps*α.

6.4.2 The Grey-box model

The blue rectangle in Fig. 6.6 encloses blocks relative to the grey-box model for the controller: the "Model estimator" and the "Kalman filter". The "Model estimator" was connected to the "Kalman filter" block, which returned in output the states of the system, thus it was directly connected to the controller. In the following sub-sections, each component of the grey-box model will be described in detail.

6.4.2.1 Model estimator

This block (Fig. 6.7) contains results of the summer simulation campaign for the building model identification, in terms of parameters estimates. Double-clicking on the "Model estimator" icon, a mask is opened that summarizes the thermal parameters inserted for the grey-box model. To feed the "Kalman filter" block, the output of the Model estimator was the equations system in state space form, representing the grey-box model, previously identified. The additional step, with respect to the experimental approach, was the introduction of a function for the parameters estimation of the building model during the run-time of the simulator. The estimator had the use of data, as input, (up to a week of data) of the simulation during the operation of the controller, then estimated the grey-box model by means of "fmincon" algorithm (finding minimum of constrained nonlinear multivariable function), provided in MATLAB. Initially, this function was disabled, but enabling the estimator, it has been possible tested the accuracy in controller prediction and applying this method for further applications, as to overcome the model dependence on the estimation period. The "getssmodel.m" in APPENDIX H explains the model identification implemented within the "Model estimator".

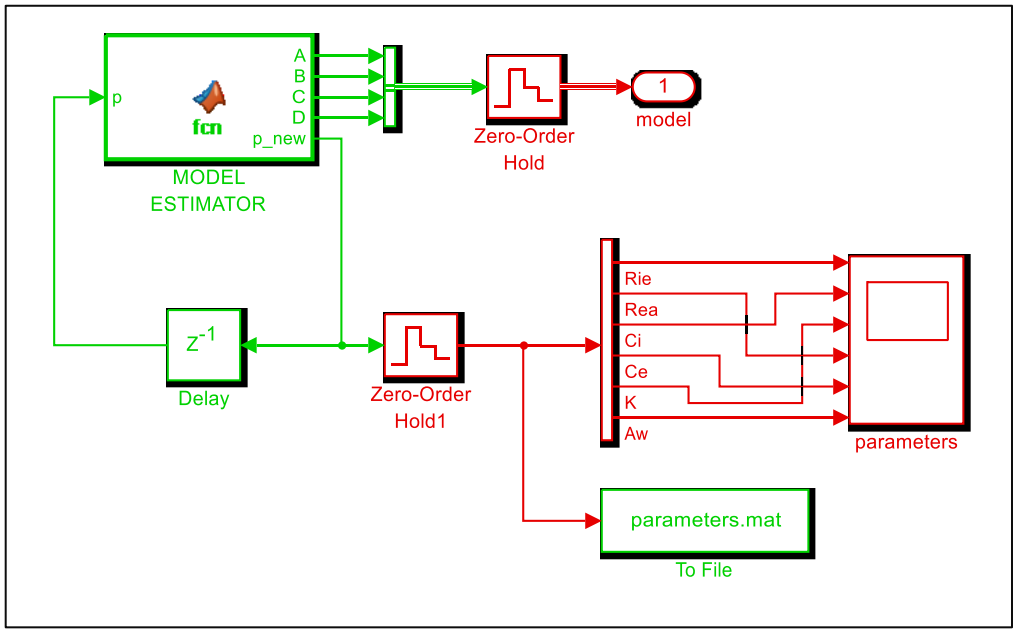

Fig. 6.7 The "Model estimator" block for generating the state space model.

6.4.2.2 Kalman filter

The "Kalman Filter" block is used to estimate states of a state-space plant model, given process and measurement noise covariance data. The state-space model can be time-varying. A steady-state Kalman filter implementation is used if the state-space model and the noise covariance matrices are all time-invariant. A time-varying Kalman filter is used otherwise. Kalman filter provides the optimal solution both to continuous and discrete-time estimations.

In this dissertation, the "Kalman filter" block received the matrix (A, B, C, D) matrices as input signals along with the current solar gain (PsSha), fan power (Pc) and measured internal temperature (yTi), then send the estimated system states (Ti, Te) to the controller. Parameters setting for the "Kalman filter" block is shown in Fig. 6.8. It is underlined that this block was essential because state "Te" was not measurable and it could be only estimated.

For the discrete-time estimation, the discrete plant is:

$$x[n+1] = A[n]\,x[n] + B[n]\,u[n] + G[n]\,w[n] \tag{6.3}$$

$$y[n] = C[n]\,x[n] + D[n]\,u[n] + H[n]\,w[n] + v[n] \tag{6.4}$$

with known inputs *u*, white process noise *w* and white measurement noise *v* satisfying:

$$E[w[n]] = E[v[n]] = 0 \tag{6.5}$$

$$E[w[n]wT[n]] = Q[n] \tag{6.6}$$

$$E[v[n]vT[n]] = R[n] \tag{6.7}$$

$$E[w[n]vT[n]] = N[n] \tag{6.8}$$

Q is the process noise covariance matrix, R is the measurement noise covariance matrix and N is the process and measurement noise cross-covariance matrix. The three matrices were set up all time-invariant. In this study, matrices G and H were not used. More information about is provided in Mathworks Documentation under "Kalman filter" section.

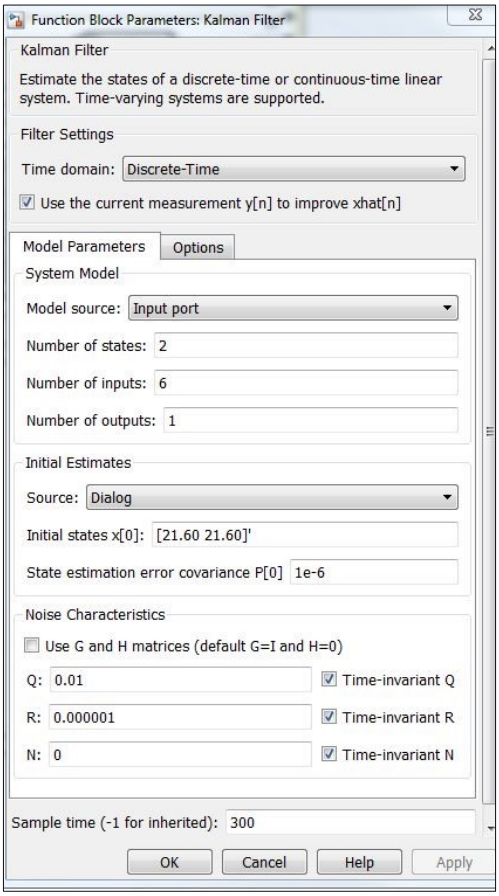

Fig. 6.8 The mask of the "Kalman filter" block implemented in the simulator.

6.4.3 The controller

The green rectangle in Fig. 6.6 concerns the model-based predictive controller. The MP controller block developed in the simulator contains the building model in its state space form, the cost function for the optimization problem, constraints and all the MPC parameters required for proper operation. Double-clicking on the "MPC" block icon, the related mask (Fig. 6.9) appears showing main parameters to be defined for running the control.

The General Problem (GP) was expressed by minimization of the cost function (6.9) subjected to constraints (6.10):

$$\min_{u} J(u) \tag{6.9}$$

$$lb \leq u \leq ub \tag{6.10}$$

In this specific case, the control action "u" was a vector of two variables, the power of the fan coil (Pc) and the shading level (SL). Thus, the Eq. 10 can be rewritten in this way:

$$-1200 \leq Pc \leq 0 \quad [W] \tag{6.11}$$

$$0 \leq SL \leq 1 \tag{6.12}$$

The cost function (J) implemented in the "MPC" block is stated as (11):

$$J(k) = \sum_{j=N_w}^{N_p} [\hat{y}(k+j|k) - r(k+j|k)]^T \cdot Q \cdot [\hat{y}(k+j|k) - r(k+j|k)] + \\ + \sum_{j=0}^{N_c-1} [u^T(k+j|k) \cdot R \cdot u(k+j|k)] \tag{6.13}$$

Cost function computation was based on provided horizons (Nw, Np, Nc), cost weights (Q, R) for a given plant with initial state (x0), disturbances prediction (d), reference prediction (r) and control sequence (u). When the setpoint "r" is "NaN", the corresponding cost is not accounted for.

The cost weight "R" is represented by a diagonal matrix, containing the weights of the two control actions (Pc and SL). The shading weight has been changed to balance the plant power, expressed in kW (wSL = $1*10^6$; wPc = 1). The cost weight "Q", related to the distance from the temperature setpoint, was set to $10*10^6$, reflecting the same priority chosen in the experimental phase, compared to the control action.

Concerning the horizons, the "Move Blocking" strategy was applied: the control horizon was used to define block inputs, i.e. the prediction horizon was divided into Np/Nc (approximated to the lowest integer) intervals of equal length, except for the last one, for the reminder. Therefore, manipulated variables (u) are fixed over time intervals in the future and degrees of freedom in optimization problem are reduced.

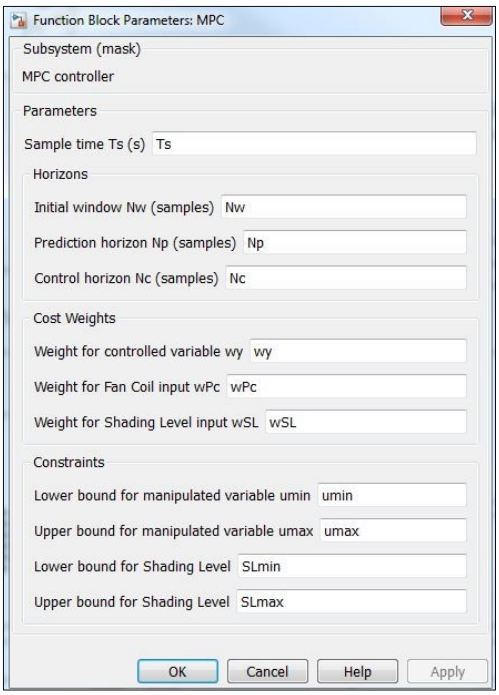

Fig. 6.9 The mask of the "MPC" block implemented in the simulator.

Referring to the GP (Eq. 6.9), the optimal solution is achieved through the MATLAB "fmincon" function with "Active Set" algorithm for constrained nonlinear optimization.

In constrained optimization, the general aim is to transform the problem into an easier subproblem that can then be solved and used as the basis of an iterative process. A characteristic of a large class of early methods is the translation of the constrained problem to a basic unconstrained problem by using a penalty function for constraints that are near or beyond the constraint boundary. In this way, the constrained problem is solved using a sequence of parameterized unconstrained optimizations, which in the limit (of the sequence) converge to the constrained problem. These methods are now considered relatively inefficient and have been replaced by methods that have focused on the solution of the Karush-Kuhn-Tucker (KKT) equations. The KKT equations are necessary conditions for optimality for a constrained optimization problem. If the problem is a so-called convex programming problem, that is, $f(x)$ and $G_i(x)$, $i = 1,...,m$, are convex functions, then the KKT equations are both necessary and sufficient for a global solution point. Refer to Mathworks Documentation "Constrained Nonlinear Optimization Algorithms" for an explanation in-depth.

The MATLAB code implemented in the MPC simulator is given in APPENDIX H.

6.5 Modelling results

6.5.1 Model identification

Defined the structure of the MPC simulator, it was necessary to provide an adequate model for the controller in order to run and test the control. In analogy of what has been done in the experimental phase, in which the grey-box model was identified from data of short-term monitoring campaigns, in this simulation phase, the identification procedure required, first of all, a set of data. Hence, the "DatasetGeneration.slx" (Fig. 6.10) was generated in Simulink to obtain data for the estimation of model parameters. The detailed model of the building, realized in Dymola, was used for generating data by using the FMU, as previously explained. In this case, the FMU received in input the fan coil power (Pc) like a random white noise, whilst the solar shading was considered inactive (SL=0). These inputs were the only ones provided in Simulink environment, while the others were deriving directly by Dymola model. In particular, weather data in input were those available of the year 2016, as done for the operation of the MPC. The simulation period was the month of July.

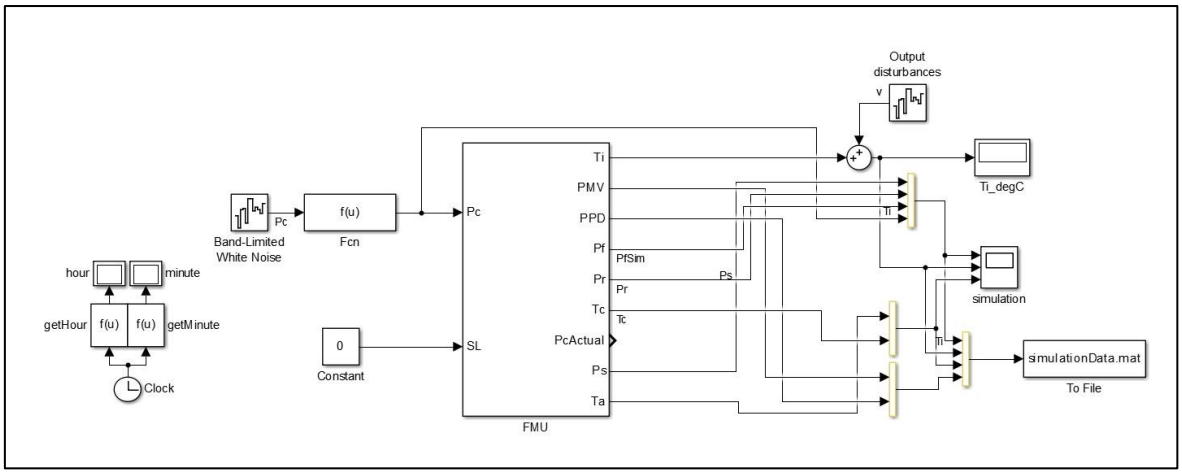

Fig. 6.10 The "DatasetGeneration" in Simulink to generate data for the model identification.

Considering that the simulation required about a week to stabilise, the two central weeks of July were believed useful for generating the data set (11-24 July 2016), while the last week was reserved for the validation phase of the grey-box models. The time-series of variables involved in the model estimation were the energy fluxes from the conditioning system (Pc, Pr), from the solar radiation (Ps) and from the equipment (Pf), together with the boundary temperatures of outdoor air (Ta) and the corridor (Tc) and the internal temperature of the test room, the office 90. Trends of these variables, extracted from the simulation data, are presented below (Figg. 6.11-6.16).

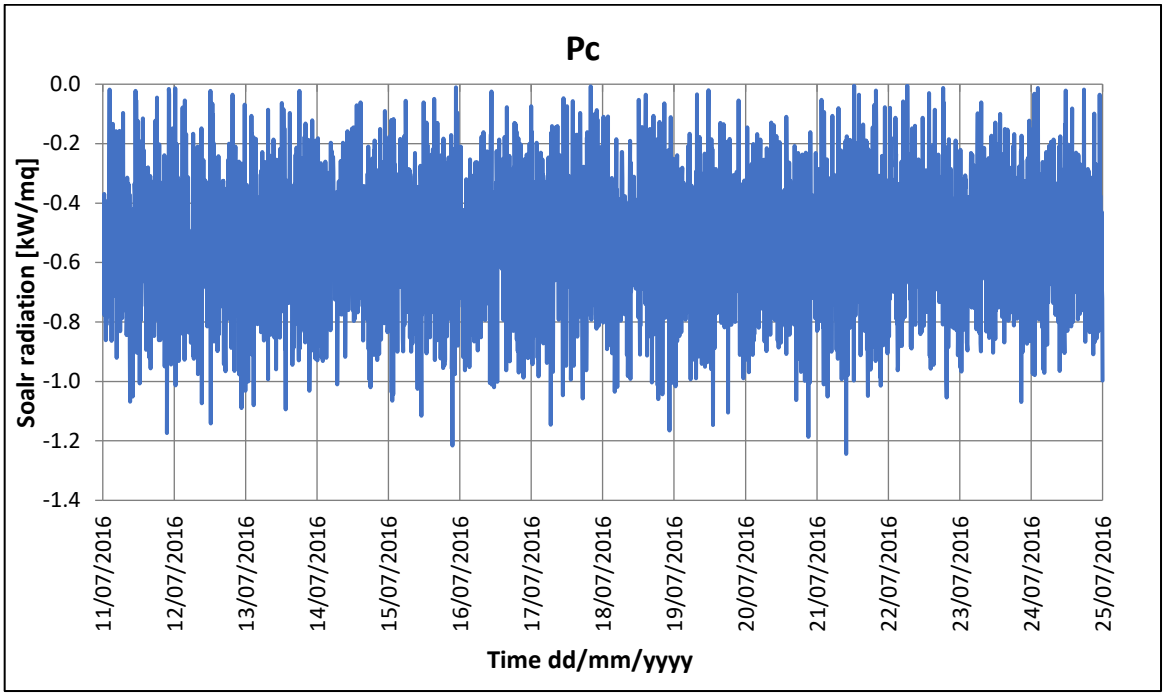

Fig. 6.11 Trend of the cooling power during the selected period.

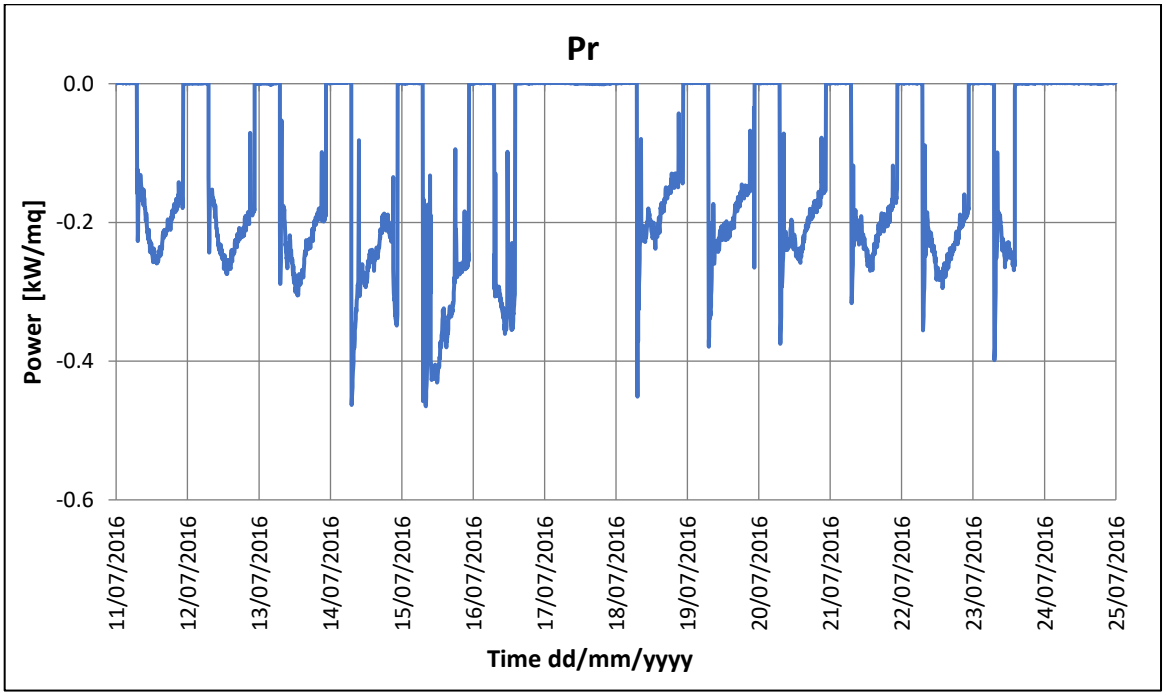

Fig. 6.12 Trend of the ventilation power during the selected period.

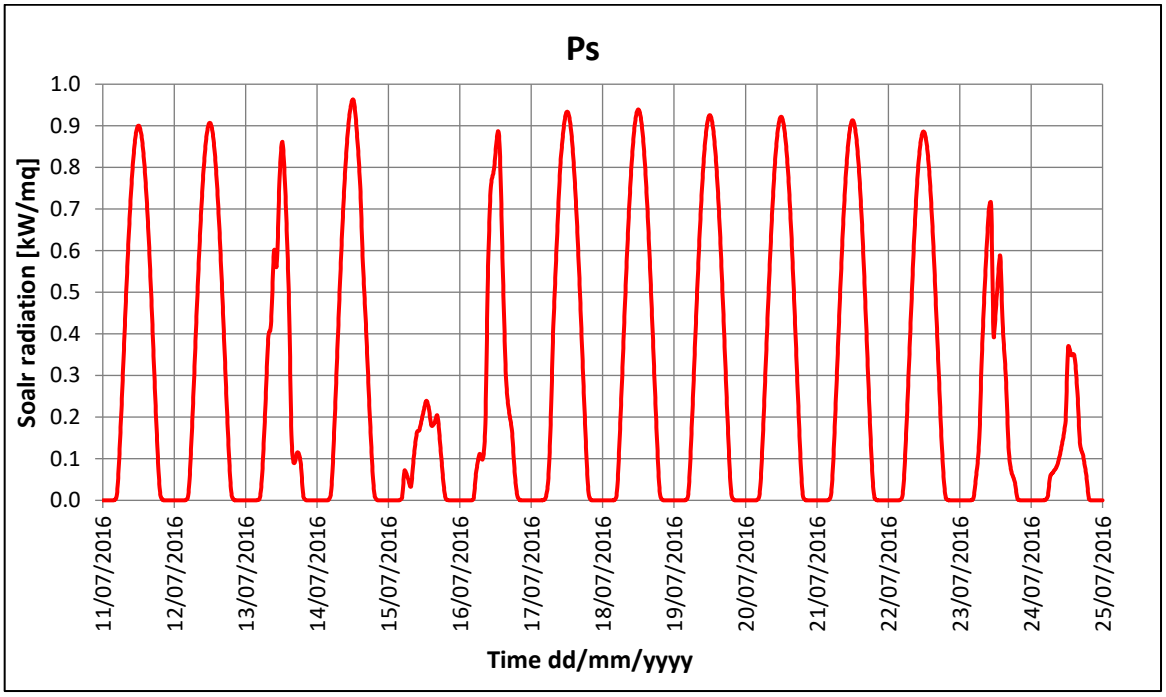

Fig. 6.13 Trend of the global solar radiation, according to weather data of year 2016, downloaded by "Weather Underground" website.

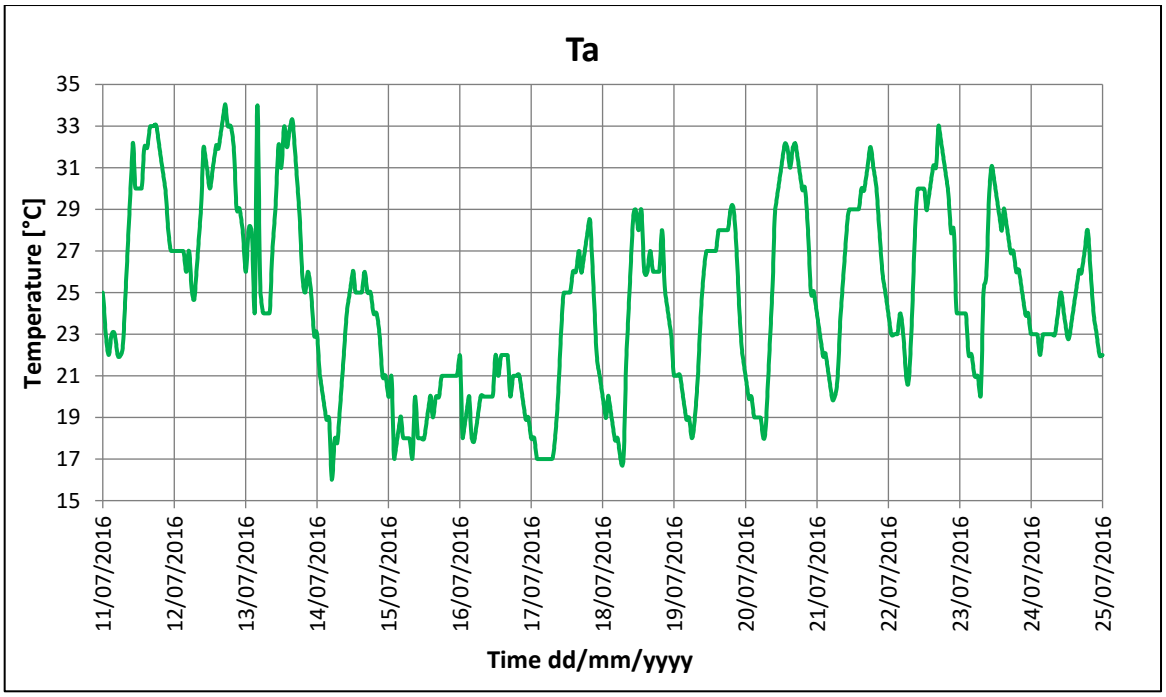

Fig. 6.14 Trend of the outdoor temperature, according to weather data of year 2016, downloaded by "Weather Underground" website.

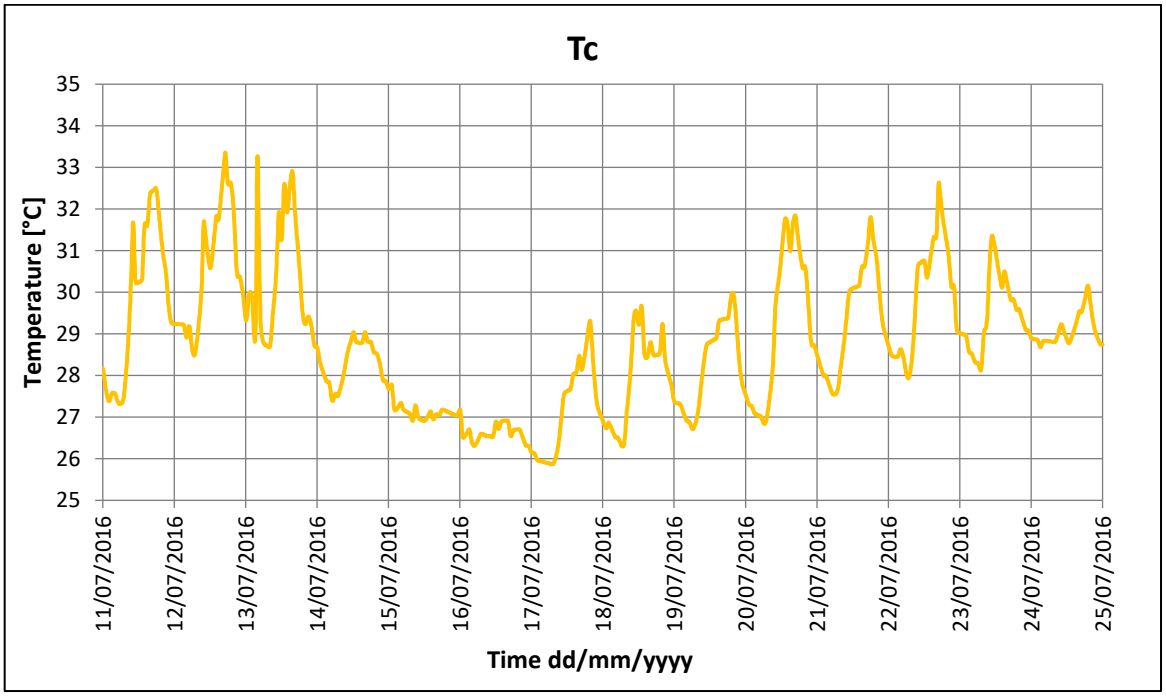

Fig. 6.15 Trend of the air temperature of the corridor, in front of the test-room, derived by the simulation during the selected period.

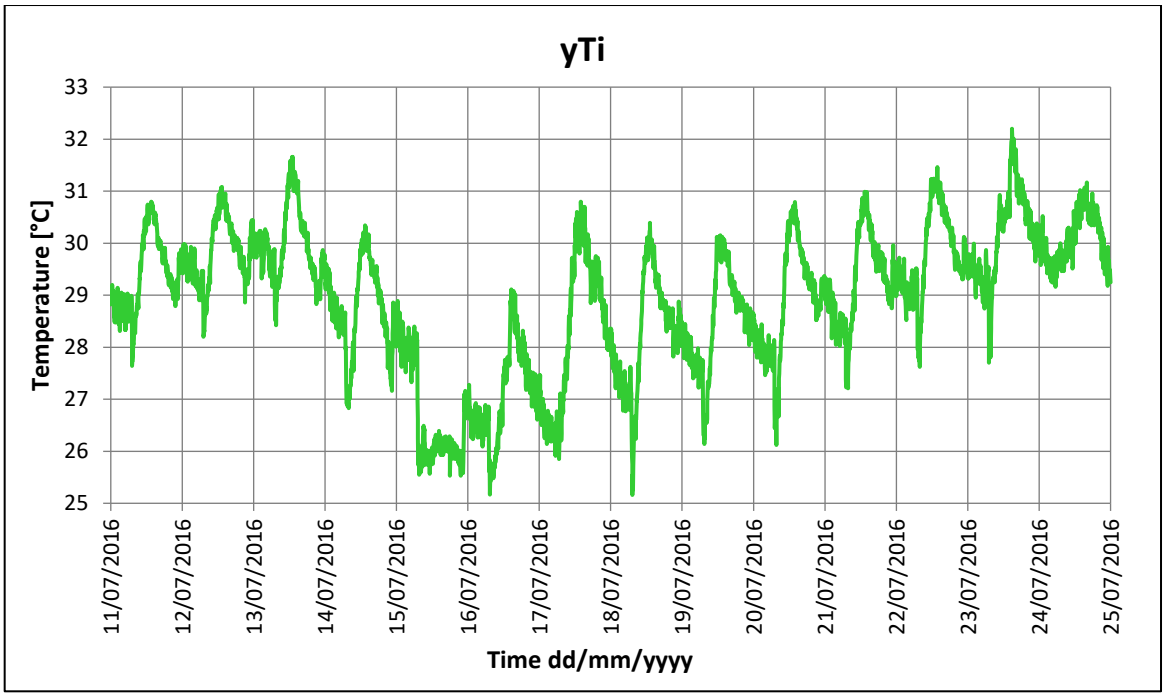

Fig. 6.16 Trend of the internal temperature of the test room during the selected period.

Defined the data set, a first grey-box model was tested, whose structure was reclaimed from the RC-network identified in the experimental phase (Fig. 4.32), thus a 2R2C network expressed by the same equations (Eq. 4.11-4.12). The estimation procedure was applied using all available data. Results of the first model tested are provided in Table 6.1, according to procedure of APPENDIX E. Then the data set was reduced (14-22 July) as to improve the RMSE value, while the structure was maintained.

Table 6.1: Results of the parameters estimation for the first grey-box model tested.

Parameter	Estimated value	Pr(>|t|)	dPen/dPar
Ti0	2.8820e+01	0.0000e+00	0e+00
Te0	2.9323e+01	0.0000e+00	0e+00
Aw	1.3638e+00	0.0000e+00	0e+00
Ce	3.3632e+00	8.4095e-10	0e+00
Ci	8.2261e-02	0.0000e+00	0e+00
e11	-2.1032e+01	0.0000e+00	0e+00
p11	-1.7811e+00	0.0000e+00	0e+00
p22	-1.0365e+01	0.0000e+00	0e+00
Pf	3.9218e-01	0.0000e+00	0e+00
Rea	2.8391e+00	6.2108e-05	0e+00
Rie	1.4612e+00	0.0000e+00	0e+00
K	4.1827e-05	9.1039e-01	0e+00

Therefore, other two 2C2R-networks were tested, structurally equal to the first grey-box model, using a reduced data set (5 days less). The second grey-box model tested was estimated using the the *fmincon* algorithm provided in MATLAB, while the thermal parameters of the third grey-box model were derived using the MLE (Maximum Likelihood Estimation) of CTSM package in R environment. Results of the second model, according to APPENDIX H, are provided in Table 6.2, whilst results of the third model tested are presented in Table 6.3, according to procedure of APPENDIX E.

Table 6.2: Results of the parameters estimation for the second grey-box model, identified using the "fmincon" algorithm of Matlab.

Parameter	Estimated value	Mean	Std%
Ti0	2.9824e+01	2.3208e+01	28.16
Te0	2.9234e+01	1.9098e+01	32.28
Aw	6.1294e-01	1.907e+00	285.24
Ce	2.0442e+00	3.6357e+00	124.20
Ci	7.7703e-02	3.2141e+00	3941.49
Pf	5.2166e-01	3.4413e-01	56.83
Rea	2.3151e+00	2.4104e+00	128.08
Rie	3.7768e+00	2.962e+00	72.00
K	0e+00	4.3578e-04	Inf

Table 6.3: Results of the parameters estimation for the third grey-model, identified using the MLE of CTSM-R.

Parameter	Estimated value	Pr(>|t|)	dPen/dPar
Ti0	2.9430e+01	0.0000e+00	0e+00
Te0	2.9764e+01	0.0000e+00	0e+00
Aw	1.3042e+00	0.0000e+00	0e+00
Ce	3.2764e+00	7.4344e-06	0e+00
Ci	8.0277e-02	0.0000e+00	0e+00
e11	-2.0564e+01	0.0000e+00	0e+00
p11	-1.4644e+00	0.0000e+00	0e+00
p22	-1.3303e+00	0.0000e+00	0e+00
Pf	4.0686e-01	0.0000e+00	0e+00
Rea	1.8965e+00	9.5596e-05	0e+00
Rie	1.4772e+00	0.0000e+00	0e+00
K	2.3554e-07	8.1495e-01	0e+00

Another grey-box model was tested using the limited data set (14-22 July), a 3C5R model (Fig. 6.17), which was defined by the following stochastic differential equations:

$$dT_i = \frac{1}{\mathrm{R}_{ie}\mathrm{C}_i}(\mathrm{T}_e - \mathrm{T}_i)\mathrm{d}t + \frac{1}{C_i}P_r\mathrm{d}t + \frac{1}{C_i}P_c\mathrm{d}t + \frac{1}{C_i}P_f\mathrm{d}t + \frac{1}{C_i}A_wP_s\mathrm{d}t + \sigma_i\mathrm{d}\omega_i \tag{6.14}$$

$$dT_{e1} = \frac{1}{\mathrm{R}_{ie1}\mathrm{C}_{e1}}(\mathrm{T}_i - \mathrm{T}_{e1})\mathrm{d}t + \frac{1}{\mathrm{R}_{ea1}\mathrm{C}_{e1}}(T_c - \mathrm{T}_{e1})\mathrm{d}t + \frac{1}{\mathrm{R}_{ea2}\mathrm{C}_{e1}}(T_e - \mathrm{T}_{e1})\mathrm{d}t + \sigma_{e1}\mathrm{d}\omega_{e1} \tag{6.15}$$

$$dT_e = \frac{1}{\mathrm{R}_{ie}\mathrm{C}_e}(\mathrm{T}_i - \mathrm{T}_e)\mathrm{d}t + \frac{1}{\mathrm{R}_{ea}\mathrm{C}_e}(\mathrm{T}_a - \mathrm{T}_e)\mathrm{d}t + \frac{1}{\mathrm{R}_{ea2}\mathrm{C}_e}(T_{e1} - \mathrm{T}_e)\mathrm{d}t + \sigma_e\mathrm{d}\omega_e \tag{6.16}$$

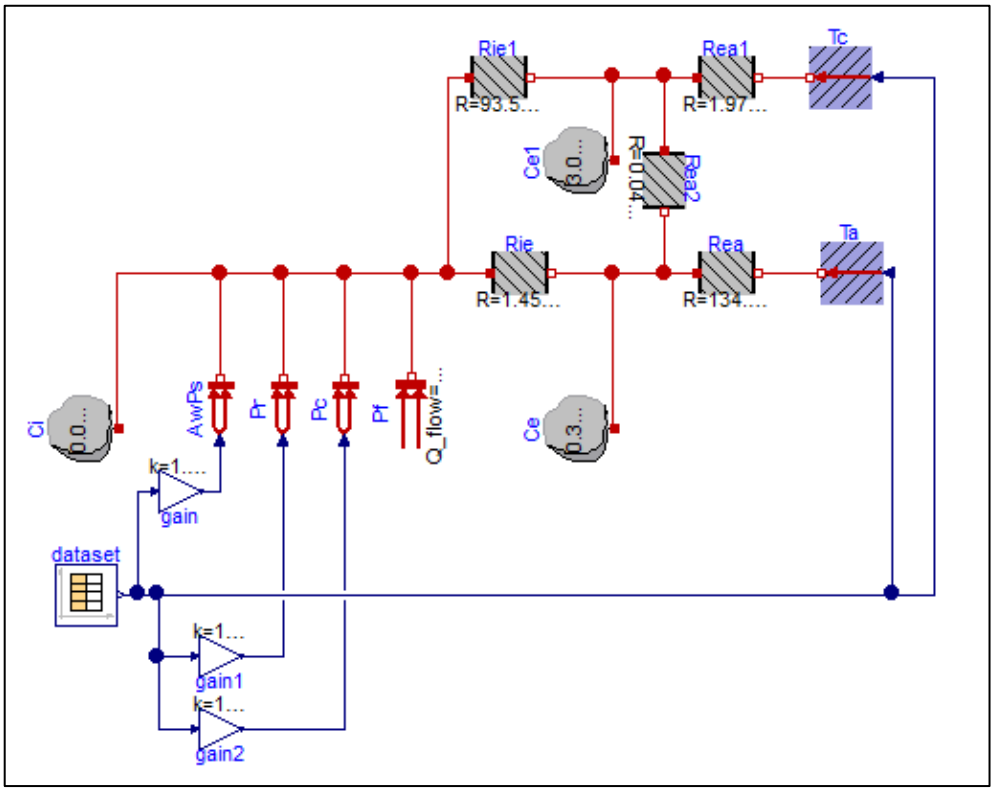

Fig. 6.17 The 3C5R network of the fourth grey-box model identified using the data set 14-22 July.

Results of this fourth grey-box model tested are provided in Table 6.4, while the RMSE values in simulation of all grey-box models tested in this simulation phase are presented in Table 6.5.

Table 6.4: Results of the parameters estimation for the fourth grey-box model tested, the 3C5R network.

Parameter	Estimated value	Pr(>|t|)	dPen/dPar
Ti0	2.9430e+01	0.0000e+00	0e+00
Te0	2.9630e+01	0.0000e+00	0e+00
Te10	2.9764e+01	0.0000e+00	0e+00
Aw	1.3135e+00	0.0000e+00	0e+00
Ce	3.5658e-01	2.9140e-04	0e+00
Ce1	3.0294e+00	3.1176e-07	0e+00
Ci	8.0107e-02	0.0000e+00	0e+00
e11	-2.8784e+01	1.9908e-06	0e+00
p11	-5.4267e+00	1.6369e-08	0e+00
p22	-3.6992e+00	2.7056e-03	0e+00
p33	8.5586e-01	5.0587e-05	0e+00
Pf	4.2310e-01	0.0000e+00	0e+00
Rea	1.3461e+02	2.1714e-01	6e-04
Rea1	1.9726e+00	4.8916e-05	0e+00
Rea2	4.2456e-02	2.9769e-06	0e+00
Rie	1.4515e+00	0.0000e+00	0e+00
Rie1	9.3516e+01	7.7587e-01	2e-04

Table 6.5: RMSE values in simulation of the grey-box models tested.

Grey-box model	Data set	RMSE value
First model – 2C2R	11-24/07/16	0.75
Second model – 2C2R	14-22/07/16	0.45
Third model – 2C2R	14-22/07/16	0.59
Fourth model – 3C5R	14-22/07/16	0.60

6.5.2 Model validation

Similarly to what was done in the experimental phase, defined the structure and estimated the thermal parameters, the reduced-order models were validated in Dymola environment, in order to establish the best model for the controller. The methodology used in this section is the same explained in par. 4.3.6.1. For this validation phase, the data set was extracted from data previously generated, corresponding to the latter week of July (25-31/07/2016). For each model, the length of the data set corresponded to one third of the data used in the identification phase. Trends of all variables involved for the validation are provided for the period chosen in Figg. 6.18-6.23.

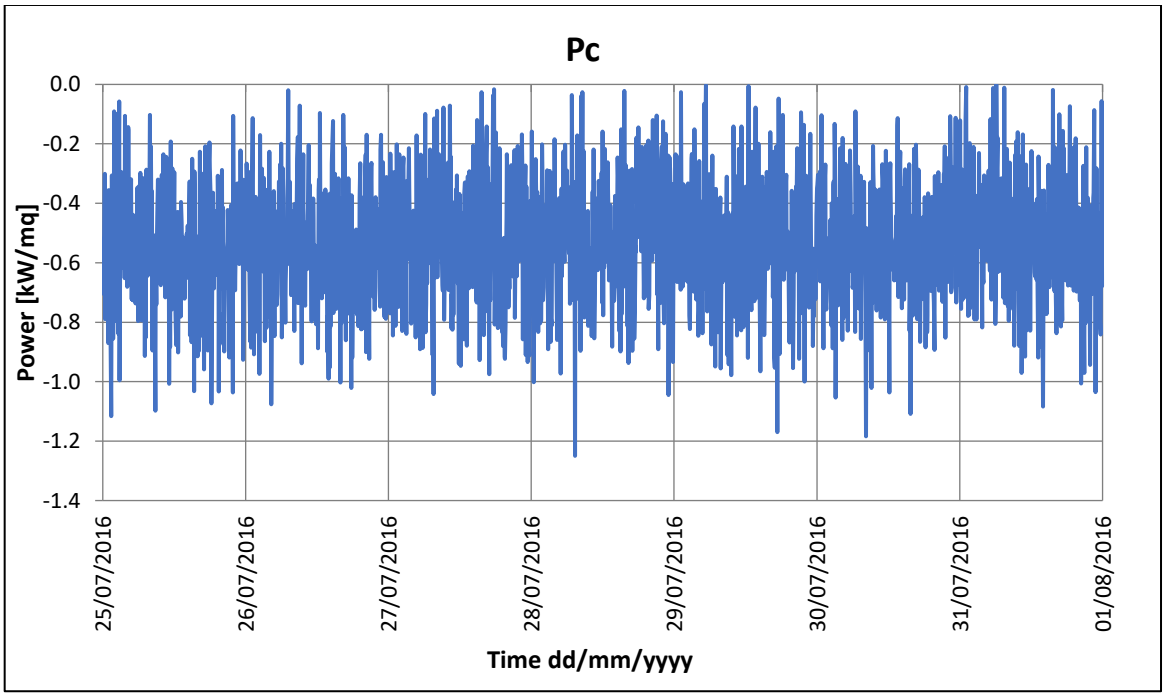

Fig. 6.18 Trend of the cooling power during the selected period.

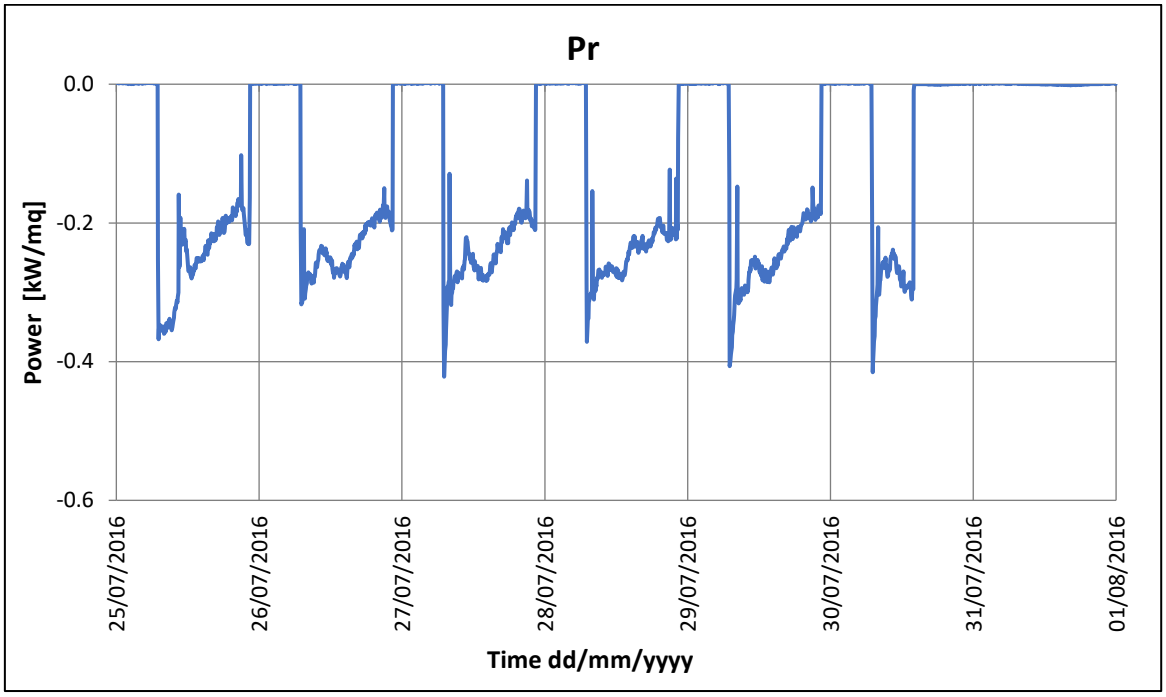

Fig. 6.19 Trend of the ventilation power during the selected period.

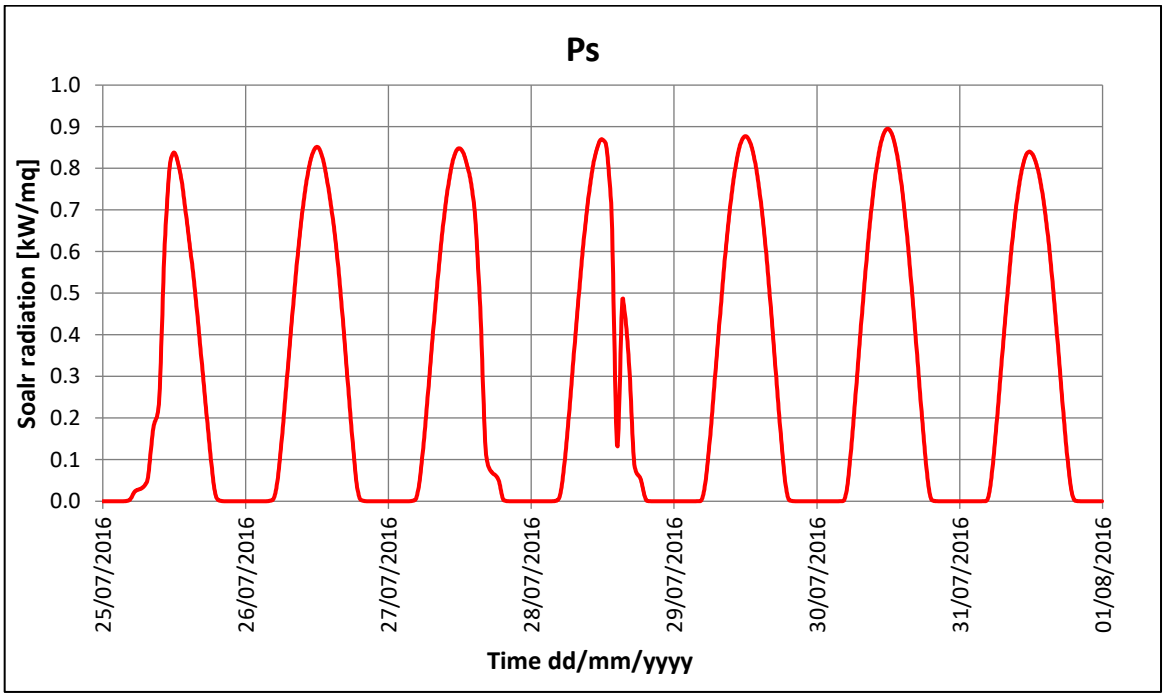

Fig. 6.20 Trend of the global solar radiation, according to weather data of year 2016, downloaded by "Weather Underground" website.

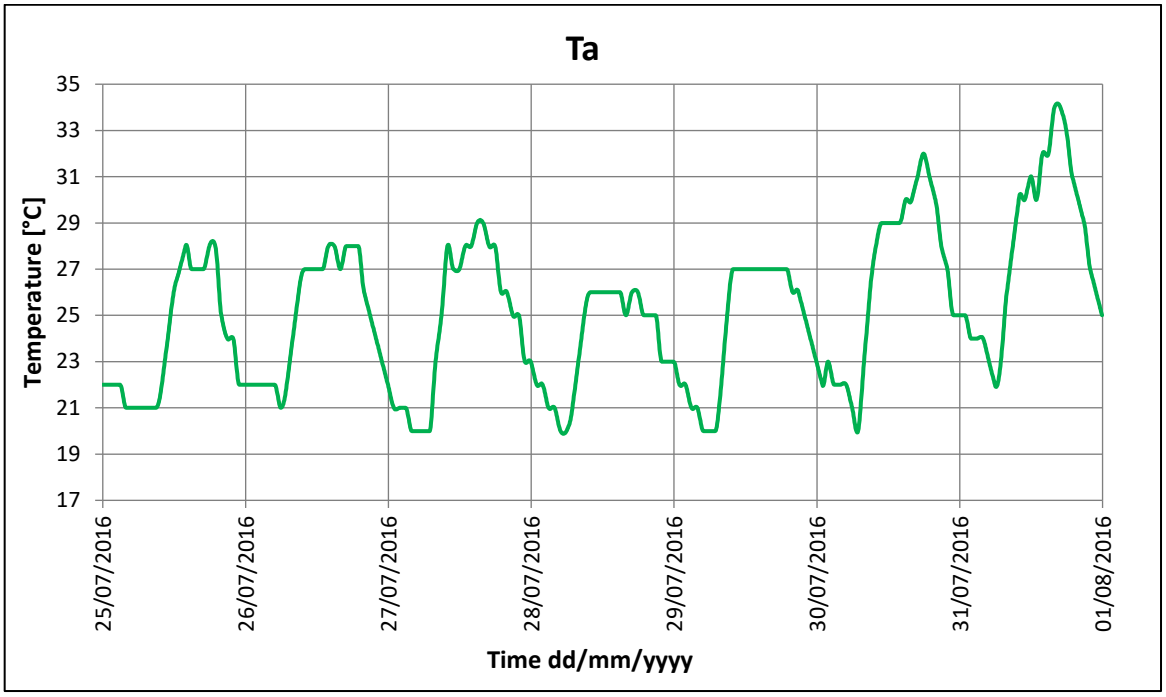

Fig. 6.21 Trend of the outdoor temperature, according to weather data of year 2016, downloaded by "Weather Underground" website.

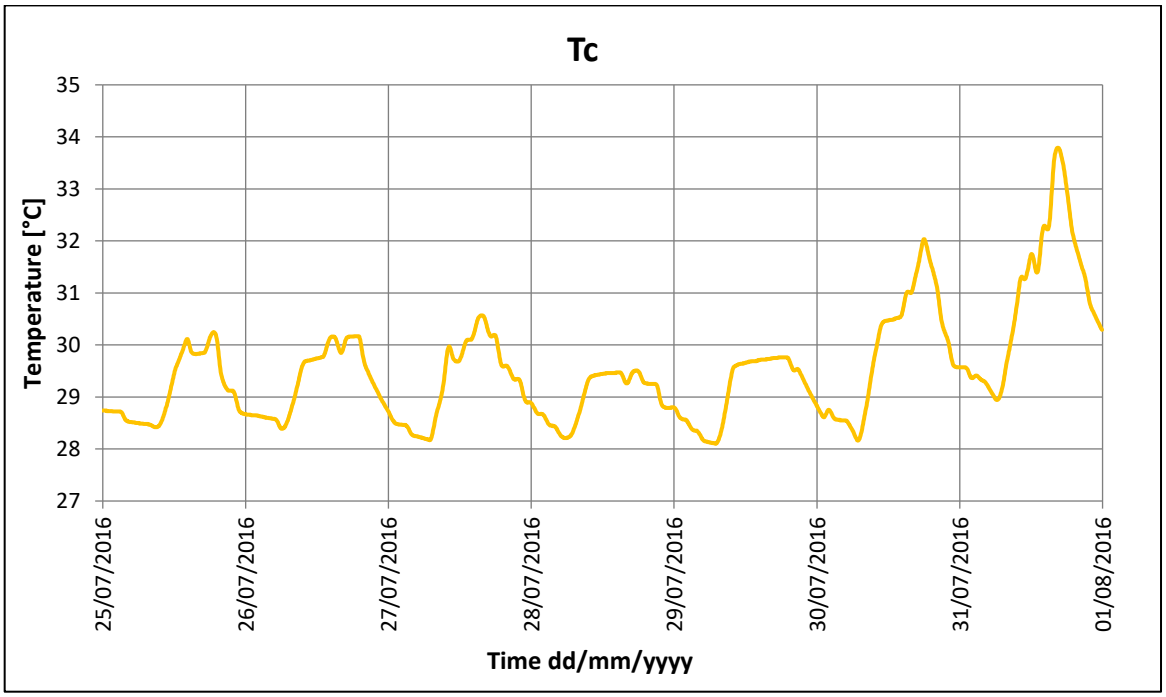

Fig. 6.22 Trend of the air temperature of the corridor, in front of the test-room, derived by the simulation during the selected period.

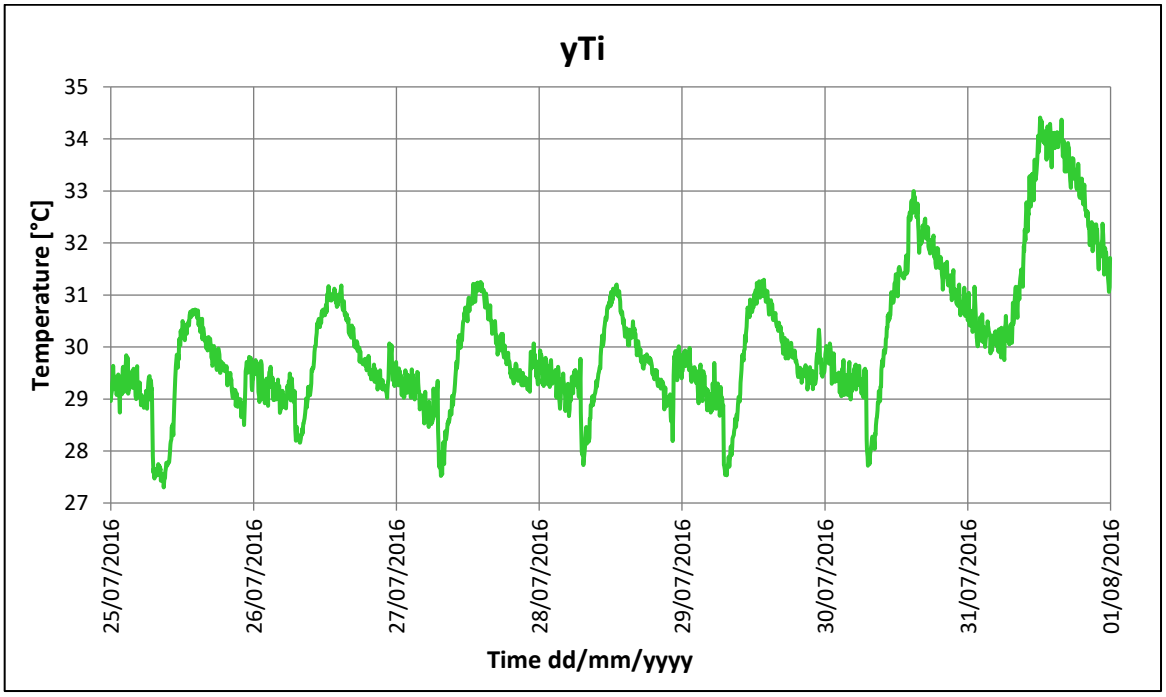

Fig. 6.23 Trend of the internal temperature of the test room during the selected period.

The 1st model was a second-order model (Fig. 6.24), which was estimated by means of CTSM-R and using the complete data set. It was validated in Dymola using 5 days of the validation data set and it returned to the end a RMSE value in simulation of 0.42°C, comparing values of the internal temperature simulated and those provided by the data set (Fig. 6.23). Results of the model validation are shown in Fig. 6.25.

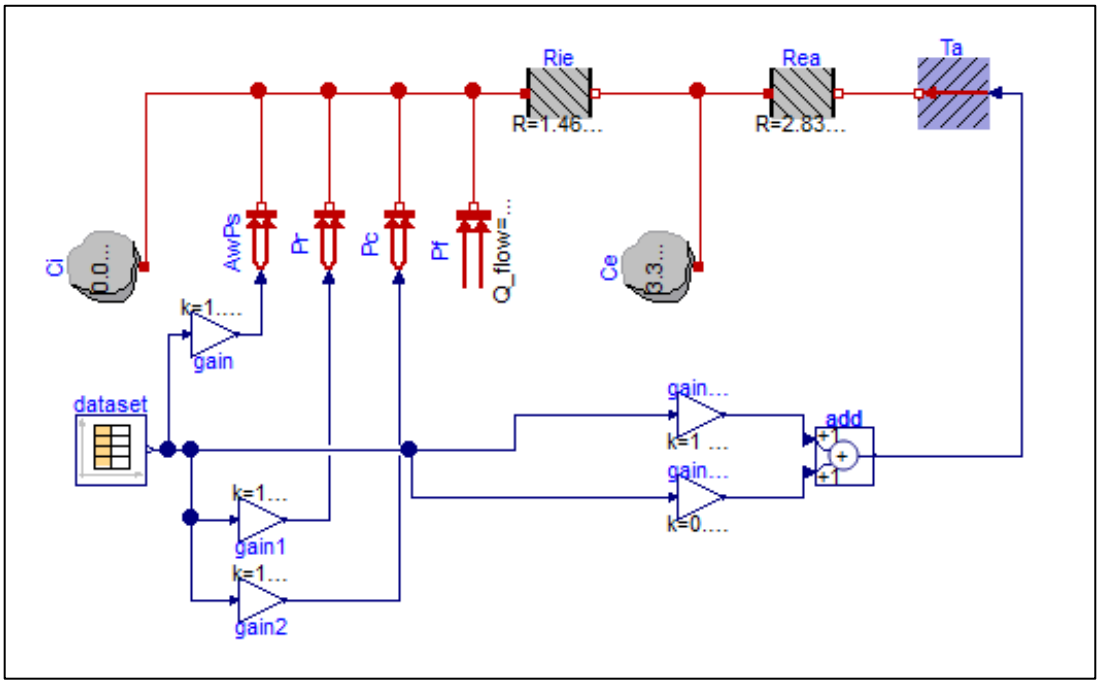

Fig. 6.24 The 2C2R network of the first grey-box model identified using the data set 11-24 July.

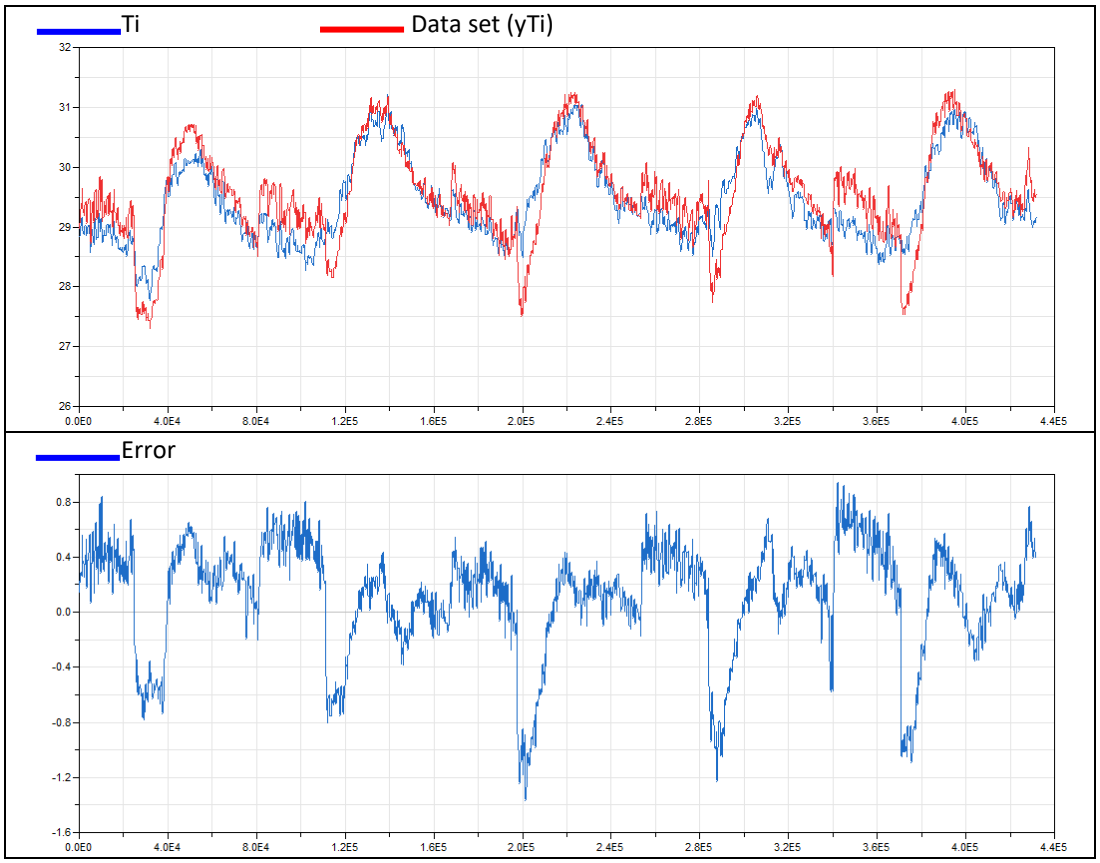

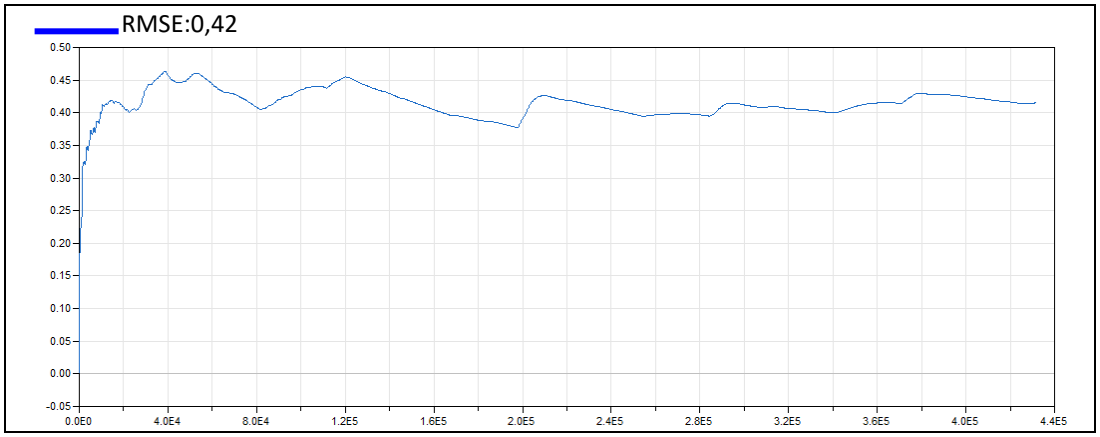

Fig. 6.25 Results of model validation for the first grey-box model tested.

The 2nd model was a second-order model (Fig. 6.26), which was estimated using the MATLAB algorithm *fmincon*. It was validated in Dymola using 3 days of the validation data set and it returned to the end a RMSE value in simulation of 0.56°C, comparing values of the internal temperature simulated and those provided by the data set (Fig. 6.23). Results of the model validation are shown in Fig. 6.27.

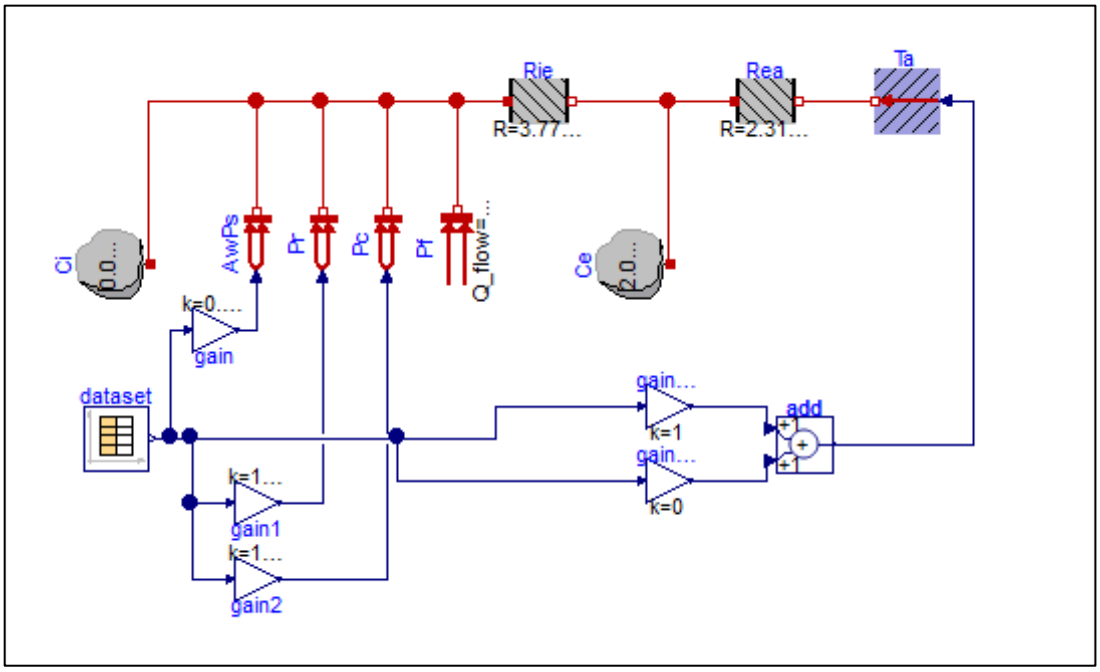

Fig. 6.26 The 2C2R network of the second grey-box model identified using the data set 14-22 July.

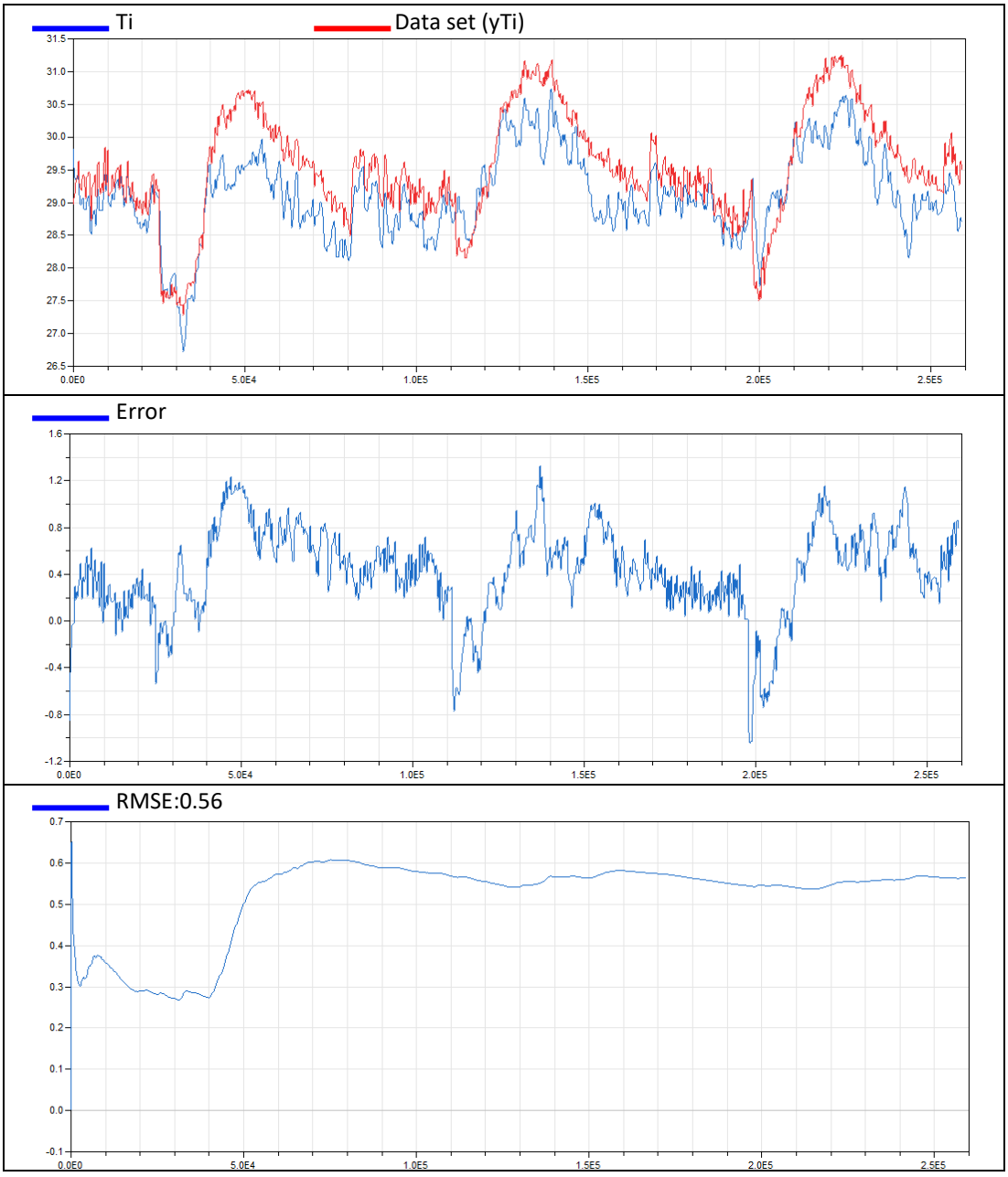

Fig. 6.27 Results of model validation for the second grey-box model tested.

The 3rd model was a second-order model (Fig. 6.28), which was estimated using the CTSM-R algorithm *MLE*. It was validated in Dymola using 3 days of the validation data set and it returned to the end a RMSE value in simulation of 0.37°C, comparing values of the internal temperature simulated and those provided by the data set (Fig. 6.23). Results of the model validation are shown in Fig. 6.29.

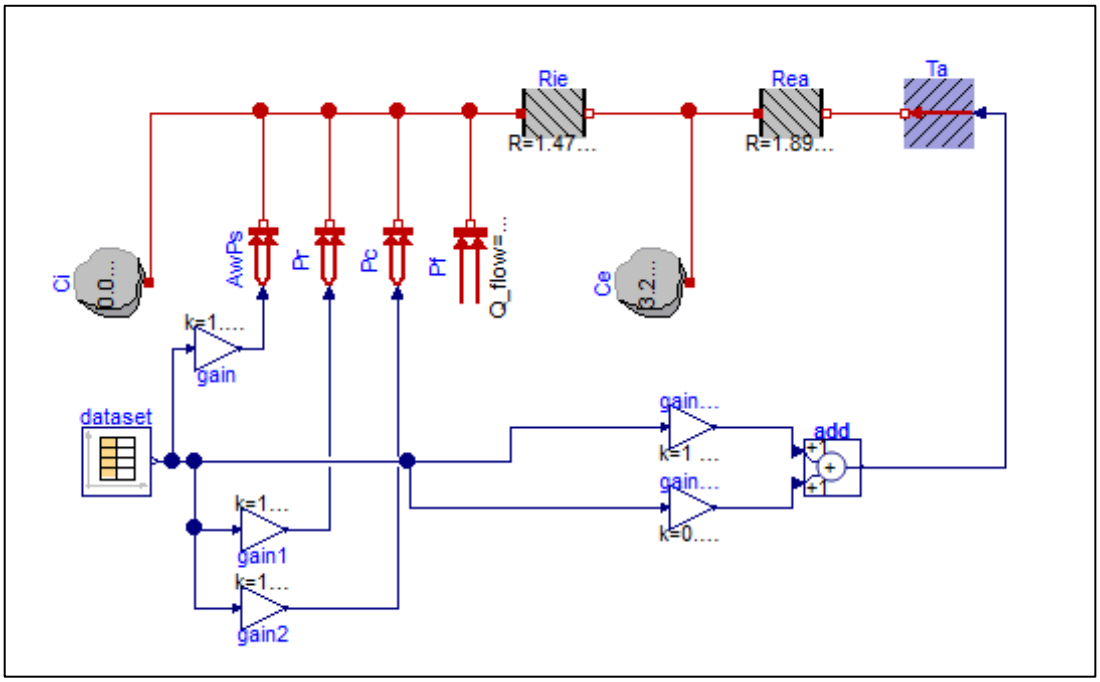

Fig. 6.28 The 2C2R network of the third grey-box model identified using the data set 14-22 July.

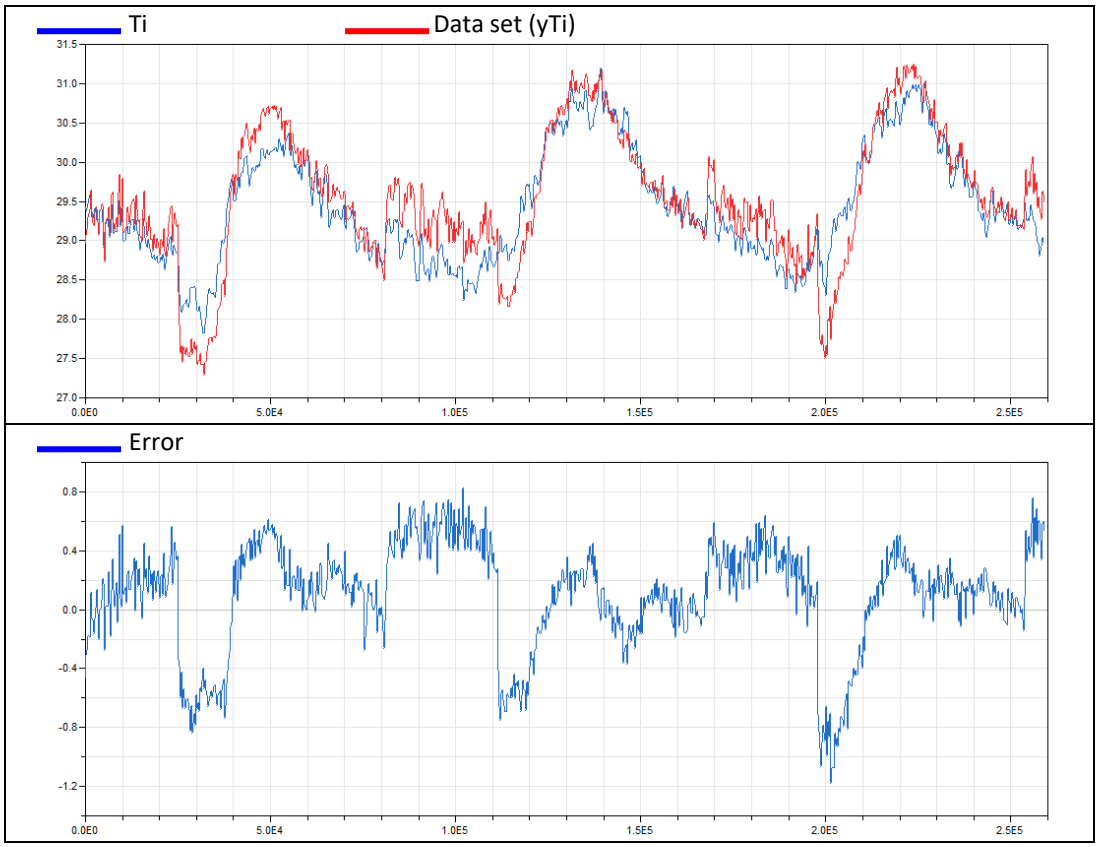

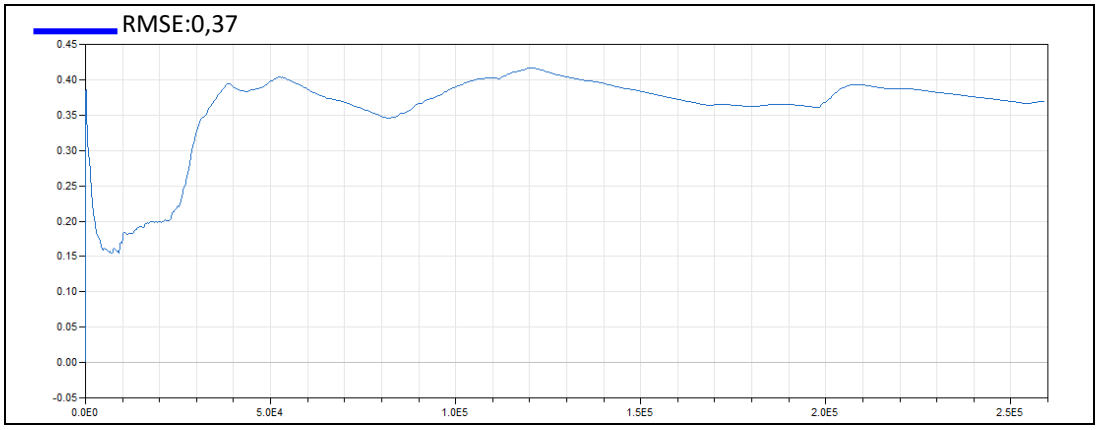

Fig. 6.29 Results of model validation for the third grey-box model tested.

The last model was a third-order model (Fig. 6.17), which was estimated by means of CTSM-R. It was validated in Dymola using 3 days of the validation data set and it returned to the end a RMSE value in simulation of 0.37°C, comparing values of the internal temperature simulated and those provided by the data set (Fig. 6.23). Results of the model validation are shown in Fig. 6.30.

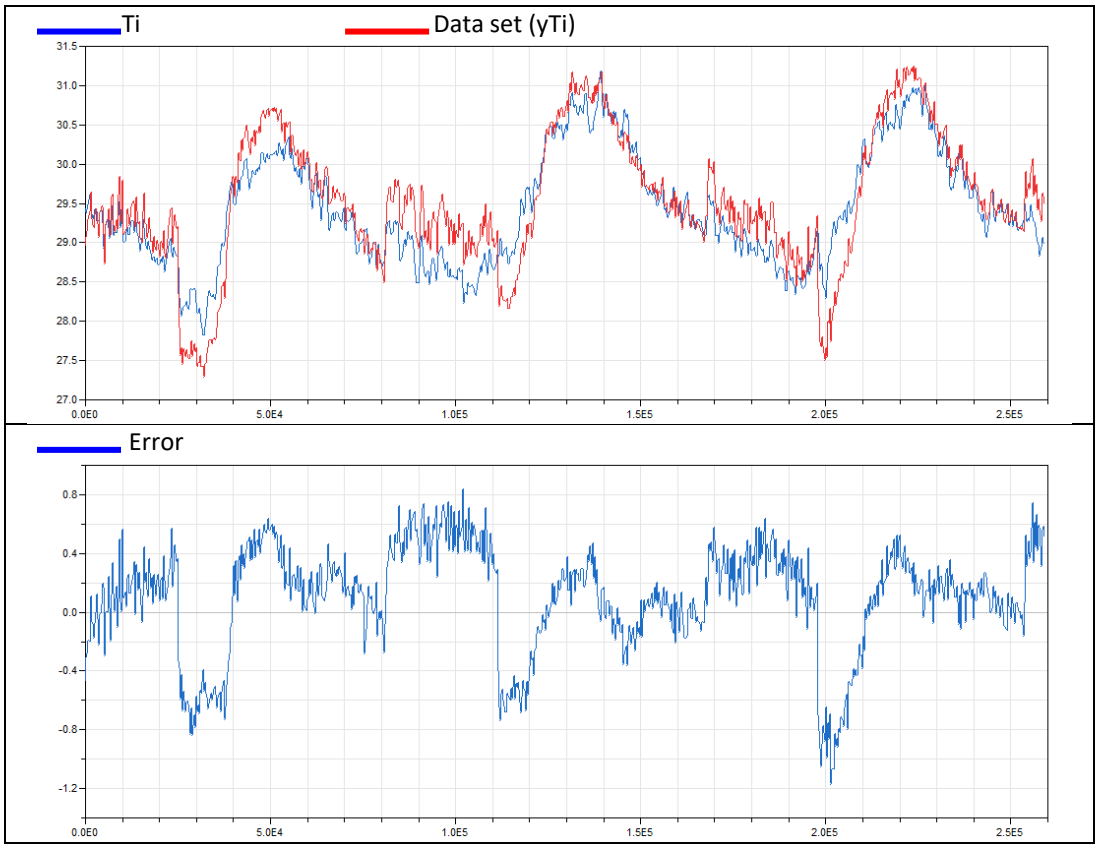

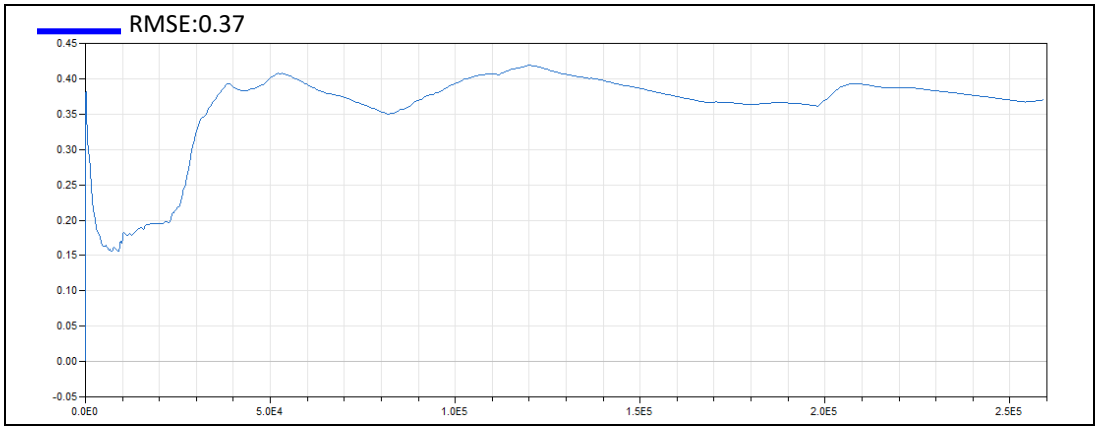

Fig. 6.30 Results of model validation for the fourth grey-box model tested.

Both considering results obtained in the identification phase and those provided by the models' validation, which are summarized in Tables 6.5 and 6.6, it turned out that the overall best model was the third grey-box model, which better represented the thermal dynamics of the testing area, without being too dependent on the data that had generated it (overfitting phenomena). Besides, its 2C2R network preserving the structure of the grey-box model for the controller of the experimental phase.

Table 6.6: RMSE values in simulation of the grey-box models validated.

Grey-box model	Data set	RMSE value
First model – 2C2R	25-29/07/16	0.4150
Second model – 2C2R	25-27/07/16	0.5649
Third model – 2C2R	25-27/07/16	0.3702
Fourth model – 3C5R	25-27/07/16	0.3703

6.6 MPC results

Defined the grey-box model for the controller, it was integrated into the simulator architecture to test the MPC operation. Since the effectiveness of this advanced control was proved during the experimental phase, testing of the MPC simulator was focus on investigating renovation scenarios, by introducing the solar shading within the detailed model and setting the proper level thanks to the optimal response of the controller. Besides, this last part of the research was also addressed to tuning of MPC parameters, that is the prediction and control horizons, in order to define the best compromise for the case study and provide suggestions for further developments. Tuning of weights in the cost function was not considered in this dissertation, because it is strictly linked to the objective of the application and to the policy governing the hypothesis of intervention on the building.

Results presented in next sections refer to a simulation period chosen within the cooling season, the month of June 2016. According to this period, all inputs of the detailed model were set, including outdoor conditions, providing the corresponding weather data in input.

6.6.1 Horizons tuning

First of all, exploiting the default settings presented in par. 6.4.3, the MPC simulator was tested for evaluating the effect of solar shading on the current building condition and its management by the controller. Hence, the horizons of the MPC simulator were set to the default values (tp=1h, Np=12, Nc=6) and the simulation was carried out for the month of June. Simulation results for the current building condition are provided in Fig. 6.31, in terms of trends of boundary conditions (top and bottom graphs) and internal temperature (central graph), which was related to the setpoint profile. Figure 6.32 shows the simulation results after the introduction of the solar shading, which trend is presented in terms of shading level ($0<SL<1$). By analysing these results, even without tuning the other parameters, it was immediately demonstrated how the shading level contributing to preserve the internal temperature from increasing too much during the period of occupancy, according to the same setpoint profile used in the experimental phase. This is particularly evident in the second part of the month, when the fan coil performance is not sufficient to contrast the effect of weather conditions, although it has operated, most of time, at maximum speed.

Following this consideration, the MPC simulator with solar shading active will be the only one used for subsequent tuning phases. Anyway, results obtained in previous simulations will be reported within tuning results for a complete comparison.

Tuning of the MPC parameters regarded the prediction and control horizons, which were initially tested separately, as to be re-joined in the end. In order to identify the best prediction horizon, the control horizon was linked to the prediction one through the relation: $Nc = Np/2$. Remembering that, within the controller, the control horizon was divided in equal time intervals to cover with the control action all the prediction period, each interval was of 10 minutes, in this first tuning phase.

Considering the internal dynamics and the solar ones and guaranteeing an acceptable computational time, the prediction time (tp), already tested for one hour, has been varied from 2 to 12 hours (Np=24 to Np=144), with a time step of two hours.

Trends of variables obtained for each horizon tested are reported in APPENDIX I, similarly to those already presented in Fig. 6.32. Whereas, the RMSE values in simulation of the entire month of June, for each prediction horizon are shown in Table 6.7.

The choice of the best prediction horizon was derived from comfort and energy assessments, considering the most critical situation, along the data set chosen, i.e. the period 22-30 June 2016.

Therefore, histograms in Fig. 6.33 show the total energy absorbed for the period identified, varying the prediction horizon.

Comfort assessments are reported according to the standards related to PMV index, as already done in Chapter 5, and evaluating also the frequency distribution of the PMV index for each prediction horizon considered.

Thus, histograms in Fig. 6.34 are provided for comfort categories, according to standard EN15251 (*EN 15251:2007*), while results of frequency distribution, generated in Excel for the PMV data of each Np tested, are displayed in Fig. 6.35. Best results are highlighted in red.

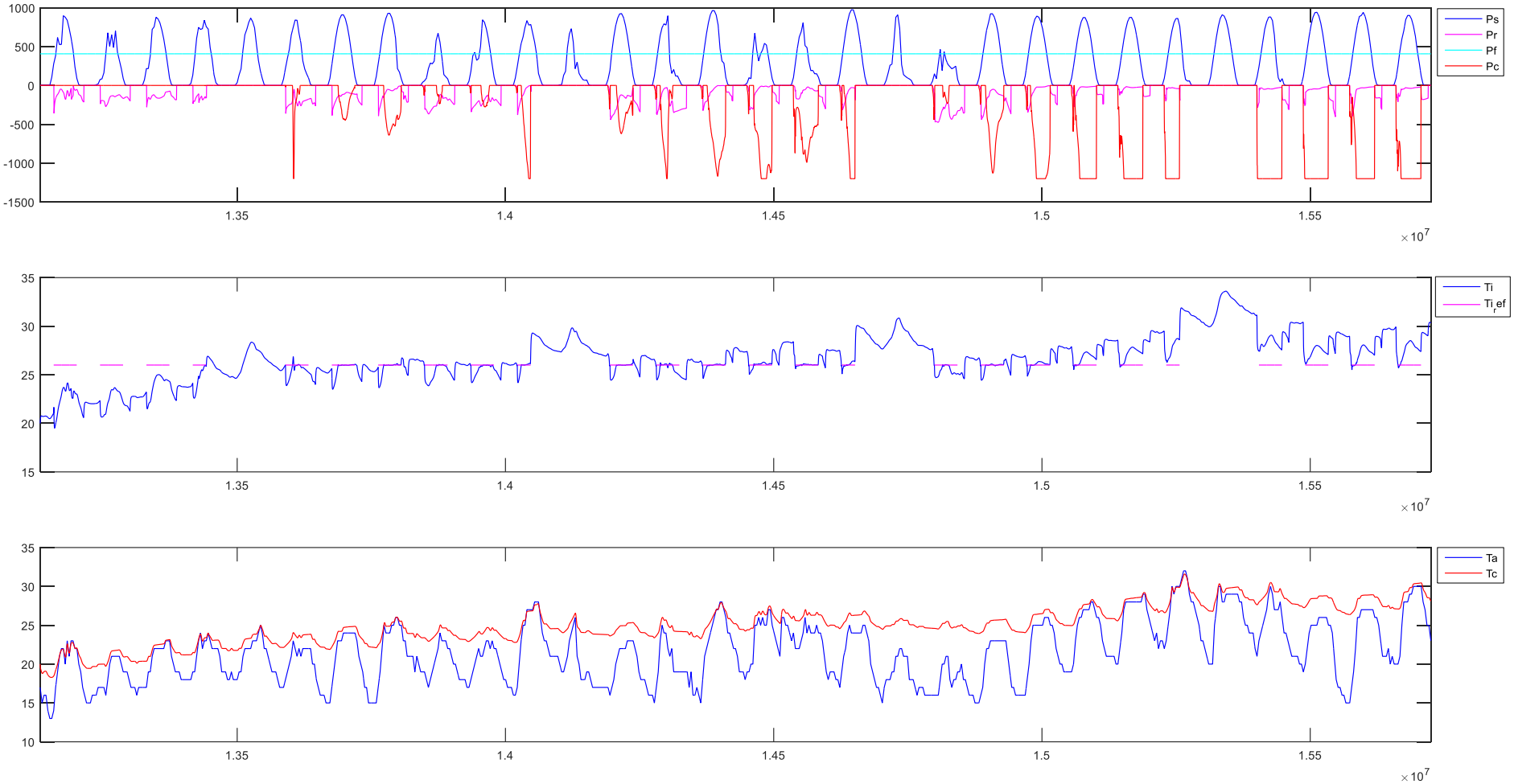

Fig. 6.31 Simulation results of the MPC simulator operating during one month of the cooling season, without solar shading management.

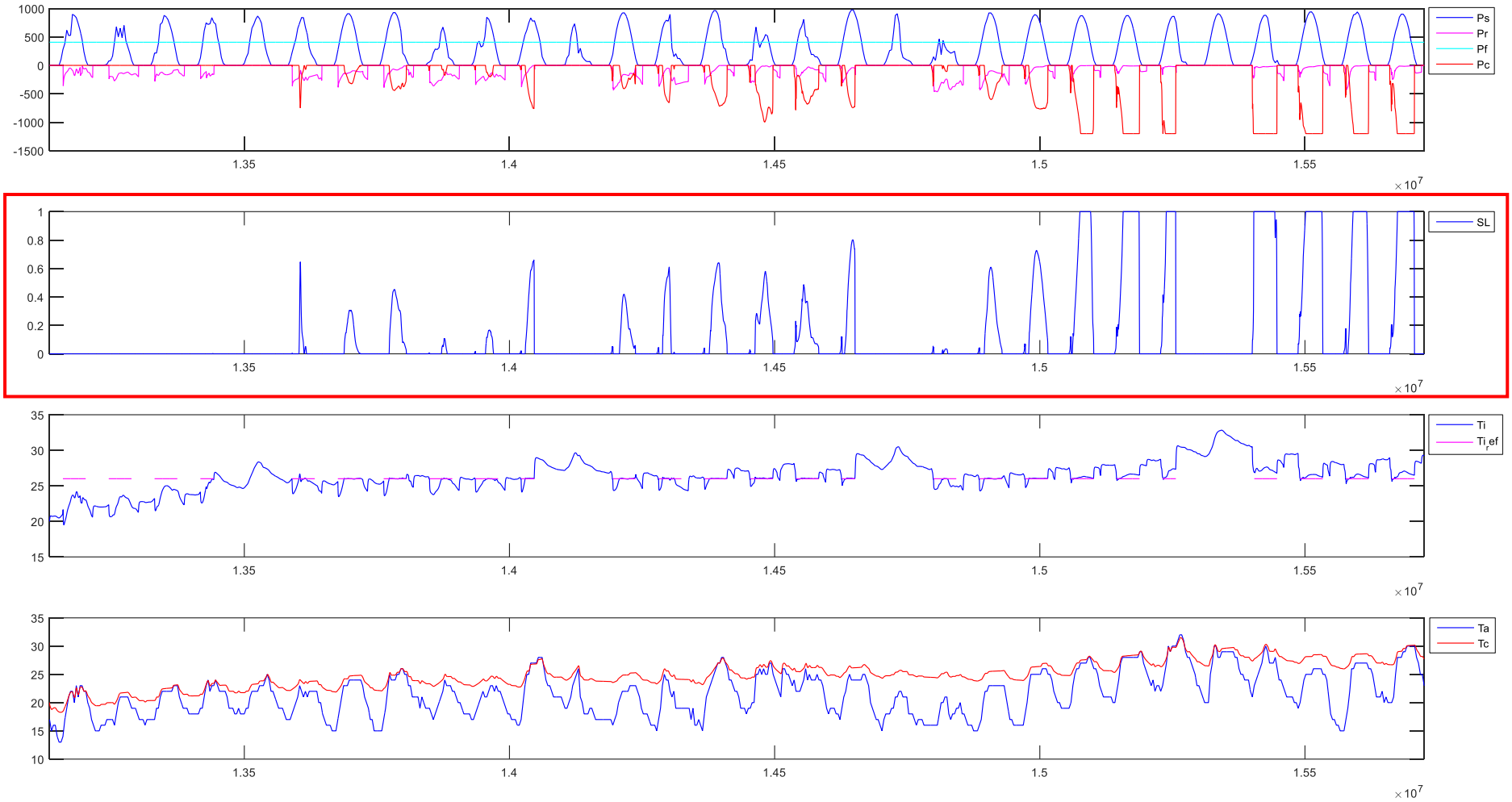

Fig. 6.32 Simulation results of the MPC simulator operating during one month of the cooling season, with solar shading management.

Table 6.7: RMSE values obtained simulating the MPC during the tuning of Np.

Np	Nc	tp [h]	RMSE value
12	6	1	0.51
24	12	2	0.50
48	24	4	0.48
72	36	6	0.47
96	48	8	0.45
120	60	10	0.44
144	72	12	0.42

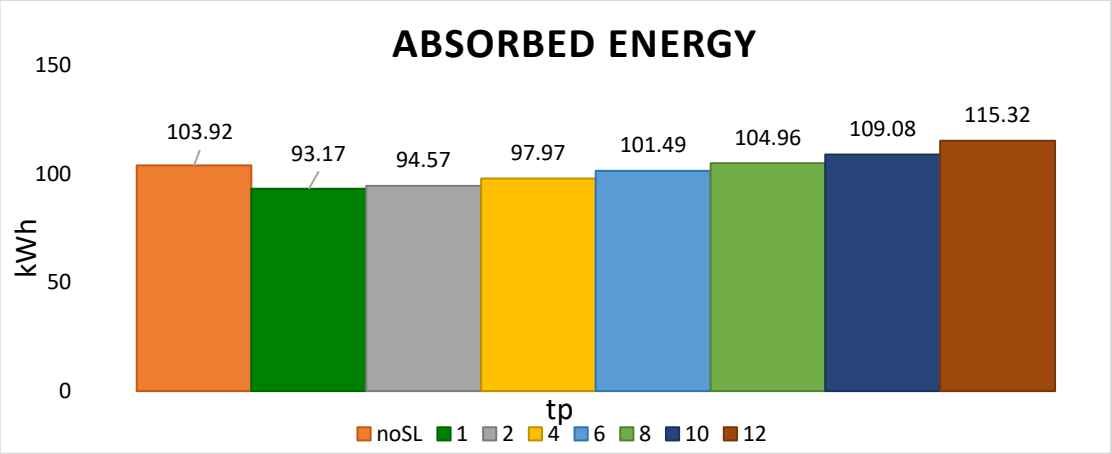

Fig. 6.33 Total energy absorbed by the plant in the simulation period for each prediction time.

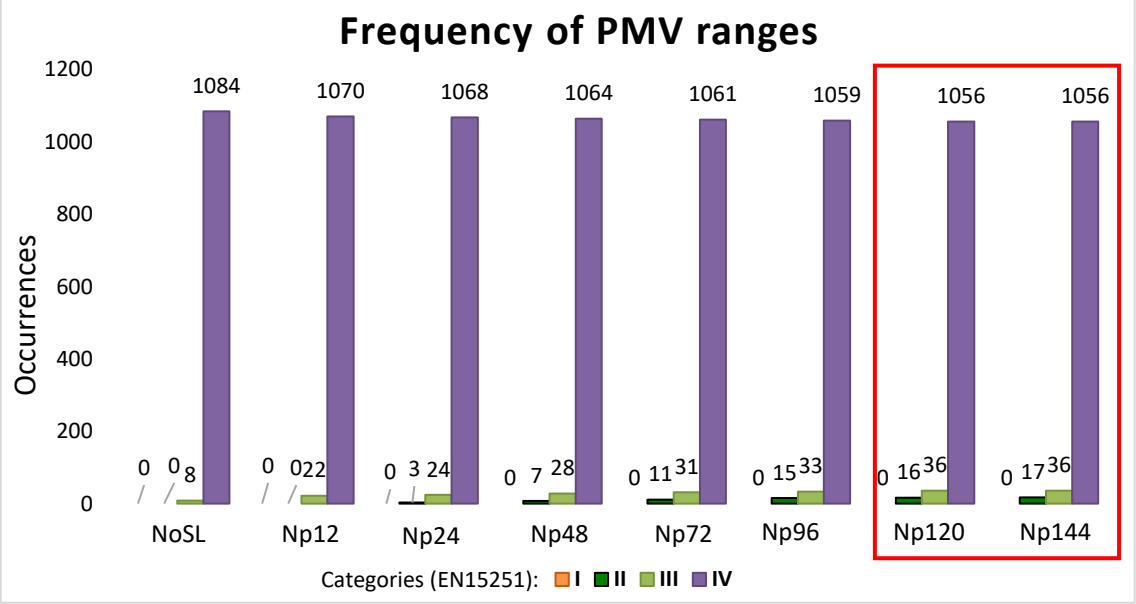

Fig. 6.34 Comfort assessment: histograms of occurrences - PMV value.

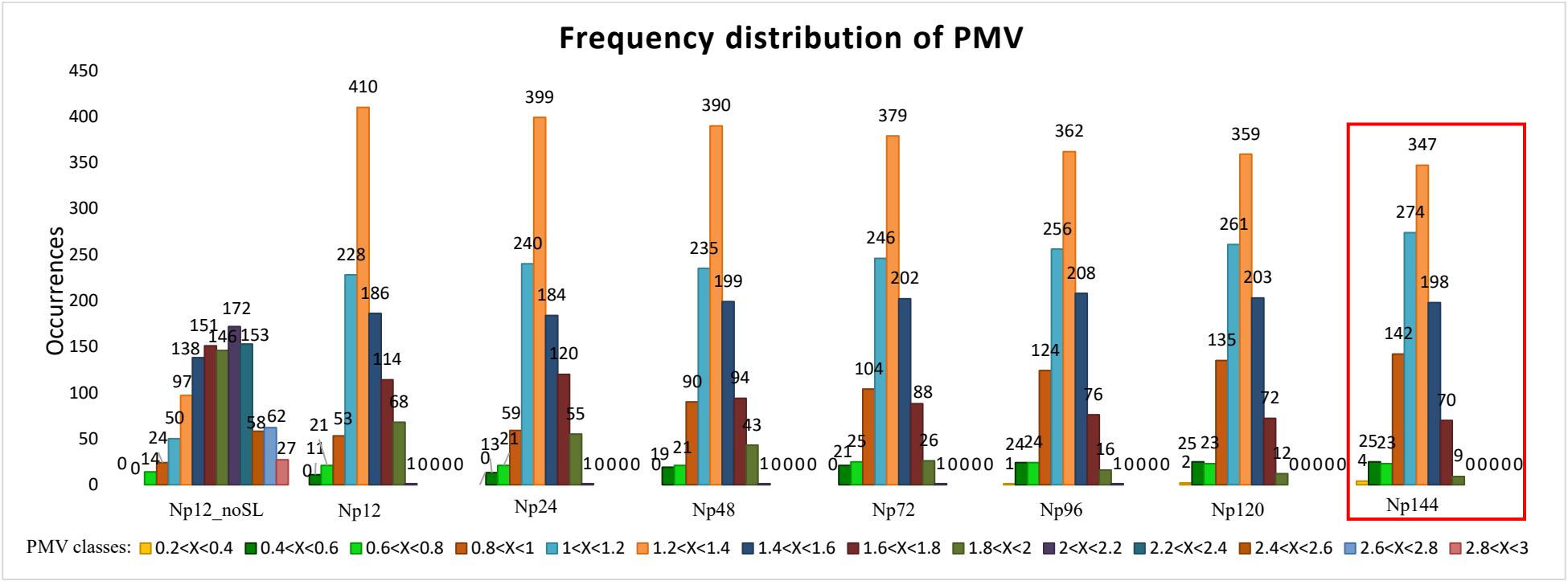

Fig. 6.35 Comfort assessment: frequency distribution - PMV value.

The second phase of tuning has mainly regarded the control horizon (Nc). The best prediction horizons of the first phase (Np=120 and Np=144) were maintained and other longer horizons were added. For the previous best horizons, corresponding to a prediction time (tp) of 10 and 12 hours respectively, different control horizons were tested. Considering an acceptable computational effort when control time is equal to one hour, longer prediction horizons were investigated as to evaluate the effect of the control action on the system. Indeed, the internal temperature of the test room is affected by the daily solar dynamics, but it also depends on the setpoint profile imposed by the occupancy schedule. Thus, extending the prediction horizon may fulfil the gap of the weekend, which often caused relevant energy demand, mostly in the beginning of the after week, consequently involving discomfort conditions. Table 6.8 summarizes the horizons tested and the resulting RMSE values in simulation.

Table 6.8: RMSE values obtained simulating the MPC during the tuning of Nc.

Np	tp [h]	Nc	RMSE value
120	10	60	0.44
		20	0.49
		10	0.49
		5	0.48
144	12	72	0.42
		24	0.48
		12	0.48
		6	0.47
288	24	24	0.40
432	36	36	0.41
576	48	48	0.40

Trends of variables obtained for each horizon tested are reported in APPENDIX I, together with those of the first tuning for the prediction horizon.

The choice of the best horizons was again derived from comfort and energy assessments, considering the most critical situation, along the data set chosen, i.e. the period 22-30 June 2016.

Therefore, histograms in Fig. 6.36 show the total energy absorbed for the period identified, varying the control horizon for the best prediction horizons and maintaining a 1-hour horizon for the longer prediction horizons.

Comfort assessments are reported according to the standards and evaluating also the frequency distribution of the PMV index, as previously done.

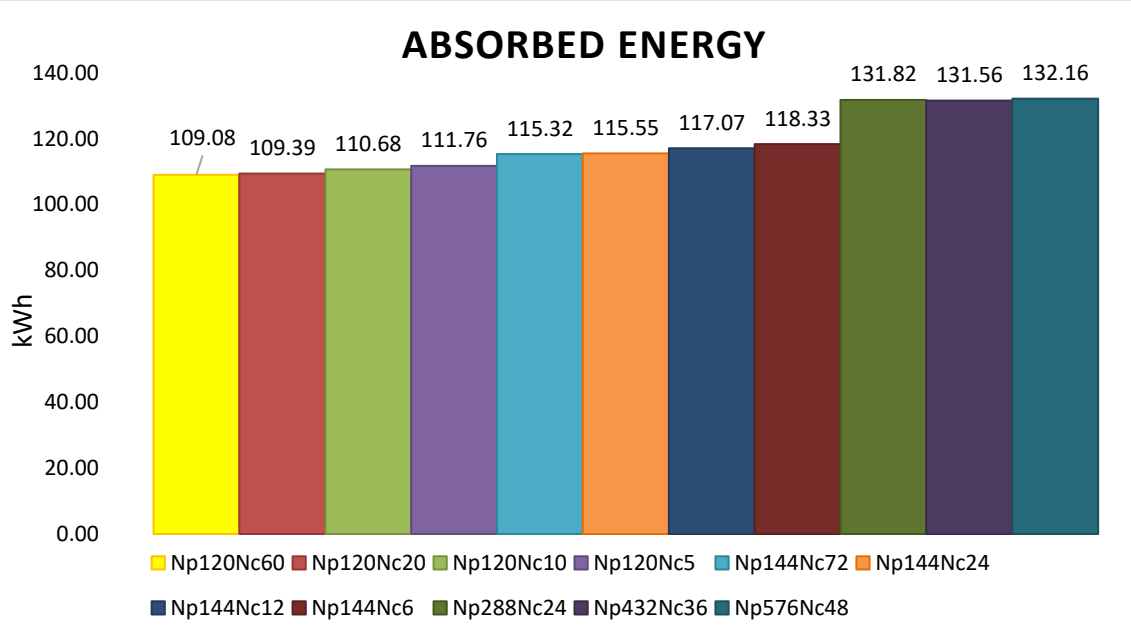

Fig. 6.36 Total energy absorbed by the plant in the simulation period for each horizon tested.

Thus, histograms in Fig. 6.37 are provided for comfort categories, according to standard EN15251 (*EN 15251:2007*), while results of frequency distribution, generated in Excel for the PMV data of each NpNc tested, are displayed in Fig. 6.38. Final best result, both of prediction and control horizon, is highlighted in red.

6.6.2 Adaptive modelling

Ultimately, the possibility of using adaptive modelling, i.e. by identifying the thermal parameters of the reduced model during the operation of the controller, has been investigated, taking from time to time the data from the system needed to derive the model for the controller itself. For this analysis, the MPC parameters were set according best results achieved in the tuning phase (par. 6.6.1), Np= 288 and Nc= 24. The "Model estimator" block was activated, enabling the on-line estimation, and a 14-day length of data set was established, defining the maximum of data to load from the simulation output.

Then, the estimator operated as described in par 6.4.2.1 and it carried out the model identification at the end of each day of simulation, using data provided up to a maximum of 14-day data.

Initially, model parameters were those of the best grey-box model identified in par. 6.5 and simulation period remained the month of June.

Results of this first test demonstrated by one side the chance to release from periodically off-line estimating the model for the controller. On the other side, the RMSE value (= 0.6 °C), compared to that of the tuning phase for the best horizons, revealed the need of refining the choice of data set. Conversely, the total energy absorbed (= 131.27kWh) during the simulation is absolutely comparable with the one of the tuning phase, meaning to suggest that adaptive modelling does not imply an increase of energy demand.

Trends of variables involved in this first test of adaptive modelling are summarized in Fig. 6.39, whilst trends of parameters estimated during the simulator working, were displayed in Fig. 6.40.

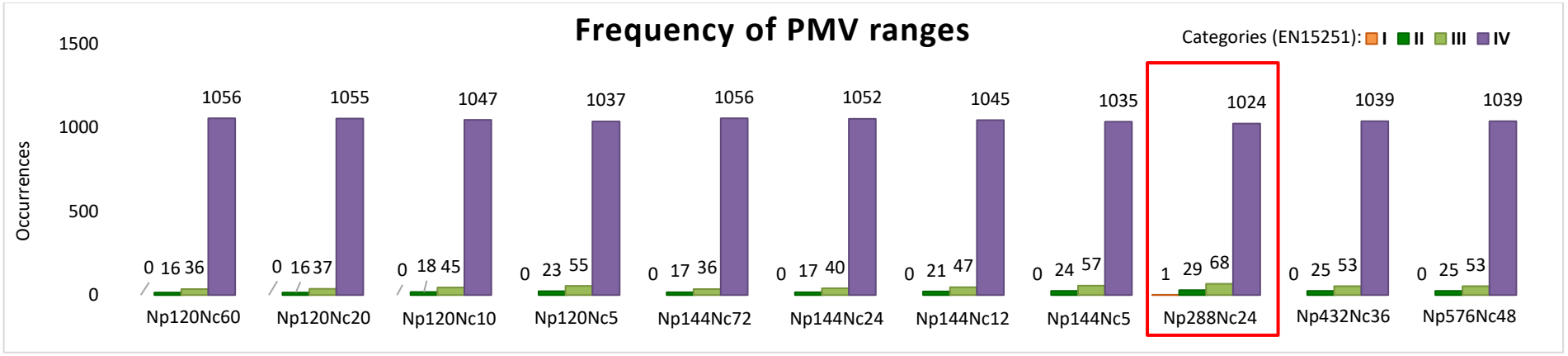

Fig. 6.37 Comfort assessment: frequency distribution - PMV value.

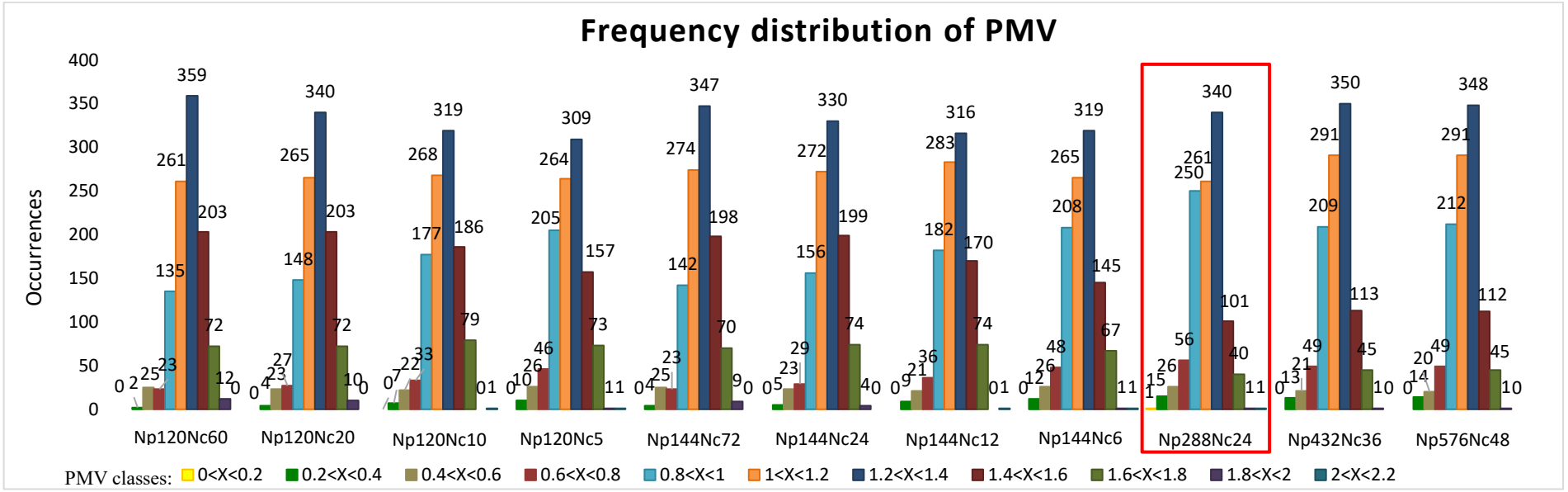

Fig. 6.38 Comfort assessment: frequency distribution - PMV value.

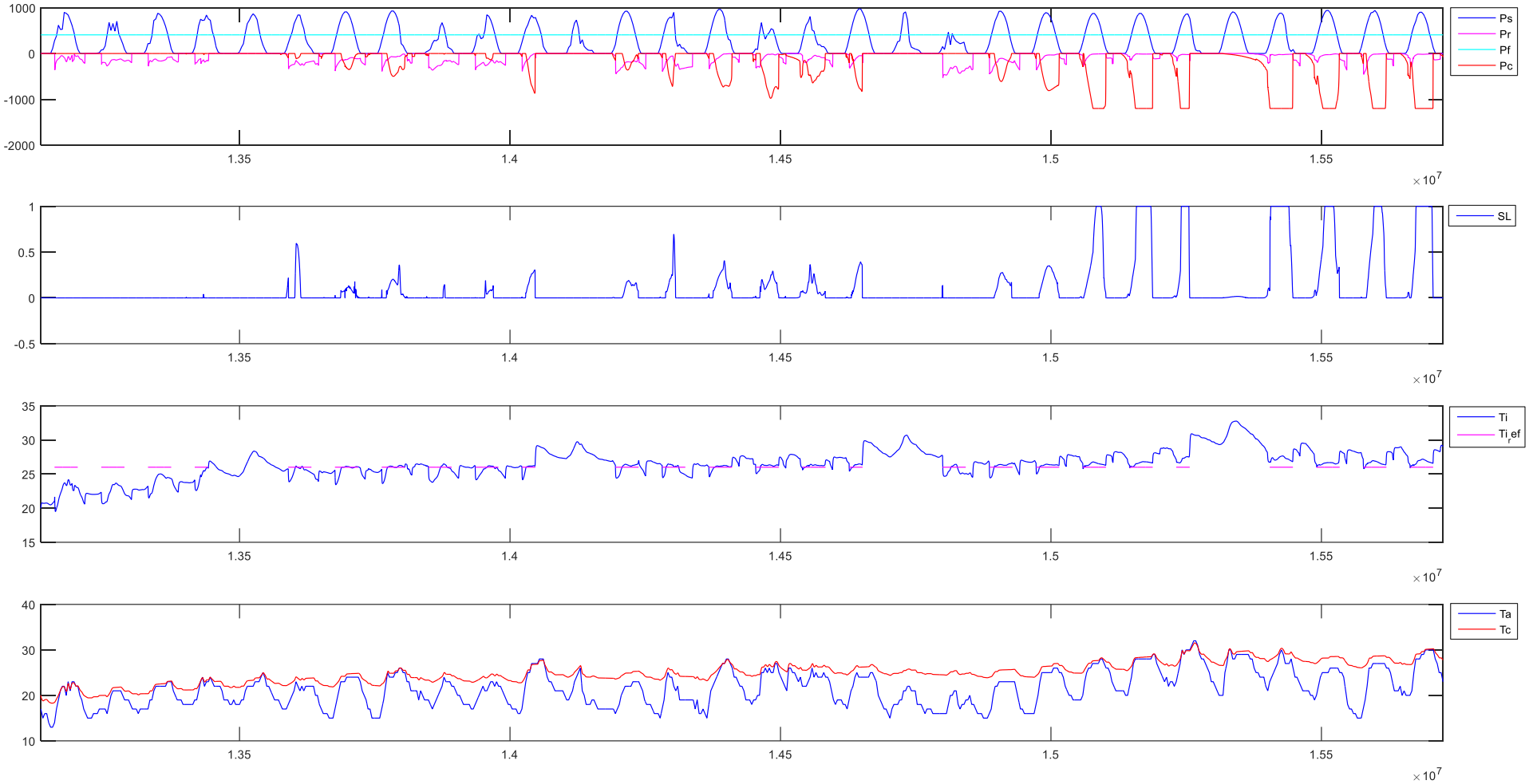

Fig. 6.39 Simulation results of the MPC simulator operating during one month of the cooling season, with adaptive modelling.

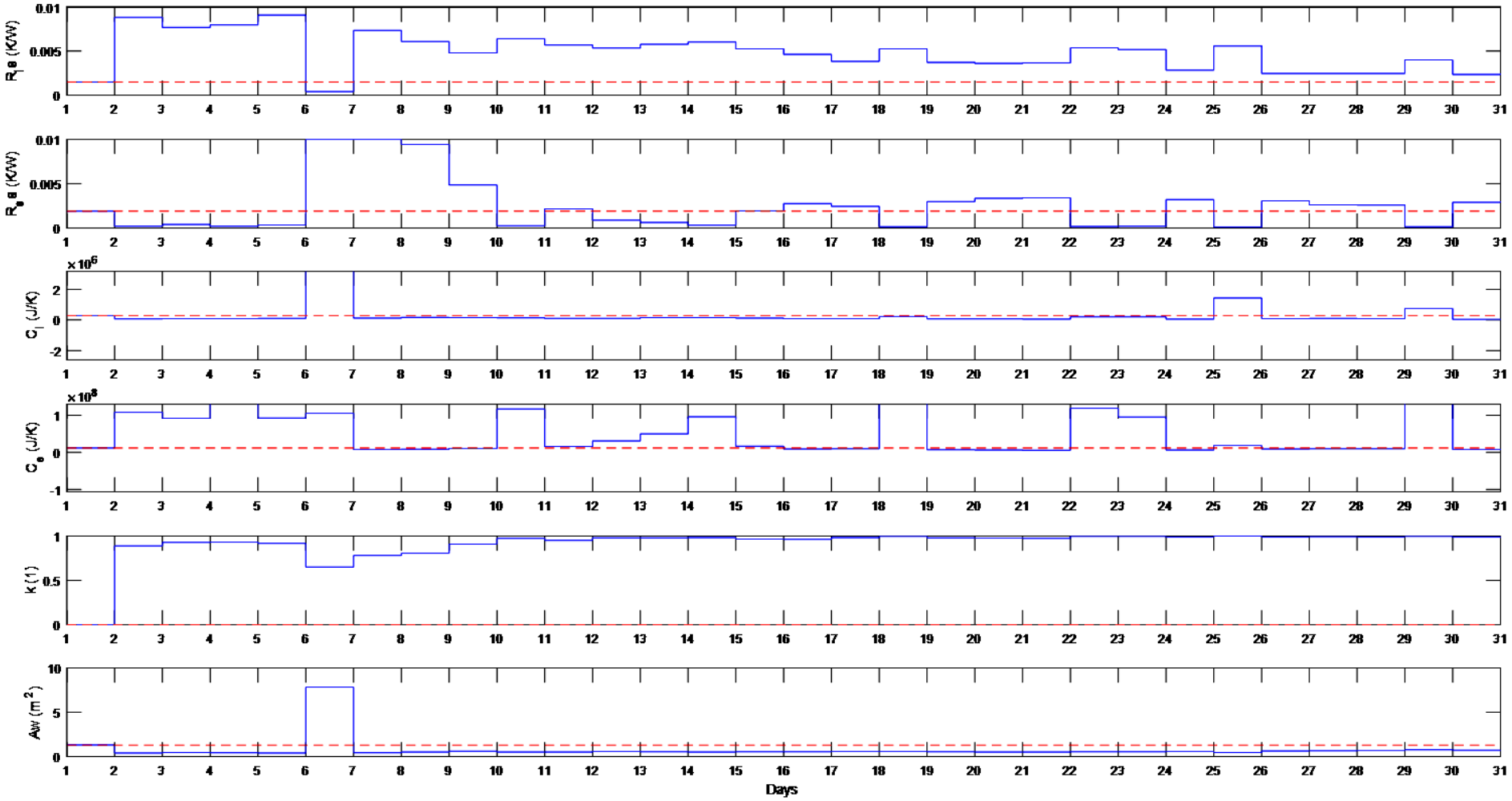

Fig. 6.40 Simulation results of the model parameters estimated by the "Model estimator", while the MPC simulator was working.

6.7 Conclusions

This chapter, exploiting results of the experimental test described in Chapter 5, presented the development of the model-based predictive control in simulation environment to test its potentiality in renovation scenarios.

Therefore, a MPC simulator, reproducing the experimental controller, was created in MATLAB and simulated in Simulink, using the detailed building model, realized in Dymola, to simulate the physical system, the university building and, particularly, the test room where the advanced control had been implemented.

First, in order to derive the suitable grey-box model for the controller, a modelling phase was developed, by applying the identification procedure, widely discussed in previous chapters of this research thesis. The generated data set was descended from output data of a simulation with a random behaviour of the plant to avoid the overfitting of the model identified with the data. The best model was, like for the experimental phase, a second-order model, which, overall, has returned better performance in the parameter estimation phase and, especially, in the validation phase.

Afterwards, a first retrofit scenario has been elaborated by introducing the solar shading within the detailed building model and the shading level as control action for the controller.

It has been demonstrated, with a first simulation during the cooling season, the beneficial effect of the shading action both for energy reduction and for improvement of comfort conditions.

Then, a tuning phase was carried out for the shading scenario, by varying the prediction and control horizons.

Results of simulation, during the month of June, revealed an expected predominant effect of solar dynamics affecting the internal temperature.

Comfort and energy assessments on simulations tested, which differed for the horizons setting, underlined that the controller could mitigated the risk of overheating by the adoption of a quite long prediction horizon, better if it is of one-day order. Indeed, a long prediction horizon allows to prevent local discomfort, mostly after the weekends.

On the contrary, the control response could be set with one-hour horizon, ensuring an effective control without affecting the computational effort of the controller. This is an important aspect to consider when the application is provided to be “plug and play” and working real time.

Another consideration to be done in this direction is the choice of weights for the cost function, which must be optimized by the controller. The balance between energy and comfort should be calibrated on the control objectives and, to a higher and comprehensive level, on the policies governing the building management.

Chapter 7

Final conclusions

This dissertation has presented a model-based predictive control to support building performance management. This chapter summarises the main contributions of this research and their impact on the field of building management systems. Interesting issues beyond the scope of this dissertation were raised during the research undertaken. They are presented in this chapter as future research in this field.

7.1 Main contributions and implications of this research

This dissertation presents the state of the art on the model-based predictive control (MPC) for buildings and the main successful implementations are documented.

The main contribution of this research is the development of an application of model-based predictive control in an existing building to support the on-going evolution and optimization of advanced controls and integrated it in processes of building performance management, from a design level to an implementation level, by establishing the necessary information related to the data collection, technological implementation and its reproducibility.

The principal findings and implications of this dissertation are presented below, demonstrating how the initial objectives stated have been achieved by the research undertaken.

The first objective of this thesis was to identify a reduced model suitable to be used in an advanced control, such the MPC, in order to reduce the computational effort of the controller, while ensuring the control reliability. This goal was accomplished by the adoption of a grey-box model, derived from experimental data of the environmental monitoring arranged for the case study. The model used was identified by a very limited data set, but neither this, nor the discrete root mean square error obtained in simulation have affected the result of the experimental test. This demonstrated the power of the grey-box model in such applications, where it is required to process many iterations in a short time.

The second and core objective concerned the MPC prototype, which has revealed its potentiality for the design and operation of real-time control strategies: once the system model has been identified, the prototype developed requires only two physical inputs (two sensors: one for the indoor temperature and one for the boundary temperature condition) and an output (a connection to communicate with the fan coil motor) while in operation.

About the third objective, the application created in LabVIEW is user-friendly and easily reproducible even for more complex systems, provided its architecture is expanded accordingly. Finally, it can be acknowledged that standard technology currently available makes integration of MPC systems in existing buildings quite feasible. More specifically, the prototype developed in this thesis, was made of a wireless sensor network, a customised connection to the conditioning system of the building, along with a programmable workbench including a user interface, a data acquisition system, a MPC loop case to manage subVIs and setpoints. Thus, this MPC framework could be seamlessly integrated in portable devices, deployable directly on site.

7.2 Further research

Some interesting issues came out during the development of this research. However, they were not addressed because they require an analysis beyond the scope of this dissertation. Some of the most relevant matters, suggesting further developments, are introduced below.

Although has been recognised and verified that grey-box models are a winning solution for deployment in advanced controls, such as the MPC, the identification of thermal parameters of the model does not always seem to be so immediate, especially in the optics, seen in Chapter 6, of taking advantage of an adaptive modelling within the MPC. This is because the estimate with the MLE algorithm (within the CTSM package in R) requires careful management of the initial conditions and parameter ranges to be estimated in order to avoid running into local minimum that may compromise the reliability of the results of estimation. Despite it was verified that even discrete RMSE values do not compromise the control, it would be good to deepen the question of model identification, especially for the purposes of its continuous estimation, as suggested by the test carried out in this thesis, using the “fmincon” algorithm in MATLAB applied to case study.

As for the application of MPC developed, considering the promising results obtained for the study case, it will be useful extending the application pursuing the objective of improving the building performance. This approach is not just about energy efficiency, that is, the energy efficiency classes

according to the minimum requirements of the recent Ministerial Decree (DM 26/06/2015), but it has the ultimate goal of returning building automation systems with increasing energy efficiency, as indicated by standard EN 15232 (*UNI EN 15232-1:2017*).

Extending the procedure tested means, at first, considering an extension of the local control, connecting multiple rooms, automating the return of some sensors measurements and allowing data communication between spaces and with a central control unit. This aspect promotes also a more efficient local control and better comfort conditions for users. Therefore, the main issue is limited to the technological effort needed to generate a central control and local applications, which should be installed to manage themselves independently, yet with the possibility of exchanging information, if needed.

After that, having reached an advanced automation level, in order to achieve even higher performance (refer to standard UNI EN 15232 for the BACS classification), it will be necessary to include additional integrated functions for multidisciplinary relationships between HVAC systems and the different building facilities, like electricity, lighting, solar shading, etc. This solution has been suggested also by this research work, by exploiting the simulated intervention scenario, to promote the integration between the advanced plant management and one of the hypothesised services, namely the solar shading.

References

Afram, A., Janabi-Sharifi, F., 2014. Theory and applications of HVAC control systems – A review of model predictive control (MPC). Building and Environment 72, 343–355. https://doi.org/10.1016/j.buildenv.2013.11.016

Andersen, K.K., Madsen, H., Hansen, L.H., 2000. Modelling the heat dynamics of a building using stochastic differential equations. Energy and Buildings 31, 13–24.

ASHRAE Standard 55 - 2010 Thermal Environmental Conditions for Human Occupancy, n.d.

Bacher, P., Madsen, H., 2011. Identifying suitable models for the heat dynamics of buildings. Energy and Buildings 43, 1511–1522. https://doi.org/10.1016/j.enbuild.2011.02.005

Bacher, P., Madsen, H., 2010. Experiments and Data for Building Energy Performance Analysis (Report), Financed by The Danish Electricity Saving Trust. Technical University of Denmark, DTU Informatics, Building 321.

Berardi, U., 2015. Building Energy Consumption in US, EU, and BRIC Countries. Procedia Engineering 118, 128–136. https://doi.org/10.1016/j.proeng.2015.08.411

Bertoldi, P., López Lorente, J., Labanca, N., European Commission, Joint Research Centre, Institute for Energy and Transport, 2016. Energy consumption and energy efficiency, trends in the EU-28 2000-2014: efficiency trends of energy-related products and energy consumption in the EU-28. Publications Office, Luxembourg.

Bolognini, F., 2016. "Experimental identification and validation of reduced order thermal models for the dynamic control of a university building."Master Thesis. Università Politecnica delle Marche.

Braun, J.E., 2003. Load Control Using Building Thermal Mass. Journal of Solar Energy Engineering 125, 292. https://doi.org/10.1115/1.1592184

Buildings.Utilities.Comfort [WWW Document], n.d. URL https://simulationresearch.lbl.gov/modelica/releases/v1.2_build1/help/Buildings_Utilities_Comfort.html (accessed 11.28.17).

Camacho, E.F., Bordons, C., 2007. Model Predictive control, Advanced Textbooks in Control and Signal Processing. Springer London, London. https://doi.org/10.1007/978-0-85729-398-5

Carrascal, E., Garrido, I., Garrido, A., Sala, J., 2016. Optimization of the Heating System Use in Aged Public Buildings via Model Predictive Control. Energies 9, 251. https://doi.org/10.3390/en9040251

Chen, T.Y., 2002. Application of adaptive predictive control to a floor heating system with a large thermal lag. Energy and Buildings 34, 45–51.

Cho, S.H., Zaheer-uddin, M., 2003. Predictive control of intermittently operated radiant floor heating systems. Energy Conversion and Management 44, 1333–1342. https://doi.org/10.1016/S0196-8904(02)00116-4

Cigler, J., Gyalistras, D., Široky, J., Tiet, V., Ferkl, L., 2013. Beyond theory: the challenge of implementing model predictive control in buildings, in: Proceedings of 11th Rehva World Congress, Clima.

Cigler, J., Siroky, J., Korda, M., Jones, C., 2013. On the selection of the most appropriate MPC problem formulation for buildings, in: 11th REHVA World Congress CLIMA 2013.

Cutler, C.R., Ramaker, B.C., 1980. Dynamic Matrix Control- A Computer Control Algorithm. Presented at the Automatic Control Conference, San Francisco.

De Coninck, R., Magnusson, F., Åkesson, J., Helsen, L., 2014. Grey-Box Building Models for Model Order Reduction and Control, in: Proceedings of the 10th International Modelica Conference. Presented at the 10th International Modelica Conference, Linköping University Electronic Press, Linköping, Sweden, pp. 657–666.

EN 15251:2007. Indoor environmental input parameters for design and assessment of energy performance of buildings addressing indoor quality, thermal environment, lighting and acoustics., n.d.

Europe 2020 indicators - climate change and energy - Statistics Explained [WWW Document], n.d. URL http://ec.europa.eu/eurostat/statistics-explained/index.php/Europe_2020_indicators_-_climate_change_and_energy (accessed 11.27.17).

Fanger, P.O., 1970. Thermal comfort: Analysis and applications in environmental engineering. Danish Technical Press.

Fanger, P.O., Ipsen, B.M., Langkilde, G., Olessen, B.W., Christensen, N.K., Tanabe, S., 1985. Comfort limits for asymmetric thermal radiation. Energy and Buildings 8, 225–236. https://doi.org/10.1016/0378-7788(85)90006-4

Freire, R.Z., Oliveira, G.H.C., Mendes, N., 2008. Predictive controllers for thermal comfort optimization and energy savings. Energy and Buildings 40, 1353–1365. https://doi.org/10.1016/j.enbuild.2007.12.007

García, C.E., Prett, D.M., Morari, M., 1989. Model predictive control: Theory and practice—A survey. Automatica 25, 335–348. https://doi.org/10.1016/0005-1098(89)90002-2

Goyal, S., Barooah, P., 2012. A method for model-reduction of non-linear thermal dynamics of multi-zone buildings. Energy and Buildings 47, 332–340. https://doi.org/10.1016/j.enbuild.2011.12.005

Grünenfelder, W., Tödtli, J., 1985. The use of weather predictions and dynamic programming in the control of solar domestic hot water systems. Presented at the Mediterranean Electrotechnical Conference (Melecon), Madrid, Spain.

Hazyuk, I., Ghiaus, C., Penhouet, D., 2014. Model Predictive Control of thermal comfort as a benchmark for controller performance. Automation in Construction 43, 98–109. https://doi.org/10.1016/j.autcon.2014.03.016

Hazyuk, I., Ghiaus, C., Penhouet, D., 2012. Optimal temperature control of intermittently heated buildings using Model Predictive Control: Part I – Building modeling. Building and Environment 51, 379–387. https://doi.org/10.1016/j.buildenv.2011.11.009

Henze, G.P., Dodier, R.H., Krarti, M., 1997. Development of a Predictive Optimal Controller for Thermal Energy Storage Systems. HVAC&R Research 3, 233–264. https://doi.org/10.1080/10789669.1997.10391376

Henze, G.P., Felsmann, C., Knabe, G., 2004a. Evaluation of optimal control for active and passive building thermal storage. International Journal of Thermal Sciences 43, 173–183. https://doi.org/10.1016/j.ijthermalsci.2003.06.001

Henze, G.P., Kalz, D.E., Felsmann, C., Knabe, G., 2004b. Impact of Forecasting Accuracy on Predictive Optimal Control of Active and Passive Building Thermal Storage Inventory. HVAC&R Research 10, 153–178. https://doi.org/10.1080/10789669.2004.10391097

Henze, G.P., Kalz, D.E., Liu, S., Felsmann, C., 2005. Experimental analysis of model-based predictive optimal control for active and passive building thermal storage inventory. HVAC&R Research 11, 189–213.

ISO Standard 7730. Ergonomics of the thermal environment - Analytical determination and interpretation of thermal comfort using calculation of the PMV and PPD indices and local thermal comfort criteria, (2006)., n.d.

Jiménez, M.J., Madsen, H., 2008. Models for describing the thermal characteristics of building components. Building and Environment 43, 152–162. https://doi.org/10.1016/j.buildenv.2006.10.029

Juhl, R., Kristensen, N.R., Bacher, P., Kloppenborg, J., Madsen, H., 2013. Ctsm-r user guide. Technical University of Denmark 2.

Kalmár, F., 2016. Summer operative temperatures in free running existing buildings with high glazed ratio of the facades. Journal of Building Engineering 6, 236–242.

Kavgic, M., Hilliard, T., Swan, L., 2015. Opportunities for Implementation of MPC in Commercial Buildings. Energy Procedia 78, 2148–2153. https://doi.org/10.1016/j.egypro.2015.11.300

Killian, M., Kozek, M., 2016. Ten questions concerning model predictive control for energy efficient buildings. Building and Environment 105, 403–412. https://doi.org/10.1016/j.buildenv.2016.05.034

Kim, J.-T., Ryu, Y.-S., Cho, H.-M., Stubbs, N., 2003. Damage identification in beam-type structures: frequency-based method vs mode-shape-based method. Engineering structures 25, 57–67.

Kontes, G.D., Valmaseda, C., Giannakis, G.I., Katsigarakis, K.I., Rovas, D.V., 2014. Intelligent BEMS design using detailed thermal simulation models and surrogate-based stochastic optimization. Journal of Process Control 24, 846–855. https://doi.org/10.1016/j.jprocont.2014.04.003

LabVIEW Control Design User Manual, 2008.

Liao, C., Barooah, P., 2010. An integrated approach to occupancy modeling and estimation in commercial buildings, in: American Control Conference (ACC), 2010. IEEE, pp. 3130–3135.

Lin, Z., Chow, T.T., Fong, K.F., Wang, Q., Li, Y., 2005. Comparison of performances of displacement and mixing ventilations. Part I: thermal comfort. International Journal of Refrigeration 28, 276–287. https://doi.org/10.1016/j.ijrefrig.2004.04.005

Liu, S., Henze, G., 2004. Impact of Modeling Accuracy on Predictive Optimal Control of Active and Passive Building Thermal Storage Inventory. ASHRAE Transactions 110, 151–163. https://doi.org/10.1007/978-3-662-07287-5_8

Ma, Y., Borrelli, F., Hencey, B., Coffey, B., Bengea, S., Haves, P., 2010. Model predictive control for the operation of building cooling systems, in: Proceedings of the 2010 American Control Conference. Presented at the Proceedings of the 2010 American Control Conference, pp. 5106–5111. https://doi.org/10.1109/ACC.2010.5530468

Ma, Y., Borrelli, F., Hencey, B., Packard, A., Bortoff, S., 2009. Model Predictive Control of thermal energy storage in building cooling systems. IEEE, pp. 392–397. https://doi.org/10.1109/CDC.2009.5400677

Ma, Y., Kelman, A., Daly, A., Borrelli, F., 2012. Predictive Control for Energy Efficient Buildings with Thermal Storage: Modeling, Stimulation, and Experiments. IEEE Control Systems 32, 44–64. https://doi.org/10.1109/MCS.2011.2172532

Maciejowski, J., 2002. Predictive Control With Constraints.

Madsen, H., Schultz, J.M., 2003. Short time determination of the heat dynamics of buildings. (No. 243). Technical University of Denmark, DTU Informatics.

Mathews, E.H., Richards, P.G., 1989. A tool for predicting hourly air temperatures and sensibles energy loads in buildings at sketch design stage. Energy and Buildings 14, 61–80. https://doi.org/10.1016/0378-7788(89)90029-7

n. 74 Decreto del Presidente della Repubblica 16 aprile 2013, Regolamento recante definizione dei criteri generali in materia di esercizio, conduzione, controllo, manutenzione e ispezione degli impianti termici per la climatizzazione invernale ed estiva degli edifici e per la preparazione dell'acqua calda per usi igienici sanitari., n.d.

Oldewurtel, F., Parisio, A., Jones, C.N., Gyalistras, D., Gwerder, M., Stauch, V., Lehmann, B., Morari, M., 2012. Use of model predictive control and weather forecasts for energy efficient building climate control. Energy and Buildings 45, 15–27. https://doi.org/10.1016/j.enbuild.2011.09.022

Orosa, J.A., Oliveira, A.C., 2011. Software tools for HVAC research. Advances in Engineering Software 42, 846–851. https://doi.org/10.1016/j.advengsoft.2011.05.028

Piccinini, A., 2016. "Design and simulation of thermal control system for large public building". Master Thesis. Università Politecnica delle Marche.

Prívara, S., Cigler, J., Váňa, Z., Oldewurtel, F., Sagerschnig, C., Žáčeková, E., 2013. Building modeling as a crucial part for building predictive control. Energy and Buildings 56, 8–22. https://doi.org/10.1016/j.enbuild.2012.10.024

Prívara, S., Široký, J., Ferkl, L., Cigler, J., 2011. Model predictive control of a building heating system: The first experience. Energy and Buildings 43, 564–572. https://doi.org/10.1016/j.enbuild.2010.10.022

Propoi, A.I., 1963. Use of LP Methods for Synthesizing Sampled-data Automatic Systems. Automatic Remote Control 24.

Qin, S.J., Badgwell, T.A., 2003. A survey of industrial model predictive control technology. Control engineering practice 11, 733–764.

Rabl, A., 1988. Parameter Estimation in Buildings: Methods for Dynamic Analysis of Measured Energy Use. J. Sol. Energy Eng 110, 52–66. https://doi.org/10.1115/1.3268237

Ramallo-González, A.P., Eames, M.E., Coley, D.A., 2013. Lumped parameter models for building thermal modelling: An analytic approach to simplifying complex multi-layered constructions. Energy and Buildings 60, 174–184. https://doi.org/10.1016/j.enbuild.2013.01.014

Reynders, G., Diriken, J., Saelens, D., 2014. Quality of grey-box models and identified parameters as function of the accuracy of input and observation signals. Energy and Buildings 82, 263–274. https://doi.org/10.1016/j.enbuild.2014.07.025

Richalet, J., Rault, A., Testud, J.L., Papon, J., 1978. Model predictive heuristic control: Applications to industrial processes. Automatica 14, 413–428. https://doi.org/10.1016/0005-1098(78)90001-8

Shaikh, P.H., Nor, N.B.M., Nallagownden, P., Elamvazuthi, I., Ibrahim, T., 2014. A review on optimized control systems for building energy and comfort management of smart sustainable buildings. Renewable and Sustainable Energy Reviews 34, 409–429. https://doi.org/10.1016/j.rser.2014.03.027

Široký, J., Oldewurtel, F., Cigler, J., Prívara, S., 2011. Experimental analysis of model predictive control for an energy efficient building heating system. Applied Energy 88, 3079–3087. https://doi.org/10.1016/j.apenergy.2011.03.009

Široky, J., Oldewurtel, F., Cigler, J., Prívara, S., 2011. Experimental analysis of model predictive control for an energy efficient building heating system. Applied Energy 88, 3079–3087.

Snyder, M.E., Newell, T.A., 1990. Cooling cost minimization using building mass for thermal storage, in: ASHRAE Transactions.

Standard EN 13779. Ventilation for non-residential buildings - performance requirements for ventilation and room-conditioning systems. (2008), n.d.

Trčka, M., Hensen, J.L.M., 2010. Overview of HVAC system simulation. Automation in Construction 19, 93–99. https://doi.org/10.1016/j.autcon.2009.11.019

UNI EN 15232-1:2017. Energy performance of buildings - Part 1: Impact of Building Automation, Controls and Building Management - Modules M10-4,5,6,7,8,9,10, 2017.

UNI EN ISO 13786:2008. Thermal performance of building components – Dynamic thermal characteristics – Calculation methods, n.d.

Wang, S., Xu, X., 2006. Simplified building model for transient thermal performance estimation using GA-based parameter identification. International Journal of Thermal Sciences 45, 419–432. https://doi.org/10.1016/j.ijthermalsci.2005.06.009

Weimer, J., Ahmadi, S.A., Araujo, J., Mele, F.M., Papale, D., Shames, I., Sandberg, H., Johansson, K.H., 2012. Active Actuator Fault Detection and Diagnostics in HVAC Systems, in: Proceedings of the Fourth ACM Workshop on Embedded Sensing Systems for Energy-Efficiency in Buildings, BuildSys '12. ACM, New York, NY, USA, pp. 107–114. https://doi.org/10.1145/2422531.2422551

Yuan, X., Anumba, C.J., Parfitt, M.K., 2016. Cyber-physical systems for temporary structure monitoring. Automation in Construction 66, 1–14. https://doi.org/10.1016/j.autcon.2016.02.005

Zhou, Q., Wang, S., Xu, X., Xiao, F., 2008. A grey-box model of next-day building thermal load prediction for energy-efficient control. International Journal of Energy Research 32, 1418–1431. https://doi.org/10.1002/er.1458

Publications

"Testing of a Tracer Gas Based Measurement Procedure to Assess Air Change Rates in Buildings" (International Symposium on Automation and Robotics in Construction and Mining, ISARC 2015, Oulu, Finland);

"Reduced order modelling for control and management of buildings" (convegno nazionale ISTeA 2015);

"Empirical approach for estimating reduced-order models of buildings" (convegno internazionale ISTeA 2016);

"Lumped parameter models for energy auditing of existing building" ("Central Europe towards Sustainable Building" (CESB), Prague 2016);

"Reduced-order models for supporting energy audits of buildings" (33rd International Symposium on Automation and Robotics in Construction, ISARC 2016, Auburn, USA);

"Design and simulation of a fuzzy supervisory control system integrated in a small public building" (33rd International Symposium on Automation and Robotics in Construction, ISARC 2016, Auburn, USA).

"Estimation of reduced-order models from empirical observations" (1st International Conference on Building, Energy, Systems and Technology, BEST 2016);

"Preliminary implementation of a MPC prototype in an office building" (ISTeA 2017 – Re-shaping the construction industry);

"Overheating phenomena induced by fully-glazed facades: Investigation of a sick building in Italy and assessment of the benefits achieved via model predictive control of the AC system" (Solar Energy 157 (2017) pagg. 830-852).

APPENDICES

Appendix A. Technical specs of Hobo wireless sensors

OVERVIEW

HOBO ZW Series wireless data nodes provide centralized monitoring of energy and environmental conditions in buildings.

Supported Measurements: Air Velocity, AC Current, AC Voltage, Amp Hour, $C0_2$, Compressed Air Flow, DC Current, DC Voltage, Differential Pressure, Gauge Pressure, Kilowatt Hours, Kilowatts, Power Factor, Pulse Signals, Temperature, Relative Humidity, Dew Point, Volatile Organic Compound, Volt-Amp Reactive, Volt-Amp Reactive Hour, Volt-Amps, Water Flow, Watt Hours, Watts, Volts, Amps, 0-10 VDC, 4-20mA.

Key Advantages:

• Provides real-time centralized data collection within a facility;
• Scales up to a network of 100 nodes sending data to a single receiver;
• Creates self-healing network to overcome obstructions in communication paths;
• Provides one year battery life at 15-minute logging intervals;
• Provides alarm notifications via email or text messages;
• Features powerful software for organizing and viewing data as well as the wireless network.

There are three types of devices in a HOBO ZW Series Wireless Network:

Data Node	Router Node	Receiver
• Records data measured by internal and external sensors • Runs on battery power for approximately one year at a 15-minute logging interval • Operates as "dual-purpose" data/router node when AC powered	• Provides connectivity to other nodes • Operates as "range extenders" that expand the reach of the wireless network • Always runs on AC power with battery backup • Can be either a dedicated router or a data node doubling as a router	• Collects and stores data as the central hub of the network • Operates as the bridge between the network and the software • Stores network information and sends commands to nodes • Runs on AC power or USB with battery backup

The HOBO ZW Series Wireless Network uses low-power 2.4 GHz 802.15.4 radio with ZigBee protocol to transmit data wirelessly across the network of router nodes and back to the receiver. The

low-power 2.4 GHz signals lose strength due to obstructions in the communication path. Placing router nodes to work around obstructions is crucial for successful communication. A backbone of router nodes is essential for strong communication within the network. The **HOBO® Data Node Deployment Guide** help identify where to strategically place router nodes to compensate for obstructions.

Devices used in this research work are underlined in red.

Part number	ZW-RCVR (Receiver)	ZW-001 (Data node)	ZW-003* (Data node)	ZW-005* (Data node)	ZW-006 (Data node)	ZW-007* (Data node)	ZW-008 (Data node)	ZW-ROUTER
Buffer memory	up to 95k measurements	5k measurements	4k measurements	3k measurements				N/A
Measurements	N/A	Temp	Temp/RH	Ext T/RH, 1 analog port 1 pulse input port	4 external analog ports	Ext T/RH, 2 analog ports	2 analog ports 2 pulse input ports	N/A
Probe size	N/A	N/A	N/A	1cm (0.38 in) dia.	N/A	1cm (0.38 in) dia.	N/A	N/A
Sample rate	N/A	1 min to 18 hrs	1 min to 18 hrs	1 min to 18 hrs	1 min to 18 hrs	1 min to 18 hrs	1 min to 18 hrs	N/A
Transmission rate	N/A	2 min & greater	2 min & greater	2 min & greater	N/A	2 min & greater	2 min & greater	N/A
Power options (included)	AC adapter, Battery Backup, USB power	AC Power Adapter, Battery Backup						
Measurement range	N/A	Temp: -20° to 70°C (-4° to 158°F)	Temp: -20° to 70°C (-4° to 158°F) RH: 5 to 95% RH	Temp: -20° to 70°C (-4° to 158°F) RH: 5 to 95% RH Analog: o to 2.5 VDC Pulse: 0 to 65,535 pulses per logging interval	Analog channels: 0 to 2.5 VDC; 0 to 5 VDC	Temp: -20° to 70°C (-4° to 158°F) RH: 5 to 95% RH	Analog channels: 0 to 2.5 VDC; 0 to 5 VDC	N/A
Accuracy	N/A	Temp: ± 0.21°C from 0° to 50°C (± 0.38°F from 32° to 122°F)	Temp: ± 0.21°C from 0° to 50°C (± 0.38°F from 32° to 122°F) RH: ± 2.5%	Temp: ± 0.21°C from 0° to 50° C (± 0.38°F from 32° to 122°F) RH: ± 2.5% Analog: ± 1.544 mV + 2%	Analog: ±1.544 mV plus 2% of reading	Temp: ± 0.21°C from 0° to 50°C (± 0.38°F from 32° to 122°F) RH: ± 2.5% Analog: ± 1.544 mV + 2%	Analog: ± 1.544 mV plus 2% of reading	N/A
Resolution	N/A	Temp: 0.02°C @ 25°C (0.04°F @ 77°F)	Temp: 0.02°C @ 25°C (0.04°F @77°F) RH: 0.03%	Temp: 0.02°C @ 25° C (0.04°F @77° F) RH: 0.03% Analog channel: 0.6 mV Pulse Channel: 1 pulse	Analog channel: 0.6 mV	Temp: 0.02°C @ 25°C (0.04°F @77°F) RH: 0.03% Analog channel: 0.6 mV	Analog channel: 0.6 mV Pulse Channel: 1 pulse	N/A
Range	Approx. 100 m (300 ft.) depending on obstructions or interference							
Dimensions	96.5 x 108 x 28 mm (3.8 x 4.25x 1.1 in)							
CE compliant	Yes							

Appendix B. Office walls composition

Office room walls composition: materials, thicknesses, thermal transmittances and surface mass.

Material	Density, ρ [kg/m^3]	Thermal conductivity, λ [W/m K]	Thickness, t [mm]	Thermal resistance, R [m^{2}K/W]
Flooring/ Roofing floor (3th/4th floor)				
Surface resistance (internal)	-	-	-	0.130
Stoneware tiles	2300	1.300	10	0.008
Alveolar Concrete screed	450	0.580	100	0.172
Reinforced concrete and hollow tiles mixed floor	2200	-	300	0.300
Plastering	1200	0.700	15	0.021
Surface resistance (external)	-	-	-	0.130
Tot.			425	0.761
Thermal transmittance U (W/m^{2}K)				1.314
Corridor ceiling				
Surface resistance (internal)	-	-	-	0.130
Internal plasterboard	900	0.250	25	0.100
Air space	-	-	400	0.426
Reinforced concrete and hollow tiles mixed floor	2200	-	300	0.300
Alveolar Concrete screed	450	0.580	100	0.172
Stoneware tiles	2300	1.300	10	0.008
Surface resistance (external)	-	-	-	0.130
Tot.			835	1.266
Thermal transmittance U (W/m^{2}K)				0.790
East/West Walls				
Surface resistance (internal)	-	-	-	0.130
Internal plasterboard	700	0.210	25	0.119
Fiberglass	16	0.046	50	1.087
External plasterboard	700	0.210	25	0.119
Surface resistance (external)	-	-	-	0.130
Tot.			100	1.585
Thermal transmittance U (W/m^{2}K)				0.631
Surface mass (kg/m^2)				35.8
North Wall				
Surface resistance (internal)	-	-	-	0.130
Plastering	1400	0.700	10	0.014
Hollow bricks	800	0.400	80	0.200
Plastering	1400	0.700	10	0.014

Surface resistance (external)	-	-	-	0.130
Tot.			100	0.488
Thermal transmittance U (W/m^2K)				2.049
Surface mass (kg/m^2)				64
South Horizontal Shielded Band				
Surface resistance (internal)	-	-	-	0.130
Steel sheet	7800	52	6	0.000
Polyurethane foam	70	0.050	55	1.100
Hardened reflective glass	2500	1.000	6	0.006
Surface resistance (external)	-	-	-	0.040
Tot.			67	1.276
Thermal transmittance U (W/m^2K)				0.784
Surface mass (kg/m^2)				65.65
South Glazing				
Surface resistance (internal)	-	-	-	0.130
Stratified inner glass	2500	1.000	7	0.007
Air space	-	-	12	0.173
Hardened reflective glass	2500	1.000	6	0.006
Surface resistance (external)	-	-	-	0.040
Tot.			25	0.356
Thermal transmittance U_g (W/m^2K)				2.809
Surface mass glass (kg/m^2)				32.5
Surface mass frame (kg/m^2)				270

Appendix C. FCU technical data

FCU technical data

Model	**Production house**	**Motor**	**Fan Power [W]**	**Number of fans**
ESTRO 1.2 mod. 2	Galletti Air Conditioning	3-speed, electric	Centrifugal, airfoil shaped blades 330	1
SPEED	**Global cooling power[1] [kW]**	**Sensible cooling power[1] [kW]**	**Water flow[1] [l/h]**	**Pressure drop[1] [kPa]**
Min speed	1,04	0,79	179	7
Med speed	1,24	0,97	213	9
Max speed	1,54	1,20	264	13
SPEED	**Heating power[2] [kW]**	**Pressure drop[2] [kPa]**	**Heating power[3] [kW]**	**Water flow[3] [l/h]**
Min speed	1,4	6	2,5	216
Med speed	1,7	8	3,0	263
Max speed	2,1	11	3,7	325
SPEED	**Pressure drop[3] [kPa]**	**Air flow [m^3/h]**	**Power consumption [W]**	
Min speed	7	178	21	
Med speed	10	233	28	
Max speed	15	319	37	

[1] Water temperature 7/12°C, air temperature 27°C dry-bulb, 19°C wet-bulb (47% RH).
[2] Water temperature 50°C, same water flow as in cooling, air inlet temperature 20°C.
[3] Water temperature 70/60°C, air temperature 20°C.

Appendix D. Indirect measurements

In this research work, it was necessary to refer to the indirect calculation for the two variables relating to the ventilation power and the conditioning power linked to the AHU and FCU inside the test room.

Calculation of the conditioning power of the FCU.

From the technical documentation obtained at the technical office of Ancona, it was not possible to obtain data on the conditioning power of the fan coil installed in the offices, nor at least the factory model.

In absence of these technical data, a calculation procedure based on on-site measurements, i.e. inside the test room, was necessary.

On July 28, 2016, a test was carried out to measure the velocity of the air supplied by the FCU that would be used to calculate the flow rate of the intake air inside the room.

The measurements were made with the help of an anemometer that was positioned alternately in three sections of the FCU air outlet section: left, right and centre.

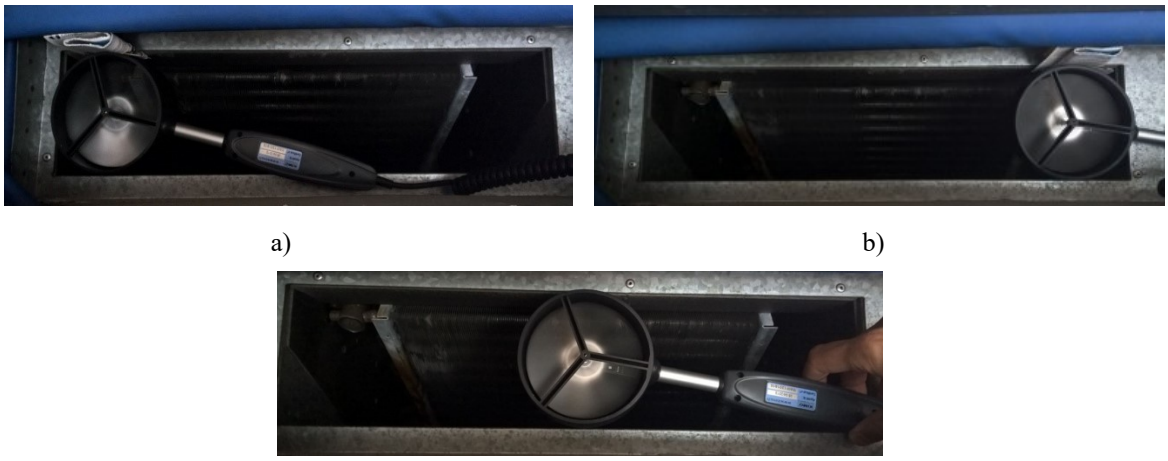

a) b)

c)

Fig. D.1 Anemometer positioned on the three sections of the FCU to detect the velocity of the airflow: a) on the left, b) on the right and c) in the centre.

The fan setting provides three different operation at 3 different level of velocity: 1, 2 and 3 that are controlled by a thermostat, which can be manually managed depending on the need of conditioning.

For each section of the battery and for each velocity level, the air velocity was recorded with a 5-second interval of acquisition. In order to better understand the measurement procedure, the measured values with the acquisition time are summarized below.

Table D.1: FCU velocities recorded during the measurement test.

CENTRE		
		ORARIO
Velocity 1	v= 1,35 m/s	11:54
Velocity 2	v=1,90 m/s	11:56
Velocità 3	v=2,5 m/s	11:58
LEFT		
Velocity 1	v= 1,17 m/s	12:08
Velocity 2	v=1,55 m/s	12:06
Velocity 3	v=2,0 m/s	12:03
RIGHT		
Velocity 1	v= 1,6 m/s	12:10
Velocity 2	v=2,24 m/s	12:18
Velocity 3	v=2,92 m/s	12:20

In order to calculate the flow rate, it was necessary to calculate, in addition to the velocity, the area of the outlet-air section. Since velocities were calculated in 3 different positions of the supply-air section, the area was divided into 3 parts, considering the centre wide section being twice as large as the other sections (Fig. D.2). As the section is 46 cm long, the side parts (A1) measure both 14 cm, while the centre part (A2) measures 18 cm.

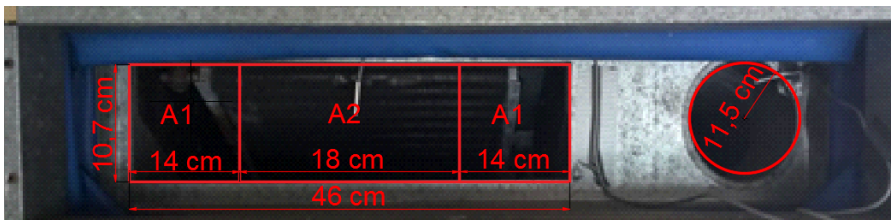

Fig. D.2: Subdivision of the outlet-air section for the calculation of the flow rate.

Then, the air flow rate was calculated for each measured velocity by multiplying it for the corresponding section of area and the average air flow rate was calculated as the sum of the individual flow rates for each velocity (Table D.2).

In conclusion, for each fan speed, a mean air flow was obtained, the values were compared with the airflow values in a technical manual of a company that constructs fan coils. In fact, since it was not possible to find information about the FCU installed in the building, it was chosen technical data

from a leading Italian company, that is Galletti SpA. From the technical data sheets of the various fan coil models, it has been identified the Model 5, having air flow rates approximately equal to those previously estimated.

ESTRO 1.2			4						4M						5					
Motore / velocità	3x			min	med	Max				min	med	Max				min	med	Max		
	6x	n°	1	2	3	4	5	6	1	2	3	4	5	6	1	2	3	4	5	6
Resa raffreddamento totale (1)		kW	1,40	1,36	1,70	1,96	2,33	2,62	1,41	1,50	1,85	2,24	2,42	2,76	1,40	1,60	2,03	2,42	2,74	2,90
Resa raffreddamento sensibile (1)		kW	1,00	1,00	1,24	1,42	1,69	1,90	1,00	1,06	1,32	1,60	1,74	1,99	1,04	1,18	1,57	1,88	2,23	2,39
Portata acqua (1)		l/h	240	234	292	337	399	449	242	258	317	384	415	473	239	275	348	415	470	498
Perdita di carico (1)		kPa	7	6	9	12	16	20	9	10	14	20	23	28	6	8	12	16	20	22
Resa riscaldamento (2)		kW	1,7	1,8	2,2	2,6	2,8	3,1	1,7	1,8	2,3	2,7	3,0	3,4	1,9	2,1	2,7	3,2	3,6	3,8
Perdita di carico (2)		kPa	5	5	8	10	13	20	7	8	11	16	18	23	5	6	10	13	16	18
Resa riscaldamento (3)		kW	2,9	3,0	3,7	4,4	4,7	5,2	2,9	3,1	3,8	4,6	5,0	5,7	3,2	3,5	4,6	5,5	6,2	6,5
Portata acqua (3)		l/h	252	267	322	382	409	456	254	270	333	405	439	500	276	308	401	480	541	574
Perdita di carico (3)		kPa	5	6	8	11	13	15	7	8	12	16	19	24	6	7	12	16	20	22
Portata aria		m3/h	196	211	271	344	380	450	196	211	271	344	380	450	211	241	341	442	528	579

Fig. D.3: Model the fan coil approximating the air flow rates estimated.

At first, in the estimation phase, these values were considered and inserted into the dataset under the column of the fan coil power (Pc). Subsequently, introducing this data into the detailed model of the building, it was noticed that these nominal values could not really describe the true functioning of the fan coil: in order to calibrate the model in Dymola, it was necessary to reduce the fan power up to about 60%.

The direct consequence was the choice of another model of fan coil which had the efficiency corresponding to the real operating, thus the choice was Model 2, with the reference values shown below.

ESTRO 1.2			1						2			3						
Motore / velocità	3x		min	med	Max				min	med	Max		min	med	Max			
	6x	n°	1	2	3	4	5	6	non disponibile			1	2	3	4	5	6	
Resa raffreddamento totale (1)		kW	0,77	0,92	1,15	1,33	1,41	1,54	1,04	1,24	1,54	1,20	1,26	1,52	1,74	1,91	2,12	
Resa raffreddamento sensibile (1)		kW	0,59	0,70	0,87	0,98	1,03	1,11	0,79	0,97	1,20	0,90	0,95	1,14	1,30	1,43	1,58	
Portata acqua (1)		l/h	132	158	197	228	242	264	179	213	264	206	216	261	298	328	364	
Perdita di carico (1)		kPa	4	5	7	10	11	12	7	9	13	8	8	11	14	17	20	
Resa riscaldamento (2)		kW	1,1	1,3	1,6	1,9	2,0	2,2	1,4	1,7	2,1	1,6	1,7	2,0	2,2	2,6	2,8	
Perdita di carico (2)		kPa	3	4	6	8	9,00	10	6	8	11	6	7	9	12	14	17	
Resa riscaldamento (3)		kW	1,9	2,3	2,7	3,3	3,5	3,8	2,5	3,0	3,7	2,8	2,9	3,5	3,7	4,4	4,9	
Portata acqua (3)		l/h	171	199	235	286	303	331	216	263	325	242	257	307	329	409	429	
Perdita di carico (3)		kPa	4	6	8	11	12	14	7	10	15	8	8	11	13	13	21	
Portata aria		m3/h	149	189	231	342	380	450	178	233	319	196	211	271	344	380	450	

Fig. D.4: Model of the fan coil used for the reference values of power at each velocity.

Therefore, the FCU power for the summer and the winter campaign was calculated as follows:

$$Ph(or\ Pc) = \rho * \lambda * Veff * A * (Tf - yTi)$$

Where ρ is the air density [kg/mc], based on the mean value of RH and temperature (*Tf)* for the period considered; λ is the specific heat of the air, settled to 1.0053 kJ/kg°C; *Veff* is the effective velocity calculated for each discrete velocity of the FCU by means of values in Table D.2; *A* is the area of the

outlet air section, equal to 0.05 mq; $(Tf - yTi)$ represents the thermal gradient, which is the difference between the supply air temperature and internal temperature of the test room, both measured by the sensors network.

Table D.2: Calculation of air flow rates for each velocity of the FCU.

Position	Velocity [m/s]	Air Section [mq]	Air flow rate [m³/s]	Mean Air flow rate [m³/s]	Mean air velocity [m/s]
V1 centre	1.35	0.021	0.028	0.072	1.37
V1 left	1.17	0.016	0.019		
V1 right	1.60	0.016	0.025		
V2 centre	1.90	0.021	0.039	0.099	1.9
V2 left	1.55	0.016	0.025		
V2 right	2.24	0.016	0.036		
V3 centre	2.50	0.021	0.051	0.13	2.48
V3 left	2.00	0.016	0.032		
V3 right	2.92	0.016	0.047		

Calculation of the ventilation power of the AHU

The calculation was carried out with the same procedure described above, the air velocity for the AHU section was considered fixed throughout the dataset period and equal to 1.9 m / s. This value was recorded by a measurement (Fig. D.5), carried out during the same test of July 28, 2016.

Fig. D.5 Anemometer positioning for the measurement of air velocity.

Appendix E. CTSM-R guide

INTRODUCTION

This document is an example of using the R package CTSM-R for grey-box modelling of the thermal dynamics of a building. A two-state model is implemented and the results are provided. The data and the model are taken from the case study of my Doctoral Thesis, i.e. the office building of the Medicine Faculty in Ancona. Data collected from an experimental campaign are used to derive the model of the test-room, an office situated on the 3rd floor of the building.

1. Initiate

To start the modelling, a few initialization steps are carried out. Note here that the working directory needs to be to the path where the files are located on the computer:

```
## @knitr init
## Init by deleting all variables and functions
rm(list=ls())

## Set the working directory
setwd(".")

## Use the CTSM-R package, note that first the package must be installed, see the Installation section in the CTSM-R Userguide
library(ctsmr)

## List with global parameters
prm <- list()
## Number of threads used by CTSM-R for the estimation computations
prm$threads <- 1
```

Then source some functions defined in the "functions" folder:

```
## @knitr sourceFunctions,cache=FALSE
## Source the scripts with functions in the "functions" folder. Just a neat way of arranging helping functions in R
files <- dir("C:/Users/.../functions", full.names=TRUE)
for(i in 1:length(files)) source(files[i])
```

Remember to insert the path where is located the folder on the pc!

2. Read the data

The data used in this example was measured in a university facility. It is a building of the nineties characterized by two longitudinal macro volumes, which define the main facades and, consequently, the main north-south orientation of the building. It houses classrooms, offices and other activities linked to the Medicine Faculty. The objective of our study is a south-facing office on the 3rd floor with internal dimension of 3.52 x 5.46 x 3.00 m (W x D x H). The glazed façade system faces south with a dimension of 3.50 x 1.67 m^2. The time series consist of five-minutes averaged values of:

- *yTi* the indoor temperature measured (°C);
- *Pc* the cooling input power of the fan coil (kW);
- *Pr* the input power of the AHU for the test-room (kW);

- *Tc* the hallway temperature (°C);
- *Ta* the ambient temperature (°C);
- *Ps* the global radiation (kW/m^2).

The climate variables were measured with a climate station right next to the building. The data is located in the file "dataset 03-07_10-07_5min.csv" which is read into a data.frame by:

```
## @knitr readData
## Read the data into a data.frame
X <- read.csv("C:/Users/.../dataset 03-07_10-07_5min.csv",sep=";",header=TRUE)
## X$t is now hours since start of the experiment. Create a column in the POSIXct format for plotting etc.
X$timedate <- asP("2016-07-03 00:00:00") + X$t * 3600
```

Plot the time series. Two helping functions (found in the "functions" folder) are used for setting up the plot of the data in Fig. 1:

```
## Plot the time series (see "functions/plotTSBeg.R" to see the plot setup function)
plotTSBeg(6)
gridSeq <- seq(asP("2016-07-03"),by="days",len=365)
##
plot(X$timedate,X$yTi,type="n",xlab="",ylab="yTi (°C)",yaxt="n") # Prepare plot
axis(2,pretty(scalerange(X$yTi,0.2)))      # y axis
abline(v=gridSeq,h=0,col="grey85",lty=3)   # Grid
lines(X$timedate,X$yTi)                    # draw lines
##
plot(X$timedate,X$Ps,type="n",xlab="",ylab="Ps (kW/mq)",yaxt="n")
axis(2,pretty(scalerange(X$Ps,0.2)))
abline(v=gridSeq,h=0,col="grey85",lty=3)
lines(X$timedate,X$Ps)
##
plot(X$timedate,X$Pc,type="n",xlab="",ylab="Pc (kW)",yaxt="n")
axis(2,pretty(scalerange(X$Pc,0.2)))
abline(v=gridSeq,h=0,col="grey85",lty=3)
lines(X$timedate,X$Pc)
##
plot(X$timedate,X$Pr,type="n",xlab="",ylab="Pr (kW)",yaxt="n")
axis(2,pretty(scalerange(X$Pr,0.2)))
abline(v=gridSeq,h=0,col="grey85",lty=3)
lines(X$timedate,X$Pr)
##
plot(X$timedate,X$Ta,type="n",xlab="",ylab="Ta (°C)",yaxt="n")
axis(2,pretty(scalerange(X$Ta,0.2)))
abline(v=gridSeq,h=0,col="grey85",lty=3)
lines(X$timedate,X$Ta)
##
plot(X$timedate,X$Tc,type="n",xlab="",ylab="Tc (°C)",yaxt="n")
axis(2,pretty(scalerange(X$Tc,0.2)))
abline(v=gridSeq,h=0,col="grey85",lty=3)
lines(X$timedate,X$Tc)
##
plotTSXAxis(X$timedate,format="%Y-%m-%d")
```

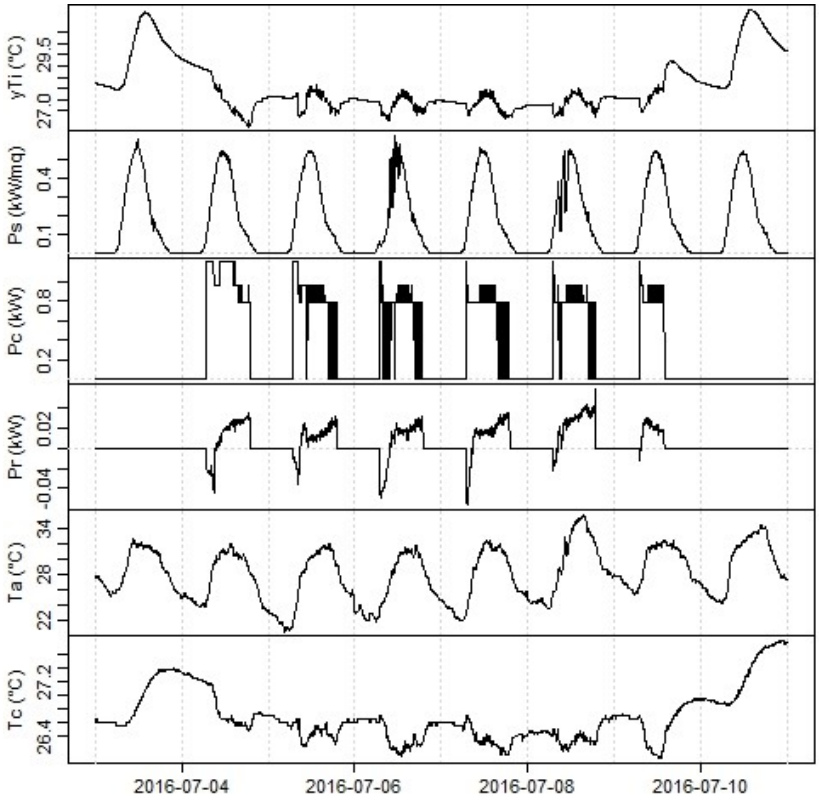

Fig. 1: Plots of the data.

3. The two-state grey-box model of the thermal dynamics of the building

The two-state grey-box model *TiTe* is defined by the following system of differential equations, which is represented by the RC-network in Fig. 2:

$$\boldsymbol{dT_i = \left(\frac{1}{R_{ie}C_i}(T_e - T_i) + \frac{A_w}{C_i}P_s + \frac{1}{C_i}P_c + \frac{1}{C_i}P_r + \frac{1}{C_i}P_f\right)dt + \sigma_i d\omega_i}$$

$$\boldsymbol{dT_e = \frac{1}{R_{ie}C_e}(T_i - T_e)dt + \frac{1}{R_{ea}C_e}\left((KT_a + (1-K)T_c) - T_e\right)dt + \sigma_e d\omega_e}$$

Together with the measurement equation:

$$\boldsymbol{Y_k = T_{ik} + e_k}$$

they are specified in CTSM-R as follows in the script below. First, a model object is generated. Then two-state equations are added and the inputs are defined.

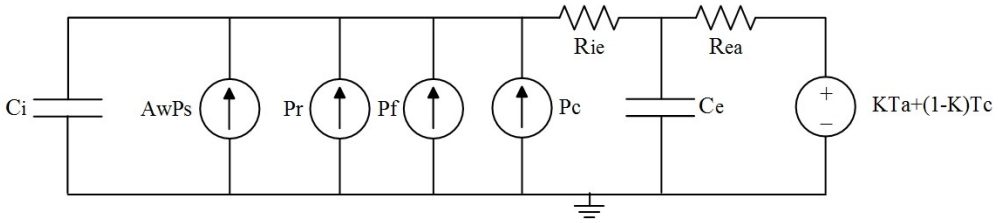

Fig. 2: RC-network equivalent of the two-state model.

Add the two-state system and define inputs:

```
## @knitr TiTeNew,tidy=FALSE
## Generate a new object of class ctsm
model <- ctsm$new()
## Add system equations and thereby also states
model$addSystem(dTi ~ ( 1/(Ci*Rie)*(Te-Ti) + Aw/Ci*Ps - 1/Ci*Pc + 1/Ci*Pr + 1/Ci*Pf)*dt + exp(p11)*dw1)
model$addSystem(dTe ~ ( 1/(Ce*Rie)*(Ti-Te) + 1/(Ce*Rea)*((K*Ta+(1-K)*Tc)-Te))*dt + exp(p22)*dw2)

## Set the names of the inputs
model$addInput(Ta,Ps,Pc,Pr,Tc)
```

Note the following for each equation:

- the deterministic part of the SDE is multiplied with *dt*;
- the stochastic part is multiplied with system noise process *dw1*;
- the variance of the system noise is *exp(p11)*, where *exp()* is the exponential function and *p11* is the parameter which is estimated. Since the variance is strictly positive, but can be very close to zero, it is advised to take the exponential function, in order to get a better numerical resolution
  in the optimization.

Now add the observation equation:

```
## @knitr addObs
## Set the observation equation: Ti is the state, yTi is the measured output
model$addObs(yTi ~ Ti)
## Set the variance of the measurement error
model$setVariance(yTi ~ exp(e11))
```

Set up the initial values of the states and parameters together with bounds for the optimization:

```
## @knitr initialValues,tidy=FALSE

## Set the initial value (for the optimization) of the value
##of the state at the starting time point
model$setParameter(  Ti = c(init=22   ,lb=0    ,ub=200) )
model$setParameter(  Te = c(init=20    ,lb=0    ,ub=200) )

## Set the initial value of the parameters for the optimization
model$setParameter(  Ci = c(init=0.5    ,lb=1E-5   ,ub=100))
model$setParameter(  Ce = c(init=0.5     ,lb=1E-5   ,ub=100))
model$setParameter( Rie = c(init=1    ,lb=1E-5   ,ub=100))
model$setParameter( Rea = c(init=1    ,lb=1E-5   ,ub=100))
model$setParameter( Aw = c(init=1    ,lb=1E-5   ,ub=100))
model$setParameter( p11 = c(init=1    ,lb=-50    ,ub=10) )
model$setParameter( p22 = c(init=1    ,lb=-50    ,ub=50) )
model$setParameter( e11 = c(init=-1   ,lb=-50    ,ub=50) )
model$setParameter( Pf = c(init=10     ,lb=0   ,ub=100))
model$setParameter( K = c(init=0.5     ,lb=0   ,ub=2))
```

Finally, run the parameter estimation and keep the results in “fit”:

```
## @knitr estimate,results="hide"
## Run the parameter optimization
fit <- model$estimate(data = X, threads = prm$threads)
```

4. Model validation

Evaluate the result of the parameter estimation for the two-state model. First an extended summary of the fit is printed with:

```
## @knitr summaryfit
print(summary(fit,extended=TRUE))
## See the summary of the estimation
```

CTSM-R model estimated:

```
Coefficients:
       Estimate  Std. Error     t value    Pr(>|t|)     dF/dPar dPen/dPar
Ti0  2.8250e+01  5.0258e-02  5.6210e+02  0.0000e+00 -1.6457e-04         0
Te0  2.7324e+01  3.0684e-01  8.9051e+01  0.0000e+00  9.7000e-06         0
Aw   1.9978e+00  6.7750e-02  2.9488e+01  0.0000e+00 -4.2711e-06         0
Ce   4.0914e+00  1.4803e+00  2.7639e+00  5.7573e-03  2.8849e-06         0
Ci   8.6999e-01  5.1081e-02  1.7032e+01  0.0000e+00 -5.3730e-07         0
e11 -7.1820e+00  1.2505e-01 -5.7435e+01  0.0000e+00  1.4062e-05         0
K    3.8102e-02  3.1021e-02  1.2283e+00  2.1947e-01  5.9971e-06         0
p11 -1.7811e+00  3.5366e-02 -5.0363e+01  0.0000e+00  6.9004e-06         0
p22 -1.0365e+01  2.9508e+00 -3.5125e+00  4.5262e-04  1.7725e-05         0
Pf   2.1363e-01  3.3657e-02  6.3472e+00  2.6478e-10  1.6811e-06         0
Rea  2.1345e+00  6.9101e-01  3.0889e+00  2.0331e-03 -6.9828e-06         0
Rie  3.3185e+00  3.7255e-01  8.9076e+00  0.0000e+00 -2.4571e-06         0

Correlation of coefficients:
    Ti0   Te0   Aw    Ce    Ci    e11   K     p11   p22   Pf    Rea
Te0 -0.08
Aw  -0.01  0.18
Ce   0.01 -0.15 -0.31
Ci  -0.01 -0.14  0.05  0.48
e11 -0.08 -0.12  0.00  0.23  0.23
K    0.00  0.13 -0.07  0.45  0.12 -0.01
p11  0.02  0.14  0.05 -0.28 -0.29 -0.73 -0.02
p22 -0.02 -0.03 -0.06  0.54  0.24  0.10  0.85 -0.13
Pf   0.00 -0.22 -0.02 -0.33 -0.09 -0.01 -0.39  0.04  0.03
Rea  0.01  0.24 -0.11  0.03 -0.15 -0.09  0.16  0.08 -0.35 -0.82
Rie  0.00 -0.31 -0.45  0.80  0.44  0.26  0.21 -0.31  0.29 -0.33  0.01
```

Then, the following **four important points are checked**:

- The p-value of the t-tests (i.e. $Pr(>|t|)$) should be below 0.05 for all parameters; if this value is not low, this can be an indication that the model is over-parametrized.
- The derivative of the objective function with respect to each parameter (i.e. $dF/dPar$) should be close to zero; if this value is not close to zero, the solution found may not be the true optimum.
- The derivative of the penalty function with respect to each parameter (i.e. $dPen/dPar$) should not be significant compared to $dF/dPar$); if this happens, the particular initial state or parameter may be close to one of its limits.
- The Correlation Matrix should not have any off-diagonal values close to -1 or 1; otherwise, it is an indication that the model is over-parametrized.

Moreover, the one-step ahead predictions and residuals are calculated, both for the one-step prediction and for the simulation:

```
## @knitr n-StepPred & simulation
## Calculate the one-step predictions of the state (i.e. the residuals)
tmp <- predict(fit, n.ahead = 1)[[1]]
## Calculate the residuals and put them with the data in a data.frame X
X$residuals1 <- X$yTi - tmp$output$pred
X$yTiHat <- tmp$output$pred
Sim <- simulate(fit)[[1]]
X$residuals2 <- X$yTi - Sim$output$sim
```

and the auto-correlation function, the periodogram and the cumulated periodogram are plotted (Fig. 3):

```
## @knitr residualsACF, fig.height=3
## Plot the auto-correlation function and cumulated periodogram in a new window
par(mfrow=c(3,1), mar=c(3, 3, 3, 3), cex=0.8)
## The blue lines indicates the 95 confidence interval, meaning that if it is
##  white noise, then approximately 1 out of 20 lag correlations will be slightly outside
acf(X$residuals1, lag.max=6*12, main="Residuals ACF", xlab="lag", ylab="acf")
## The periodogram is the estimated energy spectrum in the signal
spec.pgram(X$residuals1, main="Raw periodogram", xlab=("frequency"), ylab=("spectrum"))
## The cumulated periodogram
cpgram(X$residuals1, main = "Cumulated periodogram")
```

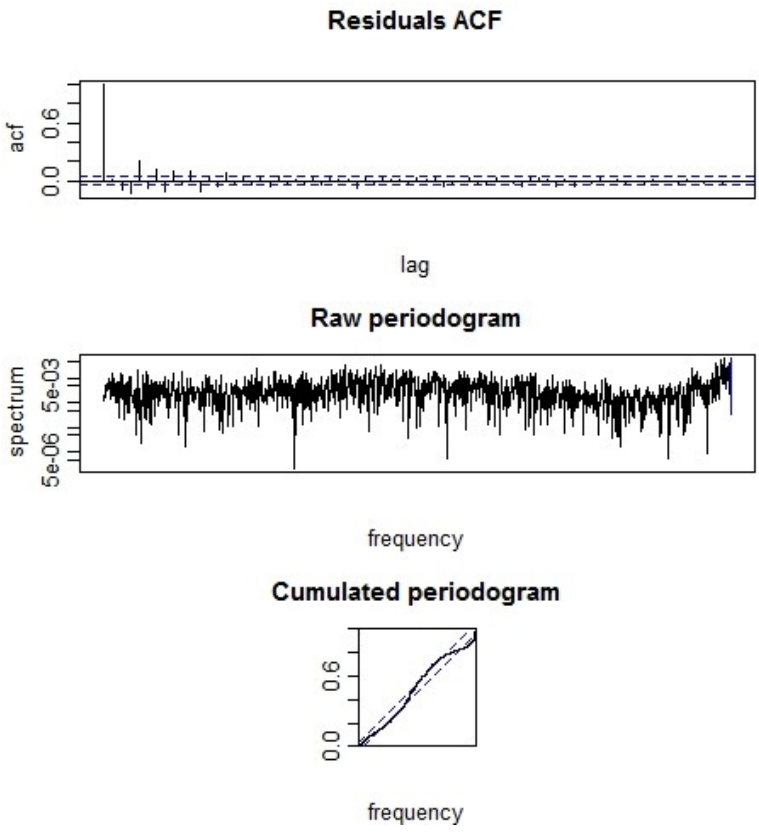

Fig. 3: Plots of residuals and periodograms.

Clearly, if the residuals are not white noise, the model lacks in the description of some dynamics of the physical system.

At the end, time series plots of the residuals and the inputs are plotted (Fig.4) and RMSE values for one-step prediction and simulation are calculated:

```
## @knitr residualsplot
## Plot the time series (see "functions/plotTSBeg.R" to see the plot setup function)
plotTSBeg(6)
gridSeq <- seq(asP("2016-07-03"),by="days",len=365)
##
plot(X$timedate,X$residuals1[,1],xlab="",ylab="ResPred (°C)",type="n")
abline(v=gridSeq,h=0,col="grey92")
lines(X$timedate,X$residuals1[,1])
##
plot(X$timedate,X$residuals2[,1],xlab="",ylab="ResSim (°C)",type="n")
abline(v=gridSeq,h=0,col="grey92")
lines(X$timedate,X$residuals2[,1])
##
plot(X$timedate,X$yTi,type="n",xlab="",ylab="yTi, yTiHat, yTiSim(°C)")
abline(v=gridSeq,h=0,col="grey85",lty=3)
lines(X$timedate,X$yTi,col=1)
lines(X$timedate,X$yTiHat[,1],col=2)
lines(X$timedate,Sim$output$sim[,1],col="blue" ,lty=2)
legend("bottomright",c("Measured","Predicted","Simulated"),
lty=1,col=c(1,2,"blue") ,bg="grey95", ncol=3,y.intersp=0,x.intersp=0.85, cex=1)
##
plot(X$timedate,X$Pc,type="n",xlab="",ylab="Pc (kW)")
abline(v=gridSeq,h=0,col="grey85",lty=3)
lines(X$timedate,X$Pc)
##
plot(X$timedate,X$Ta,type="n",xlab="",ylab="Ta (°C)")
abline(v=gridSeq,h=0,col="grey85",lty=3)
lines(X$timedate,X$Ta)
##
plot(X$timedate,X$Ps,type="n",xlab="",ylab="Ps (kW(mq)")
abline(v=gridSeq,h=0,col="grey85",lty=3)
lines(X$timedate,X$Ps)
##
plotTSXAxis(X$timedate,format="%Y-%m-%d")
```

RMSE VALUE FOR ONE-STEP PREDICTION:

```
> sqrt(mean((X$residuals1[,1])^2))
[1] 0.06542987
```

RMSE VALUE IN SIMULATION:

```
> sqrt(mean((X$residuals2[,1])^2))
[1] 0.2272381
```

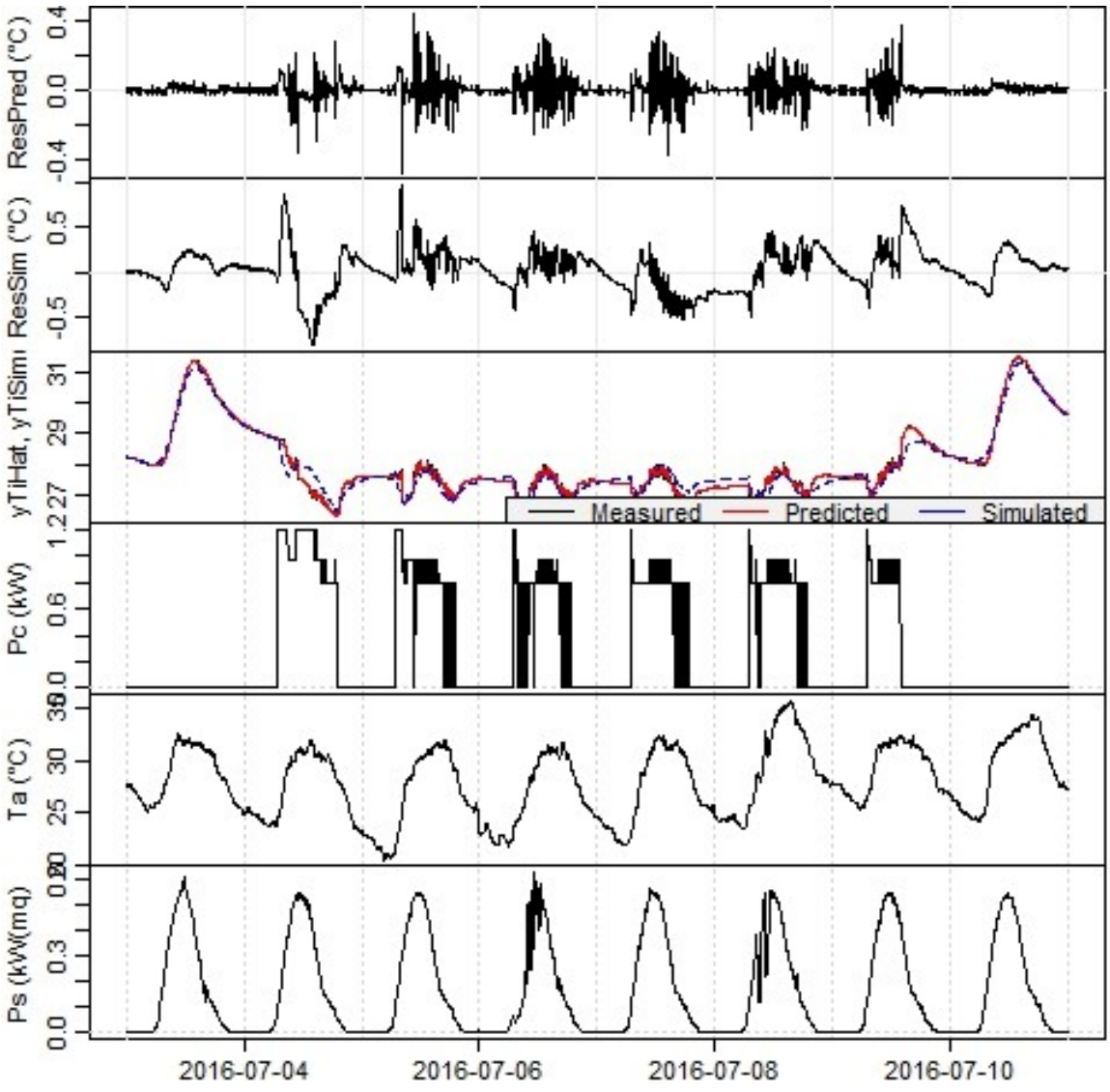

Fig. 4: Final plots.

Appendix F. Sensors network general data

SENSOR NETWORK CONFIGURATION							
Measure	**Sensor type**	**Model**	**Acquisition system**	**Rate**	**Position**	**Range**	**Accuracy**
INDOOR COMFORT MONITORING STATION							
Air temp. and velocity	Draught probe	54T33	ComfortSense main frame	5 min	Centre of the room, 2,5m from the window - H 0,10m Centre of the room, 2,5m from the window - H 0,60m Centre of the room, 2,5m from the window - H 1,1m	0.05-5 m/s, indicates up to 10 m/s	0-1 m/s: ± 2% OR* ± 0.02 m/s 1-5 m/s: ± 5% OR* 5-10 m/s: ±10% OR*
Relative Humidity	Capacitive Hygrometer	54T37	ComfortSense main frame	5 min	Centre of the room, 2,5m from the window - H 1,9m	0-100% RH	+2% RH (0-10°C); +1.5% RH (10-30°C); +2% RH (30-45°C)
Operative temperature	Ellipsoidal-thermometer	54T38	ComfortSense main frame	5 min	Centre of the room, 2,5m from the window - H 0,6m	0-45°C	±0.5 K (0-10°C); ±0.2 K (10-40°C); ±0.5 K (40-45°C)
Air temp.	Thermo hygrometer	ZW-003	Hobo ZW Series Wireless Network	1 min	Centre of the room, 2,5m from the window - H 1,1m	-20°C÷+70°C	±0.21 °C (0-50°C)
Air temp.	Thermo hygrometer	ZW-003	Hobo ZW Series Wireless Network	1 min	Corridor - H 2,5 m	-20°C÷+70°C	±0.21 °C (0-50°C)
Air temp.	Thermo hygrometer	ZW-003	Hobo ZW Series Wireless Network	1 min	Eastern adjacent office - H 2,5 m	-20°C÷+70°C	±0.21 °C (0-50°C)
Air temp.	Thermo hygrometer	ZW-003	Hobo ZW Series Wireless Network	1 min	Western adjacent office - H 2,5 m	-20°C÷+70°C	±0.21 °C (0-50°C)
FANCOIL MONITORING STATION							
External air temp.	Thermo hygrometer	ZW-007	Hobo ZW Series Wireless Network	1 min	Fancoil outlet - H 2,8 m	-20°C÷+70°C	±0.21 °C (0-50°C)
External air temp.	Thermo hygrometer	ZW-007	Hobo ZW Series Wireless Network	1 min	AHU outlet - H 2,8 m	-20°C÷+70°C	±0.21 °C (0-50°C)
Air velocity	Thermo-anemometer	VT 200	Probe+Data Logger	1 min	Fancoil outlet/AHU outlet - H 2,8 m	0,25÷35 m/s	±3% of reading ±0,1m/s (0,25÷3 m/s), ±1% of reading ±0,3m/s (3,1÷35 m/s)
GLAZED FAÇADE MONITORING STATION							
Surface temp.	Platinum resistor	PT100	NI-9217	5 min	Center of the leftmost glazed module - H 1,40 m	-40°C÷+80°C	0,05°C

Surface temp.	Platinum resistor	PT100	NI-9217	5 min	Center of the central glazed module - H 1,40 m	-40°C÷+80°C	0,05°C
Surface temp.	Platinum resistor	PT100	NI-9219	5 min	Inter-modules frame - H 1,5 m	-40°C÷+80°C	0,05°C
Surface temp.	Platinum resistor	PT100	NI-9219	5 min	Floor frame - H 0,03 m	-40°C÷+80°C	0,05°C
Surface temp.	Platinum resistor	HFP01	NI-9219	5 min	Center of the leftmost horizontal shielded band - H 0,7 m	-40°C÷+80°C	0,05°C
Thermal flow	Platinum resistor	HFP01	NI-9219	5 min	Center of the central horizontal shielded band - H 0,7 m	-2000to +2000W/m^2	+5/-5%

ACQUISITION SYSTEMS SPECS

Model	Production house	Analogic Channels	Digital Channels	Acquisition rating	PC Connection
E-Log (ELO305)	LSI Lastem	8 differential, 16 single-ended	4	5 minutes	RS232
ComfortSense main frame	LSI Lastem	Up to 16 input channels and 2 output channels with build in A/D converter		5 minutes	Usb
NI 9217	National Instruments	16		5 minutes	Usb
NI 9219	National Instruments	12		5 minutes	Usb
NI 9401	National Instruments		8	5 minutes	Usb
Hobo ZW-RCVR	Onset Computer Corporation			1 minute	Usb

Appendix G. MATLAB code for WUforecast subVI

1st File implemented

"wfr.m":

Contents

- intialisation
- get current condition and forecast


```
function [Tac,Taf,Psc,Psf,status] = wfr(p,Ts)
% Provides the weather condition and forecast vectors for temperature and
% solar radiation. When network connection fails, it retruns status=0 and
% uses last available predictions to provide condition and forecast.
%
% [Tac,Taf,Psc,Psf,status] = wfr(p,Ts)
%
% status = 1 if network connetcion works, 0 otherwise
```

intialisation

```
persistent Taf_last Psf_last T_last;
if isempty(T_last), T_last=clock; end
[c, f]=wuforecast('LIPY');
```

get current condition and forecast

```
if (~isempty(c) && ~isempty(f))
    [fr]=wuforecastresample(c, f, Ts);
    Tac=fr(1,1).temperature;
    Psc=fr(1,1).sun.GHI;
    Taf=zeros(p+1,1);
    Psf=zeros(p+1,1);
    for i=1:p+1
        Taf(i)=fr(1,i).temperature;
        Psf(i)=fr(1,i).sun.GHI;
    end
    status=1; % says that internet works
    % store values for the net iteration
    Taf_last=Taf;
    Psf_last=Psf;
    T_last=clock;
else
    if (~isempty(Taf_last) && ~isempty(Psf_last))
        % when time elapsed overpass sampling interval, previous prediciton
        % is shifted on step ahead
        et=etime(clock, T_last);
        es=floor(et/Ts); % number of sampling steps elapsed
        Tac=Taf_last(es+1);
        Psc=Psf_last(es+1);
        Taf=[Taf_last(es+1:end); Taf_last(end)*ones(es,1)];
```

```
        Psf=[Psf_last(es+1:end); Psf_last(end)*ones(es,1)];
    else
        Tac=[];
        Psc=[];
        Taf=[];
        Psf=[];
    end
    status=0; % says that internet doesn't work
end

return
```

2nd File implemented

"wuforecast.m":

Contents

- GET WEATHER DATA
- Export raw data
- Export structured data
- Add missing solar radiation data to current observation and forecasts
- INIT
- RHO = 1 - 0.0335*sin(2 * pi * (DayOfYear - 94)/365)


```
function [current, forecast, raw]=wuforecast(location)
```

GET WEATHER DATA

NB: the following code is related to DICEA account at wunderground.com ! The number of allowed queries is limited to 500calls per day and 10 calls per minute. Do not exceed the number of allowed queries!!! Do not make unauthorized use of this account!!!

```
% Get current condition data from web service
%fullURL =
['http://api.wunderground.com/api/1ae15a859280b1f1/hourly/conditions/q/' location
'.json'];
fullURL = ['http://api.wunderground.com/api/1770387007f54d92/conditions/q/'
location '.json'];
isValid=false;
Nreq=1;
while isValid==false && Nreq<=3,
    [json,netStatus]=urlread(fullURL,'Timeout',10);
    if netStatus==0,
        current=[];
        forecast=[];
        raw=[];
        return;
    end
    rawCurrent = parse_json(json);
    if isfield(rawCurrent{1},'current_observation'),
        isValid=true;
```

```
    else isValid=false;
    end
    Nreq=Nreq+1;
end
if isValid==false,
    current=[];
    forecast=[];
    raw=[];
    return
end

% Get forecast data from web service
fullURL = ['http://api.wunderground.com/api/1770387007f54d92/hourly/q/' location
'.json'];
isValid=false;
Nreq=1;
while isValid==false && Nreq<=3,
    [json,netStatus]=urlread(fullURL,'Timeout',10);
    if netStatus==0,
        current=[];
        forecast=[];
        raw=[];
        return;
    end
    rawForecast = parse_json(json);
    if isfield(rawForecast{1},'hourly_forecast'),
        isValid=true;
    else isValid=false;
    end
    Nreq=Nreq+1;
end
if isValid==false,
    current=[];
    forecast=[];
    raw=[];
    return
end
```

Export raw data

```
raw.current=rawCurrent{1}.current_observation;


raw.forecast=rawForecast{1}.hourly_forecast;
```

Export structured data

```
% Current condition
rc=raw.current;
dateStr = rc.local_time_rfc822(find(rc.local_time_rfc822==',',1)+1:end-6); %
'Fri, 17 Jun 2016 12:43:22 +0200'
current.time.string =  datestr(dateStr,'yyyy/mm/dd HH:MM:SS'); % converts to
'yyyy/mm/dd HH.MM.SS'
[current.time.year, ...
 current.time.month, ...
 current.time.day, ...
 current.time.hour, ...
 current.time.minute, ...
 current.time.second] = datevec(dateStr); % extract time fields
current.skyCondition = rc.weather; % string
current.temperature = rc.temp_c; % °C
```

```
current.relativeHumidity = str2double(
rc.relative_humidity(1:find(rc.relative_humidity=='%',1)-1) ); % convert textual
percentage to number
current.windDirection = rc.wind_degrees; % degrees
current.windSpeed = rc.wind_kph * 3.6; % converts kph to m/s
current.pressure = str2double(rc.pressure_mb) * 100; % converts from mB to Pa
current.dewpoint = rc.dewpoint_c; % °C
current.sun.GHI = str2double(rc.solarradiation); % GHI. Global irradiation on
horizontal plane at ground level (Wh/m2)
current.precipitation = str2double(rc.precip_1hr_metric); % mm/h
current.icon.url = rc.icon_url; %
 current.icon.icon = rc.icon; %
% location
current.location.stationID = rc.station_id;
 current.location.full = rc.observation_location.full;
 current.location.latitude = str2double(rc.observation_location.latitude);
 current.location.longitude = str2double(rc.observation_location.longitude);
 current.location.elevation =
str2double(rc.observation_location.elevation(1:find(rc.observation_location.eleva
tion==' ',1)-1))*0.3048; % m (converted from feet to meters)

% Forecasts
N = numel(raw.forecast);
% Pre-allocation
forecast(N).time.string = [];
forecast(N).time.year = [];
forecast(N).time.month = [];
forecast(N).time.day = [];
forecast(N).time.hour = [];
forecast(N).time.minute = [];
forecast(N).time.second = [];
forecast(N).skyCondition = [];
forecast(N).temperature = [];
forecast(N).relativeHumidity = [];
forecast(N).windDirection = [];
forecast(N).windSpeed = [];
forecast(N).pressure = [];
forecast(N).dewpoint = [];
forecast(N).sun.GHI = [];
forecast(N).precipitation = [];
forecast(N).icon.url = [];
forecast(N).icon.icon = [];
forecast(N).location = [];
% Forecasts readings
for n=1:N,
    rf=raw.forecast{n};
    dateStr = [rf.FCTTIME.year '/' rf.FCTTIME.mon_padded '/'
rf.FCTTIME.mday_padded ' ' ...
               rf.FCTTIME.hour_padded ':' rf.FCTTIME.min ':' rf.FCTTIME.sec]; %
'dd/mm/yyyy HH:MM:S'
    forecast(n).time.string = [dateStr num2str(zeros(1,2-
length(rf.FCTTIME.sec)))]; % converts to 'yyyy/mm/dd HH.MM.SS'
    [forecast(n).time.year, ...
     forecast(n).time.month, ...
     forecast(n).time.day, ...
     forecast(n).time.hour, ...
     forecast(n).time.minute, ...
     forecast(n).time.second] = datevec(dateStr); % extract time fields
    forecast(n).skyCondition = rf.condition; % string
    forecast(n).temperature = str2double(rf.temp.metric); % °C
    forecast(n).relativeHumidity = str2double(rf.humidity); % percentage
    forecast(n).windDirection = str2double(rf.wdir.degrees); % degrees
    forecast(n).windSpeed = str2double(rf.wspd.metric); % m/s
```

```
    forecast(n).pressure = str2double(rf.mslp.metric) * 100; % converts from mB
to Pa
    forecast(n).dewpoint = str2double(rf.dewpoint.metric); % °C
    forecast(n).sun.GHI = NaN; % GHI. Global irradiation on horizontal plane at
ground level (Wh/m2)
    forecast(n).precipitation = str2double(rf.qpf.metric); % mm/h
(qpf=Quantitative Precipitation Forecasts)
    forecast(n).icon.url = rf.icon_url; %
    forecast(n).icon.icon = rf.icon; %
    forecast(N).location = current.location;
end
```

Add missing solar radiation data to current observation and forecasts

```
current.sun = sunData(current.location, current);


for n=1:N,
    forecast(n).sun = sunData(current.location, forecast(n));
end
function [sun] = sunData(location, wd)
% SUNDATA [sun] = sunData(location, wd)

% shading coefficients computed by correlating condition with hystorical
conditions={'chanceflurries' 'chancerain' 'chancesleet' 'chancesnow'
'chancetstorms' 'clear' 'cloudy' 'flurries' 'fog' 'hazy' 'mostlycloudy'
'mostlysunny' 'partlycloudy' 'partlysunny' 'sleet' 'rain' 'sleet' 'snow' 'sunny'
'tstorms' 'unknown'};
% shading coefficients for corresponding conditions
k =        {1.00             0.33         1.00          0.50         0.64
1.00    0.43     1.00       0.52  0.89   0.43          0.79          0.79
0.43          0.50    0.33   1.00    0.50   1.00    0.64      1.00     };
% % radiation data for Ancona during whole year 2015
% conditions={'clear' 'partlycloudy' 'mostlycloudy' 'rain' 'tstorms' 'hazy' 'fog'
'unknown'};
% k = [1.00 0.79 0.43 0.33 0.64 0.89 0.52 1.00]; % shading coefficients for
corresponding conditions

todayDate = [wd.time.year wd.time.month wd.time.day];
Rad = suncycle(location.latitude, location.longitude, todayDate, 24);
%tomorrowDate = datevec( datenum(todayDate) + 1);
%todayRad = suncycle(location.latitude, location.longitude, todayDate, 24);
%tomorrowRad = suncycle(location.latitude, location.longitude, tomorrowDate, 24);
%Rad=[todayRad tomorrowRad];

sun=wd.sun;
sun.clearSkyGHI = Rad(wd.time.hour+1); % Clear sky GHI. Clear sky global
irradiation on horizontal plane at ground level (Wh/m2)
if isnan(sun.GHI) || isempty(sun.GHI)
    curConditionIndex = ismember(conditions,wd.icon.icon);
    if sum(curConditionIndex)>0
        sun.GHI = sun.clearSkyGHI * k{curConditionIndex};
    else
        sun.GHI = []; % Default value assigned is empty
    end
end


function [r,rs,t,d,z,a] = suncycle(lat,lon,date,n)
```

Appendix H. MATLAB code for MPC simulator

"fminestimate" (function using "fmincon" algorithm for estimation of model parameters):

This function generates estimates starting from random initial conditions, which are different for each iteration with a rough tolerance, at first instance. Then, the estimation is refined acting on the tolerance. This function works better if the upper bounds imposed are not too big. The number of iterations executed is function of the number of parameters involved.

Contents

- Objective function to be minimized
- minimization
- display results
- simulate estimated model
- plot results


```
function [xfinal,xm,xv,r,yy,t]=fminestimate(y,u,Ts,lb,ub)
%FMINESTIMATE estimate parameters of reduced order model that fits the
% provided measures y and u within the provided bounds lb and ub.
%
% [xfinal,mx,vx,r,yy,t]=fminestimate(y,u,Ts,lb,ub)
%
% x = [ Ti0, Te0, Ci, Ce, Rie, Rea, Aw, k  ] with lb<x<ub
% Ts = sampling interval (hours) of provided measures y, u
% u = [Ps Pc Pr Pf Ta Tc]
%
% Example of usage:
%   Ts=1/12;
%   lb=[20 20 0.01 0.01 0.01 0.01 0 0];
%   ub=[35 35 50 50 10 10 10 1];
%   x=fminestimate(yTi,[Ps Pc Pr Pf Ta Tc],Ts,lb,ub);
%
%   sys=genssmodel(x(3),x(4),x(5),x(6),x(7),x(8));
%   [r,v,yy,t]=modelfittest(sys,[x(1) x(2)]',yTi,[Ps Pc Pr Pf Ta Tc],Ts);
```

Objective function to be minimized

```
fun = @(x) (costfunction(x,y,u,Ts));

% [r,v,yy]=modelfittest(sys,[20 20]',y,u,300);
```

minimization

```
disp('%%%%%%%%%%%%%%%%%%%% EVALUATION OF RANDOM CASES %%%%%%%%%%%%%%%%%%%%');
numberOfPars = size(lb,2);
for iter=1:numberOfPars^2
disp(['------------------------- ITERATION N° ' num2str(iter) '------------------
-------']);
    opt=optimset('Display','iter','TolFun',1e-
3,'MaxFunEval',10*numberOfPars^2,'MaxIter',numberOfPars^2,'Algorithm','active-
set');
    % x = fmincon(fun,x0,A,b,Aeq,beq,lb,ub,nonlcon,options)
    x0 = lb + rand(1,numberOfPars).* (ub - lb);
    [x(iter,:) fval(iter)] = fmincon(fun,x0,[],[],[],[],lb,ub,[],opt);
end

% find the best solution
disp('%%%%%%%%%%%%%%%%%%%% REFINEMENT OF BEST SOLUTION %%%%%%%%%%%%%%%%%%%%');
[fmin minIndex]=min(fval);
x0=x(minIndex,:);
xm=mean(x);
xv=var(x);
% Refine estimate
% opt=optimset('Display','iter','TolFun','','MaxFunEval','','MaxIter','');
opt=optimset('Display','iter','TolFun',1e-
6,'MaxFunEval',2000,'MaxIter',2000,'Algorithm','active-set');
[xfinal, fval, exitflag, output] = fmincon(fun,x0,[],[],[],[],lb,ub,[],opt);
xpercent = 100 * sqrt(xv) ./ xfinal;
disp('%%%%%%%%%%%%%%%%%%%%%%%%%%%%%%%%%%%%%%%%%%%%%%%%%%%%%%%%%%%%%%%%%%%%%%%');
```

display results

```
disp('Estimation results:');
disp(['Ti0=' num2str(xfinal(1)) ' - mean=' num2str(xm(1)) ' - std%='
num2str(xpercent(1))]);
disp(['Te0=' num2str(xfinal(2)) ' - mean=' num2str(xm(2)) ' - std%='
num2str(xpercent(2))]);
disp(['Ci=' num2str(xfinal(3)) ' - mean=' num2str(xm(3)) ' - std%='
num2str(xpercent(3))]);
disp(['Ce=' num2str(xfinal(4)) ' - mean=' num2str(xm(4)) ' - std%='
num2str(xpercent(4))]);
disp(['Rie=' num2str(xfinal(5)) ' - mean=' num2str(xm(5)) ' - std%='
num2str(xpercent(5))]);
disp(['Rea=' num2str(xfinal(6)) ' - mean=' num2str(xm(6)) ' - std%='
num2str(xpercent(6))]);
disp(['Aw=' num2str(xfinal(7)) ' - mean=' num2str(xm(7)) ' - std%='
num2str(xpercent(7))]);
disp(['k=' num2str(xfinal(8)) ' - mean=' num2str(xm(8)) ' - std%='
num2str(xpercent(8))]);
```

simulate estimated model

```
sys=genssmodel(xfinal(3),xfinal(4),xfinal(5),xfinal(6),xfinal(7),xfinal(8));

[r,v,yy,t]=modelfittest(sys,[xfinal(1) xfinal(2)]',y,u,Ts);

disp('-----------------');
disp(['rms=' num2str(r)]);
```

plot results

```
figure; hold on;
plot(t,y,'r:');
plot(t,yy,'b');
title('Measured (red) and simulated (blue) output');
xlabel('time (s)');
ylabel('output'),
end



function [J]=costfunction(x,y,u,Ts)
% Define continuous time thermal system
%   genssmodel(  Ci,  Ce, Rie, Rea,  Aw,  k )
sys=genssmodel(x(3),x(4),x(5),x(6),x(7),x(8));
J=modelfittest(sys,[x(1) x(2)]',y,u,Ts);
end
```

“initialize.m” (initialization of the controller):

```
% Sampling interval
Ts=300; % (s)

% MPC tuning parameters
Nw=1;        % default   1
Np=12;       % default  12
Nc=6;        % default   6
wy=10*1e6;   % default  10e6
wu=1;        % default  1
wPc=1;       % default  1
wSL=1e6;     % default 1e6
umin=-1200; % default -1200
umax=0;      % default  2100
SLmin=0;     %
SLmax=1;     %

% load dataset
load('dataset2016_300.mat');
t0=eval(get_param(bdroot(gcb),'StartTime'));

% approx to the closest integer hour
step=Ps.time(2)-Ps.time(1);
t0=round(t0/step)*step;

% get row corresponding to start time
r=find(Ps.time==t0);
nr=size(Ps.time,1);

% remove values before start time
Ps.signals.values = Ps.signals.values(r:nr);
Ps.time = Ps.time(r:nr)-Ps.time(r);
Ta.signals.values=Ta.signals.values(r:nr);
Ta.time=Ta.time(r:nr)-Ta.time(r);
Tref.signals.values=Tref.signals.values(r:nr);
Tref.time=Tref.time(r:nr)-Tref.time(r);
```

“control.m” (computation code of the controller):

```
function [Pc,SL]=control2(wh,yt,xh,par)
% Computes the MPC control sequence with disturbances wh, reference yt and
% estimated state xh. The SS predictive model is internally generated.
%
% u  = control action
% wh = disturbance predictions
% yt = output setpoint
% xh = state estimation (from Kalman Filter)
% par = parameters for the MPC algorithm
%         par.Ts = sampling interval
%         par.Nw = intial window
%         par.Np = prediction horizon
%         par.Nc = control horizon
%         par.wy = output error weights
%         par.wu = control action weights
%         par.umin = lower bound on u
%         par.umax = upper bound on u


persistent u0;

% MPC tuning parameters
Ts=par.Ts;
Nw=par.Nw;
Np=par.Np;
Nc=par.Nc;
wy=par.wy;
wPc=par.wPc;
wSL=par.wSL;
Pcmin=par.umin;
Pcmax=par.umax;
SLmin=par.SLmin;
SLmax=par.SLmax;

% SS dicrete time model
A=par.A;
B=par.B;
C=par.C;
D=par.D;
nd=5; % number of disturbance variables (assumed to be the last ones in the input
vector)

% Creation of the discrete-time dynamic model for the system
plant = ss(A,B,C,D,Ts);

% Check if integral action is used, then trasform model in the integral form
% TODO:
% ......................................

% Setup optimization problem
n=size(plant.a,1); % number of state variables
m=size(plant.b,2)-nd+1; % number of input variables
p=size(plant.c,1); % number of output variables
Q=wy*eye(p);
R=[wPc 0; 0 wSL];
umin=repmat([Pcmin SLmin],Nc,1);
umax=repmat([Pcmax SLmax],Nc,1);

% Add predictions
```

```
%r=repmat(reshape(yt,1,numel(yt)),Np,1); % keep reference constant over all the
horizon...... FIXIT!
r=yt;
%d=repmat(reshape(wh(1,:),1,numel(wh(1,:))),Np,1); % keep disturbances constant
over all the horizon...... FIXIT!
d=wh(1:Np,:);

% Init starting values for search
if (isempty(u0) || size(u0,1)~=Nc || size(u0,2)~=m)
    u0=zeros(Nc,m);
end

% Minimize cost function subject to bound constraints
options = optimoptions(@fmincon,'Algorithm','active-
set','Display','off','TypicalX',umax-umin); % 'interior-point','active-
set','sqp','sqp-legacy','trust-region-reflective'
[U,fval,exitFlag] = fmincon(@(u)
costFunction(u,plant,xh,d,r,Nw,Np,Nc,Q,R),u0,[],[],[],[],umin,umax,[],options);

%disp(['time=' num2str(get_param(bdroot(gcb),'SimulationTime')) 's -> exitFlag='
num2str(exitFlag)]);

% returns and stores first control action
Pc=U(1,1);
SL=U(1,2);
u0=[U(2:end,:) ; ...
    U(end,:)        ];

return



function J=costFunction(u,plant,x0,d,r,Nw,Np,Nc,Q,R)
% Compute cost function based on provided parameters Nw,Np,Nc,Q,R for given
% plant with intial state x0, disturbances prediction d, reference
% prediction r and control sequence u.
% When setpoint r is NaN, the corresponding cost is not accounted for.
%
% input vector:
% u = [u1(1)  u2(1)  ...  um(1) ;
%      u1(2)  u2(2)  ...  um(2) ;
%      ...    ...    ...  ...   ;
%      u1(Nc) u2(Nc) ...  um(Nc);
%
% initial state vector:
% x0 = [x1(0) x2(0) ... xn(0)];
%
% disturbance vector:
% d = [d1(0)  d2(1)  ...  dnd(1) ;
%      d1(2)  d2(2)  ...  dnd(2) ;
%      ...    ...    ...  ...   ;
%      d1(Np) d2(Np) ...  dnd(Np);
%
% reference vector:
% r = [r1(0)  r2(1)  ...  rp(1) ;
%      r1(2)  r2(2)  ...  rp(2) ;
%      ...    ...    ...  ...   ;
%      r1(Np) r2(Np) ...  rp(Np);
%
% weighting matrices:
% Q = eye(p) * wy;
% R = eye(m) * wu;
%
% horizons:
```

```
% Nw, Np, Nc = Start, prediction and control horizons. The control horizon
% is used to define block inputs: i.e. the prediction horizon is divided
% into floor(Np/Nc) intervals of equal lenght but he last one.


% get dimensions
n=size(plant.a,1); % number of state variables
nd=size(d,2); % number of disturbance variables (assumed to be the last ones in
the input vector)
m=size(plant.b,2)-nd; % number of input variables
p=size(plant.c,1); % number of output variables

% complete U with Np-Nc values equals to the last value of U
%u=[u; repmat(u(end,:),Np-Nc,1)];

% inplement input blocking based on ratio Np/Nc: if Np=12 and Nc=5, then 5
% blocks are generated with lenght 2, but the last one that has lenght 3.
block=floor(Np/Nc); % block lenght
u = reshape(repmat(u,1,block)', m+1, block*Nc)'; % replicates each row 'block'
times
u = [u; repmat(u(end,:),Np-block*Nc,1)]; % add last rows up to Np

% FIXIT: chek if is better to use all zeros to complete matrix... probably
% this is better when integral form is used.
% ................................................

% compute shading correction
for i=1:Np
    SL=u(i,2);
    Ps=d(i,1);
    d(i,1) = shading(Ps,SL);
end
Pc=u(:,1:end-1);

% simulate ss model
r=[r(1,:); r]; % add one row to be coherent with the indeces of y
tt=[0:plant.Ts:Np*plant.Ts]';
y=lsim(plant,[Pc d;zeros(1,m+nd)],tt,reshape(x0,1,numel(x0)));
% sum over Np
Jy=0;
Ju=0;
for i=1:Np,
    if i>=Nw
        r( i+1, isnan(r(i+1,:)) ) = y( i+1, isnan(r(i+1,:)) ); % sets to the
value of y the setpoint for NaN entries (thus disabling cost for that instant)
        Jy = Jy + (y(i+1,:)-r(i+1,:))*Q*(y(i+1,:)-r(i+1,:))';
        Ju = Ju + u(i,:)*R*u(i,:)';
    end
%     if i<=Nc
%         Ju = Ju + u(i,:)*R*u(i,:)';
%     end
end
% get total cost
J=Jy+Ju;
return



function PsSha = shading(Ps,SL)
%#codegen
a_min=0.152; % alpha min
a=(a_min - 1) * SL + 1; % alpha
PsSha=Ps*a;
```

"getssmodel.m" (identification of the grey-box model in the "Model estimator"):

```
function [A,B,C,D,p] = getssmodel(p,Ts,option)

Rie=p(1);
Rea=p(2);
Ci=p(3);
Ce=p(4);
K=p(5);
Aw=p(6);
[A,B,C,D] = greybox(Rie,Rea,Ci,Ce,K,Aw,Ts); % Ts=0 -> continuous time model
numDays = 14; % number of days for estimating the model

% if option=='const', disable online estimation
if strcmp(option,'const'),
    return
else
    % LOAD DATASET from simulation output
    if exist('simulationData.mat','file'),
        load('simulationData.mat'); % load 'simout' variable
        simout=simout';
        nSamples = size(simout,1); % Number of available samples
        if ~isempty(simout) && nSamples>=86400/Ts, % check if datatset is sufficiently rich
        (>= 1 day)
            nFirst = max(nSamples-86400*numDays/Ts, 1); % First sample selected for
            estimation is numDays before last sample
            Ps=simout(nFirst:nSamples,2); % power W -> Ps, Pr, Pf, Pc
            Pr=simout(nFirst:nSamples,3);
            Pf=simout(nFirst:nSamples,4);
            Pc=simout(nFirst:nSamples,5);
            Ti=simout(nFirst:nSamples,6); % temperature °C -> Ti, Ti_ref
            Ti_ref=simout(nFirst:nSamples,7);
            Te=simout(nFirst:nSamples,8); % temperature °C -> Te, Ta, Tc
            Ta=simout(nFirst:nSamples,9);
            Tc=simout(nFirst:nSamples,10);
        else
            return
        end
    else
        return
    end
    % ESTIMATE MODEL
    if strcmp(option,'greyest'),
        % prepare dataset for estimation
        data = iddata(Ti, [Pc, Ps, Pr, Pf, Ta, Tc], Ts, 'Name', 'Grey-box heat dynamics
        model');
        data.InputName = {'Pc', 'Ps', 'Pr', 'Pf', 'Ta', 'Tc'};
        data.InputUnit = {'W', 'W', 'W', 'W', '°C', '°C'};
        data.OutputName = 'Ti';
        data.OutputUnit = '°C';
        data.Tstart = 0;
        data.TimeUnit = 's';

        % prepare grey box model and estimation parameters
        mi = idgrey(@greybox,{'Rie', Rie; 'Rea', Rea; 'Ci', Ci; 'Ce', Ce; 'K', K; 'Aw',
        Aw},'cd',{}, 0);
        mi = setpar(mi, 'label', 'default');
        % specify bounds and parameters to be stimated
        for i=1:6
            mi.Structure.Parameters(i).Free = true;
        end
        mi.Structure.Parameters(1).Minimum = 1e-4; mi.Structure.Parameters(1).Maximum = 1e-1;
        mi.Structure.Parameters(2).Minimum = 1e-4; mi.Structure.Parameters(2).Maximum = 1e-1;
        mi.Structure.Parameters(3).Minimum = 1e5;  mi.Structure.Parameters(3).Maximum = 1e9;
        mi.Structure.Parameters(4).Minimum = 1e5;  mi.Structure.Parameters(4).Maximum = 1e9;
        mi.Structure.Parameters(5).Minimum = 1e-2; mi.Structure.Parameters(5).Maximum = 1;
        mi.Structure.Parameters(6).Minimum = 0.1;  mi.Structure.Parameters(6).Maximum = 10;

        % prepare estimation parameters
        opt = greyestOptions;
        opt.Regularization.Lambda = 1;
        opt.Regularization.R = 1;
        opt.Regularization.Nominal = 'model'; % 'zero' or 'model' to pull parameters to
```

```
        initial values or to zero
        opt.SearchMethod = 'auto';
        opt.Display = 'on';
        opt.Focus = 'simulation'; % 'stability' 'prediction' 'simulation'
        opt.DisturbanceModel = 'estimate';

        % estimate grey box model
        sys = greyest(data, mi, opt);
        p=getpvec(sys);
        %cov=getcov(sys);
        % sys.NoiseVariance % The variance (covariance matrix) of the model innovations, e.
    else % 'fmin'
        %   Ti0 Te0 Ci   Ce   Rie  Rea  Aw   k
        lb=[10  10  0.01 0.01 0.01 0.01 0.01 0];
        ub=[35  35  50   50   10   10   10   1];
        p=fminestimate(Ti,[Ps/1000 Pc/1000 Pr/1000 Pf/1000 Ta Tc],Ts/3600,lb,ub);
        %  Rie,      Rea,      Ci,            Ce,            K,   Aw
        p=[p(5)/1000,p(6)/1000,p(3)*3600*1000,p(4)*3600*1000,p(8),p(7)];
    end
    [A,B,C,D] = greybox(p(1),p(2),p(3),p(4),p(5),p(6),Ts); % Se Ts=0 -> continuous time model
end

return
```

Appendix I. Tuning of MPC parameters

TUNING MPC PARAMETERS: PERIOD 01-30 JUNE 2016

FILE: "MPCxBuildings_v2_5_shading_final4.slx"

DEFAULT SETTINGS:

Sampling interval

```
Ts=300s;
```

MPC tuning parameters:

Horizons

```
Nw=1;
Np=12;
Nc=6;
```

Weights of the cost function

```
wy=10*1e6;
wu=1;
wPc=1;
wSL=1e6;
```

Constraints of the cost function

```
umin=-1200;
umax=0;
SLmin=0;
SLmax=1;
```

TUNING Np:

1. tp= 2h; Np = 24; Nc = 12

SIMULATION RESULTS: >> load('simulationData_2h.mat')>> plotSimulationDataSL

Root mean square error computed only for Ti>Ti_ref: **RMSE = 0.49956°C**

Absorbed energy: **E = 133.7034kWh**

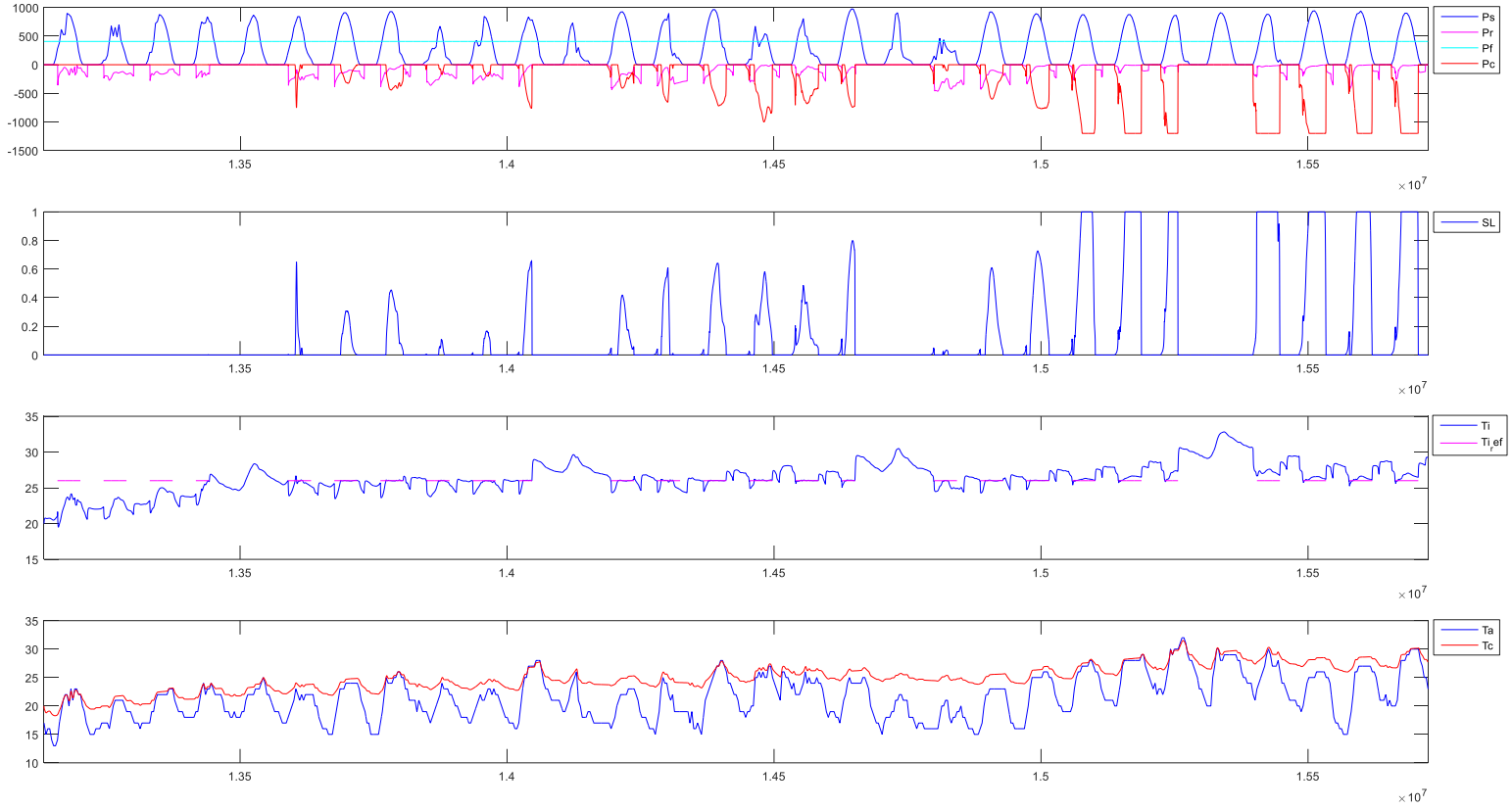

2. tp= 4h; Np = 48; Nc = 24

SIMULATION RESULTS: >> load('simulationData_4h.mat') >> plotSimulationDataSL

Root mean square error computed only for Ti>Ti_ref: **RMSE = 0.48253°C**

Absorbed energy: **E = 137.7893kWh**

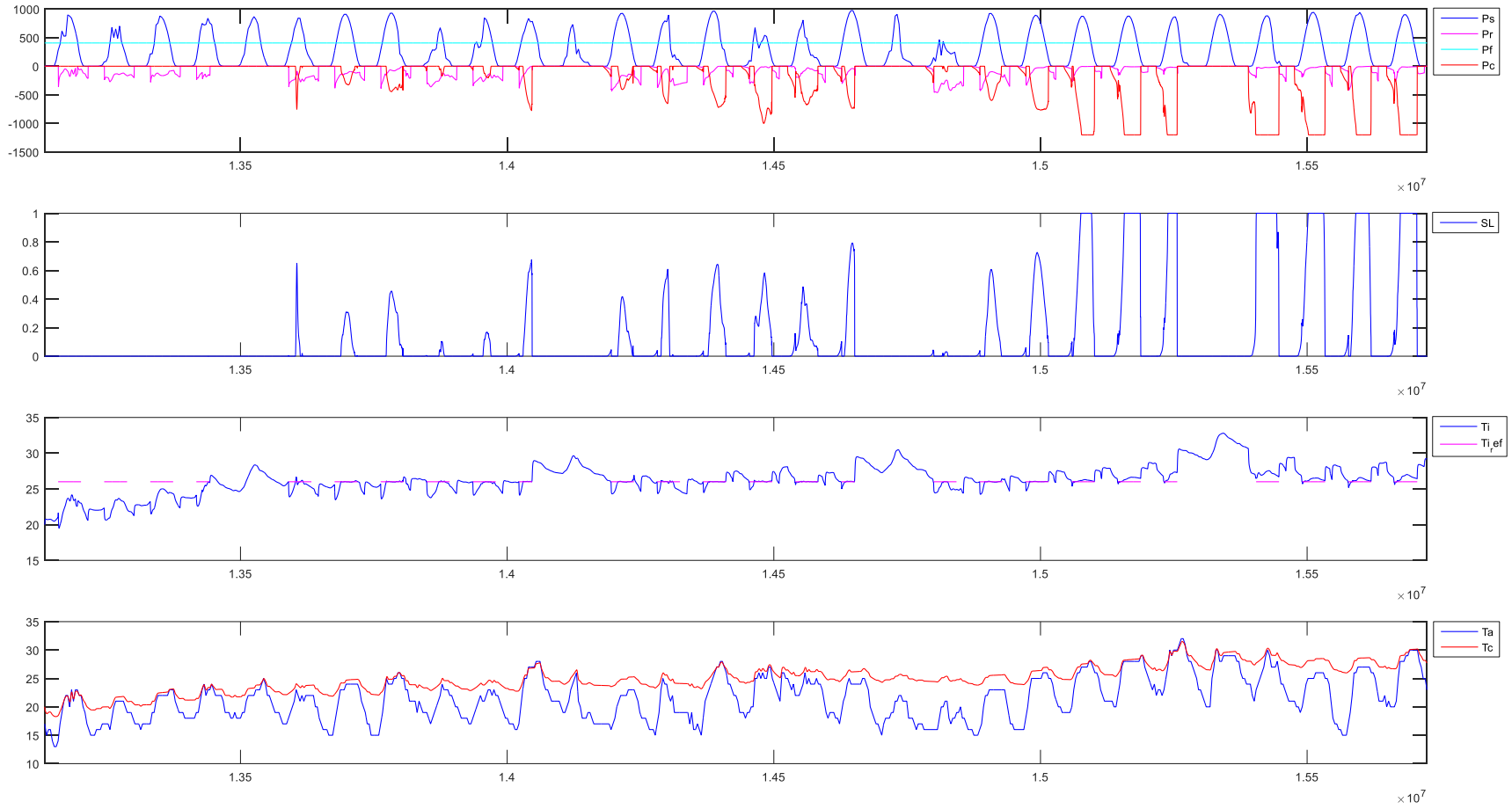

3. tp= 6h; Np = 72; Nc = 36

SIMULATION RESULTS: >> load('simulationData.mat') >> plotSimulationDataSL

Root mean square error computed only for Ti>Ti_ref: **RMSE = 0.46628°C**

Absorbed energy: **E = 142.5604kWh**

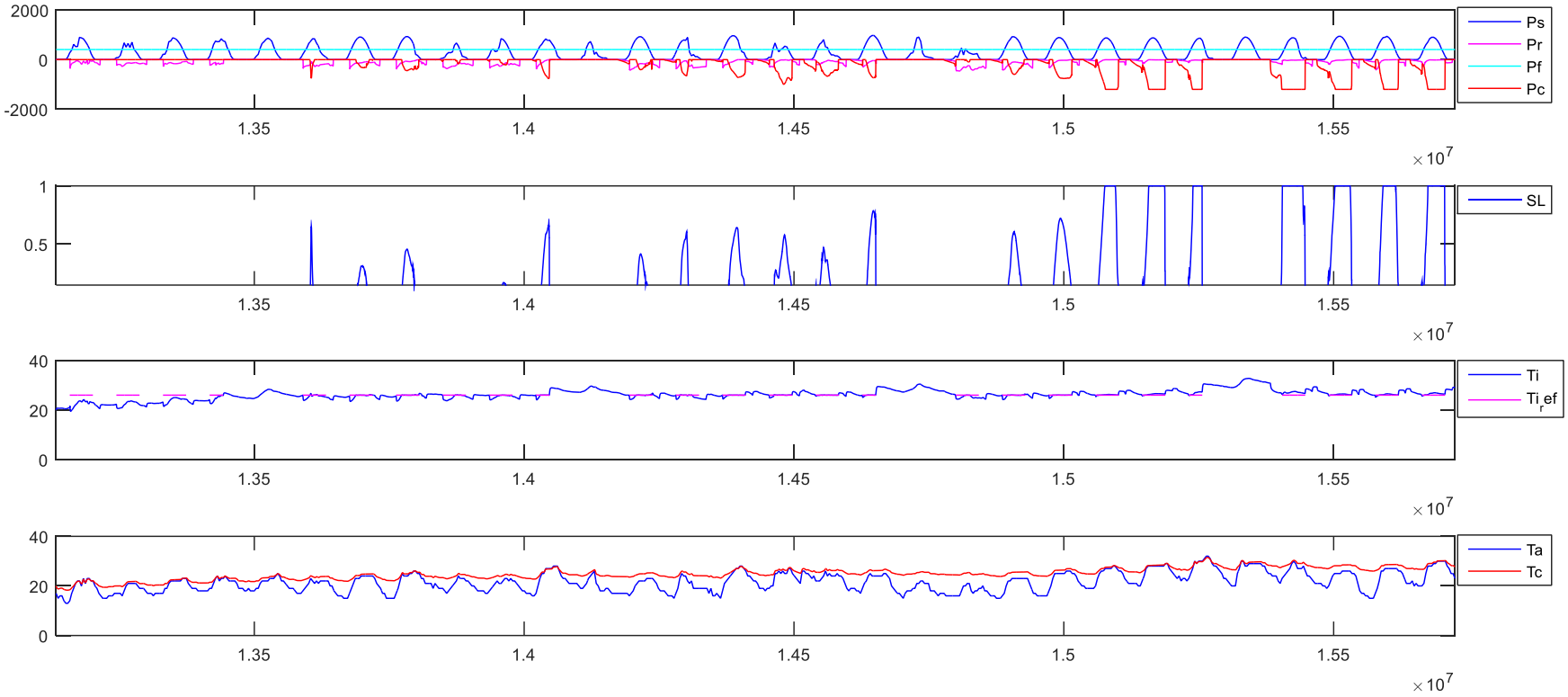

4. tp= 8h; Np = 96; Nc = 48

SIMULATION RESULTS: >> load('simulationData.mat') >> plotSimulationDataSL

Root mean square error computed only for Ti>Ti_ref: **RMSE = 0.44918°C**

Absorbed energy: **E = 147.2231kWh**

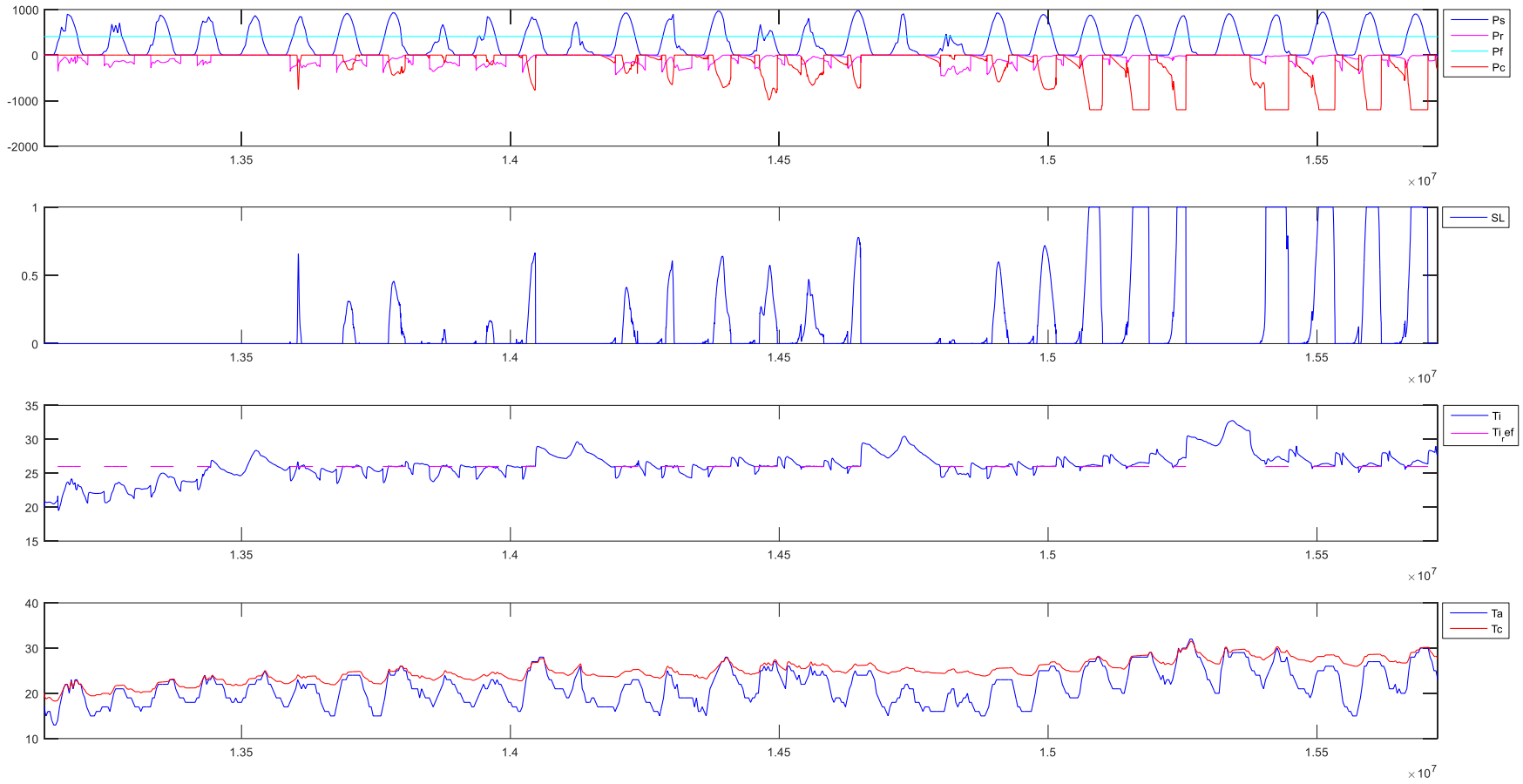

5. tp= 10h; Np = 120; Nc = 60

SIMULATION RESULTS: >> load('simulationData.mat') >> plotSimulationDataSL

Root mean square error computed only for Ti>Ti_ref: **RMSE = 0.4361°C**

Absorbed energy: **E = 152.2549kWh**

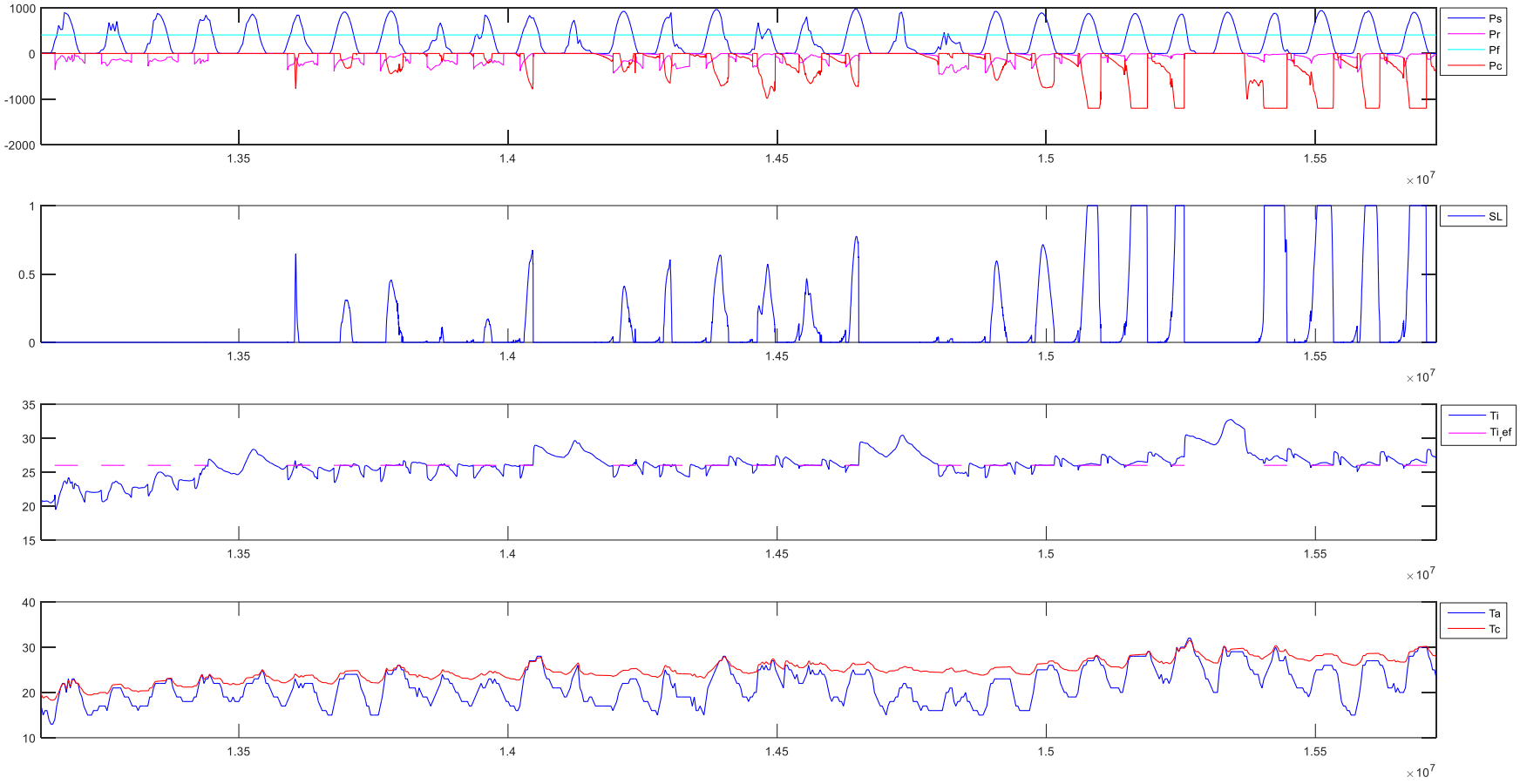

6. tp= 12h; Np = 144; Nc = 72

SIMULATION RESULTS: >> load('simulationData.mat') >> plotSimulationDataSL

Root mean square error computed only for Ti>Ti_ref: **RMSE = 0.42327°C**

Absorbed energy: **E = 159.195kWh**

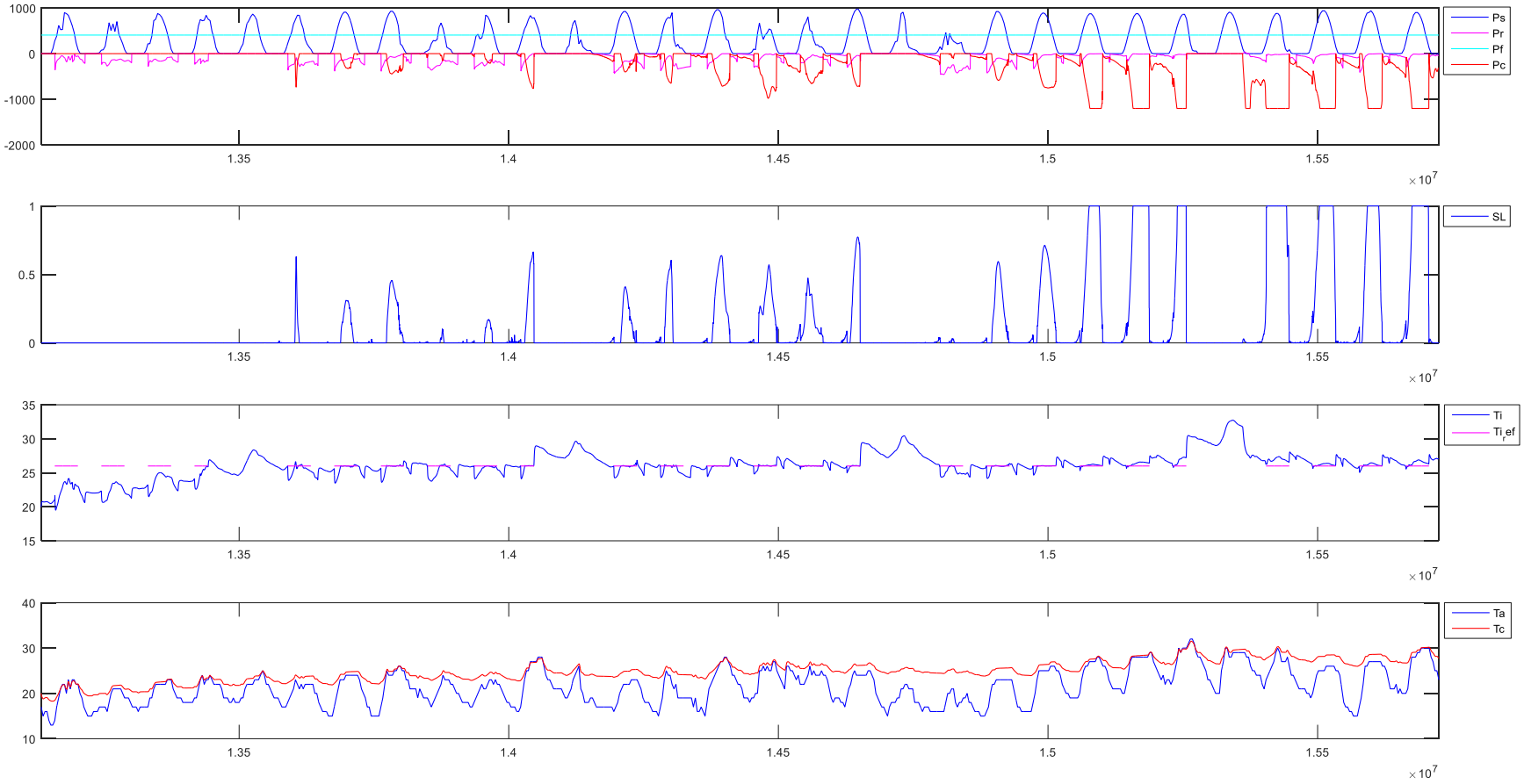

TUNING Nc:

1. tp= 10h; Np = 120; Nc = 20

SIMULATION RESULTS: >> load('simulationData.mat') >> plotSimulationDataSL

Root mean square error computed only for Ti>Ti_ref: **RMSE = 0.49156°C**

Absorbed energy: **E = 151.8705kWh**

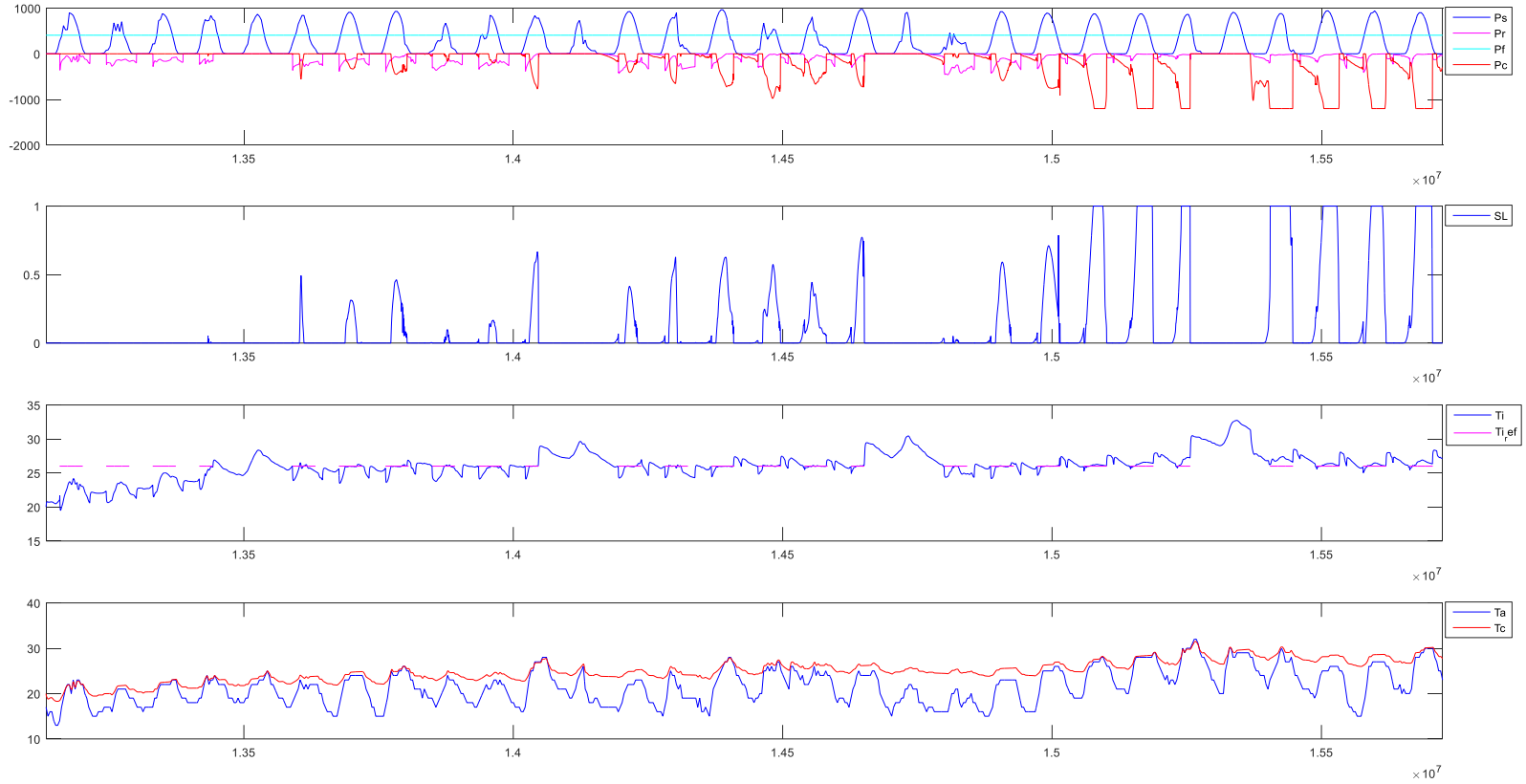

2. tp= 10h; Np = 120; Nc = 10

SIMULATION RESULTS: >> load('simulationData.mat') >> plotSimulationDataSL

Root mean square error computed only for Ti>Ti_ref: **RMSE = 0.48991°C**

Absorbed energy: **E = 154.5975kWh**

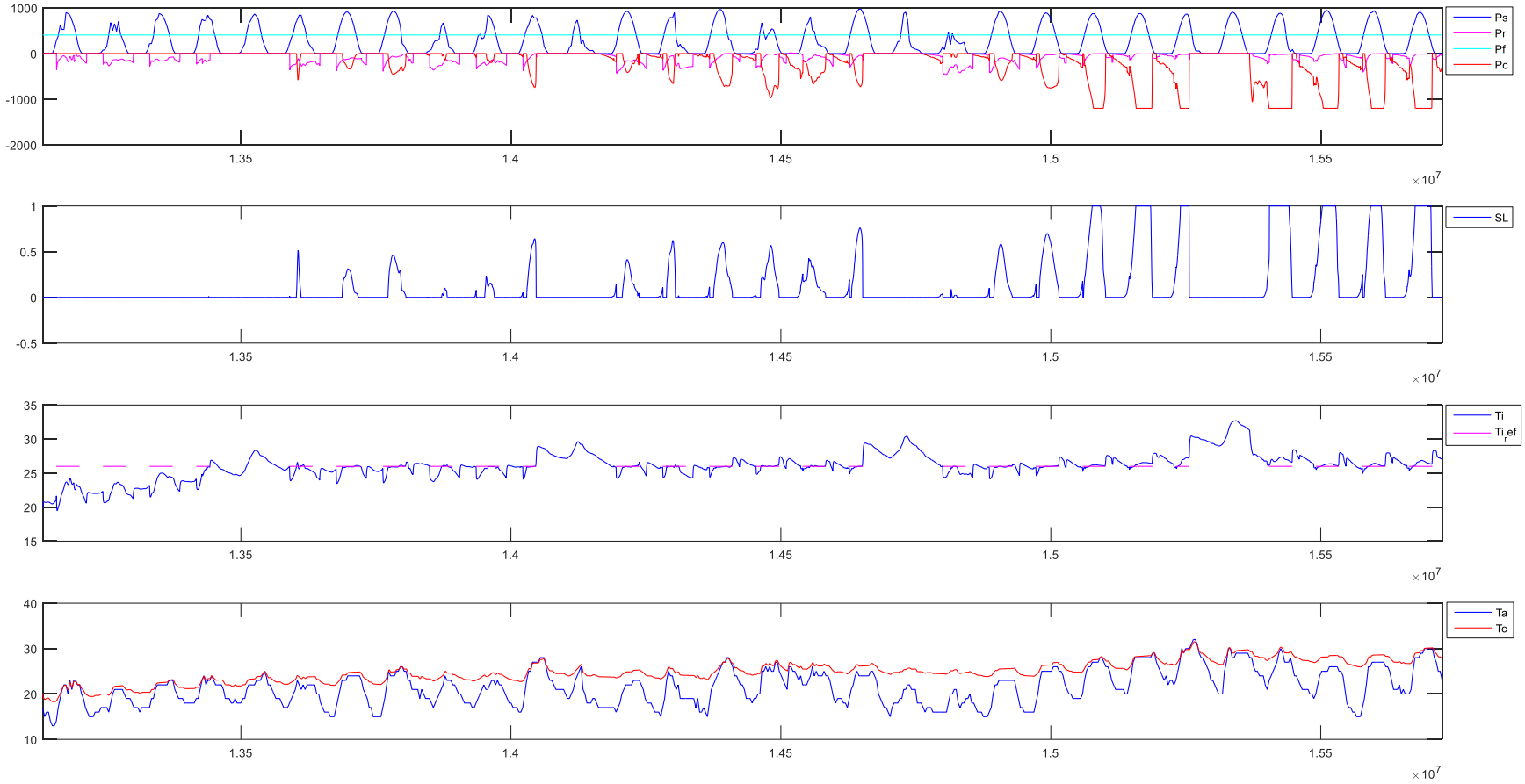

3. tp= 10h; Np = 120; Nc = 5

SIMULATION RESULTS: >> load('simulationData.mat') >> plotSimulationDataSL

Root mean square error computed only for Ti>Ti_ref: **RMSE = 0.47999°C**

Absorbed energy: **E = 154.7471kWh**

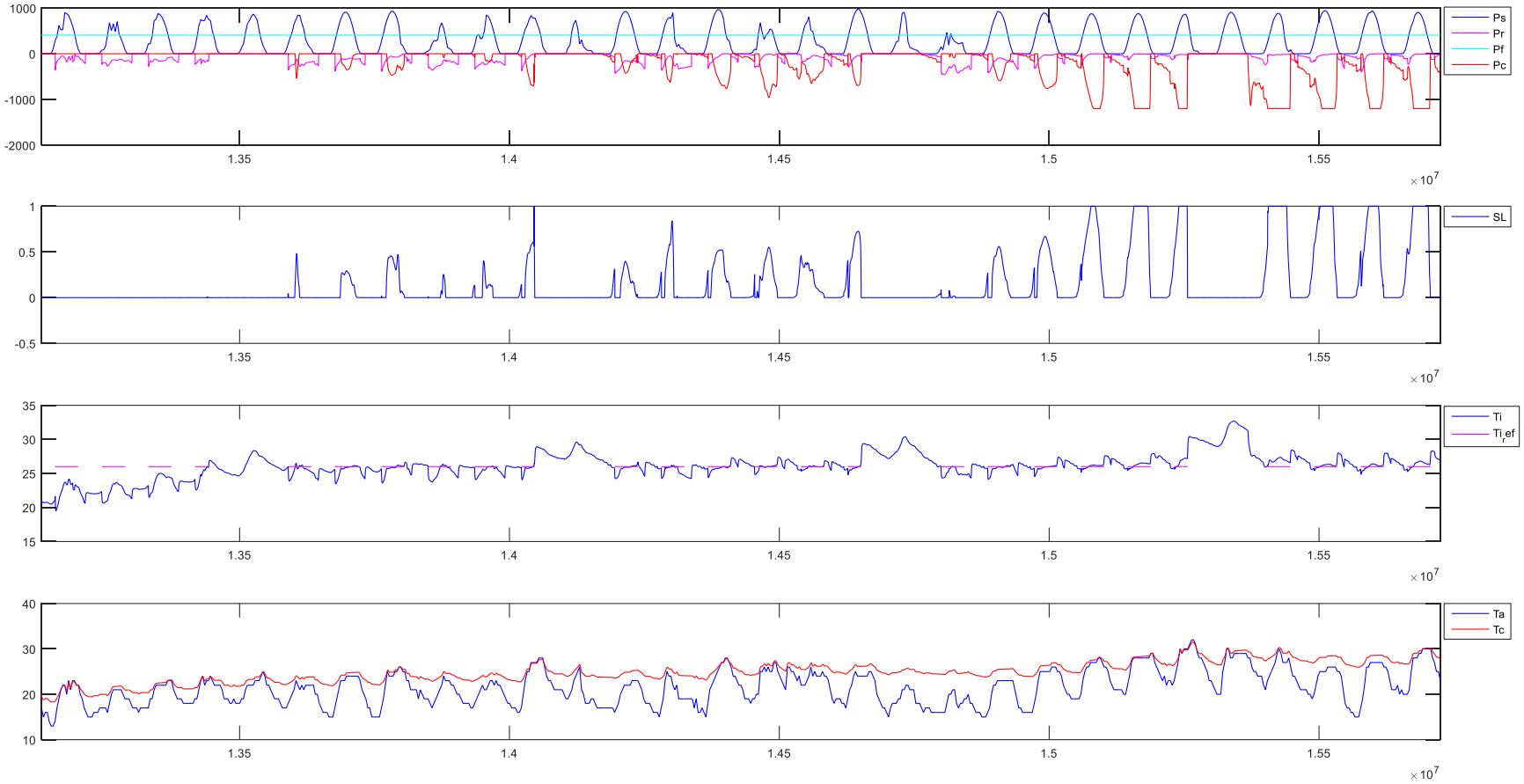

4. tp= 12h; Np = 144; Nc = 24

SIMULATION RESULTS: >> load('simulationData.mat') >> plotSimulationDataSL

Root mean square error computed only for Ti>Ti_ref: **RMSE = 0.48029°C**

Absorbed energy: **E = 158.5903kWh**

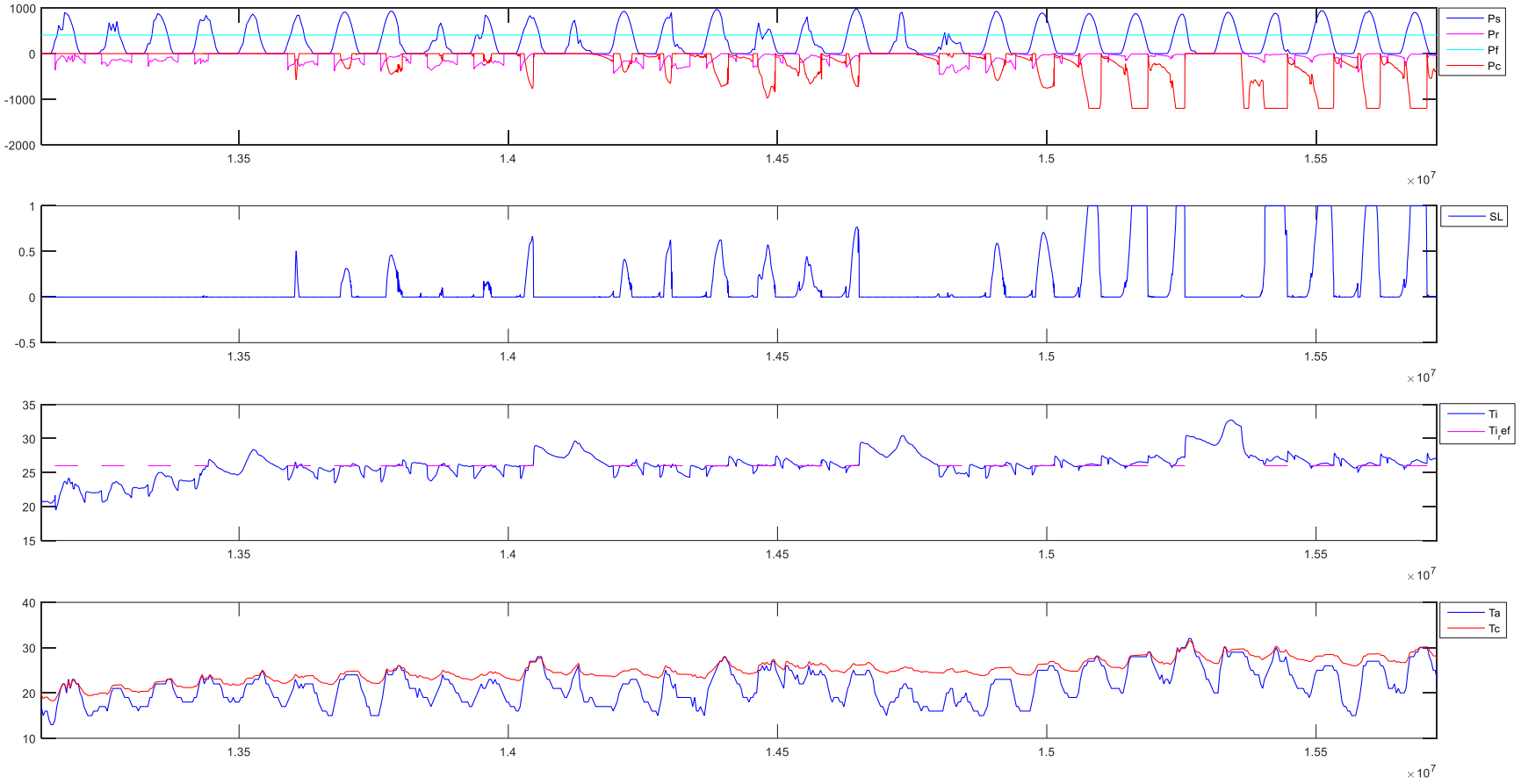

5. tp= 12h; Np = 144; Nc = 12

SIMULATION RESULTS: >> load('simulationData.mat') >> plotSimulationDataSL

Root mean square error computed only for Ti>Ti_ref: **RMSE = 0.47603°C**

Absorbed energy: **E = 161.8359kWh**

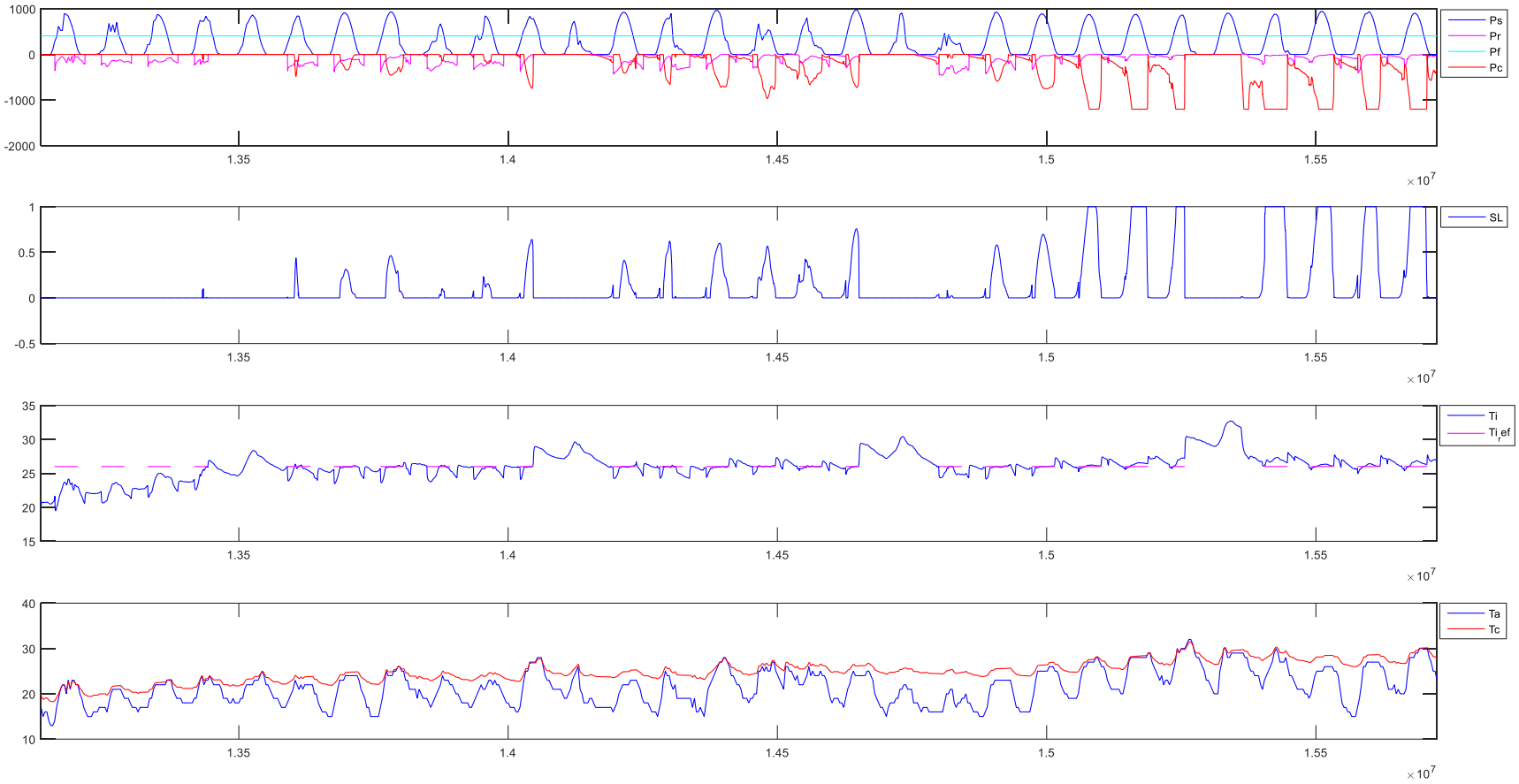

6. tp= 12h; Np = 144; Nc = 6

SIMULATION RESULTS: >> load('simulationData.mat') >> plotSimulationDataSL

Root mean square error computed only for Ti>Ti_ref: **RMSE = 0.4666°C**

Absorbed energy: **E = 162.0875kWh**

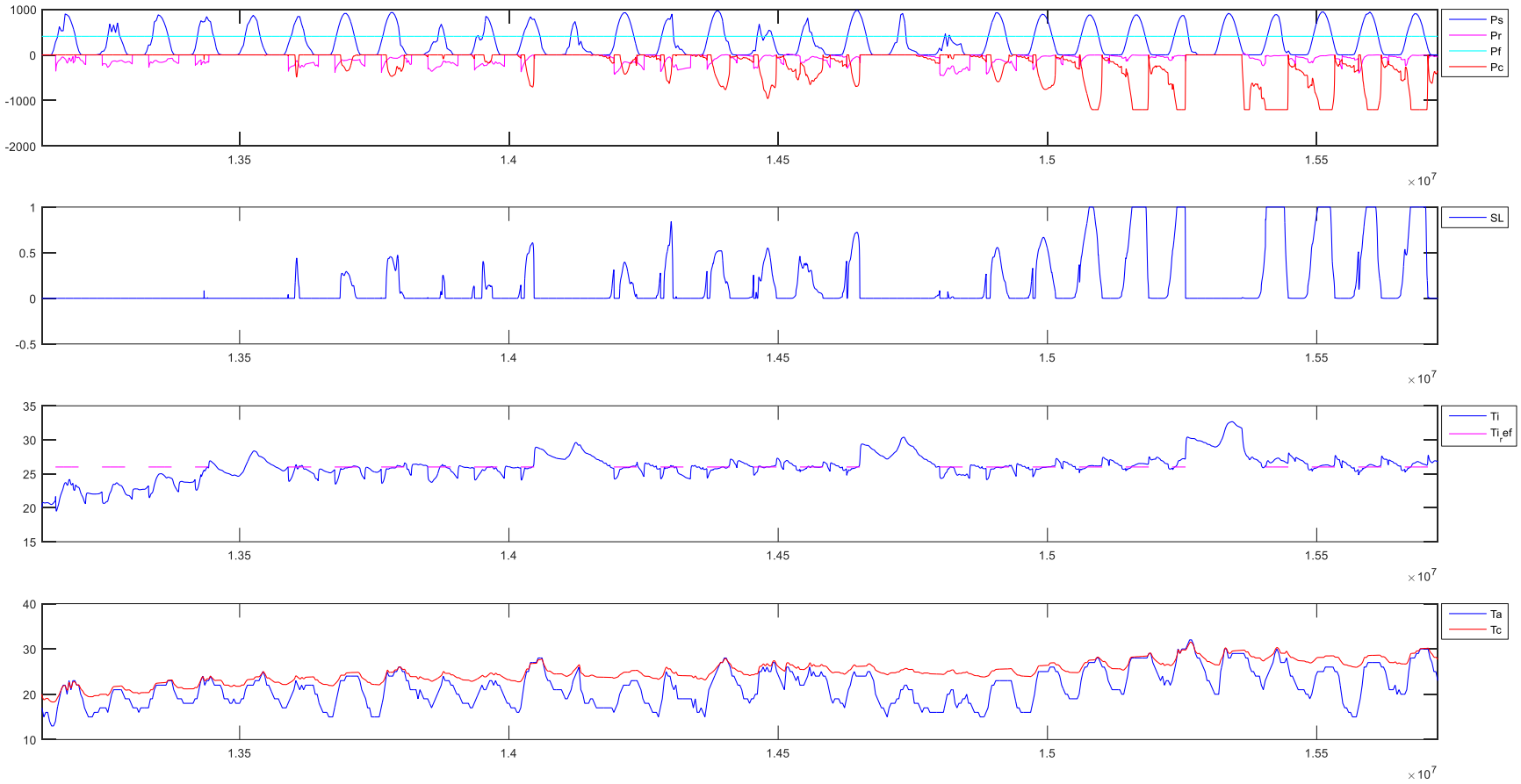

7. tp= 24h; Np = 288; Nc = 24

SIMULATION RESULTS: >> load('simulationData.mat') >> plotSimulationDataSL

Root mean square error computed only for Ti>Ti_ref: **RMSE = 0.39635°C**

Absorbed energy: **E = 176.9034kWh**

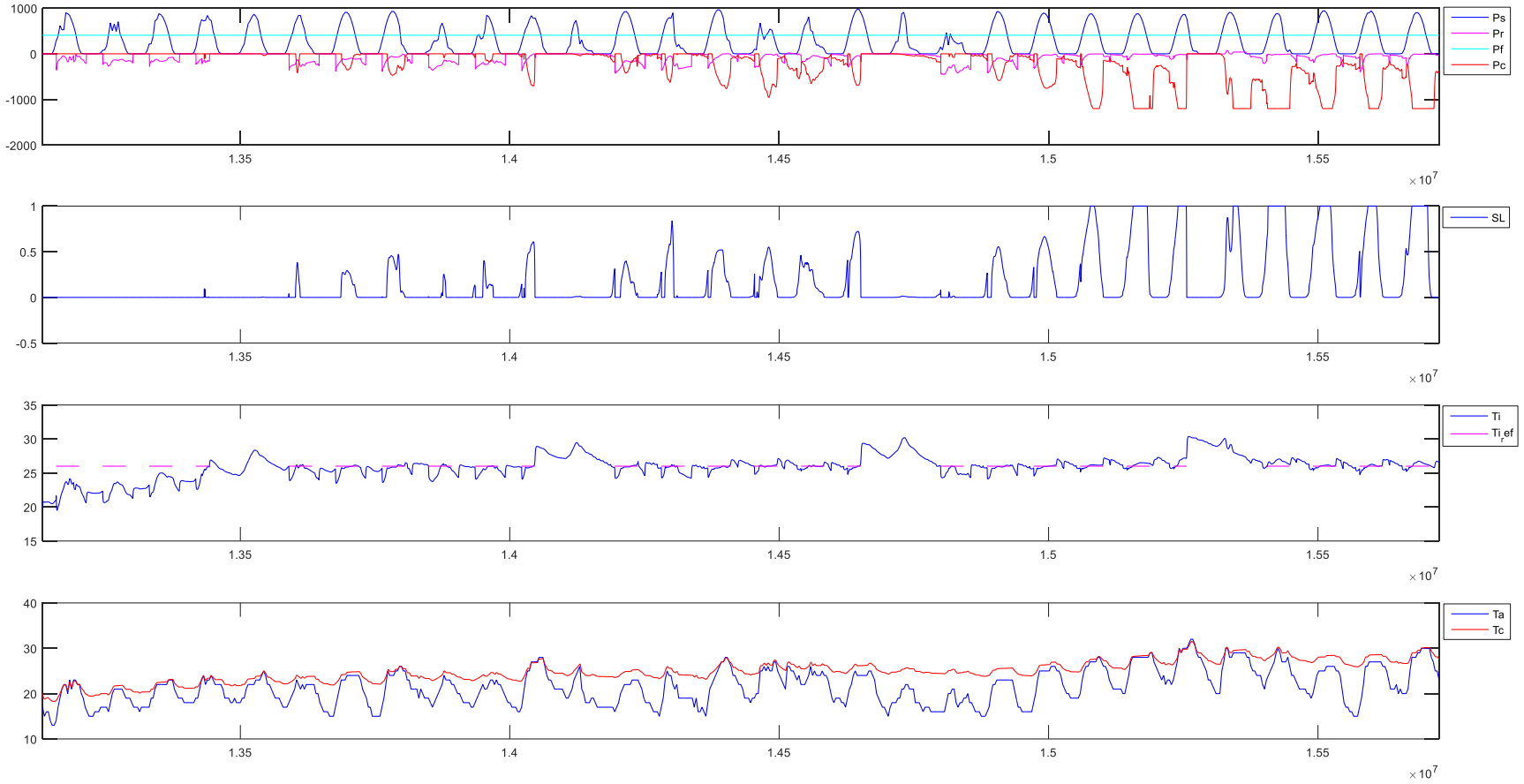

8. tp= 36h; Np = 432; Nc = 36

SIMULATION RESULTS: >> load('simulationData.mat') >> plotSimulationDataSL

Root mean square error computed only for Ti>Ti_ref: **RMSE = 0.4094°C**

Absorbed energy: **E = 177.5282kWh**

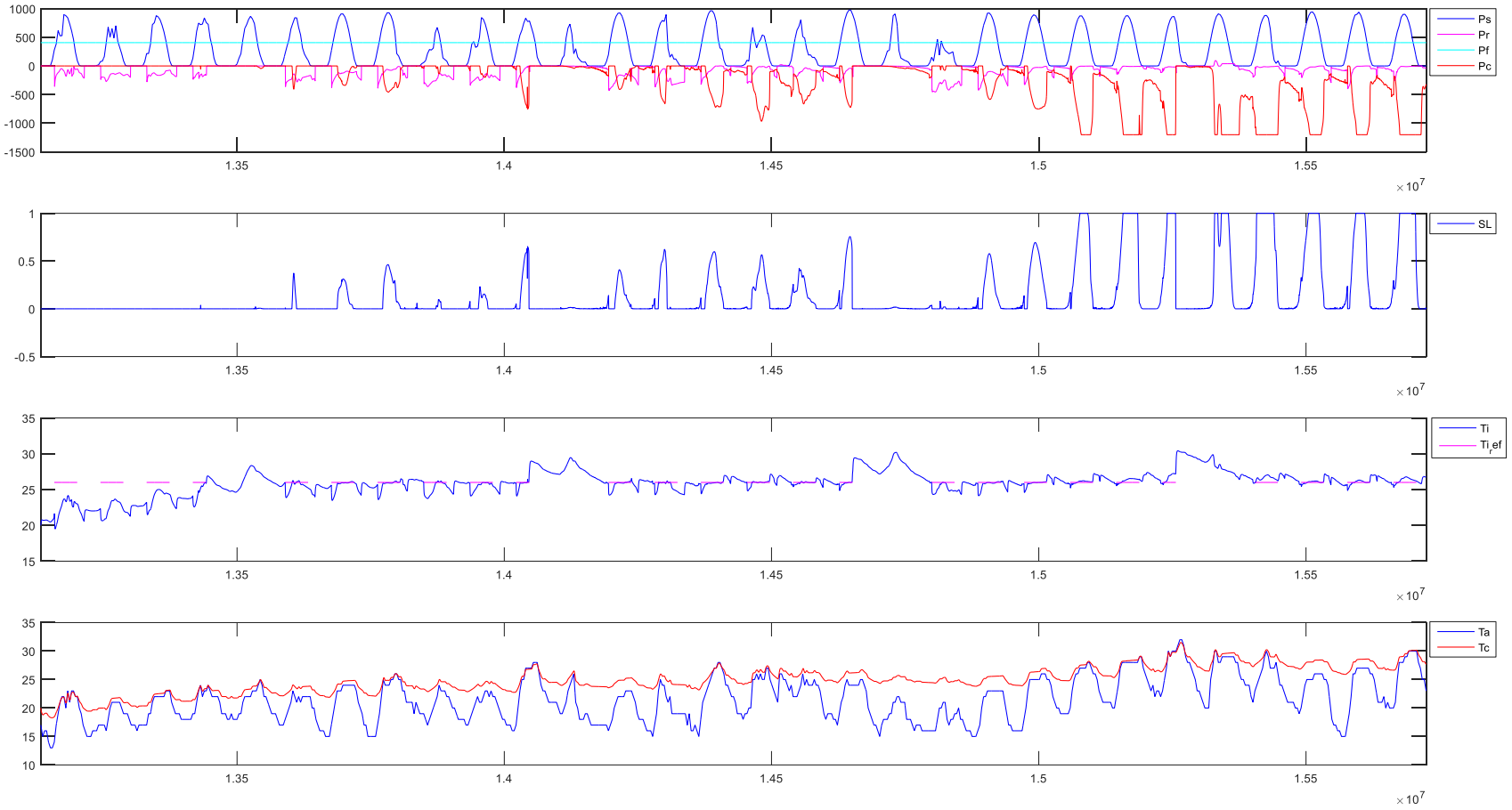

9. tp= 48h; Np = 576; Nc = 48

SIMULATION RESULTS: >> load('simulationData.mat') >> plotSimulationDataSL

Root mean square error computed only for Ti>Ti_ref: **RMSE = 0.40069°C**
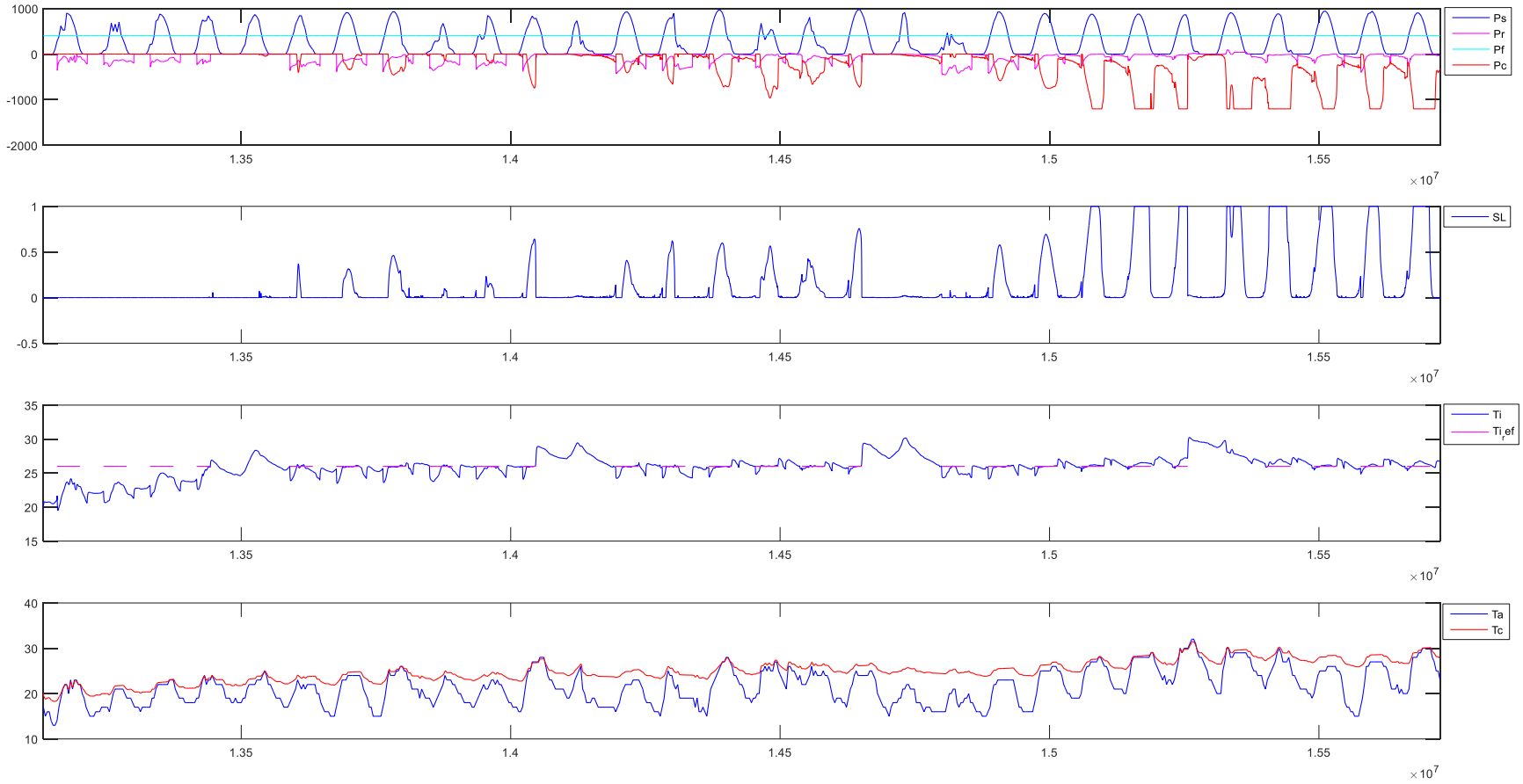
Absorbed energy: **E = 178.3667kWh**